December 28, 2022 Docket No. 52-050

U.S. Nuclear Regulatory Commission
ATTN: Document Control Desk
One White Flint North
11555 Rockville Pike
Rockville, MD 20852-2738

SUBJECT: NuScale Power, LLC Submittal of the NuScale Standard Design Approval Application Part 2 – Final Safety Analysis Report, Chapter 4, "Reactor," Revision 0

REFERENCES:
1. NuScale letter to NRC, "NuScale Power, LLC Submittal of Planned Standard Design Approval Application Content," dated February 24, 2020 (ML20055E565)
2. NuScale letter to NRC, "NuScale Power, LLC Staged Submittal of Planned Standard Design Approval Application," dated November 21, 2022 (ML22325A349)
3. NuScale letter to NRC, "NuScale Power, LLC Requests the NRC staff to conduct a pre-application readiness assessment of the draft, 'NuScale Standard Design Approval Application (SDAA),'" dated May 25, 2022 (ML22145A460)
4. NRC letter to NuScale, "Preapplication Readiness Assessment Report of the NuScale Power, LLC Standard Design Approval Draft Application," Office of Nuclear Reactor Regulation dated November 15, 2022 (ML22305A518)

NuScale Power, LLC (NuScale) is pleased to submit Chapter 4, "Reactor," Revision 0, in support of Part 2, "Final Safety Analysis Report," (FSAR) of the NuScale Standard Design Approval Application (SDAA) (Reference 1). NuScale submits the chapter in accordance with requirements of 10 CFR 52 Subpart E, Standard Design Approvals. As described in Reference 2, the enclosure is part of a staged SDAA submittal. NuScale requests NRC review, approval, and granting of standard design approval for the US460 standard plant design. Section A of Enclosures 1 and 2 contain Chapter 4, "Reactor," Revision 0 in support of Part 2, FSAR.

From July 25, 2022 to October 26, 2022, the NRC performed a pre-application readiness assessment of available portions of the draft NuScale FSAR to determine the FSAR's readiness for submittal and for subsequent review by NRC staff (References 3 and 4). The NRC staff reviewed draft Chapter 4. NuScale is enclosing information in this submittal that: 1) closes gaps identified between the draft SDAA Chapter 4 and technical content generally expected by the NRC; and 2) resolves identified technical issues that may have adversely impacted acceptance, docketing, or technical review of the application. NuScale's responses to Reference 4 for Chapter 4 observations are in section B of Enclosures 1 and 2.

The technical report that supports Chapter 4, "Reactor" is included in Section C of Enclosures 1 and 2.

NuScale requests that the proprietary content (Enclosure 1), be withheld from public disclosure in accordance with the requirements of 10 CFR § 2.390. The enclosed affidavits (Enclosures 3 and 4) support this request. Enclosure 3 pertains to the information proprietary to NuScale, denoted by double braces (i.e., "{{ }}"). Enclosure 4 pertains to the information proprietary to Framatome Inc. (formerly AREVA Inc.), denoted by brackets (i.e., "[ ]"). Enclosure 1, Section C has also been determined to contain Export Controlled Information. This information must be protected from disclosure per the requirements of 10 CFR § 810.

This letter makes no regulatory commitments and no revisions to any existing regulatory commitments.

If you have any questions, please contact Mark Shaver at 541-360-0630 or at mshaver@nuscalepower.com.

I declare under penalty of perjury that the foregoing is true and correct. Executed on December 28, 2022.

Sincerely,

Carrie Fosaaen
Senior Director, Regulatory Affairs
NuScale Power, LLC

Distribution: Brian Smith, NRC
Michael Dudek, NRC
Getachew Tesfaye, NRC
Bruce Bavol, NRC
David Drucker, NRC

Enclosure 1: SDAA Part 2 Chapter 4, "Reactor," Revision 0, (proprietary)
Enclosure 2: SDAA Part 2 Chapter 4, "Reactor," Revision 0, (nonproprietary)
Enclosure 3: Affidavit of Carrie Fosaaen, AF-131682
Enclosure 4: Affidavit of Morris Byram, Framatome Inc.

Enclosure 1:

SDAA Part 2 Chapter 4, “Reactor,” Revision 0, (proprietary)

NuScale Power, LLC
1100 NE Circle Blvd., Suite 200 Corvallis, Oregon 97330 Office 541.360.0500 Fax 541.207.3928
www.nuscalepower.com

Enclosure 2:

SDAA Part 2 Chapter 4, “Reactor,” Revision 0, (nonproprietary)

Contents

Section A

NuScale Power, LLC
1100 NE Circle Blvd., Suite 200 Corvallis, Oregon 97330 Office 541.360.0500 Fax 541.207.3928
www.nuscalepower.com

NuScale US460 Plant
Standard Design Approval Application

Chapter Four
Reactor

Final Safety Analysis Report

Revision 0

TABLE OF CONTENTS

LIST OF TABLES

LIST OF FIGURES

LIST OF FIGURES

CHAPTER 4 REACTOR

4.1 Summary Description

The NuScale Power Module is a self-contained nuclear steam supply system composed of a reactor core, a pressurizer, and two steam generators integrated within the reactor pressure vessel and housed in a compact steel containment vessel.

Chapter 4 provides a summary of the

- reactor and the reactor core design.
- fuel rod and fuel assembly design.
- core control and monitoring components.
- nuclear and thermal-hydraulic design.
- reactor vessel internals and control rod drive system materials.
- control rod drive mechanism design.

4.2 Fuel System Design

The results summarized in this section show that the NuScale Power Module (NPM) fuel design demonstrates acceptable performance.

Section 4.2.1 presents the design bases for the fuel assembly, the control rod assembly (CRA), and the surveillance programs. Section 4.2.2 provides a description of the fuel, the components that comprise the fuel assembly, and the CRA. Section 4.2.3 provides the design evaluation that demonstrates how the design bases are met. Section 4.2.4 discusses fuel and CRA testing and inspection.

The fuel system design evaluations described in this section are supported by the technical report in Reference 4.2-1. Applicability of the Framatome methodologies referenced throughout this section to the NPM fuel system design is documented in Reference 4.2-2 and Reference 4.2-3 as supplemented by Reference 4.2-4. Evaluations presented in this section are performed to bound operation at full power and include consideration of power changes for startup, shutdown, and power changes that result in a new steady-state power level (i.e., baseload operation).

COL Item 4.2-1: An applicant that references the NuScale Power Plant US460 standard design and wishes to utilize non-baseload operations will provide justification for the fuel performance codes and methods corresponding to the desired operation.

4.2.1 Design Bases

The fuel system is designed to satisfy the following criteria

- The fuel system is not damaged as a result of normal operation and anticipated operational occurrences (AOOs) (General Design Criterion (GDC) 10).
- Fuel damage during postulated accidents is not severe enough to prevent control rod insertion when it is required (GDC 27).
- Core coolability is maintained, even after postulated accidents (Principal Design Criteria (PDC) 35 and 10 CFR 52.137).
- The number of fuel rod failures is not underestimated for postulated accidents as evaluated in Chapter 15 against applicable radiological consequences requirements.

The fuel assembly structural integrity is assured by setting limits on stresses and deformations due to various loads and by preventing the assembly structure from interfering with the functioning of other components. Three types of loads are considered:

- non-operational loads, such as those due to shipping and handling
- loads during normal operation and AOOs
- loads during infrequent events and postulated accidents

4.2.1.1 Cladding

The fuel rod cladding is a zirconium alloy called M5® that is approved for use in the "Evaluation of Advanced Cladding and Structural Material (M5®) in PWR Reactor Fuel" report (Reference 4.2-5).

4.2.1.1.1 Mechanical Properties

The fuel rod cladding properties are defined in Reference 4.2-5.

4.2.1.1.2 Stress-Strain Limits

The methodology and design criteria for analyzing cladding stress are provided in Reference 4.2-5.

The cladding stress analysis follows the guidelines of Section III of the American Society of Mechanical Engineers (ASME) Boiler and Pressure Vessel Code (BPVC), which provides guidance for establishing stress intensity limits. The stress intensity limits are listed in Reference 4.2-1 and are based on unirradiated yield strength, as approved in Reference 4.2-5. The use of unirradiated values is conservative because irradiation increases the yield and ultimate tensile strengths for zirconium-based materials like M5® cladding.

A cladding buckling analysis determines that the cladding does not buckle when the rod internal pressure is at a minimum and the system pressure is at a maximum, as presented in Reference 4.2-5.

For cladding strain, the maximum uniform hoop strain (elastic plus plastic) in the cladding does not exceed 1 percent (Reference 4.2-5).

4.2.1.1.3 Fatigue and Vibration

The effect of cyclical loadings on the clad is determined by calculating the clad cumulative fatigue usage factor and ensuring it does not exceed 0.9. The analysis method is consistent with the procedure for fatigue analysis in Section III of the ASME BPVC.

The design criterion for fretting is that wear at the fuel rod and grid contact points is limited and precludes fuel cladding failure. Fretting is further described in Section 4.2.3.5.7.

4.2.1.1.4 Chemical Properties

Chemical properties of the cladding are discussed in Reference 4.2-5.

Maintaining the oxide thickness on the cladding within a prescribed limit precludes external hydriding as a cladding failure mechanism. The external cladding oxide thickness limit is reported in Reference 4.2-1.

4.2.1.2 Fuel Material

4.2.1.2.1 Thermal-Physical Properties

The thermal-physical properties of the fuel are presented in the COPERNIC code topical report (Reference 4.2-6).

4.2.1.2.2 Fuel Densification and Fission Product Swelling

Fuel densification and swelling are modeled using the methodology in Reference 4.2-6. The COPERNIC code evaluates cladding strain, fuel temperature, and rod internal pressure using the fuel densification model and the swelling model.

4.2.1.2.3 Fuel Pellet Chemical Properties

Fuel pellet chemical properties are controlled through a rigorous testing and inspection program to demonstrate that each lot of pellets conforms to design requirements and criteria as described in Section 4.2.4.3.

4.2.1.3 Fuel Rod Performance

The critical design bases include fuel rod internal pressure, cladding creep collapse, cladding fatigue, cladding strain, corrosion, and centerline fuel melt under conditions of normal operation, AOOs, and postulated accidents. Reference 4.2-1 provides additional details concerning the design-basis for normal operations and AOOs.

Section 4.4 addresses critical heat flux design criteria. Section 15.4 addresses reactivity-initiated accidents, reactivity insertion accidents, and fuel centerline temperatures.

4.2.1.4 Spacer Grids

The spacer grids are designed to maintain the fuel rods in a coolable configuration (PDC 35 and 10 CFR 50.46), and ensure CRA insertion for AOOs and postulated accidents (GDC 27).

4.2.1.4.1 Mechanical, Chemical, Thermal, and Irradiation Properties of Grids

The strength criteria of the fuel assembly grid components are based on mechanical strength testing of prototypes, including static and dynamic crush testing.

The grids are tested to establish a 95 percent confidence level of the mean allowable crushing stress limit for both the unirradiated and a simulated irradiated condition. These limits are sufficient to demonstrate that, under worst-case combined seismic and loss-of-coolant accident (LOCA) events, the fuel assemblies remain in a coolable geometry. The design limits are detailed in Reference 4.2-1.

The allowable grid clamping loads during fuel shipment are based on static crush strength testing for static stiffness and elastic load limits. The spacer grids maintain their structural integrity under the maximum lateral shipping loads and the maximum clamping loads. The spacer grid springs are designed to maintain acceptable fuel rod grip forces from the limiting 6 g lateral (transverse) and 4 g axial (longitudinal) shipping loads.

Spacer grid slip load input to the analytical models of the fuel assembly used in the horizontal and vertical faulted analyses are established by mechanical testing.

4.2.1.4.2 Vibration and Fatigue of Grids

The interface between the fuel rods and the spacer grids is maintained throughout the life of the fuel assembly and prevents fuel rod fretting failure.

4.2.1.4.3 Chemical Compatibility of Grids with other Core Components

Spacer grid materials, as listed in Table 4.2-1, are compatible with the reactor coolant based on operating experience in pressurized water reactors (PWRs) in the United States.

4.2.1.5 Fuel Assembly Structural Design

The design bases for evaluating the structural integrity of the fuel assemblies is established by setting design limits on stresses and deformations due to various non-operational, operational, and abnormal loads.

The thermal-hydraulic design basis is presented in Section 4.4.

4.2.1.5.1 Non-Operational Loads

The fuel assembly is designed for the maximum non-operational loads experienced during shipping and handling. The non-operational load limit is 4 g axial (longitudinal) and 6 g lateral (transverse).

4.2.1.5.2 Normal Operating Conditions and Anticipated Operational Occurrences

The fuel assembly component structural design uses the stress categories and strength theory presented in Section III of the ASME BPVC. The stress intensities for fuel assembly structural components are less than the ASME Code Section III Level A service limits, buckling of the guide tube does not occur, and the cumulative fatigue cycles are be less than fatigue lifetime as presented in Reference 4.2-1.

4.2.1.5.3 Infrequent Events and Postulated Accidents

Seismic loadings typically produce the worst-case faulted loads. The LOCA loads are combined with the seismic loads to evaluate fuel assembly structural adequacy. Fuel assembly structural design criteria are established in

Reference 4.2-7. The fuel assembly structural component stresses under abnormal conditions are evaluated primarily using the methods outlined in Reference 4.2-7 and Reference 4.2-3. Component acceptance criteria are discussed in Reference 4.2-1.

4.2.1.5.4 Growth Allowance

A fuel assembly nozzle-to-fuel rod shoulder gap allowance is provided to maintain positive clearance between the fuel rods and the nozzles during the entire fuel assembly lifetime.

A fuel assembly-to-reactor internals gap allowance is provided to maintain a positive core plate gap during the entire fuel assembly lifetime.

4.2.1.5.5 Fuel Assembly Liftoff

The fuel assembly does not unseat or lift off during worst case hydraulic loads during normal operation and AOOs.

4.2.1.5.6 Guide Tube Buckling

Guide tube evaluations demonstrate that buckling does not occur. In addition, the primary and primary-plus-secondary stresses are confirmed to be lower than the material allowable stresses in the ASME BPVC.

4.2.1.5.7 Fuel Assembly Distortion

Axial alignment of the spacer grids on adjacent fuel assemblies is maintained for the life of the fuel assembly, and assembly distortion does not lead to control rod drop issues for the life of the assemblies.

4.2.1.5.8 Fuel Rod Bow

Fuel rod bowing is evaluated with respect to the mechanical and thermal-hydraulic performance of the fuel assembly (Reference 4.2-8). The fuel assembly design precludes excessive rod bow during its operational lifetime to minimize impacts on critical heat flux and linear heat generation rate.

4.2.1.5.9 Control Rod Drop Times

The fuel assembly does not experience permanent deformations during AOOs that would cause the CRA drop time to increase beyond the drop time used in Chapter 15. Precluding permanent fuel assembly deformation during AOOs is met by demonstrating the fuel assembly component stresses remain below the limits defined in Section 4.2.1.5.2.

4.2.1.5.10 Loss-of-Coolant Accident and Seismic Loading

The fuel assembly is designed to remain operable during and after an operating basis earthquake (OBE) and to maintain structural integrity, a coolable geometry, and CRA insertion capability during and after a safe shutdown earthquake (SSE) and LOCA. Fuel assembly performance following an SSE and LOCA is demonstrated by meeting the limits defined in Section 4.2.1.5.3.

4.2.1.5.11 Material Compatibility

Table 4.2-1 provides a list of fuel assembly components and their materials. The selection of fuel assembly materials is based on extensive operating experience and their compatibility with the service environment and with each other. Each material is optimized for resistance to adverse changes in material properties from irradiation, and is evaluated for strength and mechanical properties for the operating temperatures and for the full service life anticipated for each component.

Each material is based on an industry standard and is modified according to specific engineering requirements, such as lowering the cobalt content in stainless steel and nickel-based alloy components, without changing the material performance, in order to reduce activation levels.

4.2.1.5.12 Corrosion

The fuel assembly structural design evaluation considers the effects of thinning from corrosion and the effects of oxide layer formation. Guide tube material corrosion allowances are established from operating experience, design verification testing, and similarities with existing designs.

4.2.1.6 In-core Control Components and Neutron Sources

To ensure efficient performance and safe shutdown of the reactor, CRAs are designed such that insertion of the CRA is not interrupted by misalignment of the CRA guide tubes during normal operation and such that CRAs can be inserted into the fuel assembly during an SSE.

Maintaining CRA insertability with respect to the fuel assembly is discussed in Section 4.2.3.5 for both normal operating and faulted conditions.

In addition, the CRAs are designed to ensure that internal pressure is within limits during normal operation, and that cladding stresses are within limits during normal, transient, and accident conditions. The CRA rod performance analyses consider the impacts of absorber material thermal expansion and irradiation.

The neutron sources are designed to meet mechanical strength requirements at both ambient and elevated temperatures, to be compatible with the materials and reactor coolant, and to be resistant to radiation degradation. Neutron sources are discussed in Section 4.2.2.9.

4.2.1.7 Surveillance Program

Section 4.2.4 discusses the testing and fuel surveillance program that is implemented to ensure the adequacy of the fuel performance and satisfy the design bases. Fuel surveillance and testing results, as they become available, are used to improve fuel design and manufacturing processes and to confirm that the design bases and safety criteria are satisfied.

4.2.2 Description and Design Drawings

A summary of the fuel assembly and CRA design is provided in Table 4.2-2 through Table 4.2-3 and in Figure 4.2-1 through Figure 4.2-11. Additional details of the fuel assembly and CRA design are provided in Reference 4.2-1.

4.2.2.1 Fuel Assembly Description

The fuel assembly is a 17x17 array of fuel rods that is designed for use with the core configuration of the NPM. The main fuel assembly parameters are listed in Table 4.2-2 and the fuel assembly and fuel rods are illustrated in Figure 4.2-1.

The fuel assembly uses five spacer grids for lateral support of the fuel rods, and 24 guide tubes with a top and bottom nozzle provide the structural support for the 264 fuel rods. Each fuel assembly includes a central instrument tube.

Each fuel assembly can be placed in any core location within the restrictions of the cycle-specific nuclear design. The fuel handling machine is designed so the fuel assembly can only be lifted in a specific angular orientation. The refueling machine then provides the correct orientation of the fuel assembly in storage, during refueling transport, and in the reactor core operating position.

4.2.2.2 Spacer Grids Description

The fuel assembly uses four HTP™ spacer grids at the intermediate and top spacer locations and one HMP™ spacer grid at the bottom location of the assembly. A summary of the materials for the spacer grids is provided in Table 4.2-1.

Each HTP™ grid is a structure of interlocking strips welded together at each strip intersection to form a 17x17 matrix of square cells. Each cross-strip is formed by resistance spot welding two stamped halves to form a doublet. The assembled doublet contains channels, slanted at the outlets, that induce a swirling pattern in the coolant flow, as illustrated in Figure 4.2-7. The channels are arranged so there is no net hydraulic torque on the fuel assembly. These channels also provide the contact surfaces that hold the fuel rods in place. Sideplates are welded to the ends of the doublets and have top and bottom lead-in tabs to avoid assembly hang-up during fuel movement.

The HMP™ spacer grid is similar to HTP™ spacer grids, except for the material of construction that provides enhanced strength and low cell relaxation during

irradiation. Additionally, the flow channels created by the doublet are straight in the HMP™ spacer grid and do not produce swirling flow around the fuel rods.

Resilient spring features are stamped into the strips that provide frictional axial restraint of each interfacing fuel rod by an interference fit of the fuel rods within each grid cell. Spring and friction contact with each fuel rod is maintained throughout the life of the fuel assembly up to the design burnup. Each spacer grid maintains eight individual line contacts per cell with each fuel rod.

To maintain axial alignment of spacer grids with adjacent fuel assemblies, the HTP™ grids are spot-welded to the guide tubes. Short Zircaloy-4 sleeves are spot-welded to the guide tube at locations above and below the HMP™ grid to fix its axial position.

4.2.2.3 Quick Disconnect Mechanism Description

A quick disconnect (QD) mechanism attaches the top nozzle to the guide tubes (Figure 4.2-4 and Figure 4.2-5). The QD design allows the top nozzle to be removed for fuel assembly reconstitution without loose parts. The design consists of a double-spline sleeve attached to the guide tube via multiple spot-welds. Machined keyway-type features within the guide tube attachment holes in the top nozzle provide either clearance for removal or restraint for securing the nozzle, based on the radial orientation of the guide tube assembly QD features.

4.2.2.4 Top Nozzle Assembly Description

The top nozzle structure (Figure 4.2-2) consists of a frame that interfaces with the reactor upper internals and the core components while providing for coolant flow. The top nozzle flow-hole pattern provides low pressure drop while satisfying strength requirements. The top nozzle design also incorporates a QD feature to attach to the 24 fuel assembly guide tubes, as presented in Section 4.2.2.3. The top nozzle assembly includes four sets of two-leaf hold-down springs.

The spring system maintains positive fuel assembly contact with the upper core plate under normal operating conditions and AOOs and also minimizes fuel assembly liftoff during seismic events to reduce fuel assembly dynamic stresses. The leaf spring sets are fastened to the top nozzle with clamp screws. The upper leaf has an extended tang that engages a cutout in the top plate of the nozzle. This arrangement maintains spring leaf retention in the unlikely event of a single leaf spring or clamp screw failure. Component materials are listed in Table 4.2-1.

4.2.2.5 Bottom Nozzle Description

The fuel assembly uses a debris-resistant bottom nozzle that includes a filter plate (Figure 4.2-3). The nozzle is constructed with a frame of deep ribs connected to the guide tubes with shoulder screws and has legs with radii that interface with the reactor internals. The frame distributes the primary loads on the fuel assembly through the bottom nozzle. The filter plate is pinned to the top of the nozzle and is held in place by the guide tubes once secured to the bottom nozzle (Figure 4.2-6).

4.2.2.6 Guide Tube Description

Each MONOBLOC™ guide tube (Figure 4.2-4) has two inside diameters (IDs) and a single outside diameter (OD). The larger ID at the top provides annular clearance that permits rapid insertion of the CRA during a reactor trip. The reduced ID section (i.e., the dashpot located at the bottom end of the tube) provides a close fit with the control rods to facilitate deceleration toward the end of the control rod travel. This deceleration limits the magnitude of the CRA impact loads on the fuel assembly top nozzle. The guide tube wall thickness at the bottom is greater in the dashpot region than at the upper end to maintain the same OD with the smaller dashpot ID. The MONOBLOC™ design provides a robust structure to minimize fuel assembly distortion and bow.

Four holes in the guide tube located just above the dashpot allow both outflow of water during CRA insertion, and coolant flow to the control components during operation. There is also a flow hole in the guide tube cap screw that enables coolant flow through the reduced diameter section and drainage of the guide tube, as well as displaced coolant venting during CRA deceleration.

The guide tubes are connected to the top and bottom nozzles as described in Section 4.2.2.3 and Section 4.2.2.5.

4.2.2.7 Fuel Rod Description

The fuel rod design consists of uranium dioxide (UO_2) pellets contained in seamless M5® zirconium alloy tubing, with end caps welded at each end (Figure 4.2-8). The use of M5® cladding is approved in Reference 4.2-5. The fuel rod length and void volume provide acceptable margin against failure by internal pressure buildup. The fuel rod uses one spring in the upper plenum to prevent the formation of fuel pellet stack gaps during shipping and handling, while also allowing for the expansion of the fuel stack during operation. The fuel stack rests on the lower end cap.

The lower end cap has a bullet-nose shape to provide a smooth flow transition in addition to facilitating insertion of the rods into the spacer grids during assembly. The upper end cap has a grippable feature that allows removal of the fuel rods from the fuel assembly if necessary.

The cylindrical fuel pellets are a sintered, high-density ceramic with a dish at each end. The edges of the pellets have chamfers that ease the loading of the pellets into the rod, and the dish and chamfer help reduce the tendency for the pellets to assume an hourglass shape during operation.

The fuel rod design can also utilize axial blanket and gadolinia fuel configurations. The geometry and design of axial blanket and gadolinia fuel rods is identical to the UO_2 fuel rod design. The only difference between standard fuel rods and those with axial blankets or gadolinia is in the composition of the fuel stack. The use of gadolinia or axial blankets in the core design is discussed in Section 4.3.

Table 4.2-2 provides a summary of the major fuel rod design parameters.

4.2.2.8 Control Rod Assembly Description

Each CRA consists of a group of 24 individual control rods fastened to a spider assembly (Figure 4.2-9). The individual rods (Figure 4.2-11) contain B_4C pellets in the upper portion of the rod and silver-indium-cadmium (AIC) absorber in the tip of the rod. The hybrid configuration of AIC and B_4C is commonly used in commercial PWRs, and is adapted to the NuScale design to reduce the total weight of the CRA. Unlike the AIC material, the B_4C can produce helium gas under neutron fluence leading to the potential buildup of gas pressure in the rod. Thus, the use of B_4C is restricted to the low flux region at the top of the rod where helium production is minimal, and the AIC material is used in the high flux region. The lower portion of the control rod contains a stack support that resides within a central hole in the AIC. The stack support is comprised of a support column that passes through the AIC central hole and a support platform, upon which the solid portion of the AIC rests (Figure 4.2-11). The stack support prevents the weight of the B_4C column and the plenum spring preload from compressing the lower AIC, which is susceptible to deformation through creep mechanisms at elevated temperatures. By eliminating the axial load acting on the AIC, the stack support reduces the creep mechanism of the lower absorber and thereby reduces cladding strain. The rod internals are sealed within a cladding tube to protect the absorber from the coolant. The tube is plugged and welded at each end.

The top ends of the control rods are fastened to a spider using a threaded and pinned joint. The upper end plug is designed with a flex joint that is able to accommodate misalignment between the control rods and the fuel assembly.

The CRA spider (Figure 4.2-9) is a one-piece, stainless steel cast array of vanes on a hub. A spring is located in the lower part of the hub to absorb the kinetic energy of the CRA and driveline following a reactor trip. The spring is preloaded and maintained within the hub by a retaining ring and tension bolt. During a refueling outage or after a reactor trip, the spring retainer rests on the fuel assembly top nozzle. The CRA is coupled to the control rod driveline through the coupling section within a cavity in the top of the hub.

Table 4.2-3 provides the nominal design parameters for the CRA, spider, and individual control rods.

4.2.2.9 Neutron Source Assemblies

The design includes primary and secondary sources. The purpose is to provide a minimum detectable neutron flux level at the source range detectors for the initial core and to allow monitoring the change in core multiplication factor during fuel loading and approach to criticality. Neutron source assemblies may be used in subsequent cycles to support the core design and fuel loading.

The primary source material is californium (Cf-252) and the secondary source material is comprised of antimony and beryllium. The source material is contained

in individual stainless steel rods that are connected to a spider hub similar to the CRA. The rods containing the source material are hermetically sealed. The neutron source assemblies are located in diametrically-opposed core positions near the core periphery as close as possible to the ex-core detectors. The neutron source assemblies are statically installed in fuel assembly locations not occupied by a CRA.

4.2.3 Design Evaluation

To demonstrate adherence to the mechanical design bases, analyses are performed to consider rod operating history, model uncertainties, and dimensional variations with interfacing nuclear and thermal-hydraulic design bases in Section 4.3 and Section 4.4. The evaluation considers the effects of normal operation power maneuvering. The performance of the fuel during AOOs and postulated accidents is presented in Chapter 15. Anticipated transients without scram are addressed in Chapter 15.

4.2.3.1 Cladding Evaluation

4.2.3.1.1 Vibration and Wear

Because of the low fuel assembly axial flow and low cross-flow between assemblies, there is little flow energy available to cause vibration in the fuel rods. The grids provide sufficient fuel rod support to prevent significant wear of the clad during the life of the fuel assembly based on operating experience, design analyses, and testing as shown in Reference 4.2-1.

A life and wear test was performed on the fuel assembly design. The life and wear results, as well as the PWR operating experience of HMP™ and HTP™ grids with M5® clad fuel rods, show the fuel design has significant margin to fretting failure for the expected operating conditions (Reference 4.2-1). Section 4.2.3.5.7 has additional discussion on the fretting evaluation.

Based on these evaluations as summarized in Reference 4.2-1, the fuel is not expected to experience flow-induced vibration or wear issues.

4.2.3.1.2 Fuel Rod Internal Pressure and Cladding Stresses

The fuel rod cladding is analyzed for stresses induced during operation using the approved methodology in Reference 4.2-5. Conservative values are used for cladding thickness, cladding ovality, oxide layer buildup, external pressure, internal fuel rod pressure, differential temperature, and unirradiated cladding yield strength in accordance with the approved methodology. The analyses of the fuel rod cladding stresses demonstrate positive margins for all operating conditions. The cladding stress safety margins are presented in Reference 4.2-1.

Analysis shows fuel rod cladding buckling does not occur. The maximum differential pressure is less than the buckling pressure and the maximum

compressive load on the fuel rod is less than the buckling critical load, thereby proving the cladding does not buckle.

Analysis in Reference 4.2-1 also shows the maximum internal pressure of the fuel rod over its designated lifetime does not exceed the reactor coolant system pressure. A burnup-dependent fission gas release model in Reference 4.2-5 is used in determining the internal gas pressure as a function of irradiation time. Demonstrating the fuel rod internal pressure is less than system pressure assures there is no cladding liftoff or reorientation of hydrides in the radial direction of the cladding.

4.2.3.1.3 Material and Chemical Evaluation

Using the methodology in Reference 4.2-6, the maximum oxide thickness is predicted to be less than the limit established in Reference 4.2-5. Bounding power histories are used in predicting the oxide thickness. The maximum predicted oxide thickness is provided in Reference 4.2-1.

The absorption of hydrogen on the inside of the cladding is minimized by tight controls on the moisture and hydrogen impurities in the rod during fabrication. The specific moisture and hydrogen content limits are provided in Reference 4.2-1.

4.2.3.1.4 Fretting and Crevice Corrosion

As described in Section 4.2.3.1.1, fretting due to flow-induced vibration is not expected due to low axial flow rates during normal operation natural circulation conditions.

Prior PWR operating experience shows crevice corrosion is not a likely corrosion mechanism for zirconium alloy cladding material. In general, zirconium alloys are resistant to crevice corrosion. In addition, coolant chemistry specifications impose tight controls for dissolved oxygen and chlorides, the contaminants often associated with crevice attack. Section 5.2 contains limits on oxygen and chlorides.

4.2.3.1.5 Stress-Accelerated Corrosion

Stress corrosion cracking is addressed for M5® in Reference 4.2-5. M5® cladding improves resistance to stress-accelerated corrosion relative to Zr-4 cladding.

4.2.3.1.6 Cycling and Fatigue

The fuel rod cladding is analyzed for the cumulative fatigue usage factor using the methodology approved in Reference 4.2-5 and the procedure outlined in the ASME BPVC. Testing determined the fatigue performance of M5® cladding. These tests have shown similar fatigue endurance performance for recrystallized cladding (including M5®) as compared to Zircaloy-4, with the

lower yield strength of the recrystallized claddings limiting the applied stresses. A fuel rod life of 10 years and a 60-year design life for the NPM are assumed. The fuel rod cladding therefore experiences approximately one-sixth of the number of transient cycles the reactor pressure vessel will experience.

The expected normal operating, upset, and test transients are evaluated to determine the cumulative fatigue usage factor experienced by the fuel rod cladding. In accordance with the ASME BPVC, faulted conditions are not included in the fatigue evaluation. Conservative inputs in terms of cladding thickness, oxide layer buildup, external pressure, fuel rod internal pressure, and differential temperature across the cladding were assumed. The results of the fatigue analysis (Reference 4.2-1) for the fuel rod show the cumulative fatigue usage factor is below the allowable limit listed in Section 4.2.1.1.3.

4.2.3.1.7 Rod Bowing Attributable to Thermal, Irradiation, and Creep Dimensional Changes

Penalties associated with rod bowing are addressed in accordance with Reference 4.2-8. Application of the rod bow penalties in the thermal and hydraulic analysis is discussed further in Section 4.4.

4.2.3.1.8 Consequences of Power-Coolant Mismatch

The consequences of power-coolant mismatch are addressed in Section 4.4.

4.2.3.1.9 Irradiation Stability of the Cladding

Considerable operating experience using M5® cladding has proven its irradiation stability. The effects of irradiation on the mechanical integrity of the cladding is accounted for using the approved COPERNIC model (Reference 4.2-6) for performing the mechanical and thermal analyses and the effects are shown to be acceptable for the approved burnup limit of 62 GWd/MTU established in Reference 4.2-5.

4.2.3.1.10 Creep Collapse and Creepdown

Creep collapse is analyzed with the methods and codes described in Reference 4.2-9 as extended to M5® cladding applications in Reference 4.2-5. Reference 4.2-1 includes an analysis of creep to evaluate the resistance of the fuel rod cladding to creep collapse. Inputs to the analysis include differential pressure, temperature gradients, and fast neutron flux. Reference 4.2-1 confirms that fuel rod creep collapse does not occur for the incore life of the fuel.

4.2.3.1.11 Cladding Strain

The cladding strain evaluation is discussed in Reference 4.2-1. The calculated linear heat rate for transients that induce cladding strain at the limit listed in

Section 4.2.1.1.2 does not limit plant operation and is much greater than the maximum transient the fuel rod is expected to experience.

4.2.3.1.12 Pellet-Cladding Interaction

Pellet-cladding mechanical interaction is assessed using surrogate criteria of transient-induced cladding strain and fuel centerline melting. The criterion for transient-induced cladding strain is discussed in Section 4.2.3.1.11 and is greater than the maximum transient peak linear heat rate the fuel rod is expected to experience. This method has been previously approved in Reference 4.2-6.

As discussed in Section 4.2.3.2.3, fuel melting does not occur during normal operation or AOOs. Fuel melting results in a large volume increase that may cause a pellet with a molten center to exert a stress on the cladding. The no centerline melting criteria precludes cladding failure and is used to show an acceptable fuel rod design.

4.2.3.2 Fuel Material Evaluation

4.2.3.2.1 Dimensional Stability

Fuel pellet dimensional stability is provided by a quality inspection program that is used for fuel pellets. Pellets are tested for resinter behavior according to criteria stipulated in the pellet manufacturing specifications. Pellets are also inspected for abnormalities such as discoloration, inclusions, pits, unground areas, cracks, and chips. All of the pellets are measured for diameter. To maintain the integrity of the fuel, the other dimensional attributes are measured based on a statistical sampling over the course of pellet grinding and inspection.

4.2.3.2.2 Potential for Chemical Interaction

Standard manufacturing testing is performed to verify fuel pellet stoichiometry (oxygen-to-uranium ratio), uranium content, and isotopic content (^{234}U, ^{235}U, ^{236}U, and ^{238}U). For fuel rods with gadolinia, the gadolinia content and stoichiometry are also measured. Microstructural examinations for grain size and internal porosity provide verification of pellet properties for limiting fission gas release.

Pellet hydrogen and fluorine content are tightly controlled to minimize the potential for hydride blister formation on the cladding inner surfaces. Introduction of unacceptable levels of hydrogen from contamination sources is further prevented by implementing visual inspections of pellets immediately following grinding and immediately before loading into the fuel rods. Testing for nitrogen, carbon, and oxygen verify sorbed gas limits within the pellets. Testing for elemental impurities and calculation of the equivalent boron content is also performed to prevent unwanted neutron absorption by tramp elements.

4.2.3.2.3 Thermal Stability

Fuel melting does not occur during normal operation or AOOs. The COPERNIC fuel performance computer code (Reference 4.2-6) is used for the centerline fuel melt analysis. COPERNIC determines the local linear heat rate throughout the fuel rod lifetime that results in centerline temperature exceeding a specified temperature limit. Staying below this local linear heat rate limit provides a high degree of assurance that fuel melting does not occur.

The local linear heat rate throughout the rod lifetime determined in the centerline fuel melt analysis is used as input to determine the limiting conditions for operation and module protection setpoints. During normal operation and AOOs, the fuel does not melt because the linear heat rate does not exceed the limit.

4.2.3.2.4 Irradiation Stability

The irradiation stability of the fuel rod is confirmed by performing analyses using the COPERNIC code (Reference 4.2-6) that analyzes the fuel throughout the life of the fuel rod.

4.2.3.3 Fuel Rod Performance Evaluation

4.2.3.3.1 Fuel Rod Performance Predictions

COPERNIC (Reference 4.2-6) is the computer code used to perform thermal and mechanical analyses to accurately simulate the behavior of a fuel rod during irradiation, and to verify the fuel rod design meets design and safety criteria. COPERNIC calculates fuel and cladding temperatures, stresses and strains, cladding thickness, and internal pressure.

4.2.3.3.2 Failure and Burnup Experience

Fuel using M5® cladding material was first inserted in a domestic reactor core in 1995 and has been used in 22 reactors and more than 7500 fuel assemblies as described in Reference 4.2-1.

4.2.3.3.3 Fuel and Cladding Temperatures

Fuel and cladding temperature analyses are described in Section 4.4.

4.2.3.3.4 Potential Effect of Temperature Transients

The fuel rod experiences many operational transients during its residence in the core. A number of thermal effects must be considered when analyzing the fuel rod performance.

The clad can be in contact with the fuel pellet at some time in the fuel lifetime. Clad-pellet interaction occurs if the fuel pellet temperature is increased after

the clad is in contact with the pellet. Clad-pellet interaction is discussed in Section 4.2.3.1.12.

Section 4.4 discusses the impact of temperature effects during anticipated operational transients including the effect from fuel rod bow, as well as other fuel rod thermal design bases.

4.2.3.4 Spacer Grids Evaluation

Structural evaluations are performed to ensure the grids maintain their configuration under postulated accidents. These analyses determined the resulting impact loads are lower than those allowed to maintain a coolable configuration and assure control rod insertion. The methodology used to perform these evaluations uses load limits derived by testing, which are provided in Reference 4.2-7.

The maximum impact load on the spacer grids due to a combined SSE and LOCA is provided in Reference 4.2-1. The OBE severity for the design is less than or equal to one-third of the severity of the SSE. 10 CFR 50 Appendix S specifies that an OBE earthquake does not need to be evaluated if its severity is less than or equal to one-third of the SSE severity; therefore, a separate OBE evaluation of the fuel assembly is not performed. Additional discussion of spacer grid performance during combined SSE and LOCA loadings is provided in Section 4.2.3.5.2.

4.2.3.4.1 Spacer Grid Dimensional Stability

The chemical, thermal, and irradiation behavior of the spacer grids is determined to be acceptable by operating experience in PWRs operating in the United States.

4.2.3.4.2 Spring Loads for Grids

The forces required to slip the HTP™ and HMP™ grids relative to the fuel rods were measured at beginning of life (BOL) conditions. This data, which represent the friction force between the grids and fuel rods, is used as input in the analytical models of the fuel assembly.

4.2.3.5 Fuel Assembly Design Evaluation

The fuel assembly design evaluation, including the fuel rods, is detailed in Reference 4.2-1 in relation to the criteria for fuel system damage mechanisms, fuel rod failure mechanisms, fuel coolability, and CRA insertion. A summary is provided in the following sections. A similar summary of the evaluations for the fuel rod design is presented in Section 4.2.3.1.

Methodologies for the fuel assembly structural and mechanical analyses adhere to the codes and methods used by Framatome as listed in Reference 4.2-4.

The results of the analyses in Reference 4.2-1 are applicable to fuel assembly operation in the NPM.

4.2.3.5.1 Fuel Assembly Structural Design Evaluation

The design criterion for the structural evaluation of the fuel assembly is that stress intensities are less than the stress limits based on Section III of the ASME BPVC. The structural design requirements for the fuel assembly are common to current Framatome PWR fuel designs and incorporate Framatome's design and incore operating experience with similar PWR fuel designs.

Evaluation results show the calculated stress intensities are less than the applicable stress limits. Fatigue usage is evaluated and found to be acceptable. ASME Code Service Level A criteria are used for normal operating conditions and Service Level D criteria are used for the LOCA and seismic (i.e., faulted) analyses. An exception to this classification is the use of Service Level C criteria for guide tubes when CRA insertability is required for the faulted analyses.

The fuel assembly component evaluations show the calculated stresses are lower than the material allowable stresses for both normal operation and faulted conditions for evaluated components. The evaluation of components for LOCA conditions conservatively considered the square root of the sum of the squares combination of the LOCA and SSE loads.

The fuel assembly components evaluated include:

Guide tubes- The guide tubes do not buckle and remain elastic, thereby ensuring the CRAs can be inserted during normal operation. Guide tube loads are evaluated for each fuel assembly span using a bounding outlet temperature. Buckling analysis considers maximum guide tube eccentricity with the fuel assembly weight, hold-down spring force, and CRA drop loads applied simultaneously. Axial conditions that result in tensile loads are also considered and include secondary loads from spacer grid slip. A positive guide tube buckling safety margin is determined for axial loading for normal operating conditions. Guide tube boiling is not predicted to occur during normal operation. Guide tube stresses are also evaluated for faulted conditions and shown to maintain CRA insertion capability by meeting the applicable criteria.

Spacer grids- The spacer grids do not deform beyond the approved limits in Reference 4.2-7 during normal operation and faulted conditions. The mechanical design bases of the spacer grids are confirmed through a series of tests on prototype 17x17 HTP™ grids as discussed in Section 4.2.4.

Top and bottom nozzles- The evaluation for normal operating conditions is performed in accordance with the ASME BPVC using a design limit of two-thirds of the collapse load limit obtained by testing.

The limit based on the maximum test load is further reduced for operating temperature conditions. Only axial loading is considered because the normal operating loads on the bottom nozzle are applied axially by the guide tubes. The maximum normal operating load used in the evaluation accounts for impact loads from a CRA drop, hold-down spring loads, and the fuel assembly mass.

The evaluation of the bottom nozzle for faulted operating conditions considers the maximum normal operating loads used in the normal operation evaluation, the assembly weight, LOCA loads, and SSE axial loads. Margin to the design limit is demonstrated in Reference 4.2-1.

The top nozzle structure is evaluated for normal operating, shipping and handling, and faulted operating loads. The limiting case is evaluated for an axial CRA drop load applied to the top nozzle structural framework. Reference 4.2-1 shows that positive margin to the design limit is maintained.

Hold-down spring- Stress analysis of the fuel assembly hold-down spring examines stresses, strains, and fatigue usage to confirm that it does not fail. The evaluation confirms that the ASME BPVC criteria are satisfied.

Structural connections- The guide tube-to-spacer grid weld connections are evaluated for the limiting applied normal operating condition loads that are caused by the grid slip loads. The applicable load limit is established in accordance with the ASME BPVC. The connections between the guide tubes, guide tube upper sleeves, and QD sleeve retainers are evaluated with ASME BPVC criteria but with applied normal operating condition loads of hold-down springs, assembly weight and CRA drop, and conservatively neglecting flow lift loading. The strength of the welded connections between the guide tubes and the guide tube lower end plugs are qualified by the manufacturing specification that bounds the predicted loads from the guide tube analysis. Stress analysis of the guide tube cap screws, threads of the guide tube lower end plugs, and seating interfaces of the guide tube upper sleeve and guide tube lower end plugs demonstrate these designs to be acceptable with positive design margins.

Fuel rod cladding- The structural evaluation of the fuel rod cladding for normal operation is discussed in Section 4.2.3.1.

4.2.3.5.2 Analysis of Combined Loss-of-Coolant Accident and Seismic Loading

The structural integrity of the fuel assembly withstands seismic, LOCA, and combined seismic with LOCA events under both unirradiated (BOL) and irradiated conditions using the methodology described in Reference 4.2-7. The fuel assembly meets the criteria to maintain structural integrity, CRA insertion, and a coolable geometry during and after an SSE and a LOCA. The horizontal and vertical loads on the components are first determined with analytical models and then combined in the evaluation of each component.

The fuel assembly response to seismic and LOCA excitations is determined using the methodology described in Reference 4.2-7 and Reference 4.2-3. The fuel assembly models used for seismic and LOCA analysis are benchmarked using properties established through full-scale prototype testing. Lateral fuel assembly models are combined to represent row configurations of fuel assemblies in the core. Row models with three, five, and seven assemblies are created, matching the core configuration. Seismic SSE and LOCA displacement time histories at the lower core plate and upper core plate are applied to the reactor core model, and the resulting fuel assembly impact loads and deflections are evaluated.

The fuel assembly is evaluated for the vertical SSE and LOCA conditions with a single assembly model described in Reference 4.2-7. Fuel assembly axial stiffness properties and drop impact characteristics are obtained from testing and used to benchmark the fuel assembly axial model. The evaluation uses vertical core plate displacement time histories determined by the seismic model (Appendix 3A).

The maximum grid impact forces obtained for SSE and SSE plus LOCA conditions for a full-core configuration of fuel assemblies are less than the allowable limits established by testing, as discussed in Section 4.2.3.4. Other fuel assembly components are evaluated for combined loads and stresses under vertical and lateral SSE plus LOCA conditions. The loads and stresses resulting from lateral SSE and LOCA excitations are the result of fuel assembly deflections under those excitations. The component stresses are shown to be less than the allowable limits based on Section III of ASME BPVC criteria. The core coolable geometry and CRA insertability are maintained for the faulted loads and the component stress intensities are less than the allowable limits.

4.2.3.5.3 Load Applied in Fuel Handling

Both the fuel assembly and individual components are evaluated for structural adequacy for shipping and handling loads in the amount of 6 g in the lateral direction and 4 g in the axial direction. The evaluations result in positive design margins to the stress limits.

4.2.3.5.4 Axial Growth

A fuel assembly top nozzle-to-fuel rod shoulder gap allowance is provided that maintains positive clearance during the assembly lifetime. The evaluation determined that a positive fuel rod shoulder gap occurs at end of life (EOL) hot conditions and considers the upper tolerance limit for fuel rod growth, minimum guide tube growth, and worst-case tolerances on the length of fuel rods and guide tubes. The evaluated minimum fuel rod shoulder gap is presented in Reference 4.2-1 and is acceptable.

A fuel assembly-to-reactor internals gap allowance is provided that maintains a positive core plate gap clearance throughout the life of the fuel assembly. The core plate gap allowance considers combined worst-case internals and

fuel assembly differential thermal expansion and irradiation-induced axial length changes of the fuel assembly. The evaluation shows a positive fuel core plate gap occurs at EOL cold conditions and considers the upper tolerance limit guide tube growth and worst-case tolerances on the length of the fuel rod and core plate separation. The minimum core plate gap is presented in Reference 4.2-1 and is shown to be acceptable.

In order to ensure axial alignment of the spacer grids with adjacent fuel assemblies, the spacer grids are affixed to the guide tubes as discussed in Section 4.2.2.2. The height of the grids is greater than the worst-case differences in grid elevation at BOL and EOL. Therefore, grid overlap between adjacent assemblies is maintained.

4.2.3.5.5 Assembly Liftoff

The fuel assembly liftoff evaluation is performed by comparing the fuel assembly weight and the fuel assembly spring hold-down load with the hydraulic forces under normal operating conditions and AOOs. Hydraulic forces are calculated using pressure loss coefficients from testing a prototypical, full scale fuel assembly. Results of the analysis show margin to liftoff for all AOOs.

4.2.3.5.6 Fuel Rod Bow

Fuel rod bowing is evaluated with respect to the thermal-hydraulic performance of the fuel assembly (Section 4.4). The fuel rod bow performance is expected to be similar to other Framatome designs and the analysis methodology discussed in Reference 4.2-8 is applicable.

4.2.3.5.7 Fuel Rod Fretting

The primary design criterion with regard to fuel rod fretting is that the design must limit fretting to preclude fuel rod failure. Fuel rod fretting and wear performance is based on the 1000 hour life and wear testing performed on a prototypical, full-scale test fuel assembly with spacer grids modified to simulate EOL conditions. Evaluation of domestic operating experience with PWR fuel assemblies incorporating M5® fuel rods, and HTP™ and HMP™ grids used on the fuel design is also considered.

The fretting operating experience for Framatome 17x17 fuel assemblies can be extended to the NuScale fuel design due to the design similarities and the lower reactor coolant system flow velocity of the NPM (the lower flow velocity results in much lower cross flow velocities compared with typical PWRs). The NuScale HTP™ and HMP™ spacer grid designs are identical to those used in Framatome 17x17 fuel assemblies, along with M5® fuel cladding.

The fuel design does not introduce additional features or characteristics other than the change to the overall length to the evaluation, which is not considered

a significant variable in fuel rod fretting. Span lengths are no greater than those used on existing PWR fuel designs.

No significant fretting marks were found on the life and wear test assembly. The life and wear testing was performed in a full-scale test channel under flow conditions that bound the operating conditions.

The life and wear test results and PWR operating experience of HTP™ grids with M5® clad fuel rods show margin against fretting failure for the expected operating conditions.

4.2.3.5.8 Corrosion

The corrosion resistance of the alloys used in the fuel assembly is demonstrated by operating experience for M5® cladding as discussed in Reference 4.2-5. This corrosion resistance is the result of both material selection and manufacturing techniques. Material standards provide high-quality base material, while controlled manufacturing processes produce components with minimum surface contamination.

Manufacturing, handling, and assembly procedures prevent contaminants from coming into contact with the metals during fabrication, welding, or annealing operations.

The low-carbon stainless steels are selected to provide resistance to corrosion. The activity levels caused by neutron activation of non-fuel components in the NPM is minimized by reducing the level of cobalt in the materials used in the fuel assemblies. Table 4.2-1 contains fuel assembly materials.

Section 5.2.3 provides information on those aspects of the reactor coolant chemistry that provide corrosion protection for stainless steels and nickel alloys.

The selection of corrosion resistant materials proven through in-reactor operation, stringent manufacturing processes, water chemistry controls, and post-irradiation inspections provide assurance that corrosion is not an issue for the fuel.

4.2.3.6 Control Rod Assembly and Burnable Poison Evaluation

As described in Reference 4.2-1, the following items are evaluated for the CRAs and shown to be acceptable for their 20 effective full power year lifetime:

- internal pressure is within limits during normal operation
- cladding stresses are within limits during normal, transient, and accident conditions
- thermal stability of the absorber material

- irradiation stability of the absorber material, taking into consideration gas release and solid and gaseous product swelling

Wear rates on the CRA rods are expected to be low in comparison to those of typical operating PWR plants with stainless steel cladding given the lower core flow rates in the design. In addition, the absence of vessel outlet flow nozzles is expected to decrease cross-flows that contribute to control rod wear in typical PWRs. In a typical PWR the flow exits the core and then turns to flow out the nozzles. In the NPM, the much lower velocity flow continues directly upward into the riser and then into the steam generators. Prototype testing using a full-scale CRA is performed to assess CRA susceptibility to wear. After initial irradiation and operation of the CRA design, inspections are performed so actual rod wear rates can be compared with the predetermined wear limits to demonstrate acceptable performance.

The CRA structure is analyzed for loads due to operational stepping, reactor trip, stuck rod, fatigue, and shipping and handling. Stresses in the components of the CRA are within limits. The CRA spring is analyzed to show it can accept the energy from a reactor trip without the spring compressing completely and without the spider hub contacting the top nozzle. These analyses are described in Reference 4.2-1.

In-reactor surveillance of CRA insertion times is performed in accordance with the technical specifications to demonstrate satisfactory performance.

As discussed previously, the burnable poison is integral with the fuel pellet in selected rods as described in Section 4.2.2.7.

4.2.4 Testing and Inspection Plan

The fuel design is similar to existing 17x17 designs that are used successfully in PWRs in the industry. The only significant design difference is the fuel assembly length. The following sections address operating experience, prototype testing, manufacturing testing and inspection, on-site receipt inspection, on-line fuel monitoring, and post-irradiation monitoring that provide confidence the fuel meets design requirements.

4.2.4.1 Operating Experience

All of the components in the fuel assembly design have relevant experience in operating plants, and both components and methods have been accepted by the NRC for commercial operation. Framatome has extensive PWR operating experience with the components and features of the fuel assembly, including the MONOBLOC™ guide tubes, HTP™ and HMP™ spacer grids, the QD top nozzle assembly, and the mesh filter bottom nozzle. The M5® fuel cladding also has extensive operating experience including Framatome's current 17x17 PWR fuel designs.

The HTP™ spacer is a proven spacer design for PWR fuel that has extensive operational experience in a number of different fuel assembly design variations that include 17x17 fuel.

The HMP™ spacer grids with straight flow channels also have an extensive operating experience base.

The M5® cladding is an advanced zirconium alloy developed and implemented by Framatome to improve corrosion resistance, reduce hydrogen uptake, and reduce irradiation growth. In 1999, the NRC approved M5® for domestic use. Since then, extensive operational experience has been gained using M5® material.

As documented in Reference 4.2-2 and Reference 4.2-4, the above experience applies to the fuel assembly design.

4.2.4.2 Prototype Testing

A prototype testing program was undertaken to determine the performance characteristics of the fuel assemblies, CRAs, and fuel assembly components such as grids, upper nozzle, and lower nozzle.

4.2.4.2.1 Assembly Testing

Testing was conducted on full-sized prototype fuel assemblies and on various assembly components. The full-size fuel assemblies were used for structural and thermal-hydraulic testing. The fuel assembly structural tests included lateral deflection tests and axial deflection tests, baffle impact tests, fuel assembly free- and forced-vibration tests, and vertical drop tests. These tests were conducted on prototypical test assemblies with grids having either BOL or EOL characteristics with the rods seated on the bottom nozzle assembly.

The fuel assembly thermal-hydraulic test scope included assembly pressure drop tests and life and wear testing for 1000 hours.

These tests, summarized in Reference 4.2-1, were conducted in accordance with approved test plans at Framatome test facilities. The test results were used in benchmarking analytical models for the fuel assembly design evaluation addressed in Section 4.2.3.5.

Static stiffness testing - Forces versus deflection tests were conducted to determine the axial and lateral stiffness of the prototype fuel assembly. In an axial stiffness test, the fuel assembly was compressed along its longitudinal axis by an application of forces at the nozzles. The lateral stiffness test consisted of loading the fuel assembly laterally near the center of the assembly at the middle spacer grid. The results of this testing are used in the fuel seismic model.

Free- and forced-vibration, and baffle impact testing - The vibration tests determine the fuel assembly lateral, dynamic response. The use of free- and

forced-vibration tests together cover higher and lower modes of the assembly natural frequency. The baffle impact test determines the assembly response to impacts with the baffle plate (or reflector). This information is used in the fuel assembly seismic model.

Fuel assembly drop testing - This test is performed to characterize the dynamic, axial structural response of the fuel assembly. The test fuel assembly is suspended a specified distance above a plate attached to a load cell. The assembly is released and allowed to fall onto the plate and load cell. The displacement of the fuel assembly bottom nozzle is measured throughout the test. This information is used in the fuel assembly seismic model.

Fuel hydraulic flow testing - Flow testing on a full-scale prototype fuel assembly was performed to establish flow component loss coefficients and other related flow characterization parameters for the fuel assembly. The form loss coefficients are used in the fuel assembly liftoff and subchannel (Section 4.4) analyses.

Fuel fretting testing - The prototype fuel assembly with EOL spacer grids was used to evaluate the fretting and wear performance at the grid-to-rod interfaces. The test was conducted for more than 1000 hours under flow conditions that bound those of the NPM. At the conclusion of the test, several test rods were inspected and showed minimal wear.

4.2.4.2.2 Fuel Assembly Component Testing

In addition to full-scale prototype testing, various components were also characterized by testing. The spacer grid design was subjected to static buckling and dynamic crush tests. The strength of the top and bottom nozzles were also tested. These test results are incorporated into the analytical models used to verify the fuel design.

4.2.4.2.2.1 Spacer Grid Testing

The mechanical design bases for the spacer grids were confirmed through a series of structural tests on prototype grids. The testing, summarized below, found that the grids provide the necessary design margins.

Dynamic impact - Dynamic crush tests were performed on HTP™ spacer grids at unirradiated conditions and irradiated simulated conditions. The tests determined the through-grid stiffness and damping values for the lateral seismic models and the crushing load limits for the grids.

Static load - The static crush characteristics (static stiffness and elastic load limit) are used to establish allowable grid clamping loads applied during shipping.

Slip load - The forces required to slip the grid relative to the fuel rods were measured at BOL conditions for both the HTP™ and HMP™ grids. The slip load values are used in the fuel assembly evaluation.

4.2.4.2.2.2 Strength Test of Top and Bottom Nozzles

Bottom nozzle - Strength testing of the bottom nozzle was performed to establish the axial load limit for evaluation. A prototype bottom nozzle was tested at room temperature in static axial compression by applying a load to 24 springs on the guide tube positions. The spring stiffness was set to be equal to the guide tube stiffness in order to simulate the load distribution of the guide tubes.

A room temperature test at maximum load was applied without collapse of the structure. This test is used to demonstrate the structural adequacy in the design evaluation by comparison with the normal operating and faulted loads, as discussed in Section 4.2.3.5.1 and Section 4.2.3.5.2.

Top nozzle - Strength testing of the top nozzle was performed to establish the axial load limit for evaluation. A prototype top nozzle was tested at room temperature in static axial compression by applying a load to the upper surface of the top nozzle that was set on 24 springs at the guide tube positions. The spring stiffness was set to be equal to the guide tube stiffness in order to simulate the real load distribution of the guide tubes.

A room temperature test was performed in which a load was applied that exceeded the design load and resulted in no plastic deformation of the structure. This tested maximum load is used to demonstrate the structural adequacy in the design evaluation by comparison with the shipping and handling, normal operating, and faulted loads, as discussed in Section 4.2.3.5.

4.2.4.2.3 Control Rod Testing

The CRA is similar to existing 17X17 CRAs except for the shorter length. The CRA drive shaft is longer than typically used in the industry. Prototype testing is performed to confirm CRA drop times and to assess the impact of the maximum expected misalignment of the fuel assembly guide tubes predicted to occur during a joint LOCA and seismic event.

The CRA drop times are calculated using a fluid dynamic computer model that predicts insertion time and impact velocity. When CRAs are dropped into a fuel assembly, the water in the guide tube is displaced through several flow paths. The fuel assembly design has 24 guide tubes, each containing two pairs of side flow holes. In addition, water is forced out through the top annulus of the guide tube and through the hole in the cap screw at the bottom of the guide tube assembly. The computer analysis for the CRA drop time is primarily best estimate but does include some conservatism. The drop time is provided in Figure 4.3-20. The control rod drop time used in Chapter 15 analysis is a more conservative bounding value. The results from the CRA drop testing, described in Section 1.5.1, validate the use of the calculated reactor trip curve shown in Figure 4.3-20 as a conservative basis for the CRA drop time.

For the impact velocity, the rod drop calculation is also primarily best estimate but does include conservatism that predicts a higher impact velocity. Testing provides confirmation that these values are conservative for their respective application. This testing is described in more detail in Section 1.5.

The ability of the CRA to insert under conditions of fuel assembly misalignment is assessed in a test that deflects the fuel assembly at the mid-height location. The CRA insertion time is measured and compared to the CRA insertion time testing performed with no deflection of the fuel assembly. The testing is performed to confirm that the CRA insertion is not significantly affected by the maximum expected misalignment.

4.2.4.3 Manufacturing Testing and Inspection

Fuel assemblies and CRAs are manufactured and inspected in accordance with a 10 CFR 50, Appendix B Quality Assurance Program as described in Chapter 17.

Manufacturing operations require adherence to cleanliness controls for components and assemblies. The cleanliness program includes controls for expendable and consumable materials that come in contact with core components.

Fuel pellets are extensively tested and inspected, including:

- dimensional inspections
- visual examinations to check for surface contamination and surface defects, including the presence of missing pellet surface
- destructive examinations for microstructure (grain pore size distribution)
- resinter densification
- chemical composition
- impurity checks, including hydrogen determination and isotopic content

Fuel rod cladding tubes are inspected for external and internal defects by approved non-destructive methods. Ultrasonic methods are used for dimensional measurements. Fuel rods have the end cap welds tested by both destructive and non-destructive means, are leak tested using helium detection equipment, and are gamma-scanned to verify the integrity and position of the internal components and the absence of unacceptable pellet gaps. Automated computer equipment maintains traceability of fuel components. Fuel pellets, fuel rod end caps, and springs are traced on a lot basis. Fuel cladding and fuel rod assemblies are traced by serial number.

Fuel assemblies undergo inspections for bow, twist, dimensional envelope, and fuel rod spacing. Visual examinations are performed as a final check on cleanliness control.

Verification of CRA and component attributes is similar to those of the fuel assemblies and is the same as for Framatome's typical domestic PWR control

components. The absorber composition is verified by an approved supplier through chemical examination. Control rod cladding tubes are inspected for external and internal defects using approved non-destructive methods. The CRAs have the end cap welds tested by both destructive and non-destructive means and are leak tested using helium detection equipment.

4.2.4.4 On-site Receipt Inspection

When fresh fuel and CRAs are received on site, written procedures are used for their inspection. Specific fuel handling procedures define the sequence in which handling and inspection take place.

Fuel shipping containers are externally inspected when received to ensure there was no damage during shipping. This inspection includes examination of the instrumentation that measures acceleration forces during shipping to ensure the forces were within limits.

Removal of the fuel from the shipping container is performed in accordance with written procedures. Following removal from the shipping container, a detailed visual inspection of the fuel assemblies and CRAs is performed. On-site fuel receipt procedures are based on the fuel fabricator's recommendations.

4.2.4.5 On-line Fuel System Monitoring

The chemical and volume control system (Section 9.3.4) contains radiation detection instrumentation that continuously monitors for radioactivity and is capable of detecting a fuel leak. In addition, the process sampling system (Section 9.3.2) contains grab sample capability that allows for more detailed assessment of the radionuclides in the primary system water. Detection of a fuel leak may result in more frequent grab sample analysis.

4.2.4.6 Post Irradiation Monitoring

A detailed surveillance program is used following irradiation of the fuel assembly and CRAs from the first licensed NPM. This program includes the schedule and criteria for inspection of selected fuel assemblies and CRAs. The program includes complete visual inspections of selected assemblies and detailed measurements to capture key attributes such as those listed below. The detailed measurements are taken to confirm the fuel is performing according to the design analyses described in Section 4.2.1. The key attributes that are assessed as part of the post-irradiation monitoring program include:

- fuel rod growth
- fuel rod bowing
- fuel assembly growth
- fuel assembly bowing
- fuel rod cladding corrosion (oxide) and crud deposition
- fuel rod cladding diameter

The post-irradiation program ensures the above characteristics are within expected values. This surveillance program spans the initial three cycles of operation of the initial licensed NPM, with provisions for during-cycle inspections if operation indicates the presence of fuel abnormalities. The surveillance program includes guidance on the disposition of failed fuel.

4.2.5 References

4.2-1 NuScale Power, LLC, "NuFuel-HTP2™ Fuel and Control Rod Assembly Designs," TR-117605-P, Revision 0.

4.2-2 NuScale Power, LLC, "Applicability of AREVA Fuel Methodology for the NuScale Design," TR-0116-20825-P-A, Revision 1.

4.2-3 NuScale Power, LLC, “NuScale Applicability of AREVA Method for the Evaluation of Fuel Assembly Structural Response to Externally Applied Forces,” TR-0716-50351-P-A, Revision 1.

4.2-4 NuScale Power, LLC, "Framatome Fuel and Structural Response Methodologies Applicability to NuScale," TR-108553-P-A, Revision 0.

4.2-5 AREVA Inc., "Evaluation of Advanced Cladding and Structural Material (M5) in PWR Reactor Fuel," BAW-10227P-A, Revision 1, June 2003.

4.2-6 AREVA Inc., "COPERNIC Fuel Rod Design Computer Code," BAW-10231P-A, Revision 1, January 2004.

4.2-7 AREVA Inc., "PWR Fuel Assembly Structural Response to Externally Applied Dynamic Excitations,” ANP-10337P-A, Revision 0, April 2018.

4.2-8 AREVA Inc., "Computational Procedure for Evaluating Fuel Rod Bowing," XN-75-32-P-A, Supplements 1-4, February 1983.

4.2-9 AREVA Inc., “Program to Determine In-Reactor Performance of BWFC Fuel Cladding Creep Collapse,” BAW-10084P-A, Revision 3, August 1995.

Table 4.2-1: Fuel Assembly Materials

Component	Material
Top nozzle	Stainless steel
Bottom nozzle frame	Stainless steel
Mesh filter plate	Alloy 286
Guide tubes; instrument tubes	Zr-4
Top connection (QD)	Zr-4 and Alloy 718
Bottom cap screw	AISI 316L stainless steel
HMP™ grid	Alloy 718
HTP™ grid	Zr-4
Fuel rod cladding	M5®
Fuel assembly leaf springs	Alloy 718
Fuel rod plenum springs	Alloy X-750
Fuel pellets	UO_2 and UO_2 plus Gd_2O_3

Note: Stainless steels are low cobalt.

Table 4.2-2: Fuel Design Parameters

Parameter	Nominal Value
Fuel Assembly Parameters	
Fuel rods per fuel assembly	264
Guide tubes per fuel assembly	24
Spacer grids per fuel assembly	5
Number of instrument tubes per assembly	1
Pin pitch (in.)	0.496
Guide tube OD (in.)	0.482
Guide tube ID (above dashpot) (in.)	0.450
Guide tube ID (in dashpot) (in.)	0.397
Fuel assembly length (excluding springs) (in.)	94.00
Fuel Rod Parameters	
Fuel stack height (in.)	78.74
Fuel rod length (in.)	85.90
Fuel rod OD (in.)	0.374
Fuel rod ID (in.)	0.326
Fuel pellet OD (in.)	0.3195
Pellet length (in.)	0.400

Table 4.2-3: Control Rod Design Parameters

Dimension	Nominal Value
CRA total mass (lb)	43
CRA total height (in.)	94.37
Control rod OD (in.)	0.381
Control rod ID (in.)	0.344
Control rod bottom end plug length (in.)	1.913
B_4C OD (in.)	0.333
B_4C stack length (in.)	62.0
AIC composition (weight percent, nominal)	80% silver, 15% indium, and 5% cadmium
AIC OD (in.)	0.336
AIC stack length (in.)	12.0
Cladding material	304L stainless steel
Height of CRA spider assembly (in.)	10.387
CRA shaft OD (in.)	1.804

Figure 4.2-1: Fuel Assembly General Arrangement

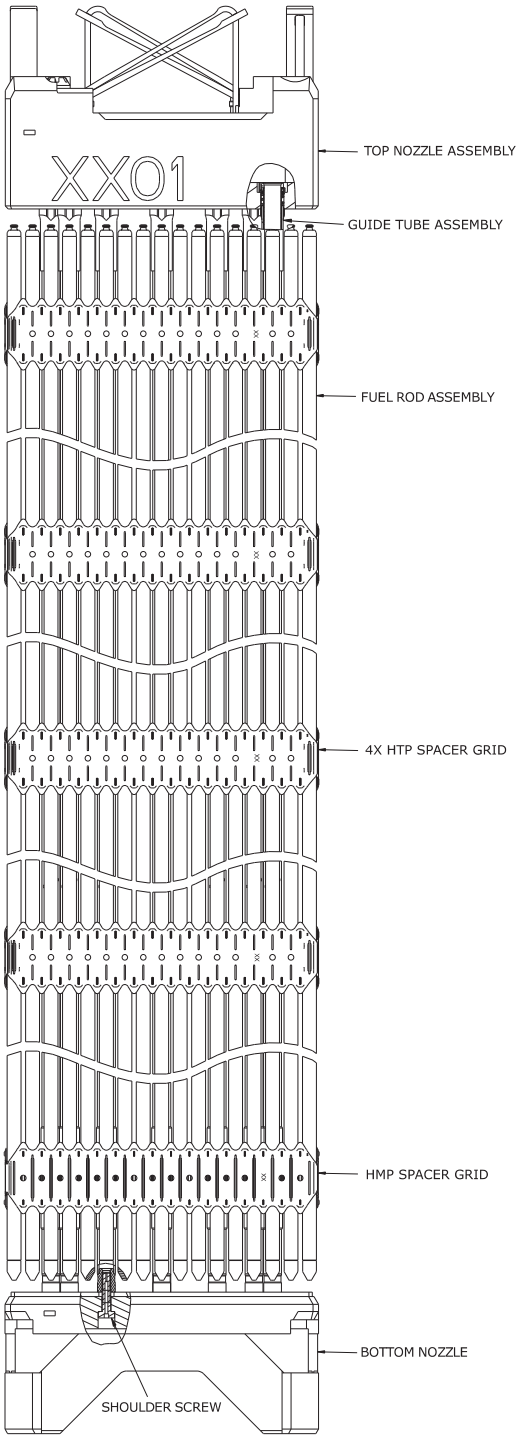

Figure 4.2-2: Top Nozzle

(nominal dimensions)

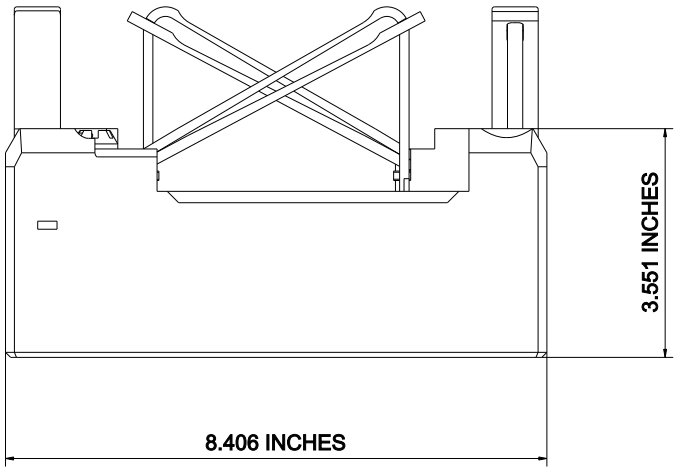

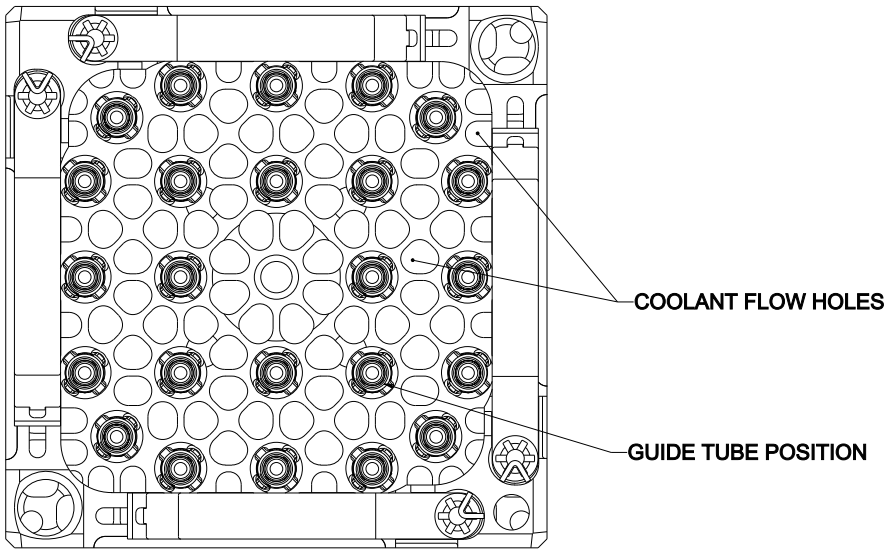

Figure 4.2-3: Bottom Nozzle

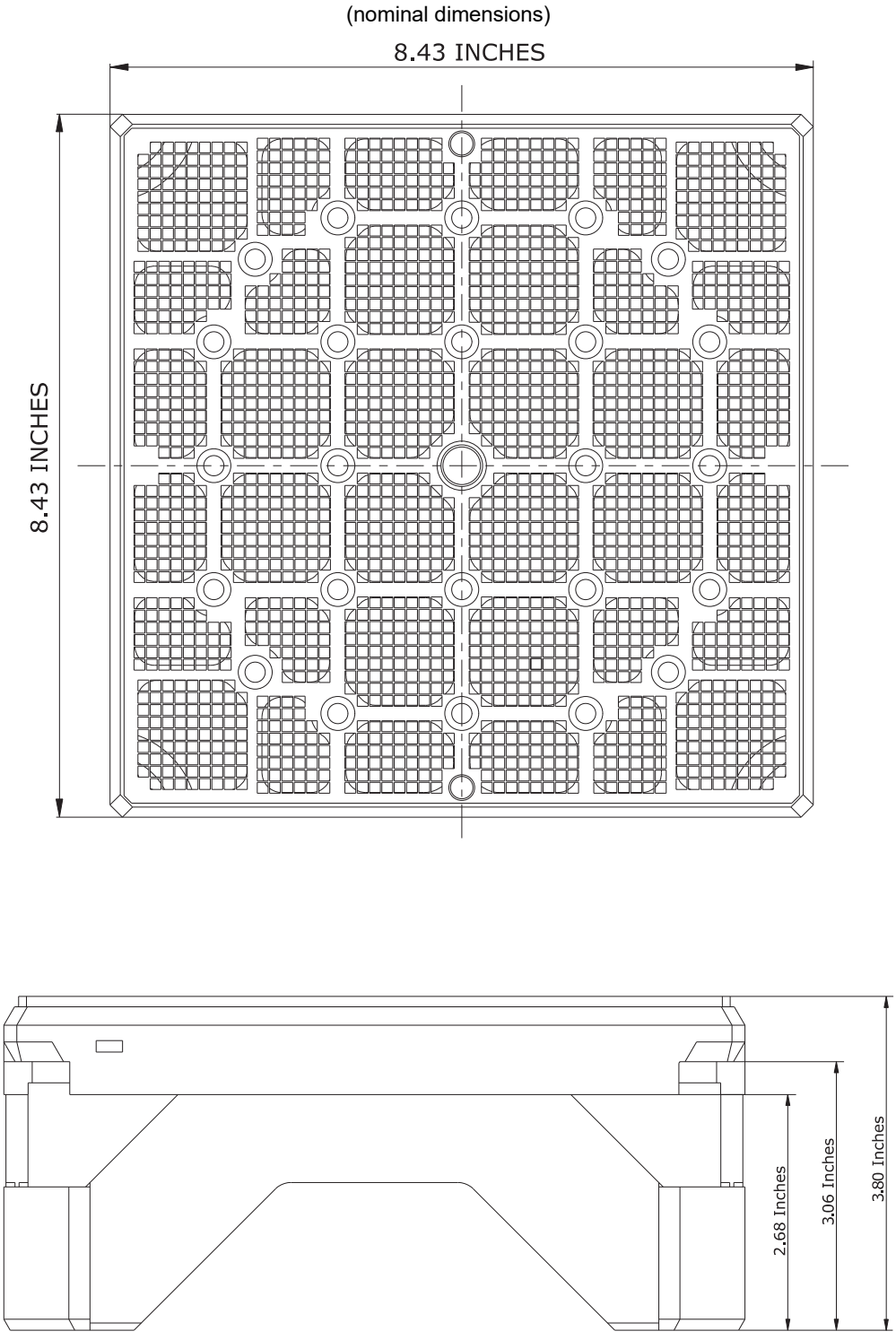

Figure 4.2-4: Guide Tube Assembly

(nominal dimensions)

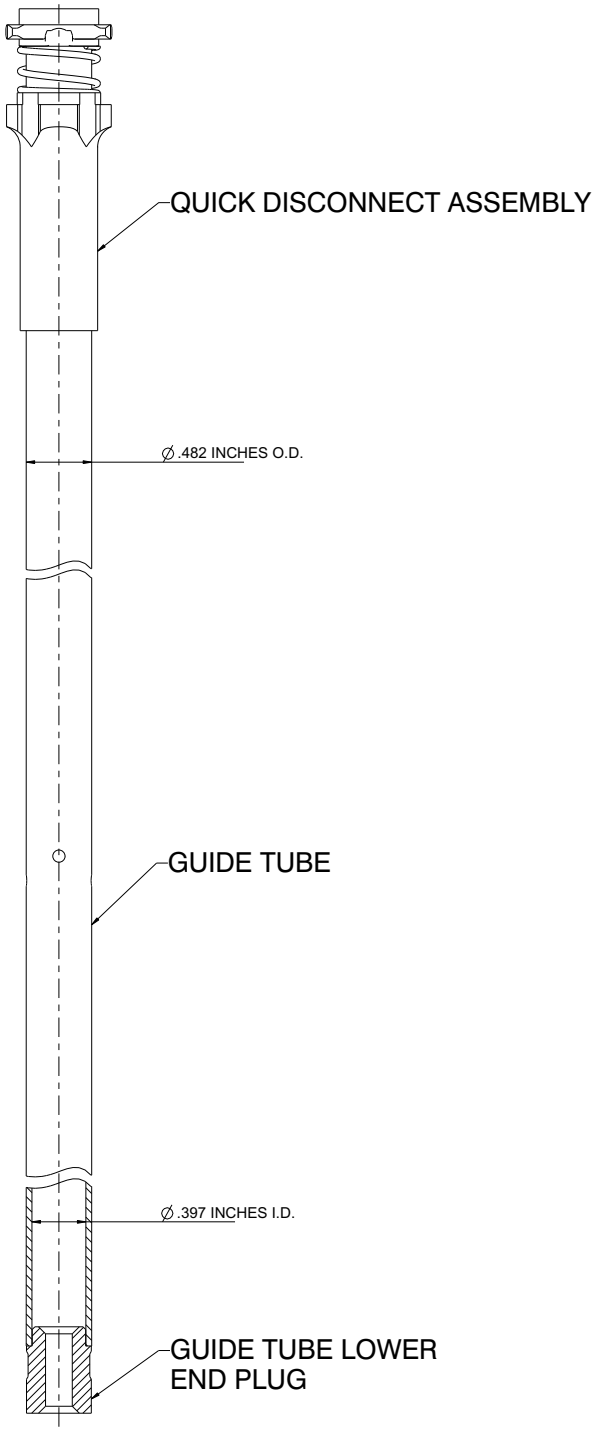

Figure 4.2-5: Guide Tube Quick Disconnect Top Nozzle Connection

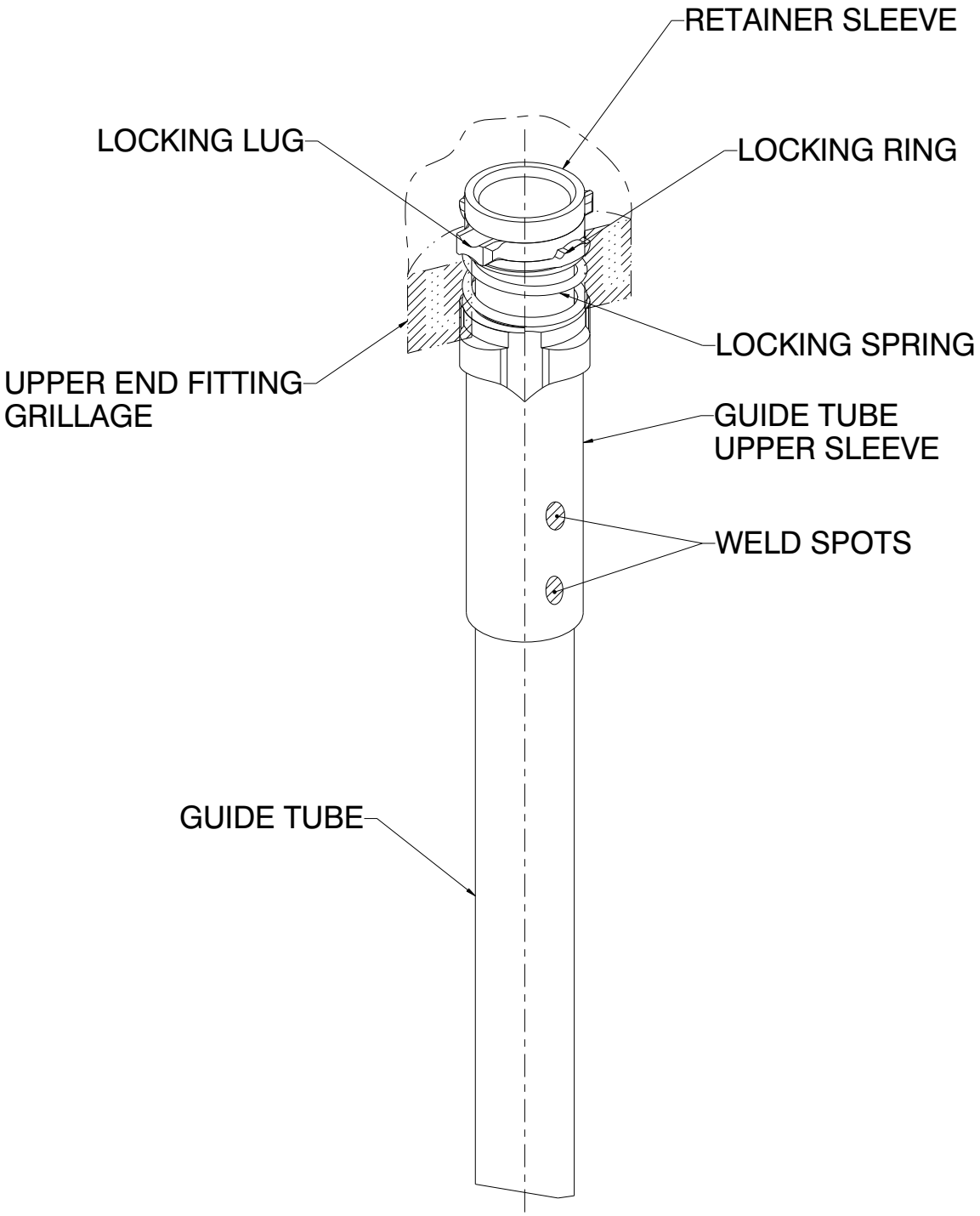

Figure 4.2-6: Cap Screw Bottom Nozzle Connection

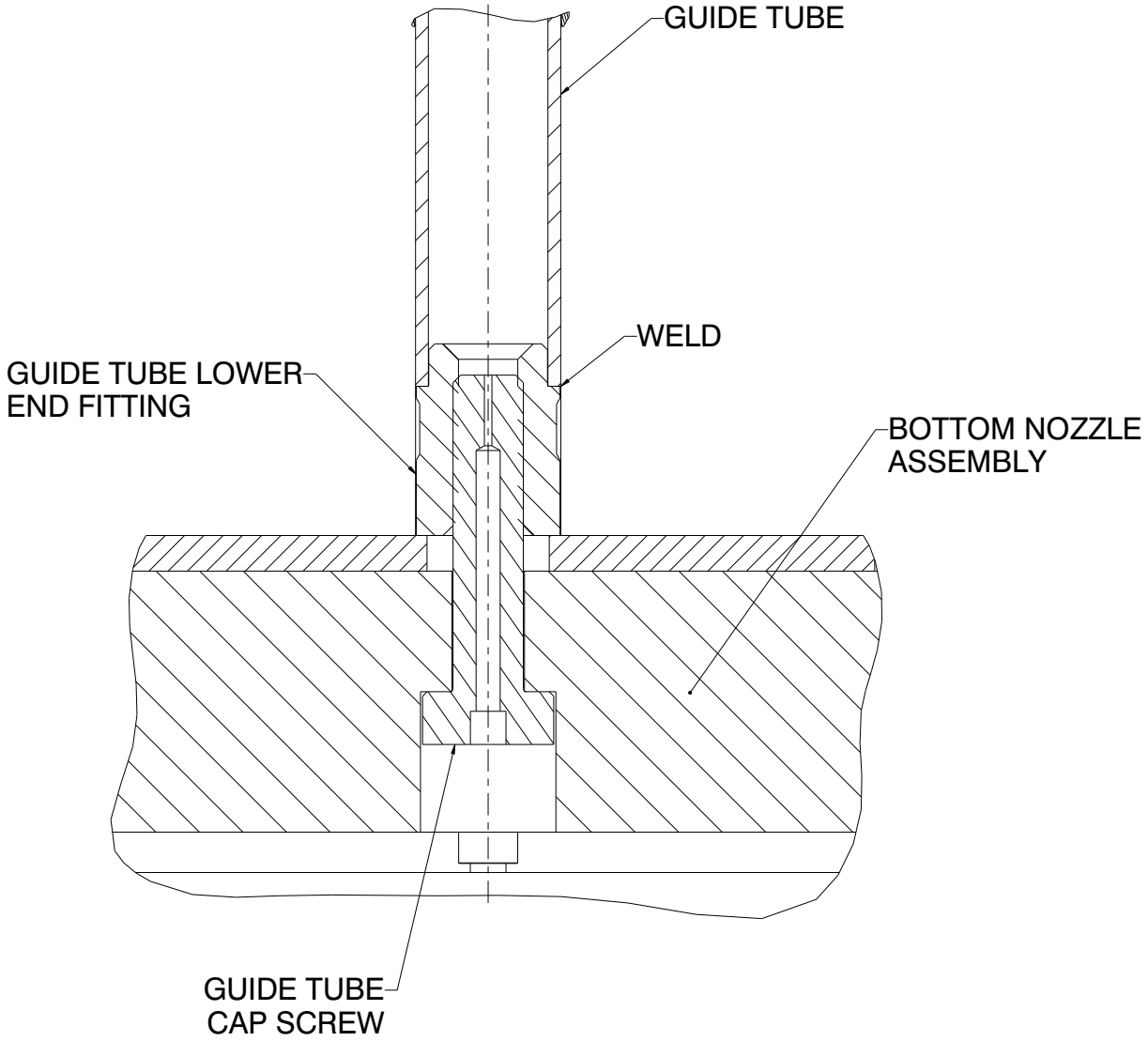

Figure 4.2-7: HTP™ Spacer Grid Characteristics

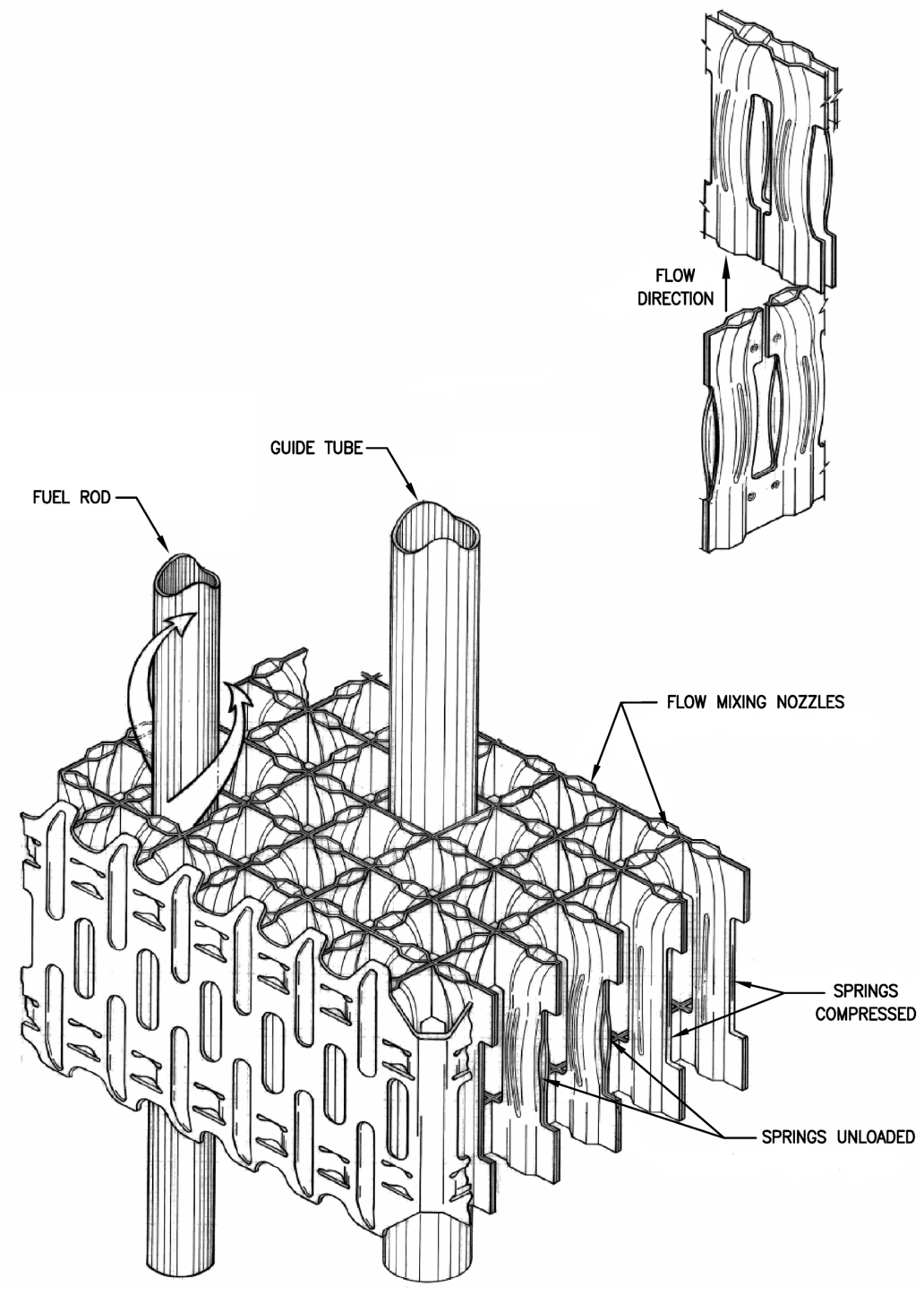

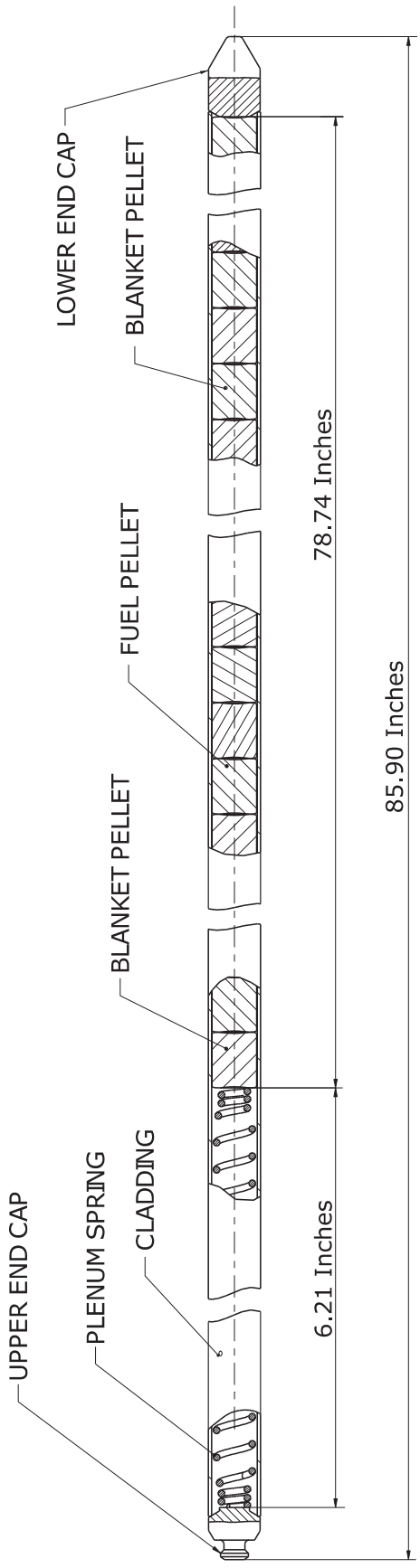

Figure 4.2-8: Representative Fuel Rod Assembly
(nominal dimensions)

Figure 4.2-9: Control Rod Assembly General Arrangement
(nominal dimensions)

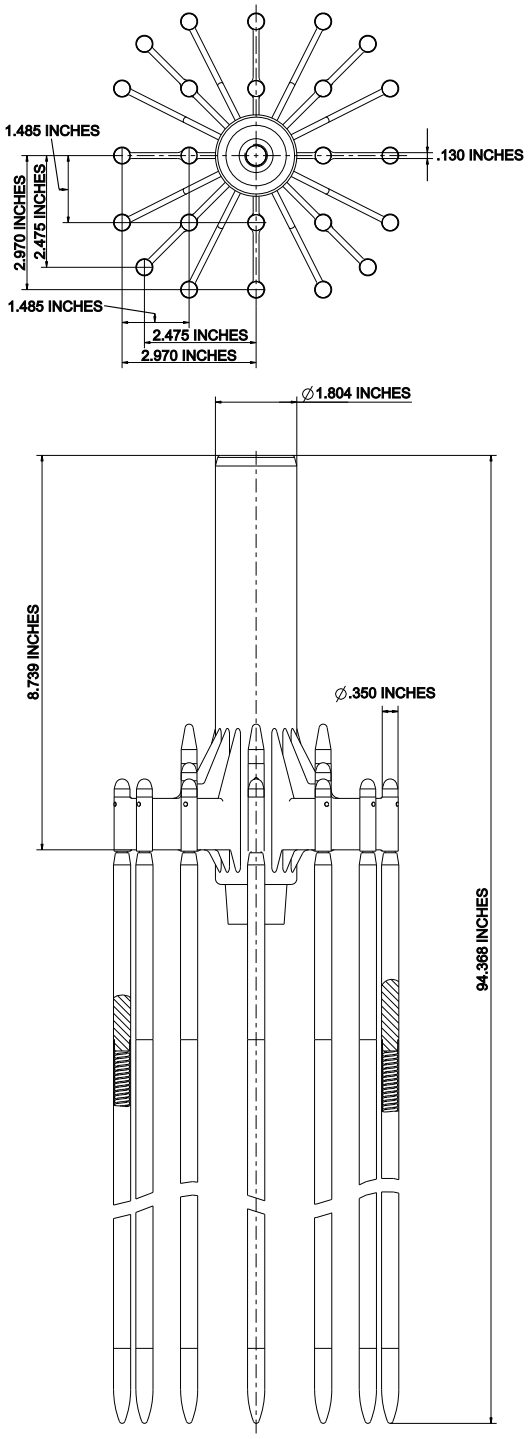

Figure 4.2-10: Control Rod Assembly Cut-Away
(nominal dimensions)

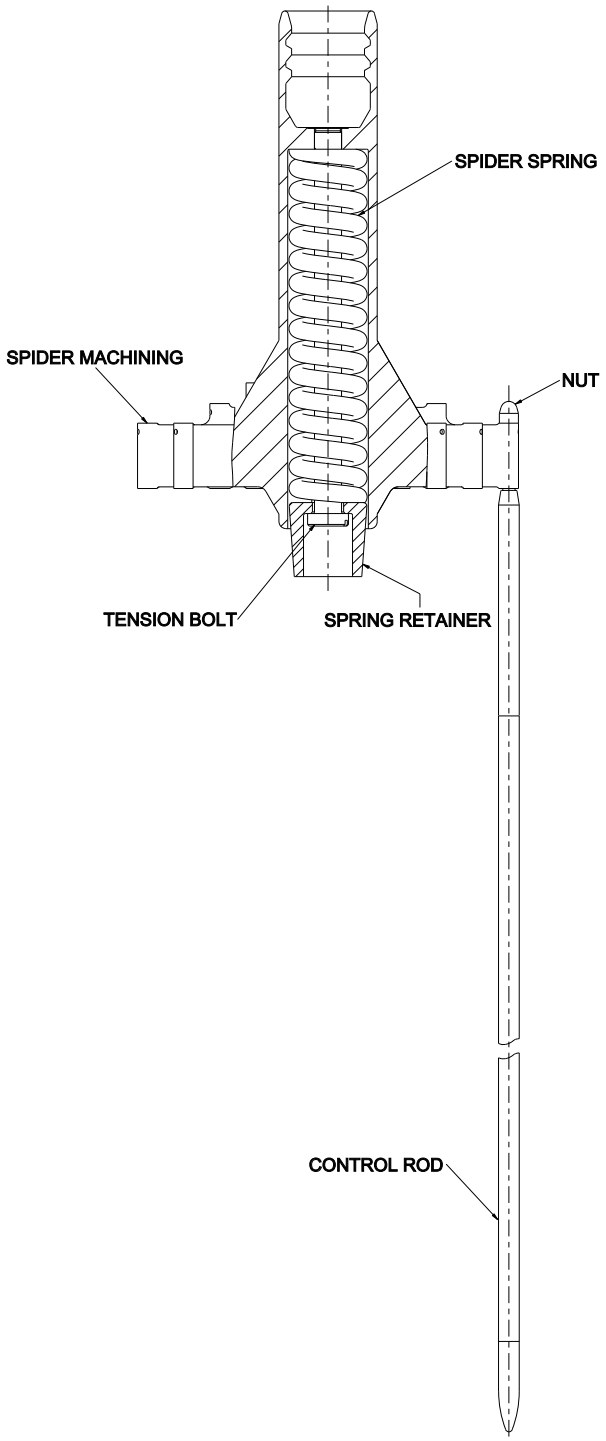

Figure 4.2-11: Control Rod Assembly Design
(nominal dimensions)

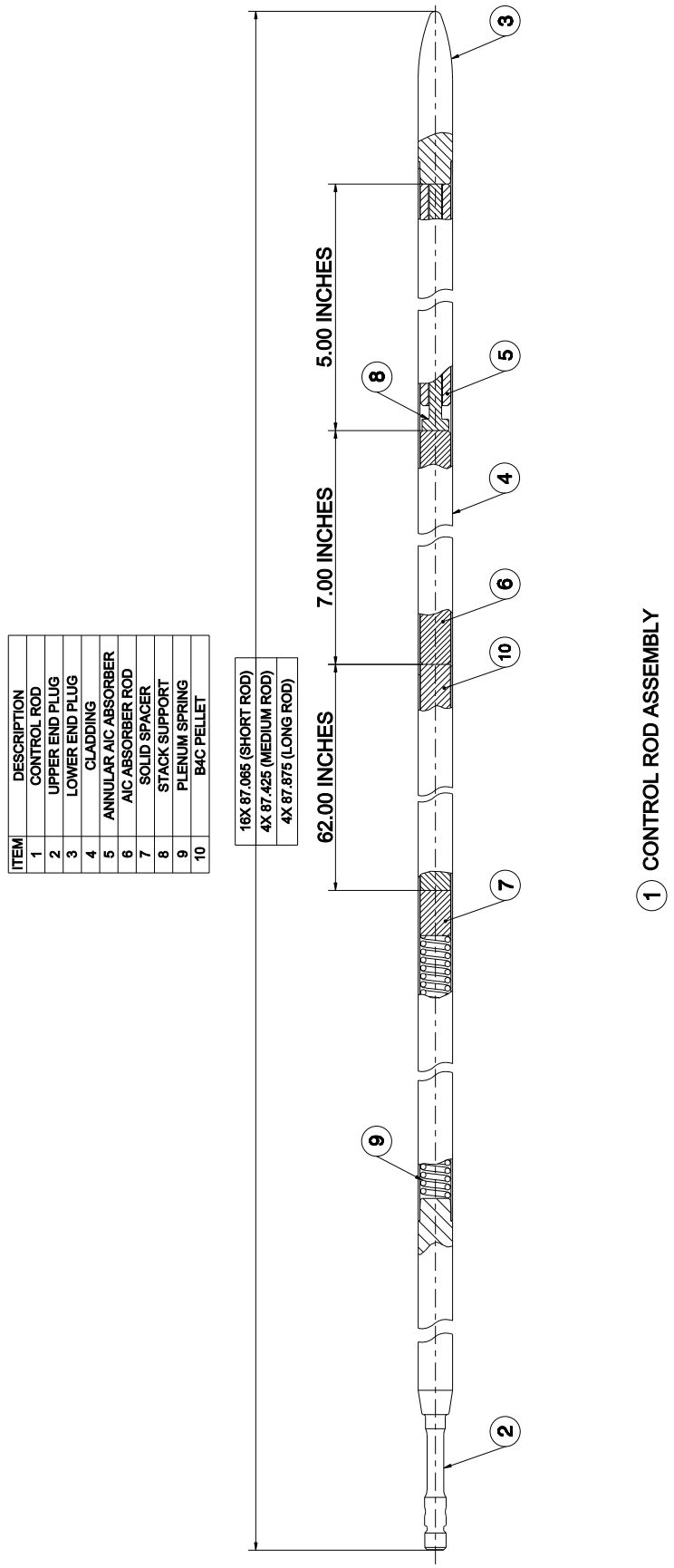

4.3 Nuclear Design

This section describes the nuclear design of the NuScale Power Module (NPM), including the design bases (Section 4.3.1), the nuclear design of the fuel and reactivity control systems (Section 4.3.2), and the analytical methods used to perform the nuclear design (Section 4.3.3). Detailed analytical results for an equilibrium fuel cycle are presented at the end of this section. The equilibrium cycle is representative of a typical fuel cycle design with limits placed on the core design that apply to the design of other cycles, including the initial and transition cycles.

4.3.1 Design Bases

The nuclear design bases for the fuel and reactivity control systems are as follows.

- The reactor core and reactivity control systems are designed with appropriate margin to ensure the specified acceptable fuel design limits (SAFDLs) are not exceeded during normal operation or anticipated operational occurrences (AOOs), in accordance with General Design Criterion (GDC) 10.
- The reactor core is designed so that in the power operating range the net effect of prompt inherent nuclear feedback tends to compensate for rapid increase in reactivity, in accordance with GDC 11.
- The reactor core and reactivity control systems are designed to ensure power oscillations that can result in conditions exceeding SAFDLs are not possible or can be reliably and readily detected and suppressed, in accordance with GDC 12.
- The reactivity control system withdrawal rate is designed to ensure SAFDLs are not exceeded for accidental withdrawal of control rods, in accordance with GDC 25.
- There are two independent reactivity control systems based on different design principles to satisfy GDC 26. The control rod drive system uses control rod assemblies (CRAs) to provide reactivity control, and the chemical and volume control system (CVCS) uses soluble boron from the boron addition system for reactivity control. The CRAs and associated rod control system are designed with a positive means for inserting the rods and reliably controlling reactivity changes during normal operation. The control rod design ensures the SAFDLs are not exceeded during an AOO assuming a single stuck CRA. The CVCS provides reactivity control associated with planned normal power changes including the effects of fuel burnup and is capable of holding the reactor subcritical during cold conditions, in accordance with GDC 26.
- The combined capabilities of the CRAs and CVCS, in conjunction with the emergency core cooling system (ECCS) supplemental boron (ESB) function, control reactivity changes under postulated accident conditions with appropriate margin for stuck rods, ensuring the capability to cool the core is maintained, in accordance with GDC 27. The CRAs with the highest worth CRA remaining fully withdrawn from the core, together with ESB recirculated into the core during ECCS operation, are capable of holding the reactor subcritical under design-basis event (DBE) conditions, including postulated accidents, for 72 hours following the event.

- The reactivity control systems limit the potential amount and rate of reactivity increase to ensure the effects of postulated reactivity accidents do not result in damage to the reactor coolant pressure boundary greater than limited local yielding nor impair the capability to cool the core, in accordance with GDC 28.

General Design Criterion 13 and GDC 20 also provide requirements to ensure SAFDLs are met. General Design Criterion 13 is discussed in Chapters 6, 7, and 9 and GDC 20 is discussed in Chapter 7.

4.3.1.1 Fuel Burnup

Fuel burnup is a measure of the depletion of the fuel based on the energy output and is measured in GWd/MTU (gigawatt days per metric ton of uranium). Core loading patterns are developed with initial excess reactivity to maintain the core critical at full power throughout the cycle as fission products in the fuel build up and fissile material depletes. Burnable poisons and soluble boron are used to compensate for this initial excess reactivity. The end of design cycle life occurs when soluble boron is essentially zero (typically 20 ppm boron or less) with the CRAs positioned to meet operational requirements (fully or close to fully withdrawn).

While there is no specific design limit on cycle average burnup, the core average cycle exposure is designed such that the peak fuel rod exposure is less than the approved value in the "Framatome Fuel and Structural Response Methodologies Applicability to NuScale" topical report (Reference 4.3-1).

Meeting the peak rod burnup limit along with the design-basis in Section 4.3.1.3 satisfies GDC 10.

4.3.1.2 Negative Reactivity Feedback

The Doppler coefficient and the moderator temperature coefficient (MTC) are the two primary reactivity feedback mechanisms that compensate for a rapid reactivity increase. The Doppler coefficient is characterized by the broadening of resonance absorption cross-sections with an increase in fuel temperature. The Doppler coefficient is negative for the fuel design. The MTC is a measure of reactivity feedback associated with a change in the moderator temperature, where changes in moderator density change the neutron energy spectrum. The MTC is negative in the power operating range. The inherent Doppler reactivity characteristics of the fuel provide rapid negative reactivity effects with an increase in fuel temperature. A corresponding increase in moderator temperature that decreases moderator density provides additional, but slower negative reactivity feedback.

The MTC and the Doppler coefficient together provide inherent reactivity control and satisfy GDC 11.

The moderator and Doppler effects are discussed in more detail in Section 4.3.2.3.

4.3.1.3 Power Distribution

The power distribution and the reactor protection system are designed to ensure the following SAFDLs are met at a 95 percent probability at a 95 percent confidence level.

- Fuel must not exceed the critical heat flux (CHF) limits under normal operating conditions and AOOs as described in Section 4.4.
- Peak fuel power under abnormal conditions, including the maximum overpower condition, must not result in fuel melting as discussed in Section 4.4.
- Fuel management is such that the values of fuel rod power and burnup meet the fuel rod mechanical integrity requirements in Section 4.2.
- Fuel is not operated at a linear power density greater than the design limit for the fuel.

These restrictions along with the burnup restriction in Section 4.3.1.1 satisfy GDC 10. The power distribution limits are discussed in more detail in Section 4.3.2.2.

4.3.1.4 Maximum Controlled Reactivity Insertion

The design places limits on the worth of the CRAs, CRA insertion depth, and maximum CRA withdrawal rate. The maximum controlled reactivity addition rate is limited, such that the SAFDLs are not violated during normal operation, AOOs, or postulated accidents.

For an accidental withdrawal of a bank of CRAs or a single CRA, the maximum withdrawal rate is established such that CHF limits are not exceeded, in accordance with GDC 25. The design maximum rod withdrawal rate is described in Section 15.4.

The maximum worth of the CRAs and the limits on CRA insertion preclude rupture of the reactor coolant pressure boundary due to a rod withdrawal or rod ejection accident (Section 15.4). The design basis presented in this section satisfies GDC 28. Control rod worth is discussed in more detail in Section 4.3.2.5.

4.3.1.5 Shutdown Margin and Subcriticality During Long-Term Cooldown

The design employs two independent means for reactivity control: CRAs and soluble boron. These two reactivity control systems satisfy the portion of GDC 26 that requires two independent reactivity control systems of different design principles. Each of the two independent means of reactivity control is capable of controlling the reactivity changes resulting from planned, normal operation.

Shutdown margin (SDM) is defined as the instantaneous amount of reactivity by which the reactor is subcritical, or would be subcritical from its present condition, assuming CRAs are fully inserted with the highest worth CRA assumed to be fully withdrawn. The SDM is maintained in accordance with the technical specifications

for all modes of operation. For normal operation, the technical specification for SDM is based on the limit used for safety analysis.

During power operations, the CVCS is used to adjust soluble boron concentration to account for reactivity changes due to core burnup and power maneuvering in order to maintain the CRAs within the power dependent insertion limits (PDILs). The PDILs ensure sufficient SDM is maintained. Using soluble boron preserves the capability of the CRAs to rapidly reduce power and protect fuel design limits upon a reactor trip, and provides a means for controlling the rate of reactivity changes resulting from planned, normal power changes (including xenon burnout) to ensure SAFDLs are not exceeded.

For AOOs, rapid CRA insertion after a reactor trip provides protection of fuel design limits. Consistent with GDC 26, the calculation of SDM includes a provision for the highest worth CRA remaining fully withdrawn from the core. When transitioning to cold conditions, the CVCS provides the necessary boron concentration to ensure the reactor remains subcritical. If the CVCS is unavailable, automatic actuation of the ECCS provides additional boron concentration via the ESB function to ensure the reactor remains subcritical for at least 72 hours following the event (Section 6.3).

For postulated accidents, rapid CRA insertion after a reactor trip provides protection of the core. As with AOOs, the CVCS is used to adjust soluble boron concentration and maintain SDM before the event. Upon actuation of ECCS, the ESB function provides additional boron concentration to ensure the reactor remains subcritical for at least 72 hours following the event (Section 6.3). For DBEs, the combined reactivity control capability of the CVCS, CRAs, and ESB ensures reactivity is controlled in accordance with GDC 26 and GDC 27, as demonstrated in Section 15.0.5.

As discussed in Section 15.0.5, diverse flow paths in the upper and lower riser barrel ensure reactor coolant system boron remains mixed during extended decay heat removal system or ECCS operation. Mixing created by these flow paths avoids a surge of diluted coolant flowing into the core from the downcomer during long-term cooling.

4.3.1.6 Stability

The design of the reactor and associated systems and the administrative controls on CRA position provide an inherently stable core with respect to axial and radial power stability. In addition, oscillations in core power can be readily detected by the fixed in-core detector system that continuously monitors the core flux distribution. Stability analyses are discussed in Section 4.3.2.7. The stability design satisfies GDC 12.

4.3.2 Nuclear Design Description

4.3.2.1 Nuclear Design Description

The core consists of 37 fuel assemblies as described in Section 4.2. Sixteen of the fuel assembly positions contain CRAs. The CRAs are organized into two banks: a regulating bank and a shutdown bank. The regulating bank contains two groups of four CRAs arranged symmetrically in the core. The regulating bank groups are used during normal plant operation to control reactivity and provide axial power shaping. The PDILs restrict the amount by which the two regulating bank groups can be inserted at power as shown in Figure 4.3-1. The shutdown bank contains two groups of four CRAs. The shutdown bank is fully withdrawn during power operation. The shutdown bank is used in the event of a reactor trip and to maintain the reactor shutdown. More information on the fuel and CRAs is provided in Section 4.2 and Section 4.6.

The fuel cycles are nominally 18 months and equivalent to a minimum 520 effective full power days. Each fuel rod may contain reduced enrichment axial blankets at the top and bottom, with a central fully enriched zone. Assemblies may also incorporate radial zoning to control power distribution and peaking within the core.

The NPM is designed with a heavy reflector to improve neutron economy. The reflector is made of stainless steel, which reflects fast neutrons back into the core and flattens the power distribution to improve fuel performance. The reflector is located between the core periphery and the core barrel; it provides the core envelope and directs flow through the core.

The soluble boron concentration is adjusted throughout the cycle to compensate for reactivity changes due to power level, fuel burnup, fission product poisoning, and burnable poison depletion. The higher concentration at beginning of cycle (BOC) balances the excess reactivity designed into the core to achieve the desired cycle length. The equilibrium cycle has an initial boron concentration of 1052 ppm.

Burnable poison in the form of gadolinia (Gd_2O_3) may be used within the fuel assemblies when needed to support the core design. The gadolinia is homogeneously mixed with the UO_2 in selected fuel rods to provide a favorable radial power distribution, hold down reactivity, and minimize power peaking within an assembly. Although gadolinia is physically compatible with UO_2, its addition to the fuel degrades some of the material properties of the UO_2. For this reason, fuel containing gadolinia is limited to a lower power generation rate than fuel containing only UO_2 based on consideration of centerline melting.

The equilibrium cycle is the basis for the reference analysis presented in this section. The exact loading patterns, initial and final positions of assemblies, and number of fresh assemblies and their placement depend on the energy requirements and the specific power history of an individual cycle. The fuel

loading pattern and fuel shuffle pattern for the reference equilibrium cycle are shown in Figure 4.3-2 and Figure 4.3-3, respectively.

Table 4.3-1 and Table 4.3-2 summarize the reactor core design parameters used in the analysis. The plant operating modes are described in the technical specifications.

4.3.2.2 Power Distribution

Power distribution calculations are discussed in the "Nuclear Analysis Codes and Methods Qualification" topical report (Reference 4.3-2). This report contains a discussion of power distribution uncertainty, including application and a means for updating the uncertainty values. Additional discussion of the power uncertainties used in thermal-hydraulic analysis is provided in Section 4.4.

4.3.2.2.1 Definitions

Enthalpy Rise Hot Channel Factor, $F_{\Delta H}$

The maximum enthalpy rise hot channel factor, $F_{\Delta H}$, is defined as the ratio of the maximum integrated fuel rod power to the average fuel rod power. The limit on $F_{\Delta H}$ is established to ensure the fuel design criteria are not exceeded and the accident analysis assumptions remain valid. This limit ensures the design-basis value for the CHF ratio is met for normal operation, AOOs, and infrequent events. The $F_{\Delta H}$ limit is representative of the coolant flow channel with the maximum enthalpy rise. This channel has the highest power input to the coolant and therefore the highest probability for CHF.

Heat Flux Hot Channel Factor, F_Q

The heat flux hot channel factor (or total peaking factor), F_Q, is the ratio of maximum local heat flux on the surface of a fuel rod to the average fuel rod heat flux. The maximum F_Q value is used to calculate the peak linear heat generation rate (LHGR). The maximum value of F_Q is used to ensure the SAFDLs are not exceeded.

Axial Peaking Factor, F_Z

The axial peaking factor, F_Z, is the maximum relative power at any axial point in a fuel rod, divided by the average power of the fuel rod.

Axial Offset

Axial offset (AO) is the ratio of the difference in power between the top half of the core and the bottom half of the core to the total core power as shown in the equation below:

$$\text{Axial Offset (fraction)} = \frac{\text{Power in Top of Core} - \text{Power in Bottom of Core}}{\text{Total Power in Core}} \quad \text{Eq. 4.3-1}$$

The AO window is defined as a function of reactor power as provided in Figure 4.3-4.

4.3.2.2.2 Radial Power

The core radial power distribution is a function of power level, core loading pattern, control rod pattern, control rod insertion, burnable poison loading, location of fresh and burned fuel assemblies, and assembly burnup throughout the cycle.

Figure 4.3-5, Figure 4.3-6, and Figure 4.3-7 show the total and radial peaking factors (F_Q and $F_{\Delta H}$) at BOC, middle of cycle (MOC), and end of cycle (EOC) as a function of power level based on a nominal cycle depletion with all CRAs out, followed by an instantaneous insertion of the regulating bank CRAs to the PDIL.

Figure 4.3-8 provides the fuel assembly relative radial power distribution at BOC, MOC, and EOC. A flat power distribution within the fuel assembly is assumed in the CHF subchannel analysis as described in Section 4.4.

4.3.2.2.3 Assembly Power

Typical radial power distributions within a fuel assembly relative to average core power are shown in Figure 4.3-9. In the case of a central assembly, the power distribution within the assembly is typically symmetric.

Figure 4.3-10, Figure 4.3-11, and Figure 4.3-12 show a pin-by-pin power distribution relative to average core power for a first batch (fresh), second batch (once burned), and third batch (twice burned) fuel assembly. These power distributions are shown for BOC and EOC.

4.3.2.2.4 Axial Power

The axial power shape is influenced by core power, the position of the regulating bank, moderator density, fission product distribution, fuel burnup, and the Doppler effect. An AO window is developed that encompasses AOs achievable during normal operation by considering depletion over various durations. The depletions consider different power levels and CRA insertions. Swings in axial xenon distribution and concentration resulting from these CRA insertions and withdrawals produce a wide range of AOs to be enveloped by

the AO window. The range of axial power shapes that is achieved while operating within allowed conditions is also used to evaluate the appropriateness of the AO window. During an operating cycle, the AO is maintained within the analytically based AO window (Figure 4.3-4) by controls specified in the technical specifications. The axial power shape can also be determined from the in-core instrumentation system (ICIS) described in Section 4.3.2.2.9.

Figure 4.3-13 provides the core average axial power shape for the equilibrium cycle at BOC, MOC, and EOC. The effect of neutron absorption by the spacer grids can be observed in the power shapes in the figure.

4.3.2.2.5 Local Power

Fuel densification has been observed in nuclear power plants due to irradiation. Densification causes the fuel pellets to shrink and in some cases results in gaps in the fuel column. These gaps, if significant, can cause reduced neutron absorption and can result in power peaking in nearby rods. Modern fuel designs and manufacturing practices have reduced the effects of this phenomenon. The subchannel analysis fuel rod modeling, discussed in Section 4.4, bounds fuel densification effects. No penalty is taken for local power spikes due to fuel densification in the fuel design.

4.3.2.2.6 Limiting Power Distributions

Limiting power distributions are used for the steady state and transient analyses. The specific assumptions for the limiting power distributions are described in more detail in Section 4.4 and Chapter 15. The values of $F_{\Delta H}$ and F_Z used in the transient analysis are confirmed bounding for cycle-specific nuclear designs.

The limiting power distributions are confirmed during operation by technical specifications that require operation within the allowed $F_{\Delta H}$, AO window, and PDILs. Section 4.3.2.2.9 discusses core monitoring to provide in-core flux measurements and power distribution for display in the control room. These indications provide further assurance the power distributions both axially and radially are not deviating from those expected and assumed in the analyses.

Radial Power Distribution

The radial power distribution is primarily determined by the cycle design. Each cycle core design is required to adhere to the maximum allowed $F_{\Delta H.}$ This design limit is then applied in the subchannel analysis as described in Section 4.4. The transient analysis applies constant radial power distributions through the evolution of transient events. For those events where radial peaking can increase during the event, an augmentation factor is used to modify the radial power distribution.

Axial Power Distribution

The core average axial flux shape can be affected by operator action. The core average axial power profile is affected by power level, control rod motion, load changes, xenon distribution, temperature changes, and cycle burnup. Axial power peaking (F_Z) does not have a limit associated with it, but the axial power distribution is limited by the allowable AO window in the technical specifications.

An analysis of the possible axial power shapes is performed to identify the bounding axial power shapes for use in the CHF and transient analyses. These shapes are generated as a function of power level, cycle burnup, control rod position, xenon distribution, and core thermal-hydraulic conditions. Bounding axial power shapes are held constant through the evolution of transients.

4.3.2.2.7 Verification of Power Distribution Analysis

The analytical methods have been benchmarked against other higher-order computer codes, experimental reactors, and against measured data from operating commercial reactors. Results of the benchmarking are discussed in detail in Reference 4.3-2 and are used to derive nuclear reliability factors (NRFs). The NRF accounts for calculational error in the nuclear methods and ensures conservatism in the safety-related application of the parameter. The NRFs can be adjusted as measurements are collected and benchmarked against the nuclear methods.

4.3.2.2.8 Testing

A startup testing program is implemented for the initial startup to confirm the nuclear design analyses are in agreement with predictions. The initial startup tests are described in Section 14.2.

Startup physics testing (low-power testing and power-ascension testing) measures the neutronic characteristics of the core and compares measurements with predictions to verify the core is operating as designed, validate the analytical models, and verify assumptions used in the safety analyses. Comparison between measured and calculated values during start-up testing is used to assess the continued applicability of the NRF values, or the data is used to update the NRF values depending on the agreement between the measured and calculated values as described in Reference 4.3-2.

There are five characteristics that must be confirmed for each newly loaded core:

- reactivity balance
- reactivity control
- power distribution

- shutdown capability
- shutdown requirement

The reactivity balance is confirmed by the measurement of the hot zero power (HZP) all rods out boron concentration. Agreement between the measured value and the predicted value means the total amount of fissile material and absorbing material in the core is consistent with the design. Reactivity control is determined by measurement of the HZP isothermal temperature coefficient (ITC) and comparison to the predicted value. Agreement means the response of the core to temperature changes is consistent with the design. Power distributions are confirmed by measuring the neutron flux throughout the core at low, intermediate, and higher power levels and comparing the measurements to design predictions. The power distribution at lower power levels must be confirmed before increasing to higher power levels. Control rod worth measurements confirm the capability of the core to be shut down, and the shutdown requirement is confirmed by measuring the power defect (reactivity difference between zero power and full power).

Additional detail on startup physics testing is provided in Reference 4.3-2.

4.3.2.2.9 Monitoring

The ICIS continuously monitors core neutron flux distribution and core inlet and outlet temperatures. The core neutron flux information is provided to the module control system to ensure power distribution is in agreement with predictions. The core inlet and outlet temperature information is provided to the module protection system to ensure adequate core cooling is being provided for post-accident conditions.

The ICIS is used to synthesize core-wide three-dimensional power distributions. These power distributions are compared to predicted core power distributions to verify the core is operating as designed. Axial power distributions are continuously monitored to validate the AO operating window and actions required by the technical specifications are initiated based on this information. Power distributions from the ICIS are used to calibrate the ex-core neutron flux detectors. When the rod position indication system is not working properly, the ICIS has the capability to determine the relative position of a stuck or misaligned control rod.

During startup, the core inlet and core exit thermocouples are calibrated against the reactor coolant system narrow- and wide-range temperature measurements. The synthesized power distribution is compared against analytical predictions to verify proper fuel loading, calibrate the ex-core detectors, measure core peaking factors, and confirm core behavior.

During normal power operation, the ICIS is used to measure the power distribution to ensure peaking factors are within limits.

During post-accident conditions, the core inlet and core outlet thermocouples are used to monitor adequate core cooling and provide the operating staff information to assist them in monitoring critical safety functions.

The ICIS instrument strings operate in 12 core locations as shown in Figure 4.3-14. Additional details on the ICIS are provided in Chapter 7.0.

The following uncertainties are considered in determining the power distribution:

- uncertainty in the measured detector signal
- uncertainty in the relationship between the detector signal and power
- uncertainty in the predicted relationship between assembly power and peak rod power

4.3.2.2.10 Power Distribution Controls

Design-basis events are analyzed from bounding initial conditions and analytical limits. Operation within these bounding conditions and analytical limits is ensured using a variety of mechanisms including technical specification Limiting Conditions for Operation (LCOs), continuous monitoring, and surveillances. Operation within the limiting power distributions is ensured by the following.

- Position of the shutdown and regulating CRA banks is determined by the rod position indication system and operation of the regulating bank within the PDILs. Operation of both banks within the technical specifications modes is ensured through a pre-defined limit and control room alarms as the limit is approached.
- Axial offset is surveilled by continuous monitoring of the flux and power distribution; AO is an LCO and alarms are used to indicate if the AO window limit is approached.
- Control rod assembly alignment is an LCO.
- In addition to power distributions, the reactor coolant system pressure, flow rate, and temperature are continuously monitored and used to verify the LCO on $F_{\Delta H}$.

The combination of administrative controls, continuous monitoring, and alarms ensures analytical limits are not exceeded and the most limiting power distributions assumed for analysis of DBEs remain bounding.

4.3.2.3 Reactivity Coefficients

Reactivity coefficients describe the dynamic behavior of the core in response to a change in plant conditions or to operator adjustments made during normal operation, as well as the core response during AOOs or accidents. The reactivity coefficients reflect changes in reactivity due to varying plant conditions, such as thermal power, moderator and fuel temperatures, or soluble boron concentration.

Because reactivity coefficients change during the cycle, ranges of coefficients are employed in transient analysis to determine the response of the plant throughout life. The results of these analyses and the reactivity coefficients used are presented in Chapter 15.

Reactivity coefficients are calculated with approved nuclear methods described in Section 4.3.3. These models and methods have been qualified and benchmarked for core design and analysis as described in Reference 4.3-2.

4.3.2.3.1 Doppler Coefficient

The Doppler, or fuel temperature, coefficient is a measure of the reactivity change associated with a change in fuel temperature. The Doppler coefficient is characterized by a decrease in reactivity with increasing temperature due to the Doppler broadening of ^{238}U and ^{240}Pu resonance absorption peaks. The Doppler coefficient becomes more negative as a function of burnup as the ^{240}Pu content increases, thereby increasing the effective ^{240}Pu resonance absorption. The Doppler coefficient is calculated by uniformly perturbing the fuel temperature to determine the least negative and most negative values for the cycle. Table 4.3-2 provides the range of the Doppler coefficient over this spectrum of parameters.

4.3.2.3.2 Moderator Coefficients

The MTC is a measure of the relative change in reactivity associated with a change in moderator temperature. The MTC is calculated over a range of power and burnup by increasing the moderator temperature from the reference temperature causing a change in reactivity. The calculation of MTC includes the effects of moderator density changes.

The MTC is constrained by design, operating practices, and administrative controls to be negative so that increases in moderator temperature in the core are accompanied by decreased reactivity. However, the MTC may be positive at startup and low power.

The primary parameters affecting MTC are soluble boron concentration, burnup, burnable poison, and power level. At higher soluble boron concentrations, the effect of increasing temperature (and decreasing moderator density) results in decreased boron density, which tends to increase reactivity, making the MTC more positive. The maximum MTC typically occurs at the beginning of a cycle at low power levels. Burnup tends to make the MTC more negative due to the decrease in boron concentration and buildup of plutonium and other fission products. The minimum MTC is typically achieved at the end of a cycle. The most negative and least negative MTC are shown in Figure 4.3-15 from zero power to full power.

For events that experience a rapid depressurization, a density-based reactivity coefficient is used. The moderator density coefficient is a change in reactivity

in relation to a change in reactor coolant pressure. A change in pressure causes a change in reactivity through a change in the coolant density.

The effects of voiding are accounted for in the density portion of the MTC.

The ITC is the change in reactivity due to the combined change in core average moderator and fuel temperature when the temperature is uniform across the core. The ITC is distinguished from the MTC, which is the change in reactivity due to a change only in moderator temperature. The ITC is important because it is the quantity that can be measured in the plant and is used to develop the NRFs for MTC as described in Reference 4.3-2.

4.3.2.3.3 Power Defect and Power Coefficient

The power defect is the sum of the reactivity contributions from a change in moderator and fuel temperatures corresponding to a change in power from full power to zero power. A three dimensional calculation is performed to determine power defect, and therefore axial redistribution is implicitly included. The maximum and minimum power defect for the equilibrium cycle is shown in Figure 4.3-16.

The power coefficient is the sum of the moderator temperature, fuel temperature, and void coefficient, and is measured over the percent change in power. The minimum and maximum power coefficient is shown in Figure 4.3-17 and is negative at all power levels as shown.

4.3.2.3.4 Differential Boron Worth

The differential boron worth is a measurement of the change in reactivity associated with a change in the boron concentration. The differential boron worth coefficient for the equilibrium cycle is provided in Figure 4.3-18.

4.3.2.3.5 Comparison of Calculated and Experimental Reactivity Coefficients

A comparison of calculated and experimental reactivity coefficients is used to derive the NRFs as described in Reference 4.3-2.

4.3.2.3.6 Reactivity Coefficients in Transient Analysis

The reactivity coefficients, specifically the moderator temperature and Doppler coefficients, are analysis inputs to Chapter 15 transients. Bounding values are used as design limits in the transient analysis. The exact values of the coefficient used in the analysis depend on whether the transient of interest is examined at the beginning of life or end of life, whether the most negative or the most positive (least negative) coefficients are appropriate to provide conservatism, and whether spatial non-uniformity must be considered in the analysis. Conservative values of coefficients, considering various aspects of analysis, are used in the transient analysis. Details and assumptions for each transient are described in Chapter 15. The reactivity coefficients used in transient analyses are confirmed bounding for cycle-specific nuclear designs.

Limiting physics parameters, and the direction that is conservative for each Chapter 15 event, is provided in Reference 4.3-2.

4.3.2.4 Control Requirements

Core reactivity is controlled by soluble boron in the reactor coolant, CRAs, and burnable poison integral to the fuel pellets, as described in the following sections.

4.3.2.4.1 Soluble Boron

The design uses natural boron for soluble boron control. The soluble boron concentration is changed to control relatively slow reactivity changes due to

- moderator temperature changes from ambient conditions to HZP.
- transient xenon and samarium poisoning due to planned power changes.
- reactivity effects of fissile inventory depletion and buildup of fission products.
- depletion of burnable poison.

Table 4.3-2 shows the boron concentrations for different modes of operation for the equilibrium cycle. The boron concentration variation for the reference equilibrium cycle is shown in Figure 4.3-19.

The addition of boron for reactivity control lowers the pH of the coolant. Lithium is added to restore coolant chemistry as discussed in Section 5.2.3.

4.3.2.4.2 Control Rod Assemblies

The 16 CRAs provide control and shutdown capability for

- shutdown margin with the highest worth rod stuck out of the core.
- reactivity compensation as a result of an increase in power (power defect, including Doppler, and moderator reactivity changes).
- fluctuation in boron concentration, coolant temperature, or xenon.
- reactivity changes from load changes.
- design-basis events with a stuck rod.
- reactivity control during long-term cooldown in conjunction with boron addition from the ESB function.

Because the excess reactivity for burnup is controlled by soluble boron and burnable poison, it is not included in control rod requirements.

Control rod assembly insertion is restricted to ensure there is sufficient negative reactivity available to maintain shutdown capability and to limit the amount of reactivity insertion possible during the rod ejection accident. When the CRAs reach the PDIL, changes in soluble boron are required to compensate for additional reactivity changes. The PDILs are set sufficiently

high to meet these criteria while being low enough that operators have a reasonable range of CRA movement for power maneuvers. In general, deeper CRA insertion is allowed at lower power levels. Operators are alerted if the PDIL is approached. The PDILs are shown in Figure 4.3-1.

The ability to accomplish shutdown is demonstrated in Table 4.3-3 for the reference equilibrium cycle. Power distribution, rod ejection, and CRA misoperation analyses are based on the arrangement of CRAs shown in Figure 4.3-14.

During a startup, the shutdown bank is withdrawn before the regulating bank withdrawal is initiated. The approach to criticality is initiated by a combination of boron dilution to the appropriate boron concentration and withdrawal of the regulating bank. Additional detail on initial startup testing is provided in Section 14.2.

4.3.2.4.3 Burnable Poisons

Gadolinia (Gd_2O_3) can be used as an integral burnable absorber in selected fuel rods to provide partial control of the excess reactivity available during the cycle and control of radial power peaking. The burnable absorber also reduces the requirement for soluble boron at the beginning of the cycle, minimizing a positive MTC during power operations at the beginning of the cycle (at power).

4.3.2.4.4 Burnup

Cycles are designed with excess reactivity to offset the effect of burnup during the cycle. Control of this excess reactivity is accomplished using soluble boron and burnable poison. The boron concentration is limited during operating conditions to maintain a negative MTC. The EOC boron concentration is discussed in Section 4.3.1.1.

4.3.2.4.5 Power Maneuvering

Power changes are normally accomplished by means of regulating CRA position or soluble boron concentration. The CRA position is limited by the PDIL to help maintain the core within the AO limits. While power maneuvering operations within the capabilities of the rod control system are anticipated to support power system demands, continuous power maneuvering of the NPM where the CRA position is used to achieve power changes is not assumed in the analysis of the representative equilibrium cycle. However, planned power maneuvers must be considered as part of a cycle-specific core design as described in the technical specifications Core Operating Limits Report. The analysis of the impact of power maneuvering on the nuclear design includes the effects on axial and radial power shapes used in the safety analysis in Chapter 15.

4.3.2.5 Control Rod Patterns and Reactivity Worth

As discussed in Section 4.3.1, the SDM is the instantaneous amount of reactivity by which the reactor is subcritical or would be subcritical from its present condition assuming all CRAs (shutdown and regulating banks) are fully inserted (while accounting for the power defect, CRAs starting at the PDIL, SDM uncertainties, and flux redistribution), except for the single CRA of highest reactivity worth, which is assumed to remain fully withdrawn.

The design limit on minimum SDM is set by the safety analysis for all power levels (including HZP) and operating modes. The limit ensures there is sufficient negative reactivity following a reactor trip, under credible operating conditions, to shut the reactor down and prevent exceeding the SAFDLs.

Allowable deviations due to misaligned CRAs are controlled by the technical specifications. The allowance for CRA misalignment is based on the uncertainty in the rod position indication system. The acceptable analytical CRA misalignment is six steps and accounts for abnormal operating conditions of the rod position indication system.

The reactivity insertion during a reactor trip is determined from the CRA drop time and differential reactivity worth versus CRA position. The CRA position versus time of travel after rod release is provided in Figure 4.3-20. This curve is based on a calculation described in Section 4.2. The results from the CRA drop testing, described in Section 1.5.1, validate the use of the calculated trip curve shown in Figure 4.3-20 as a conservative basis for the CRA drop time. A more conservative bounding CRA drop time is used in the Chapter 15 analyses. The reactivity worth versus CRA position is calculated by a series of steady-state calculations at various CRA positions, assuming the CRAs are at the PDIL as the initial position in order to minimize the initial reactivity insertion rate. The CRA with the highest worth is assumed stuck out of the core, and the flux distribution is assumed to be skewed to the bottom of the core. The reactivity worth versus CRA position is provided in Figure 4.3-21.

Table 4.3-4 and Table 4.3-5 provide the CRA worth for the individual CRA that is stuck out of the core at HZP with the remaining CRAs starting from the all rods out or PDIL positions. Figure 4.3-22 through Figure 4.3-25 provide the differential and integral rod worth for the regulating bank at BOC, MOC, and EOC for various power levels.

The loss of CRA worth due to depletion of absorber material is negligible. A conservative calculation over a 20 effective full power year CRA lifetime demonstrates that less than 2.5 percent of the boron in the upper portion of the CRA is lost due to depletion. The silver-indium-cadmium in the lower portion of the CRA is also evaluated for a loss of worth because of depletion and shown to have an insignificant impact on the available worth of the CRAs over their lifetime. Typical reactor operation with the rods withdrawn from the core while at full power limits the potential for CRA absorber depletion. Rod worth is confirmed at the beginning of each cycle during start-up physics testing.

Pressurized water reactor (PWR) operating experience has identified a phenomenon associated with potential boron build-up on the fuel rods that could affect SDM. Build-up of boron in crud at the top of the core can cause the reactivity at the bottom of the core to increase. Such a redistribution of power adversely affects the worth of the CRAs. The uncertainty analysis of the CRA worth includes comparisons to operating data from existing PWRs. Also, constant monitoring of core AO and comparison of that offset to predicted values identifies build-up of boron on the cladding surface during operation. Further, post-irradiation examinations as described in Section 4.2 measure oxide build-up and crud deposition on the fuel rods to ensure boron deposits on the cladding do not adversely affect the rod worth.

4.3.2.6 Criticality of the Reactor During Refueling

Criticality during a refueling is prevented by maintaining an effective neutron multiplication factor (k_{eff}) of 0.95 or less at all times. Refueling is performed with CRAs inserted in the fuel assemblies. Calculation of the required boron concentration for refueling assumes the two highest worth CRAs are not inserted.

Criticality of fuel assemblies outside the reactor is precluded by adequate design of fuel transfer and storage facilities and by administrative control procedures. Additional discussion of fuel assembly criticality when removed from the reactor is provided in Section 9.1.1.

4.3.2.7 Stability

The reactor core is designed to ensure power oscillations that can result in conditions exceeding SAFDLs are not possible and can be readily detected and suppressed. The NPM is inherently stable with regard to power oscillations due to the overall negative reactivity coefficients at power. Therefore, only xenon-induced power distribution oscillations require evaluation. There are three potential modes of oscillations possible in PWRs - azimuthal, radial, and axial. Azimuthal oscillations are not likely because of the inherent size and symmetry of the core loading pattern. Radial and axial oscillations are evaluated at BOC and EOC for the equilibrium cycle.

The parameter used to characterize the stability of an oscillation is the stability index, which measures the rate of decay of the oscillation over the oscillation period. The rate at which the oscillation decreases is expressed by an exponential function of the form:

$$A(t) = A_0 e^{\alpha t} \qquad \text{Eq. 4.3-2}$$

where A(t) is the time dependent oscillation amplitude (1/hr), A_0 is the initial value, and t is time.

The oscillation stability index, α, is obtained using equation:

$$\alpha = \frac{1}{T}\ln\left(\frac{A^{n+1}}{A^{n}}\right) \qquad \text{Eq. 4.3-3}$$

where T is the oscillation period (in hours) and n is oscillation number.

A positive stability index indicates the oscillations are diverging and therefore, unstable. A negative stability index indicates the oscillations are converging, and therefore, stable. A stability index of zero indicates a neutrally stable oscillation.

There are two modes of xenon oscillation that are evaluated, axial and radial oscillations. The stability calculations are performed using the SIMULATE5 code at various times during the equilibrium cycle.

4.3.2.7.1 Axial Oscillations

The oscillations are initiated by inserting and then withdrawing the regulating bank from the PDIL after sufficient time elapses for xenon to redistribute in the core. The axial xenon oscillations are then observed. Stability calculations are performed at various times in core life from 25 percent to 100 percent power.

4.3.2.7.2 Radial Oscillations

Radial oscillations are initiated by instantaneously inserting a single CRA, which results in both radial and axial oscillations.

As shown in Table 4.3-6 for both axial and radial oscillations, the stability indices are negative (i.e., stable) and the NPM is stable with respect to xenon oscillations.

The ICIS continuously monitors power distribution in the core and allows prompt detection of an axial or radial xenon oscillation.

4.3.2.7.3 Stability Methodology Comparison with Experimental Data

As stated above, SIMULATE5 calculations are used to demonstrate the core is stable with respect to axial and radial xenon oscillations. The ability of SIMULATE5 to accurately predict xenon oscillations is dependent on the code's ability to accurately predict reactivity feedback effects, including Doppler and moderator temperature feedback. Validation of the SIMULATE5 code to accurately predict xenon transient behavior is performed by modeling xenon transient behavior from operating PWRs and comparing predictions against measured data (Reference 4.3-3). The code vendor, Studsvik Scandpower, compared SIMULATE5 predictions of transient xenon behavior from Westinghouse three-loop PWRs Ringhals-2, Ringhals-3, and Ringhals-4. The code was used to model load follow and coast down maneuvers, which demonstrated the ability of SIMULATE5 to accurately predict xenon

transients. The code is demonstrated to accurately predict moderator and fuel temperature reactivity effects for the core in Reference 4.3-2.

The ability of the code to predict xenon transient behavior for the NPM is demonstrated by the accurate predictions against measured data for operating PWRs and the accurate predictions of reactivity feedback effects for the core.

4.3.2.8 Neutron Fluence

The heavy neutron reflector, the core barrel, and the water annuli protect the vessel from radiation damage by attenuating neutrons originating in the core and gamma rays originating from both the core and structural components.

The Monte Carlo N-Particle transport code (MCNP6) version 1.0 (Reference 4.3-4) is used to perform the vessel fluence calculations. NuScale's fluence calculation methodology technical report (Reference 4.3-5) is used to calculate neutron fluence on the NPM pressure vessel and containment vessel.

4.3.3 Analytical Methods

The nuclear analysis is performed with the Studsvik Scandpower Core Management Software simulation tools. These simulation tools include the lattice physics code CASMO5, the linkage code CMSLINK5 for nuclear data library generation, and the core simulator code SIMULATE5 for power distribution and stability calculations. These codes and the modelling methodology are described in detail in Reference 4.3-2. The SIMULATE-3K code is used for transient core physics calculations and is described in detail in NuScale's rod ejection accident methodology topical report (Reference 4.3-6). In addition, the MCNP6 code is used to perform fluence calculations.

These codes are used to perform both steady-state and transient neutronic analyses of light water reactors for core design and input to safety analysis.

As described in Reference 4.3-2, the methodology for the design and analysis of a single core is independent of the presence of other NPMs. A conservative neutron flux attenuation analysis, which considers the barriers between modules (several feet of both borated water and concrete wall) confirms the neutron flux contributed by the next closest NPM operating at full power has an insignificant neutronic impact on the reactor core of a neighboring NPM.

CASMO5

CASMO5 is a multi-group transport theory physics code that uses two-dimensional methods of characteristics transport theory for fuel assembly analysis and isotopic depletion. Cross sections and group constants are generated based on a wide range of potential conditions and cover several hundred energy groups and isotopes. CASMO5 uses the ENDF/B-VII cross section library. CASMO5 calculates eigenvalue results, power and flux distributions, reaction rates, and flux discontinuity factors for

individual or multiple assemblies in two dimensions. Multi-group cross section and discontinuity factor data is required for the generation of a cross section library.

CMSLINK5

CMSLINK5 collects input generated by CASMO5 and compiles the data into a single binary library with functional dependencies represented in multi-dimensional matrices of data. The format of the library is readily available for downstream use in both SIMULATE5 and SIMULATE-3K.

SIMULATE5

SIMULATE5 performs steady-state three-dimensional reactor analysis using the multi-group nodal diffusion equation. Thermal-hydraulic capabilities are coupled to the neutronic solution and over depletion state points; neutronic and thermal-hydraulic iterations ensure convergence and agreement of operating conditions, nuclear data, power distributions, and assembly exposure. SIMULATE5 is used to perform core design and optimization, develop a neutronic characterization of the core by determining reactivity feedback coefficients and CRA worth, calculating axial and radial power and flux distributions, and calculation of other values required as input for safety analysis. Also, SIMULATE5 calculation results are used as input into the plant monitoring system.

SIMULATE-3K

SIMULATE-3K is used for transient reactor core analysis where a quasi-steady-state assumption is not valid. SIMULATE-3K has the same computational foundation as SIMULATE5 and requires a model that is initialized in SIMULATE5 as input, but has been extended for transient applications.

MCNP6

MCNP6 is a general-purpose code that can be used for neutron, photon, electron, or coupled neutron photon electron transport. The code treats an arbitrary three dimensional configuration of materials in geometric cells bounded by first and second degree surfaces and some special fourth-degree surfaces. Point-wise (continuous energy) cross section data are available with MCNP6. The MCNP6 code is a higher fidelity code than CASMO5/SIMULATE5 and is used for code-to-code comparisons of the CASMO5, CMSLINK, SIMULATE5 suite of codes in Reference 4.3-2.

4.3.4 References

4.3-1 NuScale Power, LLC, "Framatome Fuel and Structural Response Methodologies Applicability to NuScale," TR-108553-P-A, Revision 0.

4.3-2 NuScale Power, LLC, "Nuclear Analysis Codes and Methods Qualification," TR-0616-48793-P-A, Revision 1.

4.3-3 Krimer, M., G. Grandi, and M. Carlsson, "PWR Transient XENON Modeling and Analysis Using Studsvik CMS," Proceedings of 2010 LWR Fuel Performance/Top Fuel/WRFPM, Orlando, Florida, September 26-29, 2010.

4.3-4 Los Alamos National Laboratory, “Initial MCNP6 Release Overview - MCNP6 Version 1.0," LA-UR-13-22924.

4.3-5 NuScale Power, LLC, “Fluence Calculation Methodology and Results,” TR-118976-P, Revision 0.

4.3-6 NuScale Power, LLC, "Rod Ejection Accident Methodology," TR-0716-50350-P, Revision 2.

Table 4.3-1: NuScale Power Module Core Description

Parameter	Value
Core	
Core diameter (in.)	59.26
Active fuel height (in.)	78.74
Mass of UO_2 per foot of assembly (lb/ft)	117
Fuel Assemblies	
Number	37
Rod array	17x17
Fuel assembly length, excluding hold-down springs (in.)	94
Fuel assembly pitch (in.)	8.466
Fuel rod pitch (in.)	0.496
Number of spacer grids	5
Grid height (in.)	1.75
Number of fuel rods	264
Number of guide tubes	24
Number of instrumentation tubes	1
Fuel Rods	
Cladding material	M5®
Cladding outside diameter (in.)	0.374
Cladding inside diameter (in.)	0.326
Fill gas	helium
Fuel Pellets	
Density, % TD	96.5
Material	UO_2 (sintered)
Diameter (in.)	0.3195
Length (in.)	0.40
Control Rod Assemblies	
Number	16
Upper absorber material	boron carbide
Lower absorber material	silver-indium-cadmium
Cladding	304L stainless steel
Fill gas	helium
Burnable Absorbing Material	
Type	integral with fuel
Material	gadolinia (Gd_2O_3)
Number	Up to 32 per assembly

Table 4.3-2: Nuclear Design Parameters (for Equilibrium Cycle)

Core Average Linear Power (kw/ft)	3.9
Heat Flux Hot Channel Factor	2.196
Maximum Enthalpy Rise Hot Channel Factor	1.4
Reactivity Coefficients	
Doppler temperature coefficient ($/F, least negative)	2.1E-03
Doppler temperature coefficient ($/F, most negative)	-4.6E-03
MTC (HZP-hot full power (HFP), least negative) ($/F)[1]	0.010 to -0.010
MTC (HZP-HFP, most negative) ($/F)[1]	-0.060 to -0.140
Boron coefficient (pcm/ppm)	-10
Effective Delayed Neutron Fraction and Prompt Neutron Lifetime	
$ß_{eff}$ BOC	0.0064
$ß_{eff}$ EOC	0.0048
Prompt lifetime BOC (10^{-5}seconds)	3.0
Prompt lifetime EOC (10^{-5}seconds)	1.0
Control Rods	
CRA requirement	Table 4.3-3
Maximum ejected rod	Section 15.4.8
Bank Worth	Figure 4.3-22 through Figure 4.3-25
Boron Concentration Limits (ppm)	
Mode 1	1900
Mode 1 (equilibrium xenon)	1400
Reduction with fuel burnup	Figure 4.3-19
Mode 2	600
Mode 3	650
Design-basis refueling[2]	1900

[1] Figure 4.3-15 provides the moderator temperature coefficient as a function of power.

[2] No xenon is assumed for the design-basis refueling boron concentration calculation.

Table 4.3-3: Reactivity Requirements for Control Rods

	BOC	MOC	EOC
Control Rod Assembly Worth (pcm)			
Total available CRA worth (a)	14920	16305	16946
Power dependent insertion limits (b)	524	666	797
Worst rod stuck out (c)	6223	5802	6679
Subtotal (a-b-c=d)	8173	9837	9470
Reactivity Allowances and Uncertainties (pcm)			
Power defect (e)	3104	3967	6036
Uncertainty (g)	608	704	412
Shutdown Margin Available (d-e-g) (pcm)	4461	5166	3022

Table 4.3-4: Individual Control Rod Assembly Worth at Hot Zero Power from All Rods Out

Time	CRA Location	Worth (pcm)
BOC	Group 1	2390
	Group 2	6360
	Group 3	3605
	Group 4	3718
MOC	Group 1	2099
	Group 2	5687
	Group 3	6035
	Group 4	6163
EOC	Group 1	2153
	Group 2	5766
	Group 3	6953
	Group 4	7051

Table 4.3-5: Individual Control Rod Assembly Worth at Hot Zero Power from Power Dependent Insertion Limits

Time	CRA Location	Worth (pcm)
BOC	Group 1	1550
	Group 2	5446
	Group 3	3585
	Group 4	3697
MOC	Group 1	1122
	Group 2	4321
	Group 3	6020
	Group 4	6146
EOC	Group 1	600
	Group 2	3549
	Group 3	6908
	Group 4	7002

Table 4.3-6: Limiting Cycle-Specific Xenon Stability Indices

Orientation	Stability Index (hr^{-1})
Axial	-0.006
Radial	-0.002

Figure 4.3-1: Power Dependent Insertion Limits

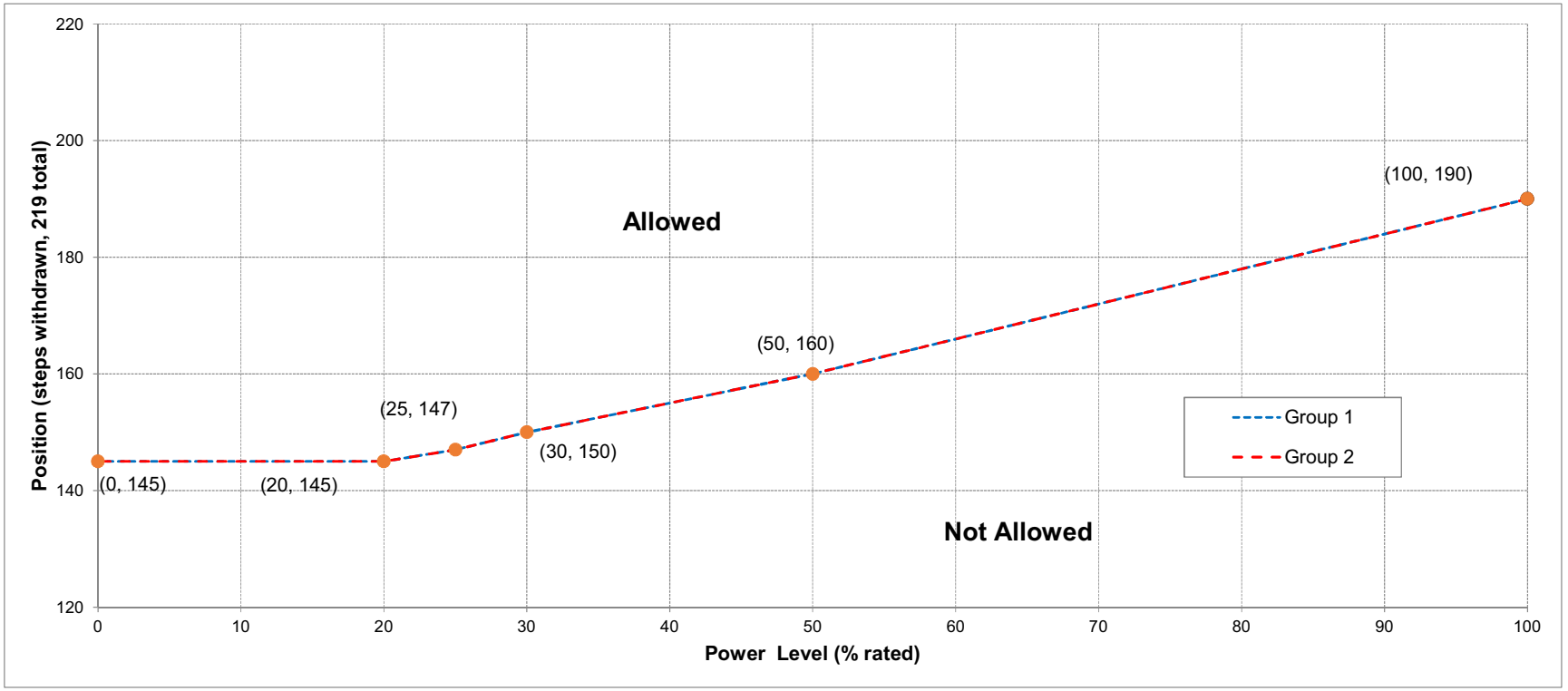

Figure 4.3-2: Fuel Loading Pattern for Reference Equilibrium Cycle

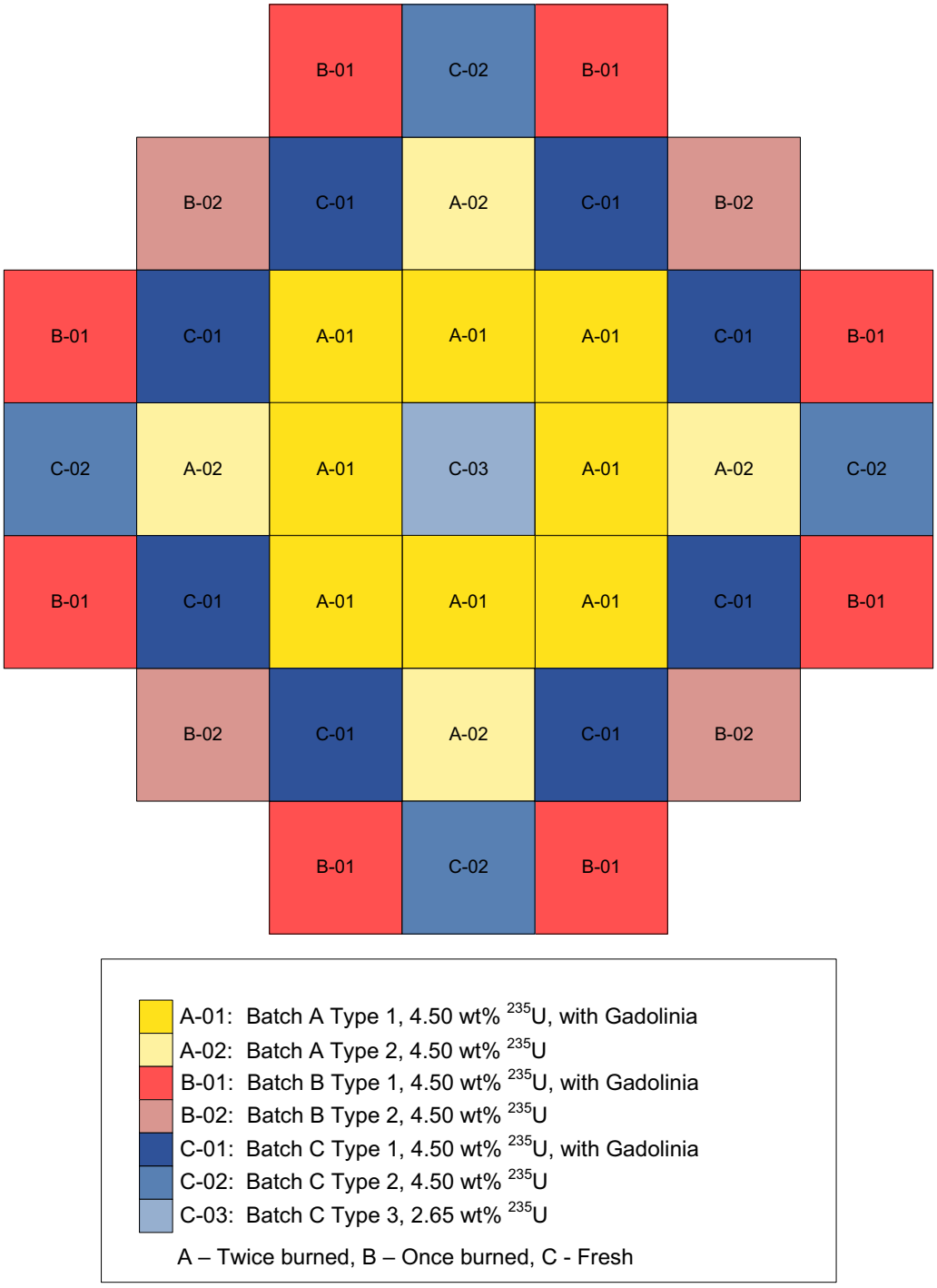

Figure 4.3-3: Shuffle Pattern for Reference Equilibrium Cycle

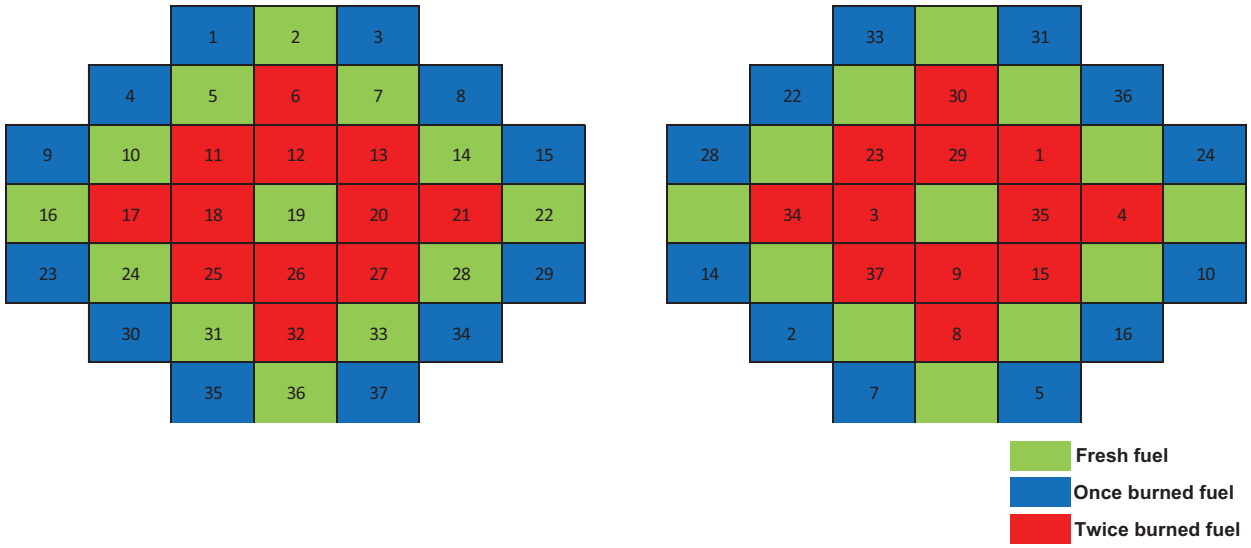

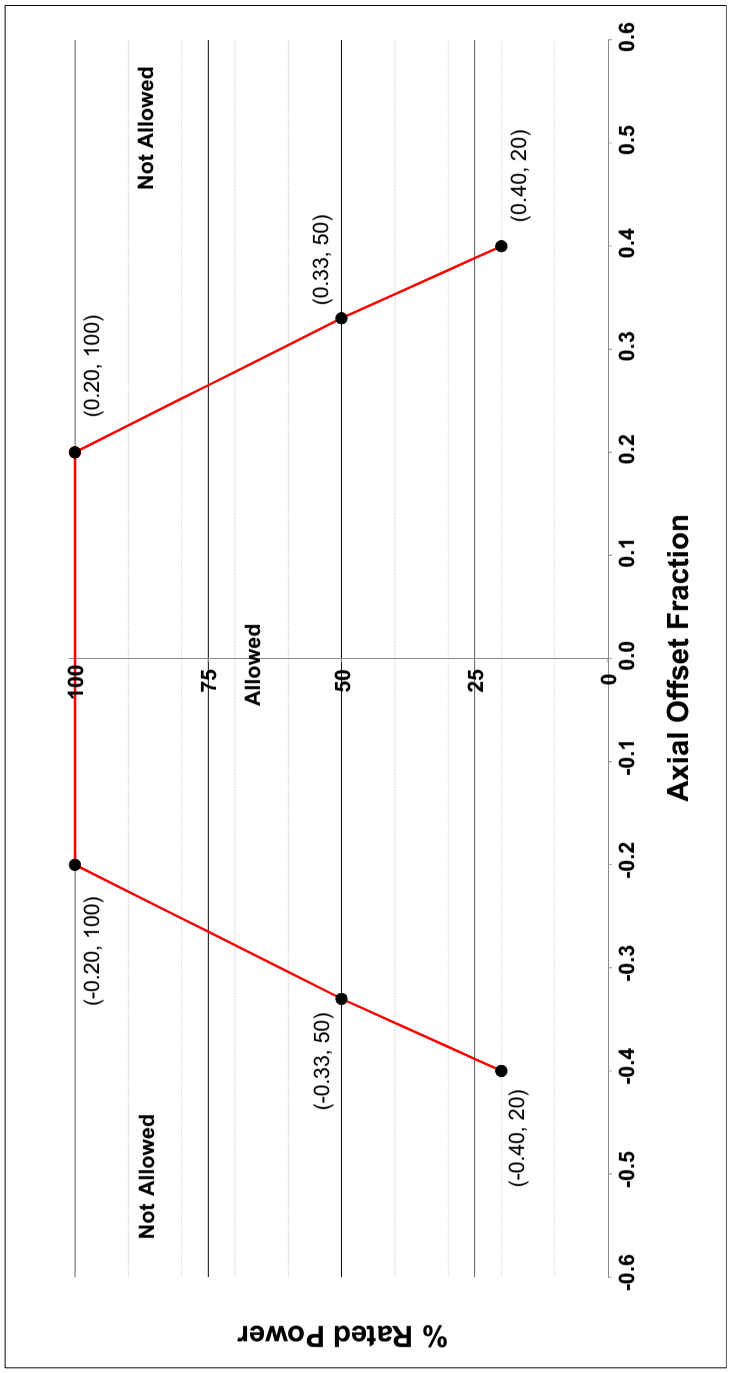

Figure 4.3-4: Axial Offset Window

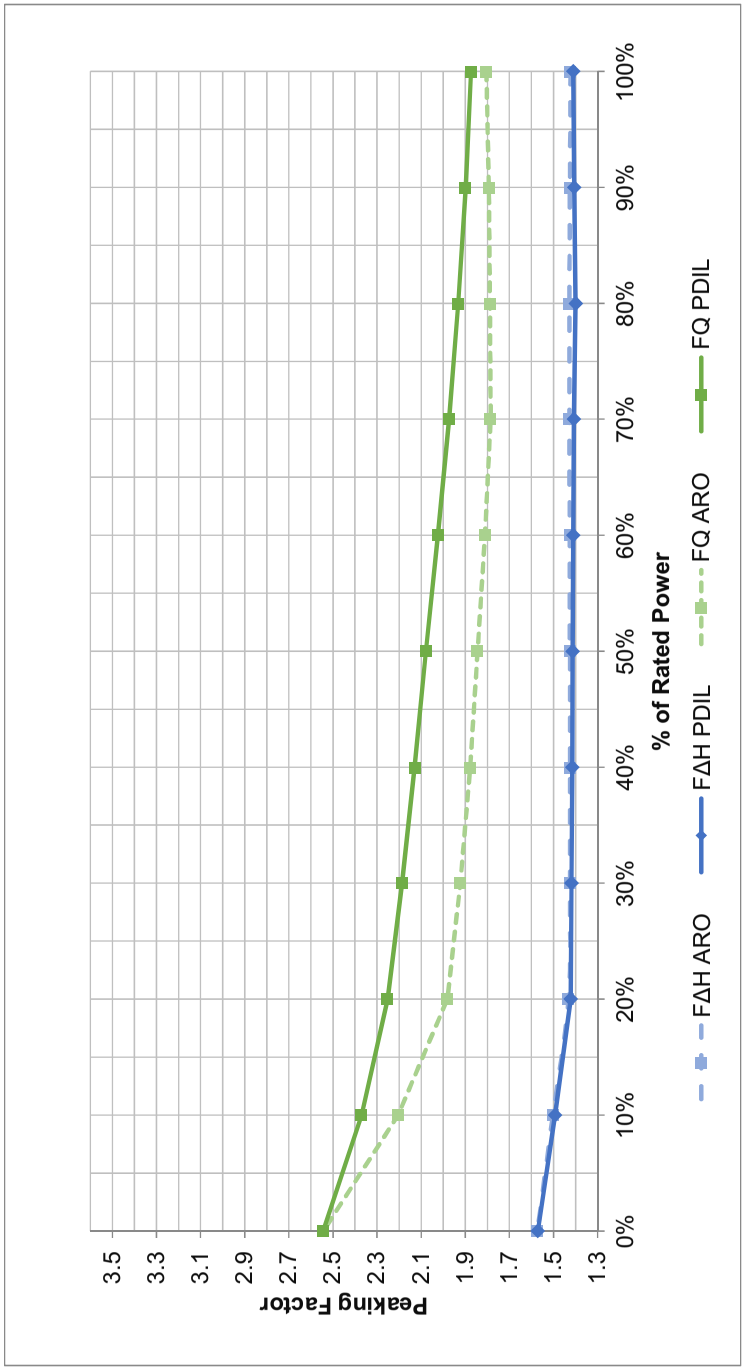

Figure 4.3-5: Power Peaking as a Function of Power Level and Rod Position at Beginning of Cycle

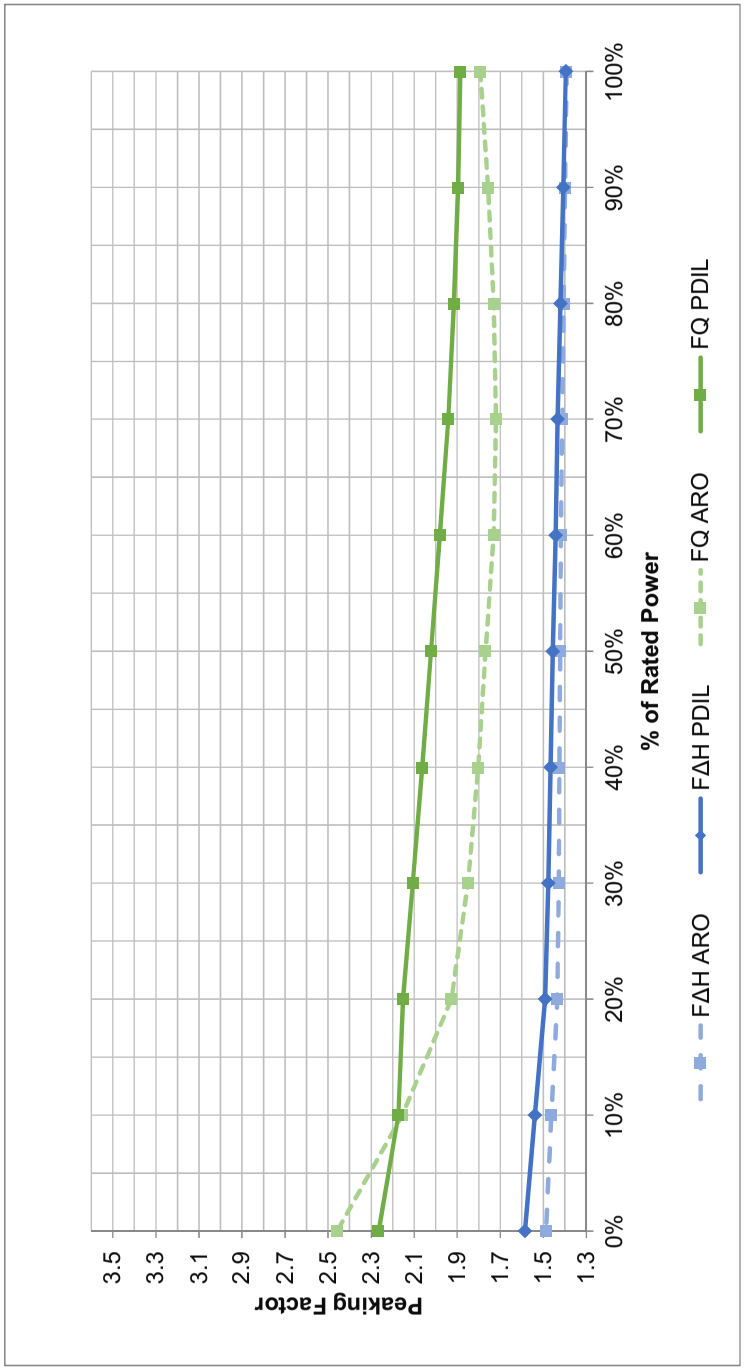

Figure 4.3-6: Power Peaking as a Function of Power Level and Rod Position at Middle of Cycle

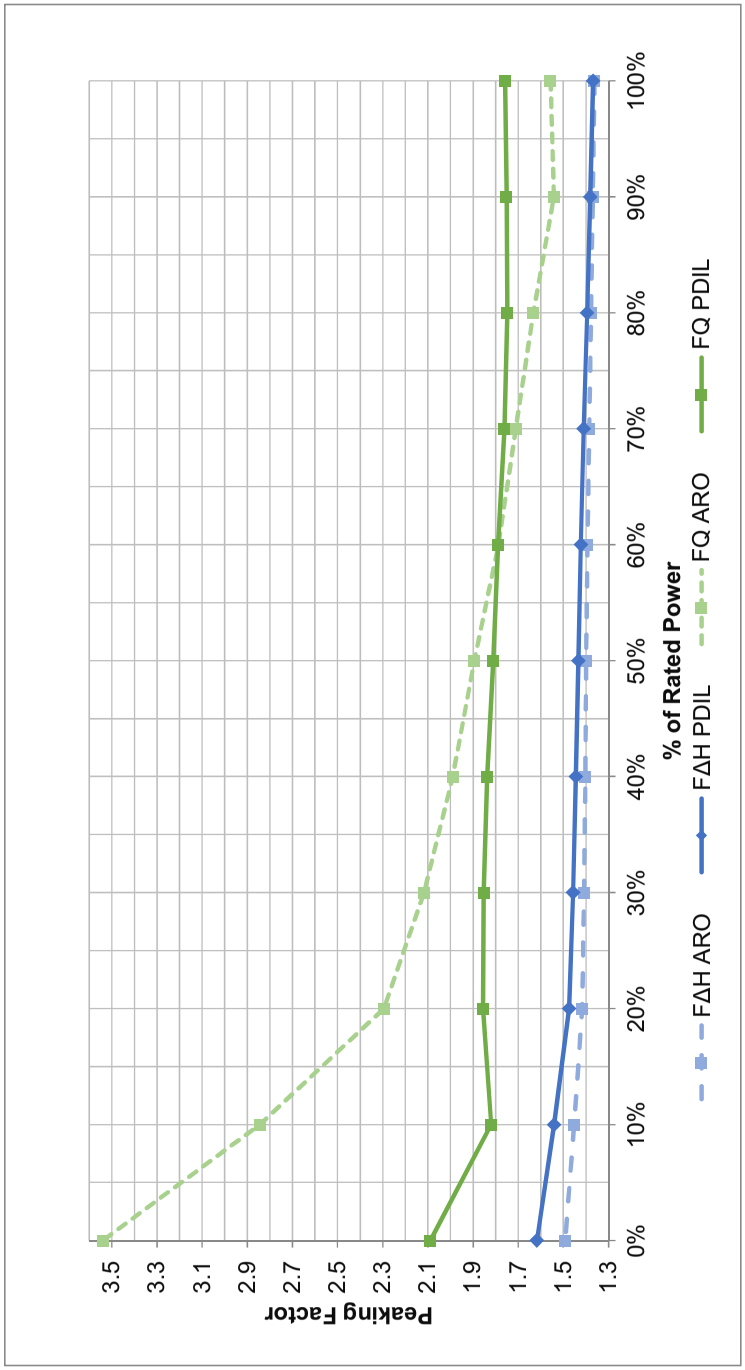

Figure 4.3-7: Power Peaking as a Function of Power Level and Rod Position at End of Cycle

Figure 4.3-8: Assembly Radial Power Distribution at Beginning, Middle, and End of Cycle

BOC

		0.747	1.134	0.742		
	0.809	1.101	1.095	1.097	0.809	
0.742	1.097	1.083	1.126	1.083	1.101	0.747
1.134	1.095	1.126	1.253	1.126	1.095	1.134
0.747	1.101	1.083	1.126	1.083	1.097	0.742
	0.809	1.097	1.095	1.101	0.809	
		0.742	1.134	0.747		

MOC

		0.746	1.048	0.742		
	0.862	1.246	1.051	1.243	0.862	
0.742	1.243	1.035	1.009	1.035	1.246	0.746
1.048	1.051	1.009	1.071	1.009	1.051	1.048
0.746	1.246	1.035	1.009	1.035	1.243	0.742
	0.862	1.243	1.051	1.246	0.862	
		0.742	1.048	0.746		

EOC

		0.756	1.027	0.753		
	0.868	1.246	1.044	1.245	0.868	
0.753	1.245	1.035	1.011	1.035	1.246	0.756
1.027	1.044	1.011	1.061	1.011	1.044	1.027
0.756	1.246	1.035	1.011	1.035	1.245	0.753
	0.868	1.245	1.044	1.246	0.868	
		0.753	1.027	0.756		

Figure 4.3-9: Typical Radial Relative Power Distribution for Central Assembly at Beginning and End of Equilibrium Cycle

Equilibrium Cycle, BOC, Central Assembly

1.02	1.05	1.08	1.10	1.12	1.13	1.14	1.14	1.15	1.14	1.14	1.13	1.12	1.10	1.08	1.05	1.02
1.05	1.10	1.14	1.18	1.21	1.24	1.23	1.23	1.25	1.23	1.23	1.25	1.21	1.18	1.14	1.10	1.05
1.08	1.14	1.21	1.28	1.30		1.31	1.31		1.31	1.31		1.30	1.28	1.21	1.14	1.08
1.10	1.18	1.28		1.35	1.35	1.32	1.32	1.35	1.32	1.32	1.35	1.35		1.28	1.18	1.10
1.12	1.21	1.30	1.35	1.35	1.37	1.34	1.34	1.37	1.34	1.34	1.37	1.35	1.35	1.30	1.21	1.12
1.13	1.25		1.35	1.37		1.38	1.39		1.39	1.38		1.37	1.35		1.24	1.13
1.14	1.23	1.31	1.32	1.34	1.38	1.36	1.36	1.39	1.36	1.36	1.38	1.34	1.32	1.31	1.23	1.14
1.14	1.23	1.31	1.32	1.34	1.39	1.36	1.36	1.40	1.36	1.36	1.39	1.34	1.32	1.31	1.23	1.14
1.15	1.25		1.35	1.37		1.39	1.40		1.40	1.39		1.37	1.35		1.25	1.15
1.14	1.23	1.31	1.32	1.34	1.39	1.36	1.36	1.40	1.36	1.36	1.39	1.34	1.32	1.31	1.23	1.14
1.14	1.23	1.31	1.32	1.34	1.38	1.36	1.36	1.39	1.36	1.36	1.38	1.34	1.32	1.31	1.23	1.14
1.13	1.24		1.35	1.37		1.38	1.39		1.39	1.38		1.37	1.35		1.25	1.13
1.12	1.21	1.30	1.35	1.35	1.37	1.34	1.34	1.37	1.34	1.34	1.37	1.35	1.35	1.30	1.21	1.12
1.10	1.18	1.28		1.35	1.35	1.32	1.32	1.35	1.32	1.32	1.35	1.35		1.28	1.18	1.10
1.08	1.14	1.21	1.28	1.30		1.31	1.31		1.31	1.31		1.30	1.28	1.21	1.14	1.08
1.05	1.10	1.14	1.18	1.21	1.25	1.23	1.23	1.25	1.23	1.23	1.24	1.21	1.18	1.14	1.10	1.05
1.02	1.05	1.08	1.10	1.12	1.13	1.14	1.14	1.15	1.14	1.14	1.13	1.12	1.10	1.08	1.05	1.02

Equilibrium Cycle, EOC, Central Assembly

0.99	0.99	0.99	1.01	1.02	1.02	1.03	1.03	1.03	1.03	1.03	1.03	1.02	1.01	1.00	0.99	0.99
0.99	0.99	1.00	1.02	1.04	1.06	1.05	1.05	1.07	1.05	1.05	1.06	1.04	1.02	1.00	0.99	0.99
0.99	1.00	1.03	1.07	1.08		1.08	1.08		1.08	1.08		1.08	1.07	1.03	1.00	1.00
1.01	1.02	1.07		1.11	1.10	1.09	1.08	1.10	1.08	1.09	1.10	1.11		1.07	1.02	1.01
1.02	1.04	1.08	1.11	1.10	1.10	1.09	1.08	1.10	1.08	1.09	1.10	1.10	1.11	1.08	1.04	1.02
1.03	1.06		1.10	1.10		1.11	1.11		1.11	1.11		1.10	1.10		1.06	1.03
1.03	1.05	1.08	1.09	1.09	1.11	1.10	1.10	1.11	1.10	1.10	1.11	1.09	1.09	1.08	1.05	1.03
1.03	1.05	1.08	1.08	1.08	1.11	1.10	1.09	1.11	1.09	1.10	1.11	1.08	1.08	1.08	1.05	1.03
1.03	1.07		1.10	1.10		1.11	1.11		1.11	1.11		1.10	1.10		1.07	1.03
1.03	1.05	1.08	1.08	1.08	1.11	1.10	1.09	1.11	1.09	1.10	1.11	1.08	1.08	1.08	1.05	1.03
1.03	1.05	1.08	1.09	1.09	1.11	1.10	1.10	1.11	1.10	1.10	1.11	1.09	1.09	1.08	1.05	1.03
1.03	1.06		1.10	1.10		1.11	1.11		1.11	1.11		1.10	1.10		1.06	1.03
1.02	1.04	1.08	1.11	1.10	1.10	1.09	1.08	1.10	1.08	1.09	1.10	1.10	1.11	1.08	1.04	1.02
1.01	1.02	1.07		1.11	1.10	1.09	1.08	1.10	1.08	1.09	1.10	1.11		1.07	1.02	1.01
1.00	1.00	1.03	1.07	1.08		1.08	1.08		1.08	1.08		1.08	1.07	1.03	1.00	0.99
0.99	0.99	1.00	1.02	1.04	1.06	1.05	1.05	1.07	1.05	1.05	1.06	1.04	1.02	1.00	0.99	0.99
0.99	0.99	1.00	1.01	1.02	1.03	1.03	1.03	1.03	1.03	1.03	1.02	1.02	1.01	0.99	0.99	0.99

Figure 4.3-10: Typical Radial Relative Power Distribution within a Batch 1 Fuel Assembly at Beginning and End of Equilibrium Cycle

BOC Batch 1

1.21	1.21	1.22	1.24	1.26	1.27	1.28	1.28	1.29	1.29	1.29	1.28	1.27	1.24	1.22	1.21	1.21
1.19	1.20	1.22	1.25	1.29	1.34	1.31	1.31	1.35	1.31	1.32	1.34	1.30	1.26	1.23	1.20	1.19
1.18	1.20	1.25	1.33	1.36		1.37	1.37		1.37	1.37		1.37	1.33	1.26	1.21	1.19
1.18	1.21	1.30		1.38	1.37	1.33	1.33	1.37	1.34	1.34	1.38	1.38		1.31	1.22	1.19
1.18	1.23	1.32	1.35	1.34	1.36	1.33	1.33	1.37	1.33	1.33	1.37	1.34	1.36	1.32	1.23	1.18
1.17	1.25		1.32	1.34		1.35	1.35		1.36	1.35		1.34	1.33		1.25	1.18
1.15	1.20	1.27	1.26	1.28	1.32	1.30	1.30	1.34	1.30	1.30	1.32	1.28	1.26	1.27	1.20	1.15
1.13	1.17	1.24	1.23	1.25	1.30	1.27	1.27	1.31	1.28	1.27	1.30	1.25	1.23	1.24	1.18	1.13
1.09	1.16		1.23	1.25		1.27	1.27		1.28	1.27		1.25	1.23		1.17	1.10
1.05	1.09	1.16	1.16	1.17	1.22	1.20	1.20	1.24	1.20	1.20	1.23	1.18	1.16	1.17	1.10	1.05
1.02	1.07	1.13	1.13	1.15	1.19	1.17	1.17	1.21	1.17	1.17	1.19	1.15	1.13	1.14	1.07	1.02
0.99	1.06		1.13	1.15		1.16	1.17		1.17	1.16		1.15	1.13		1.06	0.99
0.94	0.99	1.06	1.09	1.09	1.11	1.08	1.08	1.12	1.09	1.09	1.11	1.09	1.10	1.06	0.99	0.94
0.88	0.92	1.01		1.05	1.05	1.02	1.03	1.06	1.03	1.03	1.05	1.05		1.01	0.92	0.89
0.82	0.85	0.90	0.96	0.98		0.98	0.98		0.99	0.98		0.98	0.96	0.90	0.85	0.82
0.74	0.76	0.79	0.81	0.84	0.88	0.86	0.86	0.89	0.86	0.86	0.88	0.85	0.82	0.79	0.76	0.75
0.64	0.65	0.66	0.68	0.70	0.70	0.71	0.71	0.72	0.71	0.71	0.70	0.70	0.68	0.66	0.65	0.64

EOC Batch 1

1.18	1.16	1.17	1.18	1.19	1.20	1.20	1.20	1.21	1.20	1.21	1.20	1.19	1.18	1.17	1.17	1.18
1.15	1.13	1.14	1.16	1.19	1.22	1.20	1.20	1.22	1.20	1.20	1.22	1.19	1.16	1.15	1.14	1.15
1.13	1.13	1.15	1.20	1.23		1.22	1.22		1.22	1.22		1.23	1.20	1.16	1.13	1.14
1.12	1.12	1.18		1.22	1.22	1.19	1.18	1.21	1.18	1.19	1.22	1.23		1.18	1.13	1.13
1.12	1.13	1.19	1.21	1.19	1.20	1.18	1.17	1.20	1.17	1.18	1.20	1.19	1.21	1.19	1.14	1.12
1.11	1.14		1.18	1.18		1.18	1.18		1.18	1.18		1.18	1.18		1.14	1.11
1.08	1.09	1.13	1.12	1.13	1.16	1.14	1.14	1.16	1.14	1.14	1.16	1.13	1.12	1.13	1.10	1.08
1.06	1.07	1.11	1.10	1.11	1.14	1.12	1.12	1.14	1.12	1.12	1.14	1.11	1.10	1.11	1.08	1.06
1.03	1.06		1.09	1.10		1.11	1.11		1.11	1.11		1.10	1.09		1.06	1.03
0.99	1.00	1.04	1.03	1.04	1.07	1.05	1.05	1.07	1.05	1.05	1.07	1.04	1.03	1.04	1.00	0.99
0.96	0.98	1.02	1.01	1.02	1.05	1.03	1.03	1.05	1.03	1.03	1.05	1.02	1.01	1.02	0.98	0.97
0.93	0.97		1.01	1.01		1.02	1.02		1.02	1.02		1.01	1.01		0.97	0.93
0.88	0.90	0.95	0.97	0.96	0.97	0.95	0.95	0.97	0.95	0.95	0.97	0.96	0.97	0.95	0.90	0.88
0.84	0.85	0.91		0.94	0.94	0.91	0.91	0.94	0.91	0.92	0.94	0.94		0.92	0.85	0.84
0.78	0.78	0.82	0.86	0.87		0.87	0.87		0.87	0.87		0.87	0.86	0.82	0.78	0.78
0.71	0.71	0.73	0.75	0.77	0.79	0.78	0.78	0.80	0.78	0.78	0.79	0.77	0.75	0.73	0.71	0.71
0.62	0.62	0.62	0.64	0.65	0.65	0.66	0.66	0.67	0.66	0.66	0.65	0.65	0.64	0.62	0.62	0.62

Figure 4.3-11: Typical Radial Relative Power Distribution within a Batch 2 Fuel Assembly at Beginning and End of Equilibrium Cycle

BOC Batch 2

1.22	1.15	1.11	1.10	1.08	1.07	1.06	1.03	1.01	0.98	0.96	0.93	0.90	0.87	0.83	0.78	0.70
1.18	1.10	1.07	1.07	1.06	1.07	1.04	1.01	1.00	0.95	0.93	0.92	0.88	0.83	0.78	0.72	0.64
1.16	1.09	1.07	1.10	1.09		1.04	1.01		0.96	0.93		0.89	0.84	0.77	0.69	0.59
1.15	1.09	1.10		1.08	1.06	1.01	0.97	0.97	0.92	0.90	0.89	0.87		0.78	0.68	0.57
1.15	1.09	1.10	1.10	1.04	1.03	0.99	0.95	0.94	0.90	0.87	0.87	0.84	0.81	0.76	0.67	0.56
1.14	1.10		1.07	1.03		0.99	0.95		0.89	0.87		0.82	0.78		0.66	0.54
1.12	1.06	1.05	1.02	0.99	0.99	0.95	0.91	0.90	0.86	0.83	0.82	0.78	0.74	0.71	0.64	0.53
1.11	1.05	1.03	1.00	0.96	0.96	0.92	0.89	0.88	0.83	0.80	0.79	0.75	0.71	0.69	0.61	0.51
1.09	1.04		1.00	0.96		0.92	0.88		0.82	0.79		0.74	0.70		0.60	0.49
1.06	1.00	0.98	0.95	0.91	0.91	0.87	0.84	0.83	0.78	0.75	0.74	0.70	0.66	0.63	0.56	0.46
1.04	0.98	0.97	0.93	0.90	0.89	0.85	0.82	0.80	0.76	0.73	0.72	0.67	0.64	0.61	0.54	0.45
1.02	0.98		0.94	0.89		0.84	0.81		0.75	0.72		0.67	0.63		0.53	0.42
0.99	0.93	0.92	0.91	0.86	0.84	0.80	0.77	0.75	0.70	0.68	0.67	0.64	0.61	0.57	0.50	0.41
0.95	0.89	0.89		0.84	0.81	0.77	0.73	0.72	0.68	0.65	0.64	0.62		0.55	0.47	0.40
0.91	0.83	0.81	0.82	0.79		0.74	0.71		0.65	0.62		0.58	0.55	0.50	0.44	0.37
0.85	0.77	0.73	0.72	0.70	0.69	0.66	0.64	0.62	0.57	0.55	0.54	0.51	0.48	0.44	0.40	0.34
0.78	0.68	0.63	0.61	0.59	0.56	0.56	0.53	0.51	0.48	0.46	0.43	0.42	0.40	0.37	0.34	0.30

EOC Batch 2

1.19	1.14	1.12	1.12	1.10	1.10	1.09	1.07	1.05	1.02	1.00	0.98	0.95	0.92	0.87	0.83	0.76
1.16	1.12	1.11	1.11	1.10	1.11	1.08	1.06	1.05	1.01	0.99	0.98	0.94	0.90	0.84	0.79	0.71
1.16	1.12	1.11	1.13	1.13		1.09	1.07		1.02	1.00		0.95	0.91	0.84	0.77	0.68
1.15	1.12	1.13		1.12	1.10	1.07	1.04	1.03	0.99	0.97	0.96	0.93		0.84	0.75	0.65
1.16	1.13	1.14	1.14	1.10	1.09	1.05	1.02	1.01	0.97	0.95	0.94	0.91	0.88	0.83	0.75	0.64
1.15	1.14		1.11	1.08		1.04	1.02		0.96	0.94		0.88	0.85		0.73	0.61
1.14	1.11	1.10	1.08	1.05	1.04	1.01	0.98	0.97	0.93	0.91	0.89	0.85	0.81	0.77	0.71	0.61
1.12	1.09	1.08	1.06	1.03	1.03	0.99	0.96	0.95	0.91	0.89	0.87	0.83	0.79	0.75	0.69	0.59
1.11	1.09		1.05	1.02		0.98	0.95		0.89	0.87		0.81	0.78		0.67	0.56
1.08	1.05	1.04	1.01	0.98	0.97	0.94	0.91	0.89	0.85	0.83	0.81	0.76	0.73	0.69	0.63	0.53
1.07	1.04	1.03	1.00	0.97	0.96	0.93	0.90	0.88	0.83	0.81	0.79	0.75	0.72	0.68	0.61	0.52
1.05	1.03		1.00	0.96		0.91	0.88		0.82	0.79		0.73	0.70		0.60	0.49
1.01	0.98	0.98	0.97	0.92	0.90	0.86	0.84	0.81	0.77	0.75	0.73	0.70	0.68	0.63	0.57	0.48
0.99	0.95	0.95		0.91	0.88	0.84	0.81	0.79	0.75	0.72	0.71	0.68		0.62	0.54	0.46
0.94	0.89	0.87	0.88	0.85		0.80	0.77		0.71	0.69		0.63	0.62	0.56	0.50	0.42
0.89	0.83	0.80	0.78	0.77	0.76	0.73	0.70	0.68	0.64	0.62	0.61	0.57	0.54	0.50	0.45	0.39
0.83	0.75	0.70	0.68	0.67	0.64	0.63	0.60	0.58	0.54	0.53	0.50	0.48	0.46	0.43	0.39	0.34

Figure 4.3-12: Typical Radial Relative Power Distribution within a Batch 3 Fuel Assembly at Beginning and End of Equilibrium Cycle

BOC Batch 3

1.11	1.10	1.11	1.11	1.12	1.13	1.13	1.13	1.13	1.13	1.13	1.14	1.13	1.13	1.12	1.14	1.20
1.07	1.05	1.06	1.06	1.08	1.10	1.08	1.09	1.10	1.09	1.10	1.11	1.09	1.09	1.08	1.10	1.16
1.06	1.04	1.06	1.07	1.09		1.08	1.08		1.09	1.10		1.11	1.11	1.09	1.09	1.15
1.07	1.05	1.08		1.10	1.09	1.08	1.08	1.09	1.08	1.10	1.11	1.12		1.12	1.10	1.16
1.06	1.06	1.09	1.09	1.08	1.08	1.07	1.07	1.08	1.08	1.09	1.10	1.10	1.13	1.12	1.12	1.17
1.07	1.08		1.09	1.09		1.08	1.09		1.09	1.11		1.11	1.13		1.14	1.18
1.07	1.07	1.08	1.07	1.08	1.09	1.07	1.08	1.09	1.08	1.10	1.11	1.09	1.11	1.12	1.12	1.18
1.07	1.07	1.08	1.07	1.07	1.08	1.07	1.08	1.09	1.08	1.09	1.10	1.09	1.11	1.11	1.13	1.18
1.06	1.07		1.07	1.07		1.07	1.08		1.08	1.10		1.09	1.11		1.13	1.17
1.05	1.05	1.06	1.05	1.05	1.06	1.05	1.06	1.07	1.06	1.07	1.09	1.07	1.09	1.09	1.11	1.16
1.05	1.05	1.06	1.06	1.06	1.07	1.06	1.07	1.08	1.07	1.08	1.09	1.08	1.10	1.10	1.11	1.17
1.05	1.06		1.07	1.08		1.08	1.08		1.08	1.10		1.09	1.12		1.12	1.17
1.04	1.04	1.07	1.08	1.08	1.08	1.07	1.07	1.08	1.07	1.09	1.10	1.09	1.12	1.11	1.10	1.15
1.05	1.04	1.07		1.10	1.10	1.08	1.08	1.10	1.09	1.10	1.12	1.12		1.11	1.10	1.16
1.05	1.03	1.05	1.08	1.10		1.09	1.10		1.10	1.11		1.11	1.12	1.08	1.09	1.15
1.06	1.05	1.05	1.07	1.09	1.11	1.10	1.11	1.12	1.11	1.12	1.13	1.11	1.10	1.08	1.10	1.16
1.10	1.09	1.10	1.11	1.13	1.14	1.14	1.15	1.15	1.15	1.16	1.16	1.14	1.14	1.13	1.14	1.20

EOC Batch 3

1.04	1.04	1.04	1.04	1.05	1.05	1.05	1.05	1.05	1.05	1.06	1.06	1.06	1.06	1.06	1.07	1.09
1.01	1.01	1.02	1.02	1.04	1.04	1.03	1.04	1.05	1.04	1.05	1.06	1.05	1.04	1.04	1.05	1.07
1.01	1.01	1.02	1.04	1.05		1.04	1.04		1.04	1.05		1.06	1.07	1.05	1.04	1.07
1.02	1.02	1.04		1.06	1.05	1.04	1.04	1.05	1.04	1.05	1.06	1.07		1.07	1.06	1.08
1.02	1.03	1.05	1.05	1.05	1.04	1.03	1.04	1.04	1.04	1.05	1.06	1.06	1.09	1.08	1.07	1.09
1.02	1.04		1.05	1.05		1.04	1.05		1.05	1.06		1.06	1.08		1.09	1.09
1.03	1.03	1.05	1.04	1.04	1.05	1.04	1.04	1.05	1.04	1.06	1.06	1.06	1.07	1.08	1.08	1.09
1.03	1.03	1.04	1.04	1.04	1.04	1.03	1.04	1.05	1.04	1.05	1.06	1.05	1.07	1.07	1.08	1.09
1.02	1.04		1.04	1.04		1.04	1.04		1.05	1.06		1.06	1.08		1.08	1.09
1.02	1.03	1.04	1.03	1.03	1.04	1.03	1.04	1.04	1.04	1.05	1.05	1.05	1.06	1.07	1.07	1.09
1.02	1.03	1.04	1.04	1.04	1.04	1.04	1.04	1.05	1.04	1.05	1.06	1.05	1.07	1.07	1.07	1.09
1.02	1.03		1.04	1.04		1.04	1.04		1.04	1.06		1.06	1.08		1.08	1.09
1.01	1.02	1.04	1.04	1.04	1.04	1.03	1.03	1.04	1.03	1.04	1.05	1.05	1.08	1.07	1.06	1.08
1.01	1.01	1.03		1.05	1.04	1.03	1.03	1.04	1.04	1.05	1.06	1.06		1.06	1.05	1.07
0.99	0.99	1.01	1.03	1.04		1.03	1.03		1.03	1.04		1.05	1.06	1.03	1.03	1.06
0.99	0.99	1.00	1.00	1.02	1.03	1.02	1.03	1.03	1.03	1.04	1.04	1.03	1.03	1.02	1.03	1.06
1.01	1.00	1.01	1.01	1.02	1.02	1.02	1.03	1.03	1.03	1.03	1.03	1.03	1.03	1.02	1.04	1.06

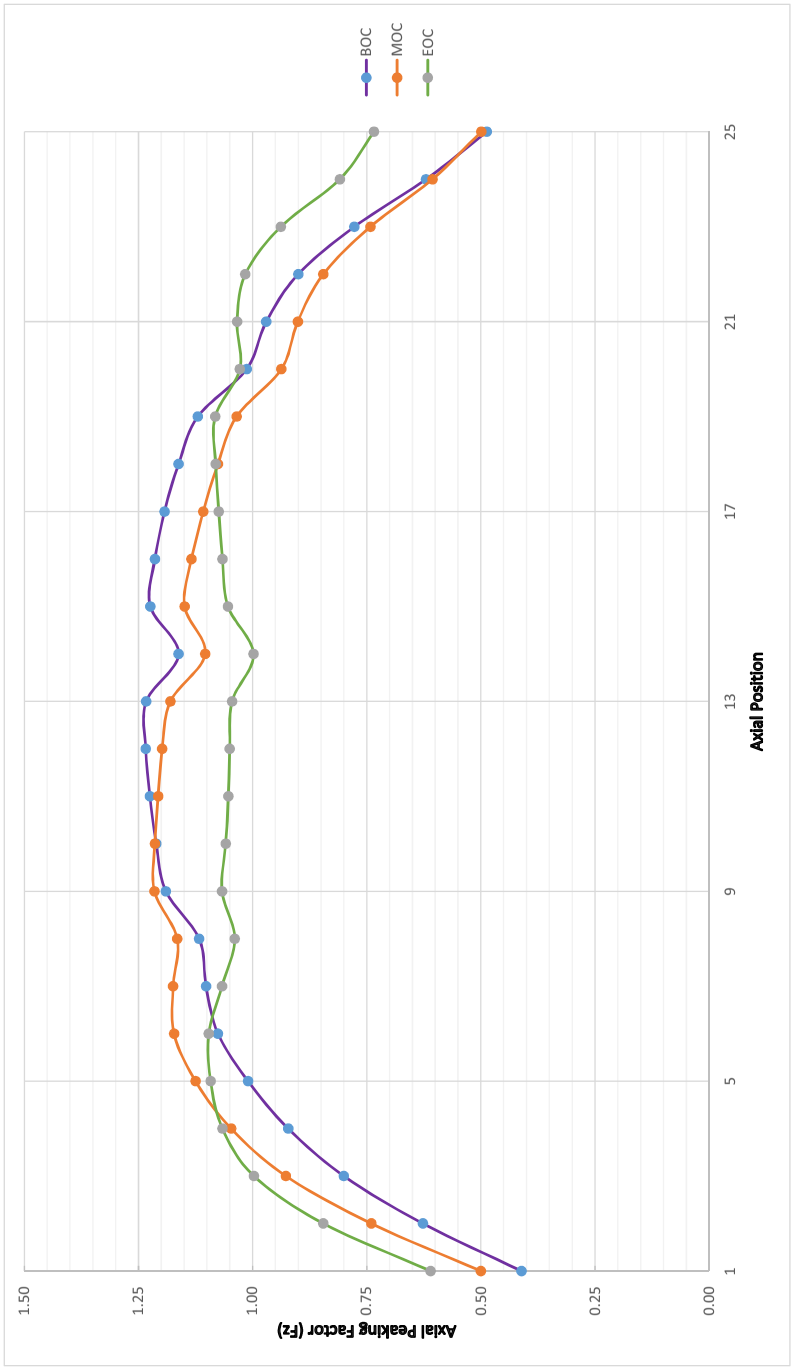

Figure 4.3-13: Axial Power Distribution at Beginning, Middle, and End of Cycle

Figure 4.3-14: Control Rod and In-Core Instrument Locations

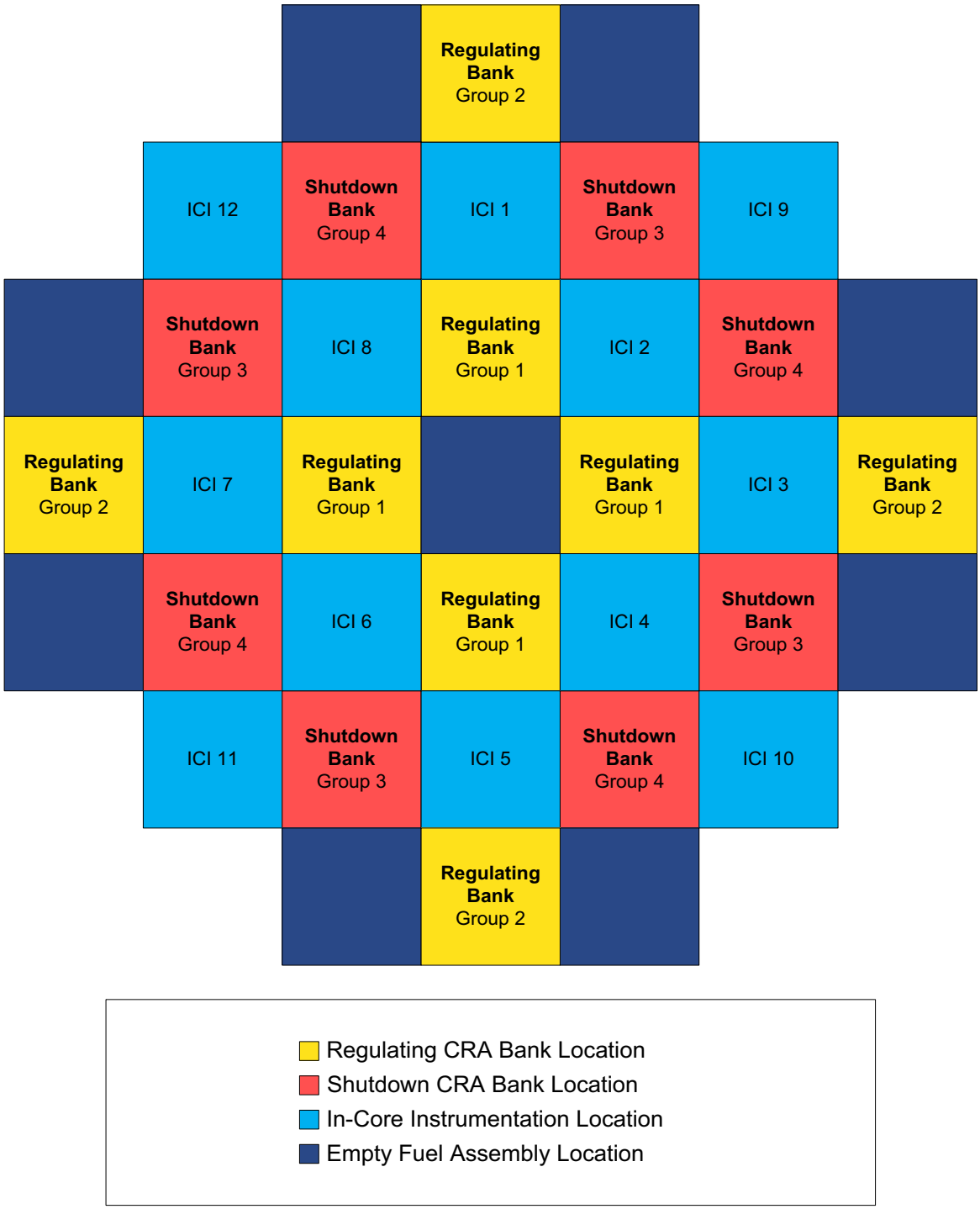

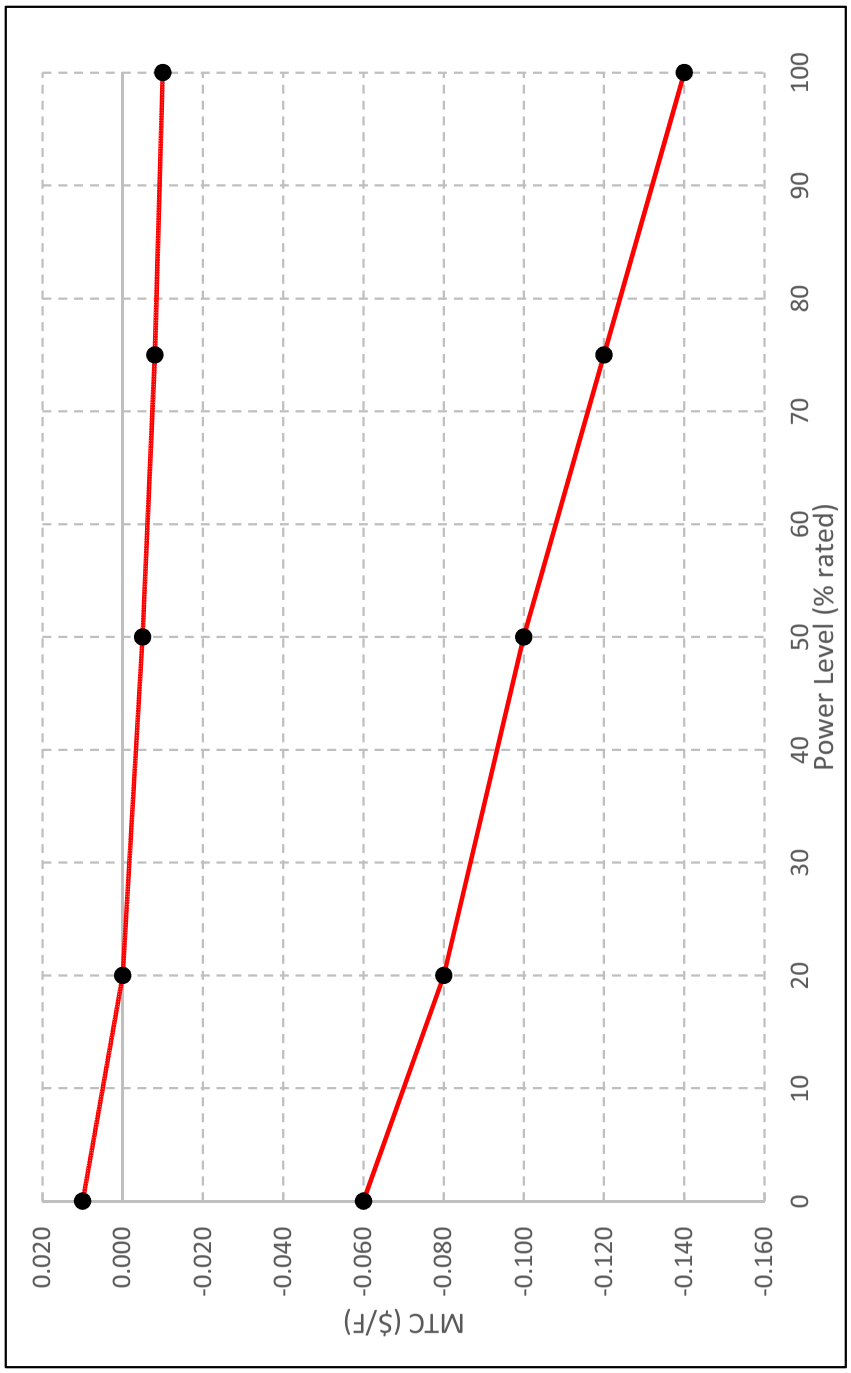

Figure 4.3-15: Moderator Temperature Coefficient of Reactivity from Zero to Full Power

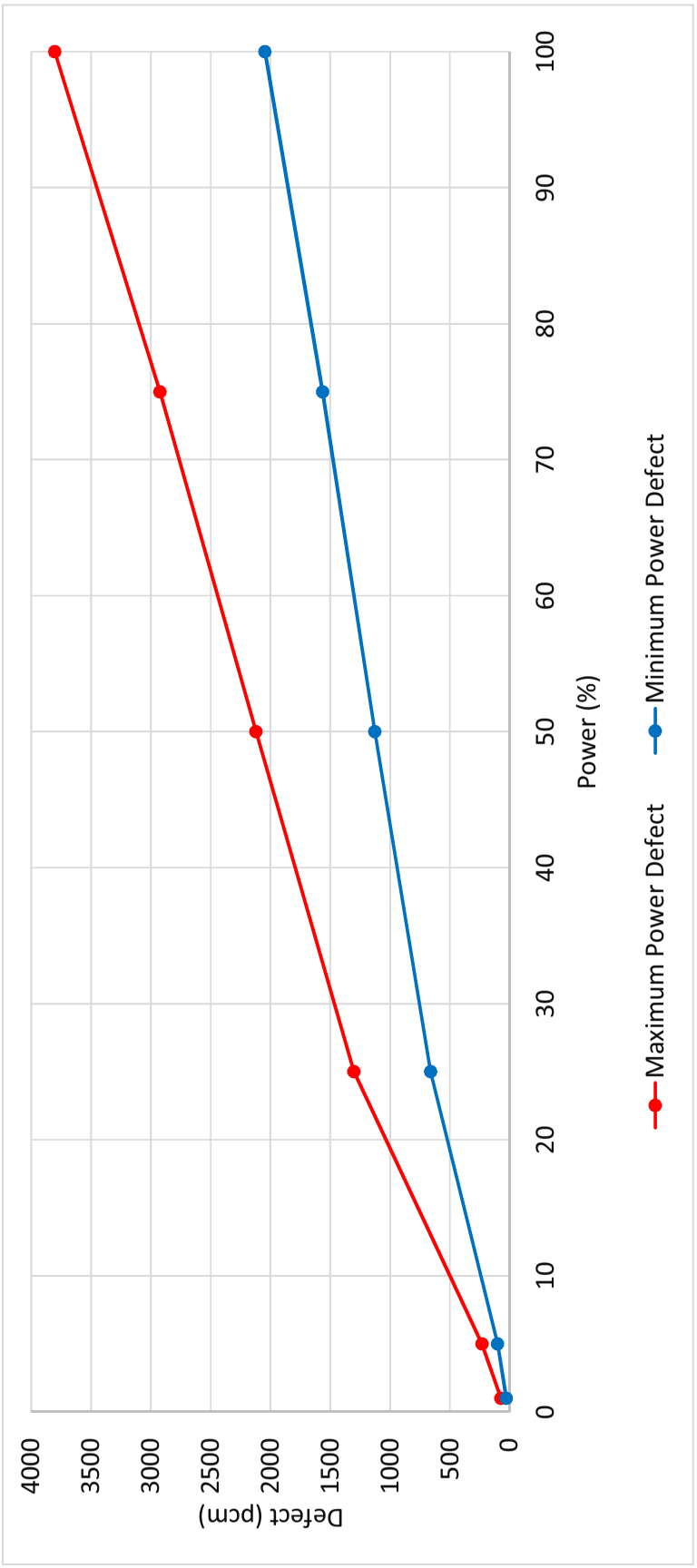

Figure 4.3-16: Maximum and Minimum Power Defect

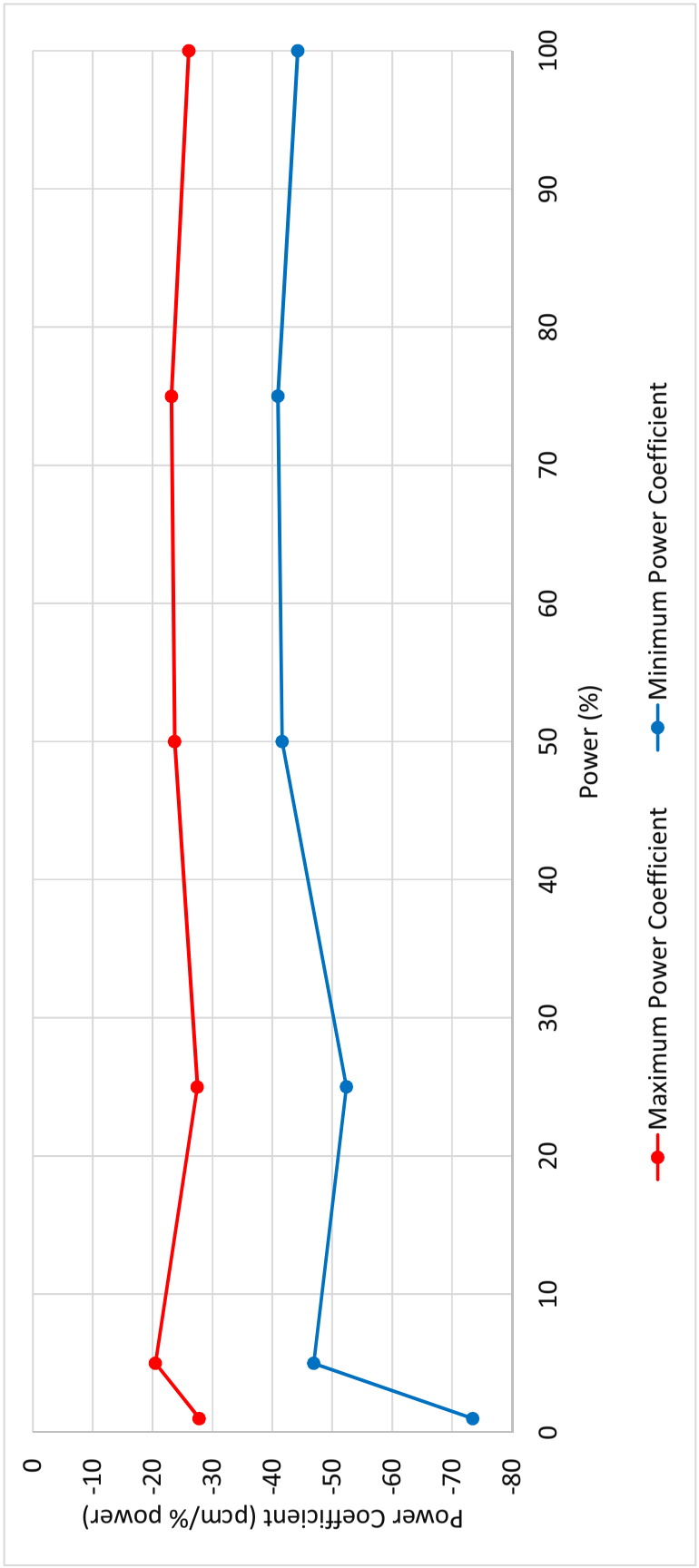

Figure 4.3-17: Maximum and Minimum Power Coefficient

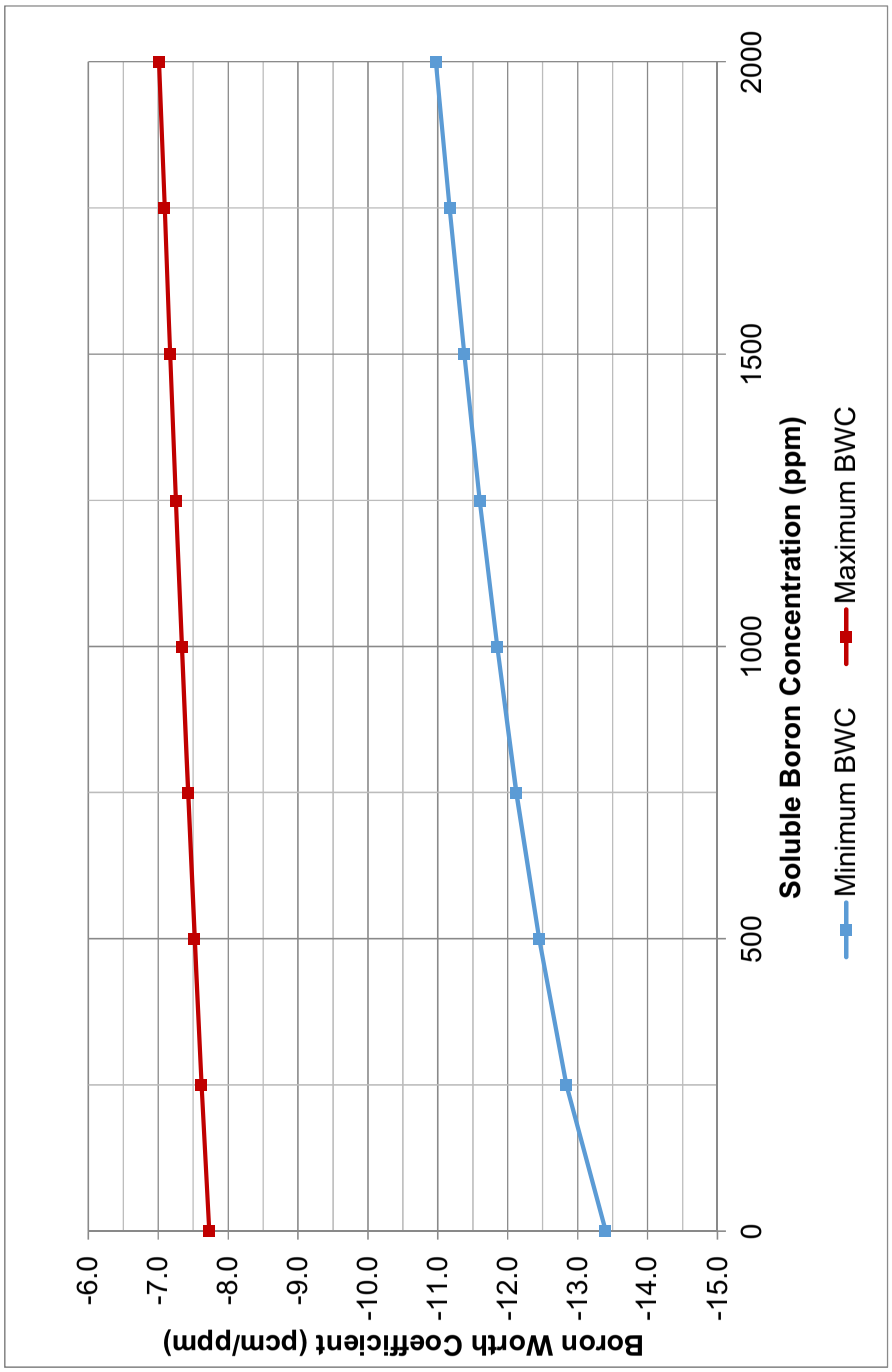

Figure 4.3-18: Differential Boron Worth Coefficient

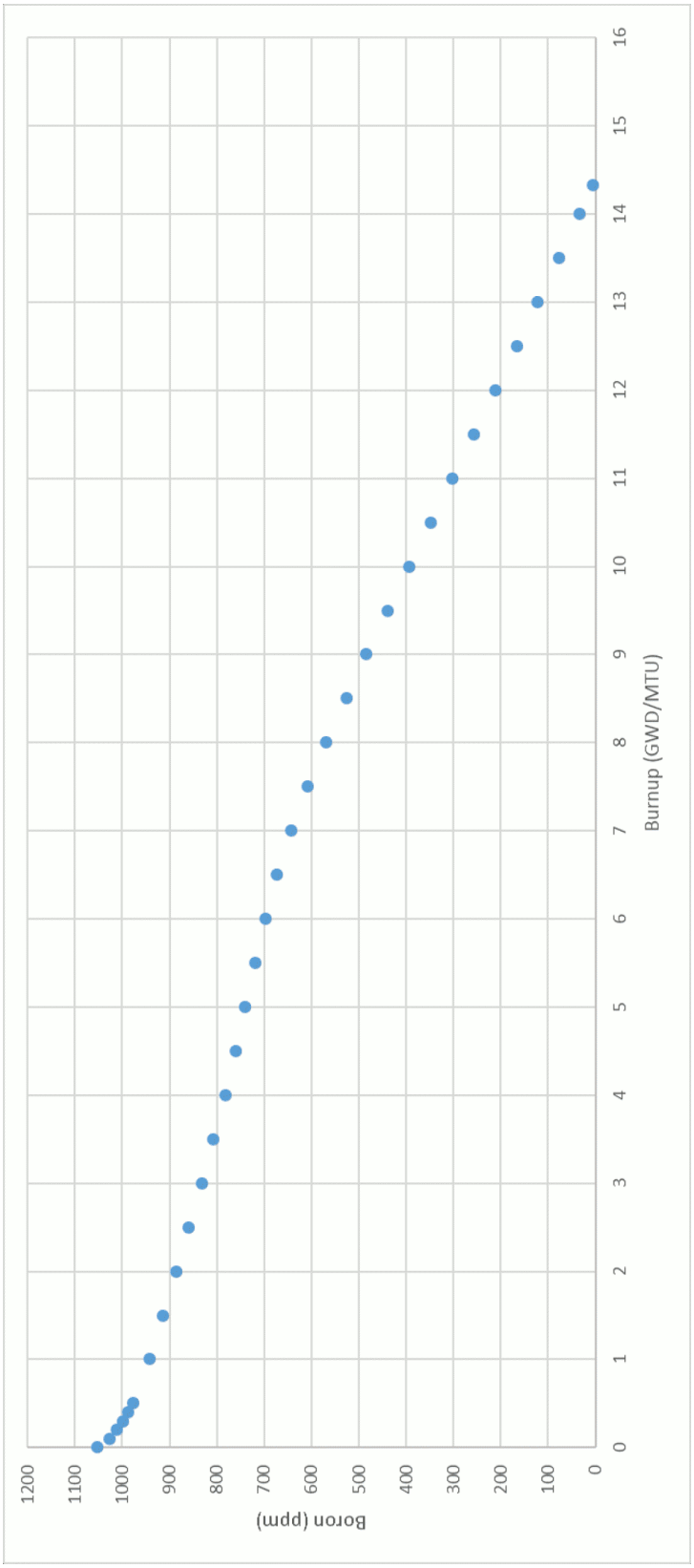

Figure 4.3-19: Boron Letdown Curve for Equilibrium Cycle

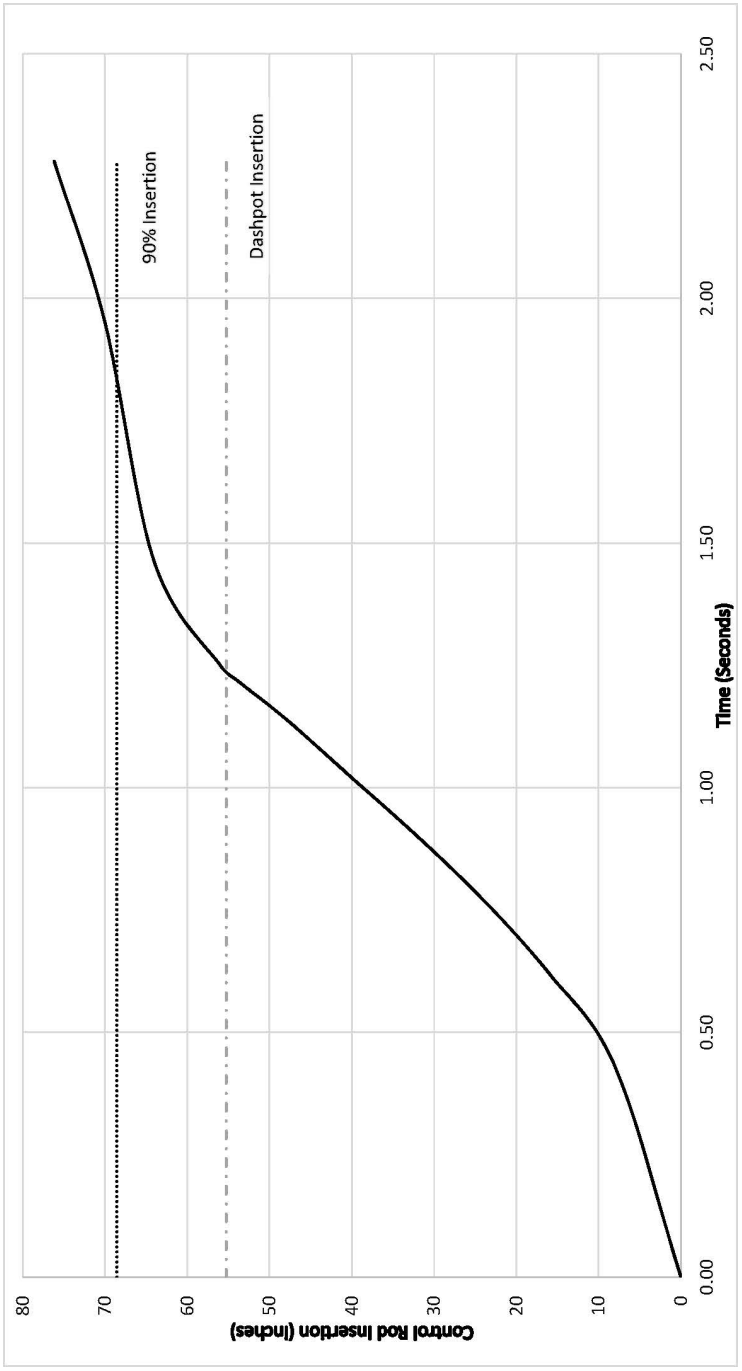

Figure 4.3-20: Control Rod Position versus Time after Trip

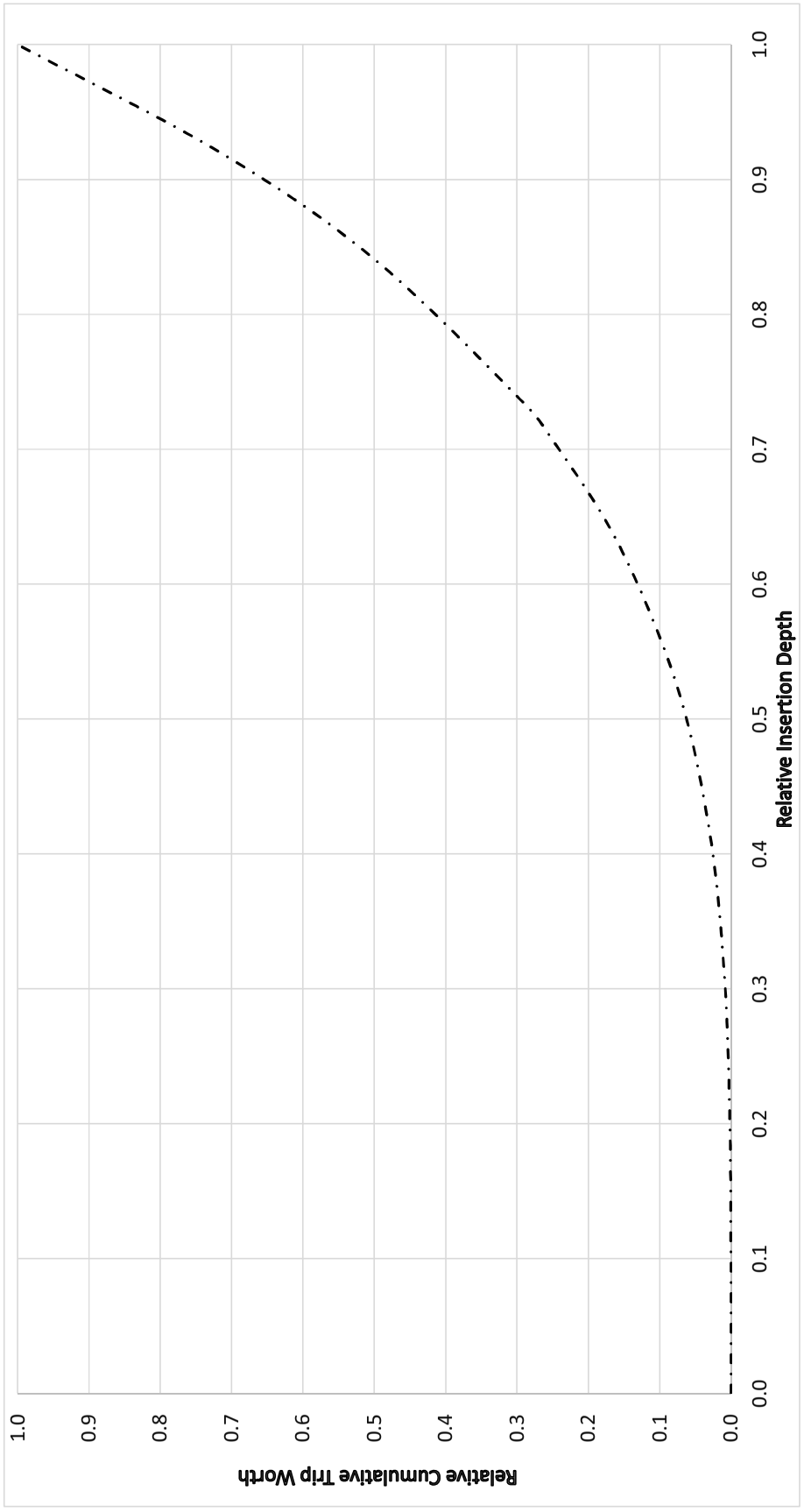

Figure 4.3-21: Reactivity Worth versus Control Rod Position

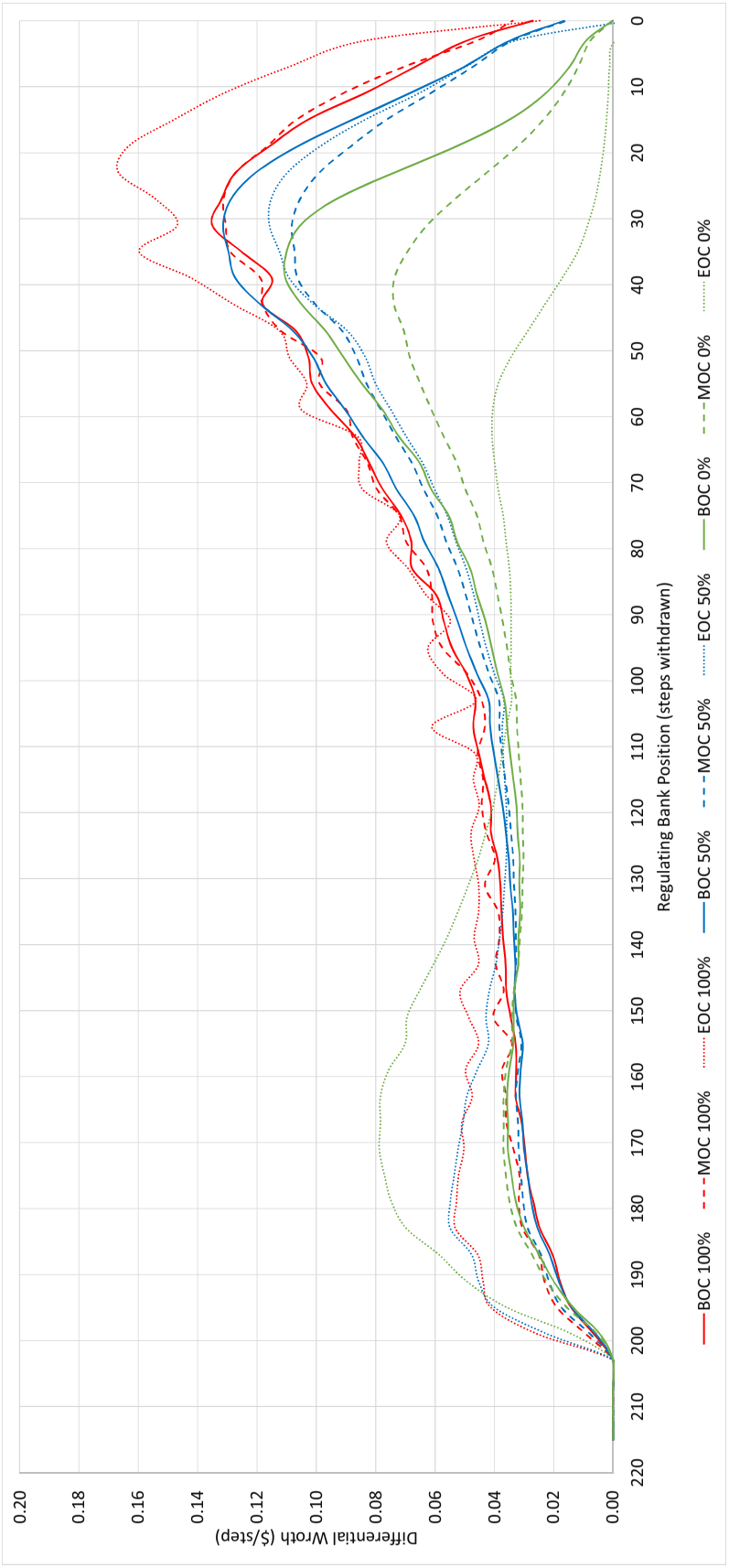

Figure 4.3-22: Differential Rod Worth for Regulating Bank from All Rods Out

Figure 4.3-23: Integral Rod Worth for Regulating Bank from All Rods Out

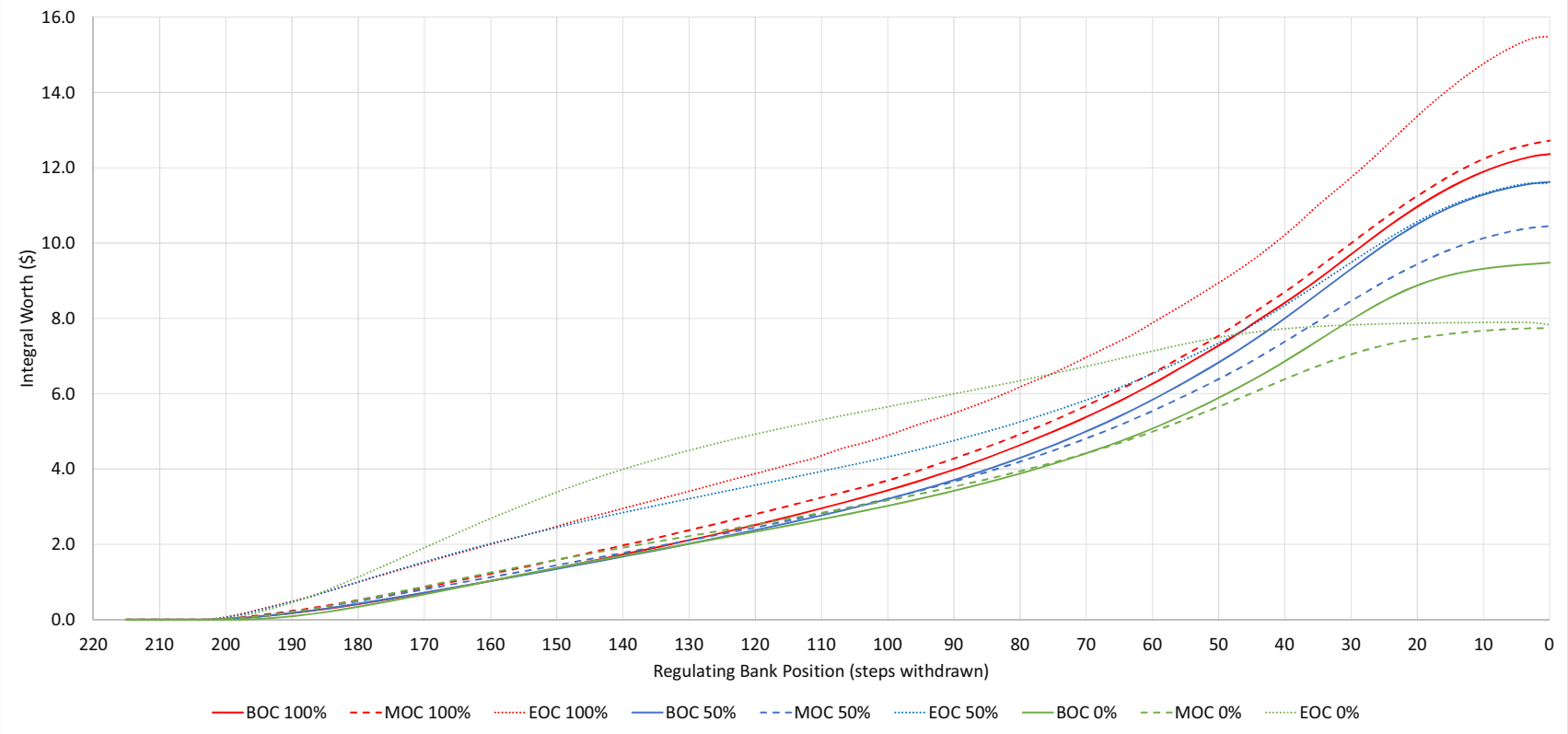

Figure 4.3-24: Differential Rod Worth for Regulating Bank from Power Dependent Insertion Limits

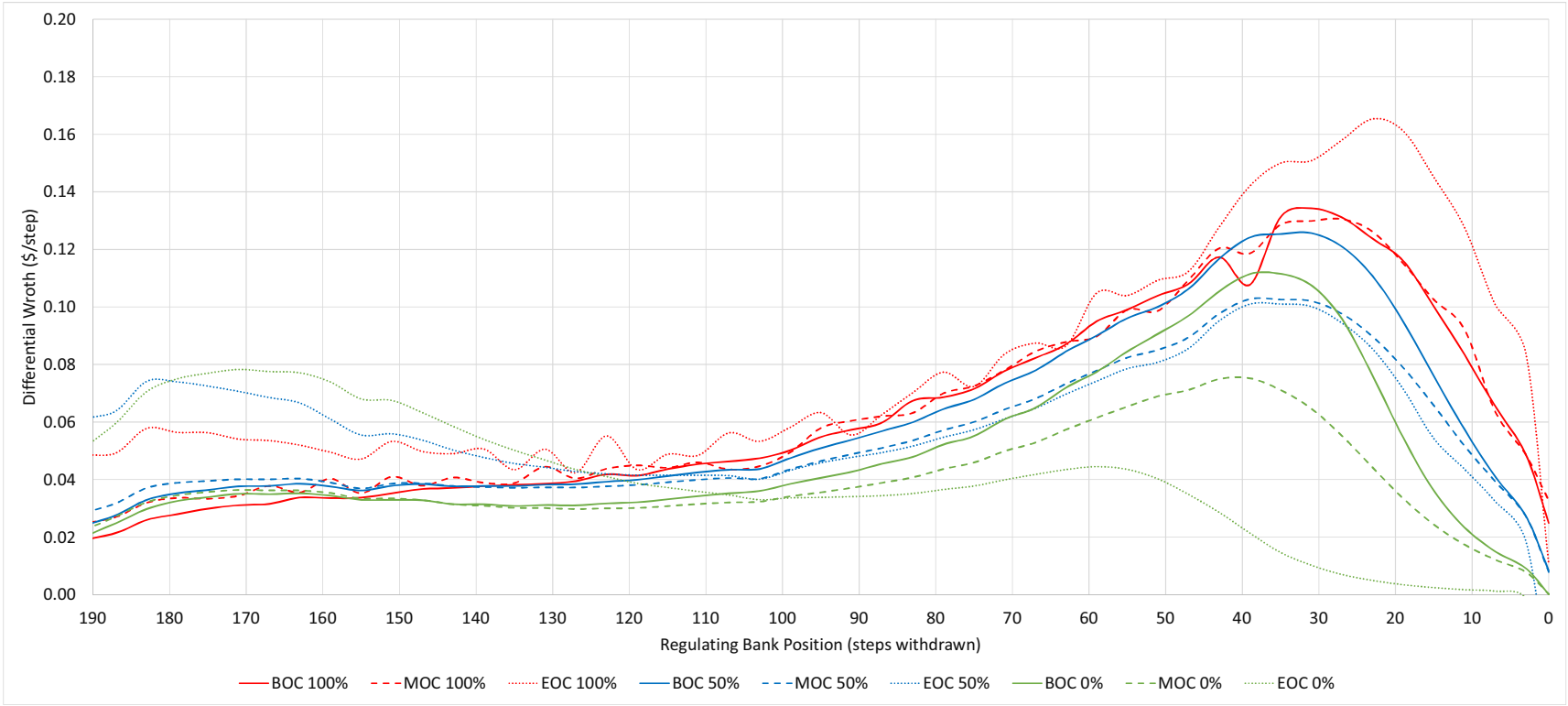

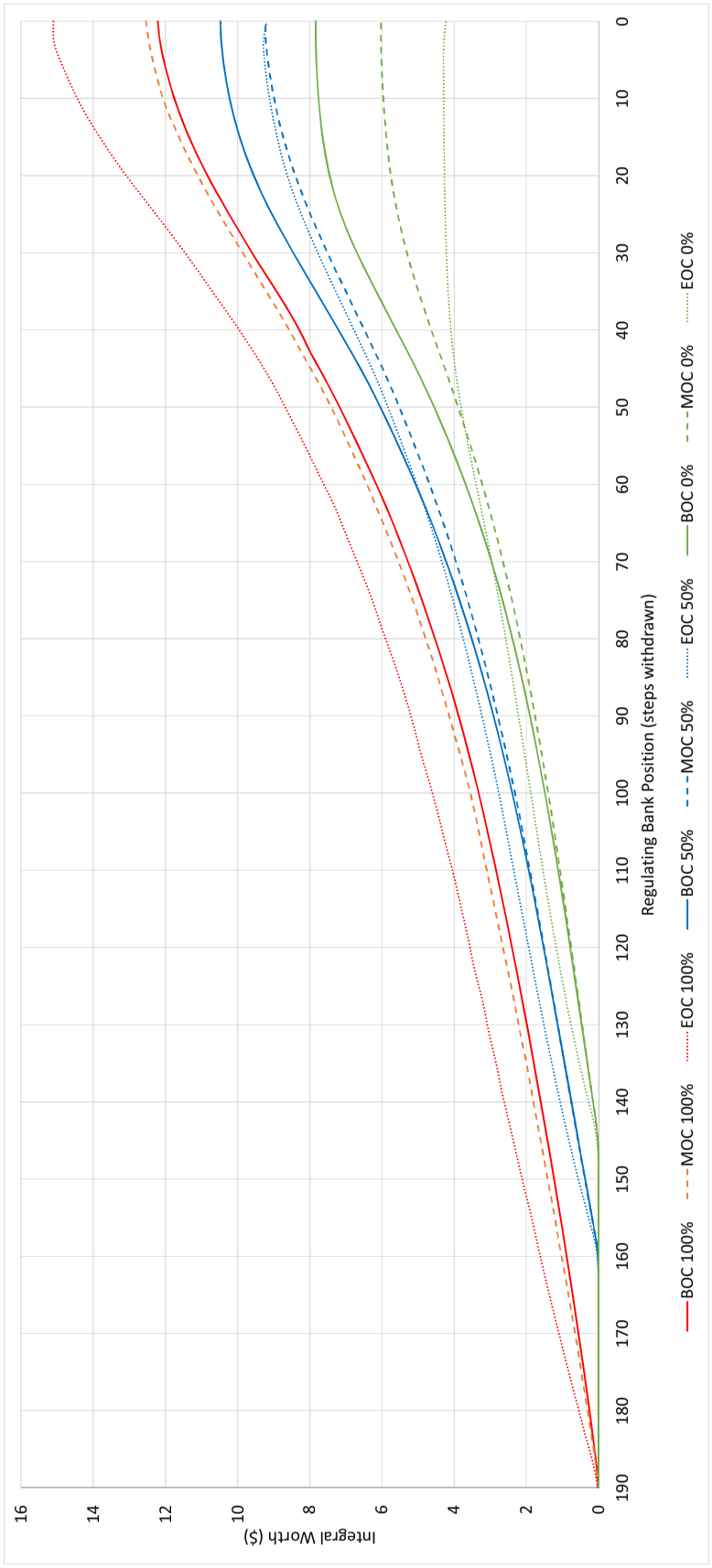

Figure 4.3-25: Integral Rod Worth for Regulating Bank from Power Dependent Insertion Limits

4.4 Thermal and Hydraulic Design

This section describes the thermal-hydraulic design of the NuScale Power Module (NPM) including the design bases (Section 4.4.1), description of the thermal-hydraulic design of the reactor core (Section 4.4.2) and reactor coolant system (RCS) (Section 4.4.3), description of the analytical methods and evaluations performed for the NPM (Section 4.4.4), the testing and verification performed to confirm analytical predictions (Section 4.4.5), the instrumentation that supports maintaining thermal-hydraulic design bases (Section 4.4.6), and flow stability as it relates to the NPM (Section 4.4.7).

4.4.1 Design Bases

Consistent with General Design Criterion (GDC) 10, the thermal-hydraulic design of the reactor core includes sufficient margin to critical heat flux (CHF) to ensure adequate heat transfer with a 95 percent probability at a 95 percent confidence (95/95) level so that specified acceptable fuel design limits (SAFDLs) are not exceeded during any condition of normal operation, including the effects of anticipated operational occurrences (AOOs) and conditions.

Consistent with GDC 12, the thermal-hydraulic design of the core includes design and operational limits that preclude power instability such that fuel design limits are not exceeded.

The design bases for the mechanical design of the fuel are discussed in Section 4.2.1. The instrumentation and controls system design features that address the monitoring requirements in GDC 13 and the protection system requirements in GDC 20 are described in Section 7.1.

4.4.1.1 Critical Heat Flux

Adequate heat transfer from the fuel cladding to the reactor coolant is provided by assuring that CHF limits are met during normal operation, AOOs, and infrequent events (IEs). NuScale-specific CHF correlations are used to ensure CHF does not occur with a 95/95 assurance level during normal operation and abnormal operating occurrences. For accidents, a small number of rods may be predicted to exceed CHF limits as long as the applicable radiological consequence requirements are met as analyzed in Chapter 15.

4.4.1.2 Fuel Temperature

For normal operation and AOOs, the fuel melting temperature is not exceeded. Analyses are performed at rated power and during transients up to the design limit burnup.

4.4.1.3 Core Flow

Flow through the core considers applicable uncertainties on a 95/95 basis. The treatment of uncertainties also considers the uncertainty on core bypass flow that accounts for flow through the fuel assembly guide tubes, instrument tubes, and the reflector block cooling channels, as discussed in Section 4.4.3.1.

4.4.1.4 Stability

Normal operation and AOO events do not lead to hydrodynamic instability as discussed in Section 4.4.7.

4.4.2 Thermal and Hydraulic Design of the Reactor Core

The NPM is a natural circulation pressurized water reactor (PWR) with integral, once-through, helical coil steam generators (SGs). Natural circulation flow rate varies with power. As a result, there is a unique steady-state flow at each power level.

Table 4.4-1 and the Subchannel Analysis Methodology topical report (Reference 4.4-1) as supplemented by Reference 4.4-2 discuss the relevant parameters for the thermal-hydraulic evaluation of core performance of the NPM.

4.4.2.1 Critical Heat Flux

Margin for protecting the fuel cladding overheating SAFDL is established by an analysis limit that accounts for testing uncertainties, manufacturing tolerances, and operational variations, such as rod bow, measurement uncertainties, and instrumentation delays. Figure 4.4-1 provides an example depiction of the NSP4 critical heat flux ratio (CHFR) limits and thermal margins.

For subchannel analysis, clad overheating can occur in off-nominal conditions, such as AOOs, IEs, and accidents. Fuel rod cladding integrity can be challenged when the heat transfer coefficient between the fuel rod clad and coolant degrades significantly because of the formation of a continuous vapor layer on the fuel rod. The degradation of the heat transfer coefficient in a two-phase flow condition is dependent on local conditions such as pressure, flow rate, coolant quality, and boiling regime. Various terms are used to describe this phenomenon, including CHF, departure from nucleate boiling, critical power ratio, boiling crisis, boiling transition, burnout, and dryout. For consistency in modeling the range of NuScale-specific phenomena, NuScale thermal margin analyses use the generic term CHF.

The parameter of interest for preventing the occurrence of CHF is the ratio of the CHF to local heat flux, or CHFR:

$$CHFR = q''_{CHF} / q''_{local} \qquad \text{Eq. 4.4-1}$$

where

q''_{CHF} = critical heat flux, and

q''_{local} = local heat flux.

Several test programs were conducted to obtain CHF test data. These programs culminated in the development of CHF correlations applicable to the NPM range

of conditions. Additional details on the CHF correlation development is provided in Section 4.4.2.5.

The CHFR design limit for the NSP4 correlation that corresponds to a 95/95 assurance level is 1.21. The NSP4 critical heat flux correlation is used to evaluate thermal margin for normal operation, AOOs, IEs, and accidents, with the exception of those characterized by rapid depressurization. Events exhibiting a rapid depressurization are evaluated using the NSPN-1 and industry-developed CHF correlations described in Reference 4.4-3. The CHFR design limit for the NSPN-1 correlation that corresponds to a 95/95 assurance level is discussed in Reference 4.4-3.

The range of applicability of the NSP4 critical heat flux correlation is contained in Reference 4.4-4, and the ranges of applicability of the NSPN-1 and industry-developed critical heat flux correlations are contained in Reference 4.4-3.

The transient response of the reactor system is dependent on the initial power distribution. Limits provided by the core design and the module protection system (MPS) ensure the NPM meets CHF design bases for AOOs. The technical specifications define the cycle-specific enthalpy rise hot channel factor and axial offset (AO) limits that must be maintained during operation. Section 4.3 provides additional discussion about the development and use of these limits.

The MPS automatically initiates the protective actions necessary to mitigate the effects of the design-basis events identified in Table 7.1-1. The MPS reactor trip functions are listed in Table 7.1-3, including the associated process variables and analytical limits.

The core design and thermal limits are developed such that the thermal margin criteria are not exceeded for normal operation and AOOs. Specifically, there is a 95/95 assurance that the hot rod in the core does not experience a CHF condition. For the purpose of this analysis, CHF is assumed to occur if the subchannel analysis-calculated CHFR is less than the allowable limit. For IEs and accidents, the total number of fuel rods that exceed the criteria are assumed to fail and are used in determining the radiological dose source term.

4.4.2.2 Linear Heat Generation Rate

A limit on peak linear heat generation rate (PLHGR) is specified (Section 4.2) to ensure the fuel overheating SAFDL is not exceeded. The design limit on PLHGR maintains the fuel temperature below the centerline melt criterion.

The total peaking factor (F_Q) is used to calculate the PLHGR. Reference 4.4-1 provides a discussion on the calculation of the PLHGR based on the average linear heat generation (LHGR) and F_Q.

4.4.2.3 Core Coolant Flow Distribution

The design uses natural circulation, and there is no active control of the core flow. The core inlet flow distribution is dependent upon the geometry of the RCS loop, including the lower core plate and bypass flow paths. The core bypass flow paths are discussed in Section 4.4.3.1. There are flow inlets for each of the fuel assemblies in the core, similar to currently licensed PWR fuel designs.

Several inlet flow distributions are evaluated in Reference 4.4-1 to understand the effect on CHF. For up to a 15-percent inlet flow reduction to the limiting fuel assembly, the flows equalize after the flow reaches approximately one-third of the active fuel length, resulting in an insignificant effect on the minimum critical heat flux ratio (MCHFR). Additionally, for a given radial power distribution, there is no sensitivity observed to the inlet flow distribution. A 5-percent reduction in the flow to the limiting fuel assembly is used in the subchannel analysis.

Core inlet flow is calculated from the total RCS flow including flow measurement uncertainty and is reduced by the nominal bypass flow. The bypass flow uncertainty is statistically applied as described in Reference 4.4-2.

4.4.2.3.1 Core Coolant Temperature Distribution

As discussed in Reference 4.4-1, the core inlet temperature distribution is a boundary condition input for steady-state and transient subchannel analysis that is dependent on nuclear steam supply system design geometry. In the helical coil SG design, the primary RCS flow is on the shell side and the secondary feedwater flow is through the tubes. The concentric geometry of the SGs relative to the core ensures symmetric coolant temperature distribution through the downcomer into the core inlet. A uniform core inlet temperature is used in the subchannel analysis for AOOs, IEs, and accidents.

4.4.2.3.2 Turbulent Mixing

The turbulent mixing model within VIPRE-01 accounts for the exchange of enthalpy and momentum among adjacent subchannels caused by turbulent flow. The coefficient for turbulent mixing and the turbulent momentum factor are the two inputs needed for this model. This mixing model is incorporated into the VIPRE-01 energy and momentum equations, which is dependent on the amount of turbulent crossflow per unit length.

The turbulent mixing coefficient is determined from thermal mixing tests and is fuel-design specific. The value for the turbulent momentum parameter is not measured and is justified based on parametric sensitivity analysis provided in Reference 4.4-1. The sensitivity study results demonstrate that the NPM base model is not sensitive to the turbulent momentum parameter.

4.4.2.4 Core Pressure Drops and Hydraulic Loads

Flow testing on a full-scale prototype fuel assembly was performed to establish flow component loss coefficients and other related flow characterization

parameters for the fuel assembly. The form loss coefficients are used in the fuel assembly liftoff analysis and the subchannel analysis. Fuel assembly pressure drop tests were performed for a range of steady-state conditions as part of the CHF testing program. Pressure drops for the fuel assembly features are included in the subchannel model corresponding to their location in the fuel assembly as described in Reference 4.4-2.

Section 4.2 confirms the fuel assemblies do not experience liftoff from the lower core plate under normal operating conditions and AOOs.

4.4.2.5 Correlations and Physical Data

Testing was performed in support of CHF correlation development. Development of the NSP4 and NSPN-1 critical heat flux correlations used data collected from testing at the Framatome Karlstein thermal hydraulic test loop (KATHY) facility on a fuel design prototypical of the NuFuel-HTP2™ fuel design (Reference 4.4-5 and Reference 4.4-3). The approved domain for the NSP4 critical heat flux correlation was extended using data obtained from testing at Stern Laboratories on a fuel design similar to the fuel design, with the exception that it did not include flow mixing grids (Reference 4.4-4). Additional discussion of the CHF test programs is provided in Section 1.5.1. Comparisons between Stern Laboratories and KATHY data can be found in Reference 4.4-5 and Reference 4.4-4.

The limiting non-loss-of-coolant accident analyses in Chapter 15 are performed using the NRELAP5 code. Once the limiting cases for each transient are identified, the thermal margin is determined using the VIPRE-01 subchannel core model with the NSP4 critical heat flux correlation analysis limit.

As discussed in Section 15.6.1 and Section 15.6.6, respectively, the analyses of an inadvertent opening of a reactor safety valve and of an inadvertent operation of the emergency core cooling system are performed using the NRELAP5 code. The loss-of-coolant accident analysis discussed in Section 15.6.5 is also performed using NRELAP5. Thermal margin for these events is determined using the NRELAP5 code with the NSPN-1 and industry-developed CHF correlations as detailed in Reference 4.4-3.

4.4.2.6 Thermal Effects of Operational Transients

The subchannel analysis approach demonstrates thermal-margin specific trips are not necessary to mitigate AOOs. The CHF analyses demonstrate safety limits are met for the operating domain described in Section 4.4.3.2.

Section 4.4.7 demonstrates hydraulic flow instabilities are precluded by reactor trip signals that occur before the development of flow instabilities so detection and suppression of hydraulic instabilities is not required.

4.4.2.7 Uncertainties in Estimates

Uncertainties or biases are incorporated into the subchannel methodology to provide conservatism. These uncertainties establish the CHF analysis limit for assessing thermal margin. Uncertainties in the CHF correlation, analytical methods, operating conditions, physical inputs, core inlet flow distribution, and core exit pressure are considered in the subchannel analysis. Table 4.4-2 lists the uncertainties applied in the statistical subchannel analysis that are calculated as described in Reference 4.4-2 for application with the NSP4 critical heat flux correlation. Uncertainties to determine the analytical limit for the NSPN-1 critical heat flux correlation are applied as discussed in Reference 4.4-3.

4.4.2.7.1 Analysis Method Uncertainties

The uncertainties in the analysis method are computer code and CHF correlation uncertainties.

4.4.2.7.1.1 Computer Code Uncertainties

The computer code uncertainties come from axial and radial modeling and from the approximations in the governing constitutive equations in the VIPRE-01 code. The adequacy of the axial and radial models are confirmed with sensitivity studies.

Code comparisons to data in applicable ranges are used to reduce code uncertainty. Most of this test validation is by benchmarking to COBRA-FLX (Reference 4.4-6), an approved subchannel analysis code with an approved Safety Evaluation Report (Reference 4.4-7). The benchmark results for VIPRE-01 compare well for conditions anticipated for NPM applications and establish that no penalty is needed for computer code calculation bias.

4.4.2.7.1.2 Critical Heat Flux Uncertainty

The CHF correlation uncertainty is measurable and is included in the 95/95 MCHFR analysis limit of the NSP4 critical heat flux correlation. The NSP4 critical heat flux correlation is developed from the local conditions derived from a simulated subchannel model of the CHF test, using the subchannel software, in this case VIPRE-01. Therefore, the uncertainty in the computer code is included in the CHF correlation and its associated design limit.

4.4.2.7.2 Uncertainty in Operating Conditions

The operating boundary conditions are input into the subchannel analysis to account for process variable uncertainty, sensor accuracy and drift, and control deviation. The values for these uncertainties are based on the instrumentation used for monitoring and are plant specific. The measurement

uncertainties are those related to core thermal power, system flow, RCS cold temperature (T_{cold}), and pressurizer pressure.

4.4.2.7.3 Uncertainties in Physical Data Inputs

The subchannel analysis considers the following uncertainties in physical data:

- enthalpy rise engineering uncertainty ($F^E_{\Delta H}$)
- heat flux engineering uncertainty (F^E_Q)
- LHGR engineering uncertainty (F^E_{LHGR})
- radial power distribution uncertainty
- fuel rod bow and assembly bow uncertainty
- core inlet flow distribution uncertainty
- core exit pressure distribution uncertainty

The enthalpy rise engineering uncertainty ($F^E_{\Delta H}$) is applied to the hot channel to account for small fabrication uncertainties related to allowable manufacturing tolerances. This factor accounts for variations in pellet diameter, pellet density, enrichment, fuel rod diameter, fuel rod pitch, fuel rod bowing, and inlet flow distribution and mixing.

The heat flux engineering uncertainty factor (F^E_Q) accounts for the small manufacturing uncertainties (pellet density, enrichment, fuel rod surface area) that affect the local heat flux.

The LHGR hot channel factor is similar to the heat flux engineering uncertainty factor, except that the fuel rod surface area uncertainty is excluded because the fuel rod outer diameter does not significantly impact the LHGR of the pellet. The LHGR engineering uncertainty (F^E_{LHGR}) is applied as a penalty on the peak LHGR for fuel centerline melt calculations.

The radial power distribution uncertainty is related to the neutronics code that is used for the radial power distribution inputs. The power of rods a few rows away from the hot rod or channel have a negligible impact on the MCHFR. With the hot rod in the subchannel model placed at the design limit $F_{\Delta H}$, and neutronic code uncertainty accounted for in the core design, no radial power distribution penalty needs to be applied in the subchannel analysis.

Fuel rod bowing can have a negative impact on CHF because of reduced flow area in the hot channel. The penalty is applied conservatively based on the methodology for rod bow in Reference 4.4-8, which is demonstrated to be applicable for the NuScale fuel design in Reference 4.4-9 and Reference 4.4-10.

The core inlet flow distribution is discussed in Section 4.4.2.3. For the subchannel analysis methodology, inlet flow distribution uncertainty is applied to the hot or limiting assembly. The open lattice of the core allows flow redistribution to occur for inlet flow imbalances and the applied flow reduction to the hot assembly has a minimal effect on MCHFR.

The open upper plenum design allows for pressure equilibrium and no core exit pressure distribution uncertainty is necessary for the subchannel analyses.

4.4.2.7.4 Critical Heat Flux Analysis Limit

Combining the uncertainties with the statistical method described in Reference 4.4-2 yields a SCHFAL of 1.33 for use with NSP4. Reference 4.4-3 describes the application of uncertainties to the NSPN-1 critical heat flux correlation resulting in an analysis limit of 1.20.

4.4.2.8 Flux Tilt Considerations

Radial tilt is a condition where the power is not symmetric between azimuthally symmetric fuel assemblies. Azimuthal power tilt is an allowable limit on operation. Once the flux tilt is beyond an allowable threshold, actions are required to remedy the condition.

The design $F_{\Delta H}$ safety limit inherently accounts for the radial tilt, expressed as:

$$F_{\Delta H}^{TS} = F_{\Delta H}(1 + T_q) \qquad \text{Eq. 4.4-2}$$

where,

$F_{\Delta H}^{TS}$ = technical specifications enthalpy rise design peaking factor,

$F_{\Delta H}$ = design limit for core design calculations, and

T_q = azimuthal tilt.

Radial tilt is evaluated in core design calculations by inducing xenon oscillations or transients. Xenon transients are triggered by inserting control rod banks or single control rods as discussed in Section 4.3.2. The maximum calculated radial peaking factor after the resulting tilt is then compared to the technical specification $F_{\Delta H}$ design peaking factor to ensure that it is below the limit. Because it is deterministically accounted for, the subchannel analysis methodology requires no additional factor to account for radial tilt as described in Reference 4.4-1.

4.4.3 Thermal and Hydraulic Design of the Reactor Coolant System

The RCS design is described in Chapter 5. Table 4.4-1 summarizes the thermal-hydraulic characteristics of the NPM. Table 5.1-2 lists the operating parameters of the RCS at various power levels.

4.4.3.1 Core Bypass Flow

The subchannel analysis considers flow through the heated core and does not credit flow that effectively bypasses the fuel rods and is not available to directly remove heat.

The reflector blocks surrounding the core have several cooling channels that allow flow to pass through the reflector blocks and flow through the fuel assembly guide tubes and instrument tube is not available to remove heat generated by the fuel rods. For the subchannel analysis, core bypass flows are accounted for in the SCHFAL.

4.4.3.2 Analytical Design Operating Restrictions

Figure 4.4-2 provides the operating map showing analytical and normal operating conditions. The dotted line with T_{cold}, T_{avg}, and T_{hot} identified represents nominal full power operating conditions. T_{avg} remains fixed above 15 percent rated thermal power; T_{cold} and T_{hot} vary as power is increased or decreased. Normal T_{avg} and RCS pressure operating ranges, excluding the T_{avg} during startup at less than 15 percent rated thermal power, are shown around the T_{avg} line.

The analytical limits on the operating range illustrated as the outer box are constrained by the following considerations:

- upper RCS pressure bound: analytical limit protects against exceeding reactor pressure vessel (RPV) pressure limits for reactivity and heatup events
- lower RCS pressure bound: analytical limit ensures riser subcooling is maintained
- left-hand temperature boundary: analytical limit on minimum temperature for criticality
- right-hand average temperature limit: analytical riser temperature limit protects against exceeding MCHFR limits for reactivity and heatup events

If the hot leg temperature is below 500 degrees F, the low pressure analytical limit is constant at 1200 psia. If hot leg temperature is above 500 degrees F, the low pressure analytical limit increases to 1850 psia. The saturation curve and a parallel, 5 degrees F margin are illustrated on the right side of the figure showing the margin to saturation in the riser based on the analytical limits shown.

4.4.3.3 Thermal Margin Limit Map

The thermal margin limit map (Figure 4.4-3) provides the inlet temperature and power level where operation is allowed to ensure that CHF is not exceeded and the core exit conditions are not at saturation. The CHF limit prevents fuel failures and the core exit saturation limit ensures margin for thermal-hydraulic stability.

A series of CHF calculations are performed for a range of power levels between hot zero power and hot full power to establish trends and operating conditions of the limiting MCHFR, and to determine the limiting axial power shapes for subchannel calculations. The limiting axial power shape for a given power level is determined based on a nuclear analysis (Section 4.3) of the possible axial power shapes that could occur for a given cycle from operation within the operating limits. The operating limits in this context are the AO window, the power dependent insertion limits, and the cycle burnup. Limiting axial power shapes for a range of power levels are determined and used to develop the thermal margin limit map.

Using the limiting axial power shapes determined from the power-flow analyses described previously, a set of thermal margin limit cases are performed with the VIPRE-01 subchannel model. These cases vary inlet temperature, pressure, and power level that result in an MCHFR at the 95/95 limit. These cases provide the MCHFR component of the thermal margin limit map. A set of thermal margin limit cases are also performed with VIPRE-01 to determine the core inlet temperature that results in core exit saturation temperature as a function of power.

Figure 4.4-3 provides a plot of the resulting thermal margin limit map that includes both the MCHFR and core exit saturation components. The saturation limits (dashed lines) correspond to the combination of core inlet temperature and power that result in core average outlet temperature being at the saturation temperature. There are two dashed lines based on the natural circulation flow rates that correspond to the allowed minimum and maximum core average temperature at each power level. The solid curve is the combination of inlet temperature and power level that results in the MCHFR being at the analysis limit. The MCHFR calculations are performed assuming the limiting radial and axial power distributions previously discussed. As shown in the figure, the CHF analysis limit portion of the thermal margin limit map for steady-state operation is well above 100 percent power.

The flow stability protection solution uses a regional exclusion solution as described in the “Evaluation Methodology for Stability Analysis of the NuScale Power Module” topical report (Reference 4.4-11) and Section 4.4.7. Section 15.9 describes stability analysis using the PIM computer code.

4.4.3.4 Power-Maneuvering Characteristics

While power maneuvering operations within the capability of the rod control system are anticipated to support power demands, continuous power maneuvering is not assumed in the analysis of the reference equilibrium cycle, as indicated in Section 4.3. However, planned power maneuvering is considered as

part of a cycle-specific core design using the methodologies described in the technical specifications. The limiting axial power shape that is described in Section 4.4.4 includes the impact of planned power maneuvering. Power control is accomplished using boron control and control rod positioning.

Section 4.3.2 describes the analysis used to generate the wide range of normal operation axial power shapes used to establish operating limits for normal steady state and power control operations. These limiting power distributions are controlled during operation by technical specifications that require operation within the AO window and within the power dependent insertion limits.

The fixed in-core flux measurements and resulting power distribution are continuously displayed in the control room and provide further assurance that the power distributions both axially and radially are not exceeded. Operation outside these limits is not allowed by the plant technical specifications.

4.4.4 Evaluation

The methodology and analysis tools (i.e., licensing methodology) used in the thermal-hydraulic design are summarized in this section and described in detail in the referenced topical reports. The VIPRE-01 code is used for steady-state and transient subchannel fuel and temperature calculations. The PIM code is used for thermal-hydraulic stability calculations and is described in more detail in Section 4.4.7. The subchannel steady-state results provided in this section and the transient results in Chapter 15 are performed in accordance with the methodology, including restrictions, defined in Reference 4.4-1 and Reference 4.4-2. The methodology is used to establish the power peaking limits and protect SAFDLs without using thermal margin-specific trips. Fuel rod thermal evaluations are performed at rated power and during transients up to the design limit burnup to verify the fuel temperature and cladding integrity design bases described in Section 4.2.1 are satisfied. These analyses also provide input for the initial fuel rod thermal conditions used in Chapter 15 transient analyses.

Conformance to GDC 10 requirements is demonstrated by establishing SAFDLs and ensuring the plant stays within the SAFDLs. These limits ensure that the fuel clad is not breached (and thus this fission product barrier remains intact), that fuel system dimensions remain within operational tolerances, and that functional capabilities are not reduced below those assumed in the safety analysis. The subchannel core thermal-hydraulic analysis determines that the MCHFR is maintained above the 95/95 limit during normal operation and AOOs, ensuring the SAFDLs are satisfied and fuel cladding integrity is demonstrated. For IEs and accidents, the total number of fuel rods that exceed the criteria and are assumed to fail is used as input for radiological dose calculation purposes.

4.4.4.1 Critical Heat Flux Correlation

The functional forms of the NSP4 and NSPN-1 critical heat flux correlations are expressed as empirical relations dependent on a number of physical parameters including:

- pressure
- cold wall factor
- boiling length
- local mass flux
- local equilibrium quality

The coefficients of the NSP4 critical heat flux correlation are determined with a cross-validation process and linear least-squares regression based on local condition parameters calculated with the VIPRE-01 subchannel thermal-hydraulics code. The form of the equation and correlation coefficients and the details of the development of the correlation are provided in Reference 4.4-5.

The coefficients of the NSPN-1 critical heat flux correlation are determined using the same process as used for NSP4 but with local conditions calculated using NRELAP5. The form of the equation and correlation coefficients with details of the development for the NSPN-1 critical heat flux correlation are provided in Reference 4.4-3.

4.4.4.2 Core Hydraulics

As discussed in Section 4.4.2.3.1, a uniform inlet temperature distribution is applied. Table 4.4-3 lists the principal flow elements in the RPV flow path and describes the flow path.

4.4.4.3 Influence of Power Distribution

The subchannel analysis basemodel is developed to bound a cycle-specific core as described in Reference 4.4-2. The model preserves limiting core conditions along with the operational envelope specified in the technical specifications. The envelope accounts for the power distribution throughout the core using design peaking factors and axial power shapes in combination with the limiting RCS parameters such as flow and pressure.

The radial power distribution for the core is characterized by the enthalpy rise hot channel factor, $F_{\Delta H}$. The $F_{\Delta H}$ is variable depending on the cycle design, exposure, fuel composition, burnable poison loading, operational history, and thermal-hydraulic conditions. As a result, the location of the peak $F_{\Delta H}$ fuel rod changes throughout an operating cycle.

A conservative core power distribution that bounds the cycle-specific or time-in-life dependent radial power distribution is used to make the radial power distribution independent of specific cycle core designs. The analysis for each

cycle loading pattern confirms this limiting radial power distribution is bounding for the fuel cycle.

The technical specifications impose a limitation on the peak value of $F_{\Delta H}$, and therefore limits the highest value for any fuel rod at hot full power. The $F_{\Delta H}$ peaking design limit is increased for lower power levels, allowing a linear increase to hot zero power.

The total peaking factor (F_Q) is determined using the $F_{\Delta H}$ peaking design limit and axial power shape local F_z peaking value. The maximum F_Q value is used to calculate the peak LHGR.

A limiting axial power shape is used in the subchannel analysis. Similar to the radial power distribution, the limiting axial power shapes are developed to be bounding and are confirmed for each cycle.

In summary, the subchannel methodology is developed to use bounding radial and axial power distributions as described in Reference 4.4-2.

4.4.4.3.1 Influence of Power Distribution During Transients

For most Chapter 15 transients that do not involve control rod assembly motion, the bounding axial and radial power distributions developed in the previous sections are conservative and are used. If the events occur from reduced power, the radial power distribution is augmented in accordance with the higher $F_{\Delta H}$ allowed at lower powers. Similarly, the limiting axial power shape for the analyzed power is used.

For Chapter 15 events that involve control rod assembly motion, such as Section 15.4 events, the radial power distribution at the time of peak core power is determined from the event-specific nuclear analysis. The bounding power distribution determined for the steady-state analysis is then augmented to reflect the higher peak $F_{\Delta H}$. The power distribution is described in more detail in Reference 4.4-2.

The core design has an imposed limitation on the peak value of $F_{\Delta H}$, and therefore the highest value for any fuel rod throughout the full range of power, time in life, and allowed control rod positions are accounted for. The applied peaking value also accounts for measurement uncertainty. The radial power distribution applies a conservative peak-to-average power peaking for the hot assembly. Engineering uncertainties related to the enthalpy rise are accounted for statistically in the CHF analysis limit.

The CHF limiting axial power shape based on core-average axial power is sufficient to be used for most transient analyses. Generally, the core-average axial power shape does not deviate significantly from the spectrum of shapes already considered within the power shapes analysis, and the subchannel limiting axial power shape is held constant during these events. The

combination of the core-average axial power shape of initiating power level with the conservative radial power distribution and core hydraulic boundary conditions from NRELAP5 provides a conservative MCHFR calculation.

4.4.4.4 Core Thermal Response

The core thermal response during AOOs, IEs, and accidents is presented in Chapter 15.

Low power and shutdown operation is described in Section 19.1.6 and the Probabilistic Risk Assessment for the operation is addressed. The NPM natural circulation design does not require mid-loop operation during shutdown conditions. The core is always submerged in a pool of water so the core is not subjected to mid-loop thermal-hydraulic conditions during refueling operations.

4.4.4.5 Analytical Methods

4.4.4.5.1 Reactor Coolant System Flow Determination

The RCS flow loop is composed of the core region, riser transition, lower and upper riser, upper riser turn to annulus, SG, downcomer transition, and downcomer to lower plenum turn. The driving force for flow is the buoyancy arising from the density differences around the RCS flow loop. The primary contributors to pressure loss in the system are the fuel assembly and SG regions. These pressure losses are confirmed by testing. The remaining pressure drops are determined analytically. The steady state flow is calculated using the thermal-hydraulic software NRELAP5.

Maximum design, best estimate (nominal), and minimum design RCS flow rates are defined as a function of reactor power level. The best estimate flow is the most likely value for the primary coolant flow rate. This flow is based on the best estimate values of the friction and form losses in the RCS loop, and the amount of core bypass flow. Maximum design flow is the highest expected value for the primary coolant flow rate. The maximum design flow accounts for uncertainties in the RCS loop form losses, the uncertainty in the core bypass flow, and the uncertainty in the heat transfer capability of the SG. The minimum design flow is the lowest expected value for the primary coolant flow rate. The minimum design flow accounts for uncertainties in the RCS loop friction and form losses (including the influence of crud and corrosion), the uncertainty in the core bypass flow, and the uncertainty in the heat transfer capability of the SG. The RCS flow uncertainties are deterministically considered by NRELAP5 from which boundary conditions are provided to VIPRE-01 for evaluation. Uncertainties in bypass flow are accounted for in the SCHFAL. Bypass flow is discussed in Section 4.4.3.1.

The thermal and hydraulic design methodology establishes the basis for the subchannel model and its application. The thermal-hydraulics of the reactor core are modeled using VIPRE-01 with a one-pass approach in which the characteristics of the hot channel are captured, including inter-channel feedback.

4.4.4.5.2 Subchannel Model

The subchannel analysis basemodel is developed in a conservative manner such that it bounds specific cycle core designs. The model is detailed in the limiting assembly with the peak power rod with decreasing detail farther away from the limiting assembly. The decreasing detail is accomplished by combining channels (called lumped channels). Sensitivity studies show that the rod power a few rods removed from the hot rod has minimal effect on the MCHFR. Other aspects of the basis for the model are discussed in Section 4.4.3 and Section 4.4.4. The design inputs to construct the subchannel model are:

- RCS conditions
  - core thermal power
  - flow rate and core bypass fraction
  - core inlet temperature
  - system pressure
- power distribution
  - radial power profile
  - axial power profile
- mechanical fuel design information
  - fuel array geometry and loss coefficients
  - pellet and clad dimensions
  - material properties for the fuel, clad, and the pellet-to-clad gap
- fuel performance data
  - gap width, fill gas volume, composition, and pressure
  - fuel centerline and volumetric average fuel temperatures
  - fuel and clad surface temperatures

The accumulation of crud has a negligible impact on flow resistances through the core. The narrowing of the subchannels as a result of crud buildup is bounded by the flow area reduction uncertainty included in the enthalpy rise engineering uncertainty discussed in Section 4.4.2.7.3. The fuel stored energy and fuel pin temperature modeling in VIPRE-01 is calibrated against values calculated using the COPERNIC fuel performance code that includes the effects of crud on the fuel rod surface as discussed in Section 4.4.4.6. The subchannel analysis considers the range of possible axial power shapes within the allowable AO window (Section 4.4.3.4). Impacts that crud may have on AO are protected by the allowed AO window set by the technical specifications. Therefore, the subchannel analysis methodology bounds the potential effects of crud and no explicit modeling of crud is included in the subchannel analysis.

Reference 4.4-1 supplemented by Reference 4.4-2 provides details about the methodology used to analyze the thermal and hydraulic response of the fuel and core coolant, including the correlations used for heat transfer, void fraction, and pressure drop. Void fractions for the equilibrium cycle are shown in Table 4.4-4.

4.4.4.6 Fuel Rod Conduction

Conduction of heat through the fuel rod directly impacts thermal margin to CHF for transient analyses. The VIPRE-01 one-dimensional conduction model is used for the fuel rod starting from the centerline of the fuel pellet outward to the cladding surface. VIPRE-01 does not explicitly model the phenomenon associated with fuel rod behavior changes caused by fuel exposure but does account for it by calibrating the VIPRE-01 fuel pin temperatures and stored energy to match or conservatively bound the fuel performance code (COPERNIC) results as described in Reference 4.4-1. Fuel conduction temperature calculations implicitly include the effects of crud deposition on the fuel rods because post-irradiation measurements include crud in the oxide profile measurement.

Table 4.4-5 provides the peak fuel temperature for the core average linear heat rate and the peak linear heat rate with both values demonstrating significant margin to fuel melting.

4.4.4.7 Fuel Design-Specific Inputs

Fuel design-specific information is used in the subchannel basemodel. Spacer grid loss coefficients and friction factor are derived from pressure drop tests. These derivations are applied in the subchannel analysis as described in Reference 4.4-1 and supplemented by Reference 4.4-2.

4.4.5 Testing and Verification

Initial testing is performed in accordance with the plant test program described in Section 14.2. Before achieving criticality and during initial power ascension, testing is performed to confirm thermal and hydraulic design parameters, such as RCS flow rate and core peaking factors, are consistent with the analyses.

Fuel assembly component surveillance is performed during refueling outages as described in Section 4.2.4.

4.4.6 Instrumentation Requirements

4.4.6.1 In-core Instrumentation System

The in-core instrumentation system uses neutron flux measurements to determine a three-dimensional power distribution in the core (Section 4.3).

Temperature is monitored to verify that proper flow rates are being used in the thermal-hydraulic analysis. The location of the fuel assemblies that contain in-core instrumentation system detectors is shown in Figure 4.3-14.

4.4.6.2 Module Protection System

Protective trips ensure that MCHFR limits are not exceeded and that fuel centerline temperature stays below the melting point. The trips also ensure that average enthalpy in the riser is less than the enthalpy of saturated liquid and that core exit quality is within the limits defined by the CHF correlation. The MPS and reactor trip functions are discussed in Section 7.1, and the credited trip signals for each event are discussed in Chapter 15.

A detect-and-suppress system is not used for stability in the NPM design because MPS protective actuations are achieved before reaching the flow stability exclusion region as discussed in Section 4.4.7.4.

The technical specifications include operating limits and system operability requirements that ensure the thermal-hydraulic performance of the core. The reactor trip setpoints in the MPS include margin-to-safety limits for the monitored parameters.

The NPM design does not include a loose parts monitoring system because

- The low fluid velocities resulting from natural circulation flow combined with a design that has only small lines entering the RPV minimizes the potential for loose parts entering or being generated in the RPV.
- The NPM design uses corrosion-resistant materials and has a Flow-Induced Vibration Program (Section 3.9) that further minimizes the potential for loose parts being generated in the RPV.
- During startup operation, a Foreign Materials Exclusion Program minimizes the potential for loose parts entering the RPV.
- Underwater vessel inspections during refueling outage verify there are no loose parts in the RPV.

In addition the fuel assembly has a mesh filter at the bottom of each fuel assembly (Section 4.2) that filters out loose parts that could enter the fuel assembly.

4.4.7 Flow Stability

The evaluation of unstable flow oscillations in the NPM includes a detailed phenomenological review of possible modes of instability and operating conditions that may result in instability. The phenomenological review identifies the limiting instability mode as natural circulation instability. Details of the methodology are provided in Reference 4.4-11, including generic boundary conditions of anticipated transients where unstable oscillations may occur. Section 15.9 demonstrates the NPM design is protected from unstable flow oscillations when operation is limited to a defined pressure-temperature exclusion zone.

The approach for stability protection in the NPM is regional-exclusion rather than detection-and-suppression. The operational domain identified with potential instability is characterized by loss of subcooling in the riser that leads to vapor generation above the core. This condition is excluded by the MPS protective actions.

In the demonstration of the methodology, no instabilities are identified to occur over the range of power evaluated because riser subcooling margin is not lost. The MPS actuation precludes onset of instability on loss of subcooling with sufficient margin to accommodate instrumentation time delays.

4.4.7.1 Phenomenological Description of NuScale Power Module Stability

The NPM design is a small modular integrated PWR. The helical coil SGs are integrated within the RPV and natural circulation drives the primary coolant flow. The density difference between the relatively high-temperature flow exiting the core and the lower-temperature flow returning through the downcomer annulus creates the natural circulation driving head.

Various feedback mechanisms are possible and special consideration is given to coupling the SG dynamics and the flow stability in the primary loop. Feedback coupling between the thermal-hydraulic phenomena and the neutron kinetics is important. Feedback coupling is of particular importance where coolant and fuel rod temperatures provide reactivity feedback, and the core power response affects the coolant temperature and the density head that drives the flow and influences its stability.

4.4.7.2 Instability Mode Classification

The instability modes are broadly classified as static or dynamic. A list of the instability modes under each category and the mechanism for each mode is described in Table 4.4-6. The relevance of each instability mode to the design is designated as not applicable, excluded as limited by other phenomena, or applicable.

4.4.7.3 Analysis Methodology

The PIM code simulates the flow dynamics in the RCS loop with optimal resolution of its stability. The extensive experience in the field of boiling water reactor stability analysis, both numerical and first principle understanding, is used in addressing single-phase natural circulation stability, which is unique to the NPM.

The PIM code applies the general theory and numerical methods of the RAMONA code, but is not a direct derivative of the coding. The PIM code has been developed independently to suit the geometry and specific needs of the NPM. The main advantage of the RAMONA-type algorithm used in PIM is the absence or insignificance of numerical damping that affects other time-domain codes, and requires extensive study and adjustment before they can be successfully benchmarked and reliably used.

Frequency-domain methods are not affected by numerical damping as much as some time-domain methods, but they are not used for the analysis as they require linearization of the governing equations. While linearization is accurate for small perturbations, and properly identifies the decay ratio and the conditions at the onset of instability, it is not suitable to analyze the stability of a highly-nonlinear system such as a natural circulation loop. A linearized model would not be able to

discover the importance of nonlinearities that may be manifested at relatively small perturbation amplitudes. However, the RAMONA-type algorithm used by PIM is capable of representing the nonlinear interactions inherent in the natural circulation flow.

The PIM code approximates the reactor vessel geometry and flow. The approximations are founded on basic assumptions regarding the geometry, the representation of the flow fields, and various interactions and feedback mechanisms. The major assumptions, their impact, and justifications are given in Reference 4.4-11.

4.4.7.4 Stability Protection Solution

Section 4.4.3.3 describes how the NPM meets GDC 12 requirements by using an operating domain that is protected by MPS reactor trips in the exclusion region where the reactor is not allowed to operate. The exclusion region, defined by the area in the operating map where stability criteria are not met, is enforced automatically by the MPS trip setpoints.

The reactor operating maps for the NPM are described in Section 4.4.3.3.

In summary, a detection and suppression solution is not used for the design. Flow stability is ensured by maintaining a suitable operating region using an exclusion region solution.

4.4.8 References

4.4-1 NuScale Power, LLC, "Subchannel Analysis Methodology," TR-0915-17564-P-A, Revision 2.

4.4-2 NuScale Power, LLC, "Statistical Subchannel Analysis Methodology," TR-108601-P, Revision 2.

4.4-3 NuScale Power, LLC, “Loss-of-Coolant Accident Evaluation Model,” TR-0516-49422-P, Revision 3.

4.4-4 NuScale Power, LLC, "Applicability Range Extension of NSP4 CHF Correlation," TR-107522-P, Revision 1.

4.4-5 NuScale Power, LLC, “NuScale Power Critical Heat Flux Correlations,” TR-0116-21012-P-A, Revision 1.

4.4-6 AREVA NP Inc., “COBRA-FLX: A Core Thermal-Hydraulic Analysis Code Topical Report,” ANP-10311P-A, Revision 0.

4.4-7 Bahadur, Sher, U.S. Nuclear Regulatory Commission, letter to Pedro Salas, AREVA NP, Inc., January 29, 2013, Agencywide Document Access and Management System (ADAMS) Accession No. ML13135A053.

4.4-8 AREVA Inc., "Computational Procedure for Evaluating Fuel Rod Bowing," XN-75-32(P)(A), Supplement 1-4.

4.4-9 NuScale Power, LLC, “Applicability of AREVA Fuel Methodology for the NuScale Design,” TR-0116-20825-P-A, Revision 1.

4.4-10 NuScale Power, LLC, "Framatome Fuel and Structural Response Methodologies Applicability to NuScale," TR-108553-P-A, Revision 0.

4.4-11 NuScale Power, LLC, "Evaluation Methodology for Stability Analysis of the NuScale Power Module," TR-0516-49417-P, Revision 1.

Table 4.4-1: Plant Reactor Design Comparison

Parameter	NuScale	US-EPR	US-APWR
Key Reactor Parameter			
Core thermal output (MWt)	250	4590	4451
System pressure (psia)	2000	2250	2250
Number of loops	NA	4	4
Inlet temperature (°F) [best estimate (BE) flow]	482	563.4	550.6
Core average temperature (°F) (BE flow)	540	596.8	588.8
Average temperature rise in core (°F) (BE flow)	116	62.7	72.1
Minimum design flow (lb/hr)	5.13E+6	173E+6	168E+6
Maximum design flow (lb/hr)	6.52E+6	195E+6	188E+6
Best estimate flow (lb/hr)	5.82E+6	180E+6	175E+6
Core bypass flow (%)	7.5	5.5	9.0
Average linear power density (kW/ft)	3.9	5.22	4.65
Peak linear power for normal operating conditions (kW/ft)	7.0	13.6	12.1
Normal operation peak heat flux (10^6 Btu/hr-ft^2)	0.245	0.460	0.421
Total heat flux hot channel factor (F_Q)	2.196	2.60	2.60
Heat transfer area on fuel surface (ft^2)	6,276	86,166	91,360
Normal operation core average heat flux (Btu/hr-ft^2)	135,927	177,036	162,000
Core flow area (ft^2)	9.79	63.6	68.0
Core average coolant mass velocity (10^6 lbm/hr-ft^2) (BE)	0.59	2.8	2.25
Core average coolant velocity (ft/sec)	3.5	16	14.1
Core			
Equivalent diameter of active core (in.)	59.26	148.3	119.7
Number of fuel assemblies	37	241	257
Fuel Assembly			
Overall fuel length (in.)	94.0	165.4	165.4
Nominal fuel weight per assembly (lb)	771	1182	1350
Rods per fuel assembly	264	264	264
Fuel Assembly pitch (in.)	8.466	8.466	8.466
Fuel rod pitch (in.)	0.496	0.496	0.496
Number of grids per assembly	5	10	11
Fuel Rod			
Cladding outside diameter (in.)	0.374	0.374	0.374
Pellet-cladding gap (in.)	0.00325	0.0033	0.0033
Cladding material	M5®	M5®	ZIRLO
Fuel column length (in.)	78.74	160	165.4
Fuel pellet diameter (in.)	0.3195	0.3195	0.322
Fuel pellet density (% theoretical density)	96.5	96.0	97

Note: More detailed information is provided for NuScale in Reference 4.4-1. Table 5.1-2 provides additional information on NuScale RCS flow.

Table 4.4-2: Subchannel Methodology Uncertainty and Bias Application

Parameter	Application
Reactor power measurement uncertainty	System code
Pressure measurement uncertainty	System code
Temperature measurement uncertainty	System code
Core inlet flow rate uncertainty	System code
Radial power uncertainty	VIPRE-01 evaluation model
Enthalpy rise peaking factor ($F_{\Delta H}$)	VIPRE-01 evaluation model
Enthalpy rise peaking ($F_{\Delta H}$) asymmetric event augmentation	VIPRE-01 evaluation model
Axial power distribution	VIPRE-01 evaluation model
Core bypass flow fraction	Statistical analysis limit
Core inlet flow distribution bias	VIPRE-01 evaluation model
Core bypass flow uncertainty	Statistical analysis limit
Enthalpy rise engineering uncertainty ($F^{E}_{\Delta H}$)	Statistical analysis limit
Heat flux engineering uncertainty (F^{E}_{Q})	Statistical analysis limit
Fuel rod bowing uncertainty	Statistical analysis limit
$F^{U}_{\Delta H}$ measurement uncertainty	Statistical analysis limit
CHF correlation uncertainty	Statistical analysis limit
Core exit pressure distribution bias	None
Core inlet temperature distribution bias	None
Assembly bowing bias	None
LHGR engineering uncertainty	Peak LHGR calculations

Table 4.4-3: Summary of Reactor Coolant System Loop Flow Elements

Flow Element	Hydraulic Phenomena
Core support blocks in downcomer	Flow through thick-edged orifice. Forward and reverse losses are considered.
Downcomer-to-lower plenum turn	Flow turning through 180 degrees along thickened corners. Forward and reverse losses are considered.
Lower core plate	Flow through thick-edged orifice. Forward and reverse losses are considered.
Core	Flow through nozzles and spacer grids
Upper core plate	Flow through thick-edged orifice. Forward and reverse losses are considered.
Control rod assembly guide tubes	Parallel flow in interstitial area of tube bundle
Control rod assembly guide tube support plate	Flow through thick-edged orifice. Forward and reverse losses are considered.
Riser transition	Flow through converging nozzle
Control rod drive shaft support	Flow through plate that is treated as spacer plates with rounded edges in a tube.
Pressurizer baffle	Flow through contraction and sudden expansion. Forward and reverse losses are the same.
Upper riser turn to downcomer	Flow turning through 180 degrees and drag from hanger braces and control rod drive shaft sleeves
Downcomer through steam generator	Flow over tubes
Downcomer transition	Flow through converging nozzle
Upper core support blocks	Flow over obstructions and drag due to blocks in downcomer
Riser holes	Flow through orifices in a thin wall in the presence of a passing flow stream. Forward and reverse losses are considered.

Table 4.4-4: Void Fractions for Equilibrium Cycle

	Beginning of Cycle	End of Cycle
Core average void fraction	0.0	0.0
Maximum void fraction	0.079	0.059

Table 4.4-5: Peak Fuel Pellet Temperatures

Linear Heating Rate	Pellet Centerline Temperature (°F)
Core average (3.9 kw/ft)	1818
Peak fuel rod (6.04 kw/ft)	2052

Table 4.4-6: Applicability of Instability Mechanisms

Instability	Mechanism	Applicable to Design	Rationale for Determination
Static Instabilities	Governed by steady-state characteristics of the system		
Flow excursion or Ledinegg instability	Determined by the relationship between the pressure drop characteristic of a boiling channel and the pressure drop characteristic imposed by an external system (e.g., a pump).	Yes	There is no possibility for negative slope of the $\Delta P(\dot{m})$ in the case of single-phase natural circulation and it can be demonstrated that in a substantially unconstricted flow path like the primary circuit in the NPM that this condition is also absent even under two-phase conditions. Reference 4.4-11 demonstrates there is no negative slope at any power at the steady-state balanced loop operating points where $\Delta P = 0$. Moreover, no negative slope was found anywhere on the curve. Therefore, the flow excursion mode is not possible in the NPM.
Boiling crisis	Higher heat flux than the flux that can be transferred by nucleate boiling.	No	Reactor operation is restricted such that a margin to boiling transition is achieved by maintaining the minimum CHF ratio above correlation limits.
Flow pattern (relaxation) instability transition	Flow regime transitions influence the pressure drop and create inflections of the pressure drop versus flow rate that may result in instability. Flow regime transitions include laminar-to-turbulent transitions and bubbly-to-annular flow transitions.	No	Flow regime transitions cannot cause instabilities in the NPM. Bubbly-to-annular flow regime transitions occur at high steam qualities and are well outside the operational range of the NPM, which is single-phase flow with minimal, if any, local subcooled boiling. Other instability modes become excited at lower steam quality in the NPM riser and, therefore, the boiling regime transitions are bounded by these other phenomena.
Flashing instability	Relevant for heaters located under a tall riser Hot (at or near saturation) liquid rises to lower pressure elevation. Evaporation at reduced pressure (flashing) drives flow disturbance.	Yes	Observed only in low-pressure systems with pressures much lower than NPM operating pressure
Bumping geysering	Periodic or chaotic oscillations caused by cyclical vapor generation in a tall riser. Similar to flashing instability, except vapor is generated in the heater and expands in the riser. Possible liquid thermodynamic metastable state (superheated) caused by low flow and lack of nucleation sites.	No	Possible only in low-pressure systems, and therefore not a primary instability mode in NPM.

Table 4.4-6: Applicability of Instability Mechanisms (Continued)

Instability	Mechanism	Applicable to Design	Rationale for Determination
Dynamic Instabilities	Governed by inertia, feedback, and overall system response.		
Pressure-drop oscillations	Oscillations are the dynamic extension of Ledinegg static instability. Pressure drop versus flow rate is a multi-valued function. Transition from one flow state to the other is accompanied by a storage mechanism, such as compressing a volume of vapor, which causes a delayed rebound and cyclical transitions ensue.	Yes	The necessary condition of a multi-valued pressure drop versus flow rate is excluded in the NPM as shown in the Ledinegg analysis.
Acoustic oscillations	Resonance of pressure waves. Thermal energy feeds and sustains the instability. In the compression phase, direct contact between the liquid phase and the heated surface is forced by collapsing a vapor film and heat transfer is enhanced while in the rarefaction phase the vapor film is reestablished, and the cycle is repeated. High velocity flow may also provide the mechanical energy to excite the standing waves.	No	There is no mechanism for feeding and sustaining this type of instability in the NPM as discussed in Reference 4.4-11.

Table 4.4-6: Applicability of Instability Mechanisms (Continued)

Instability	Mechanism	Applicable to Design	Rationale for Determination
Density-wave oscillations	Occurs in vertical heated channels with or without boiling. Any flow perturbation at the inlet generates effects that propagate (wave) up the channel. Decreasing inlet mass flow rate results in increasing the flow enthalpy and lowers the density either by liquid expansion in the case of single-phase flow or through increased vapor generation. At steady state or quasi-steady state, or for very low frequency perturbation, the inlet flow perturbation generates a negative feedback so that the system returns to its initial state and is stable. Specifically, a perturbation decreasing the inlet mass flow rate results in lowering the density in the channel, thus increasing the buoyancy pressure head, which tends to restore the original flow rate. However, dependent on the frequency of the perturbation, sufficiently strong delayed feedback can be destabilizing. Delay mechanism is the time to propagate the density wave to transverse the heated channel length. For resonant frequency, the delayed effects of perturbation reach the channel exit at the time the inlet perturbation reverses phase and the original perturbation is reinforced. At this frequency, the system is destabilized given sufficiently strong feedback, which can occur when the power is increased. For a single-phase heated channel, instability is conceivable only for long heated channels as the density change of liquid due to change in enthalpy is relatively small. Conversely, boiling increases the mixture density response to enthalpy change, making a boiling channel less stable compared to the single-phase case. In addition, in the two-phase case, the feedback from an initial inlet flow perturbation is not limited to density head, but includes the response of friction pressure drop, which is significant due to the two-phase multiplier.	Yes	Density wave instability is seldom observed without compounding factors in nuclear systems. While density waves are present normally in a heated channel, they can occur in a heated channel connected to a tall adiabatic riser as in the simplified boiling water reactor natural circulation. Density wave instability is a concern for the flow in the secondary side of the SG of the NPM and must be addressed. Density waves in the primary circuit are part of a compound interconnected phenomena of a potential natural circulation riser instability and must be addressed as an integral process with various components.
Xenon instability	Pure neutronic phenomenon.	No	Xenon stability calculations for the NPM core demonstrate that these oscillations are highly stable as a pure instability mode. Refer to Section 4.3.

Table 4.4-6: Applicability of Instability Mechanisms (Continued)

Instability	Mechanism	Applicable to Design	Rationale for Determination
Natural circulation instability	Natural circulation system includes two legs: a riser and a downcomer. The dynamics of the flow in the two legs depends on the heater source and heat sink, and their respective location. The natural circulation instability mechanism of interest for the NPM has the heater located under a tall riser and the heat sink located near the top of the cold leg. A perturbation increasing the flow rate results in a reduction in the heater exit temperature and an increase in its density. The density perturbation travels up the riser and there is a time delay before the new density is distributed throughout the length of the riser. This delayed feedback is negative because the difference in temperature between the riser and the cold leg is diminished reducing the density difference that drives the flow. If this delayed negative feedback is sufficiently strong, the flow is destabilized and undergoes growing oscillations. The riser boils in the case of high friction in the loop that reduces flow, or if power input is sufficiently increased. The density response to an enthalpy perturbation is much higher in the case of phase change than in the case of single-phase thermal expansion. The boiling natural circulation loop can be destabilized more readily than a single-phase loop.	Yes	Natural circulation instability is a possible mode for the NPM and is evaluated in depth. The evaluation includes other compounding phenomena not discussed in the description of the fundamental instability given above. These compounding phenomena include the feedback from nuclear reactivity and the dynamics of the heat exchanger.
Thermal stratification oscillations	An extension of natural circulation instability that occurs when the heat source is at a higher elevation than the cooling sink. In this case, the heating of the water does not produce a reliable buoyancy-induced flow, the liquid becomes stratified, and periodic back-and-forth oscillations occur.	No	The NPM does not meet the required condition of the heat source being at a higher elevation than the cooling sink.
Coupled Compound Instability Modes	Compound instability modes include secondary phenomena that influence or modify the primary mechanism significantly.		
Parallel channel instability	Common headers alter the boundary conditions under which a single channel would have operated. The common pressure drop boundary condition allows for multiple oscillation modes depending on the phase difference among the oscillations in each channel. The fixed pressure drop boundary condition is destabilizing and, therefore, a set of two channels connected in parallel are less stable than a single one. For two channels oscillating out of phase, the common pressure drop fluctuation is eliminated (in the linear limit) as the effects of the flow oscillations in the two channels cancel out.	No	Parallel channel instability in the NPM core is dispositioned in Reference 4.4-11 and is not a concern.

Table 4.4-6: Applicability of Instability Mechanisms (Continued)

Instability	Mechanism	Applicable to Design	Rationale for Determination
Primary circuit flow coupling to secondary side of SG	Discussion is in Reference 4.4-11.	Yes	SG secondary-side flow coupling to the RPV-side flow is restricted to the effects of the total secondary flow. Out-of-phase flow oscillations in the tubes are self-cancelling and result in no net oscillatory effects.
Neutronic coupling with natural circulation instability	Takes effects of the neutron reactivity feedback into account. A flow increase perturbation at the core inlet reduces the core exit temperature at constant power. Reduced moderator temperature adds positive reactivity and the power is increased if the moderator temperature coefficient is negative. Power increase offsets core exit temperature reduction and the reactivity response becomes milder (reduced gain). However, the time delay involved in these processes could reinforce the perturbation if the resulting phase shift is large.	Yes	The reactivity-to-power and power-to-heat flux phenomena are important and are included in stability evaluations of the primary coolant flow in the NPM. Reference 4.4-11 provides the rational for this conclusion.
NPM circulation instability	Stability of the flow in a natural circulation loop with constant heater power and constant density cold leg is compounded to include reactivity-to-power feedback. Ideal SG assumption is relaxed with more realistic modeling of the heat transfer dynamics. System operating conditions may include parts in which the flow is two-phase because of subcooled boiling in the core and flashing in the riser.	Yes	The main NPM instability mode is natural circulation instability, also called riser instability mode. Evaluations rely on detailed numerical techniques in which a dynamic system is constructed using nonlinear equations the conservation of mass, momentum, and energy. Equations and governing equations for fission power dynamics and heat transfer.

Figure 4.4-1: Example Critical Heat Flux Ratio Limits and Thermal Margins

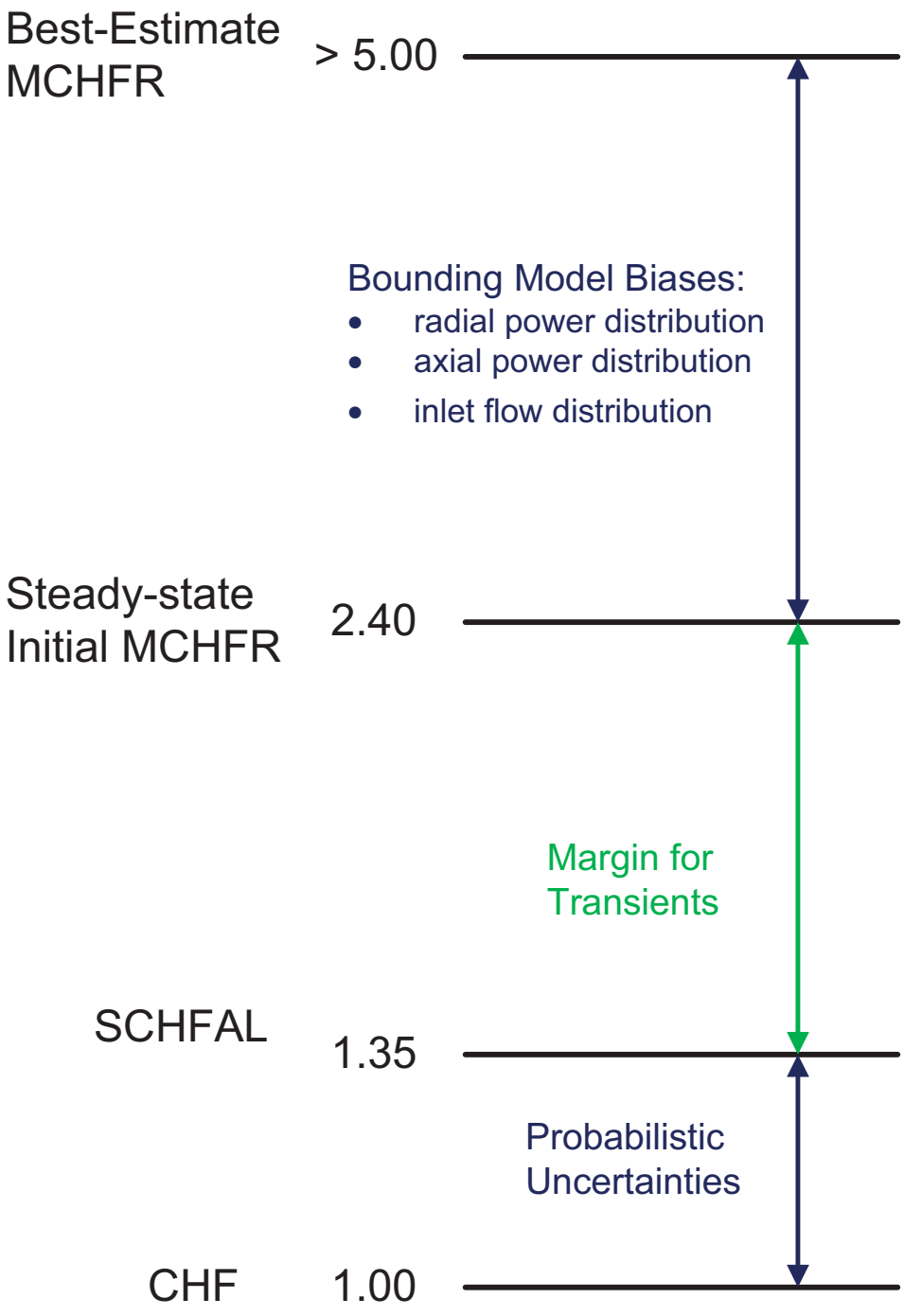

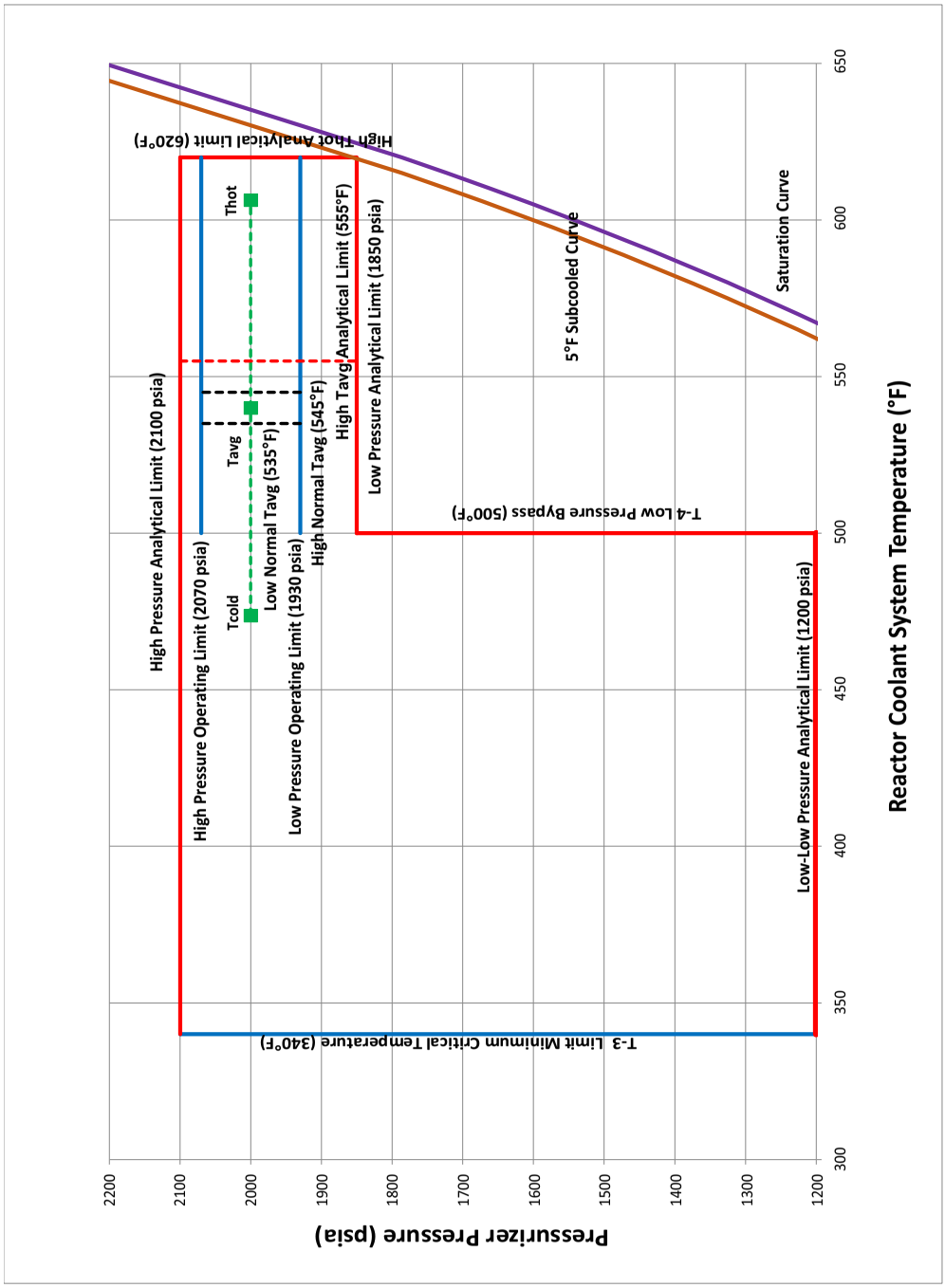

Figure 4.4-2: Analytical Design Operating Limits

Figure 4.4-3: Thermal Margin Limit Map

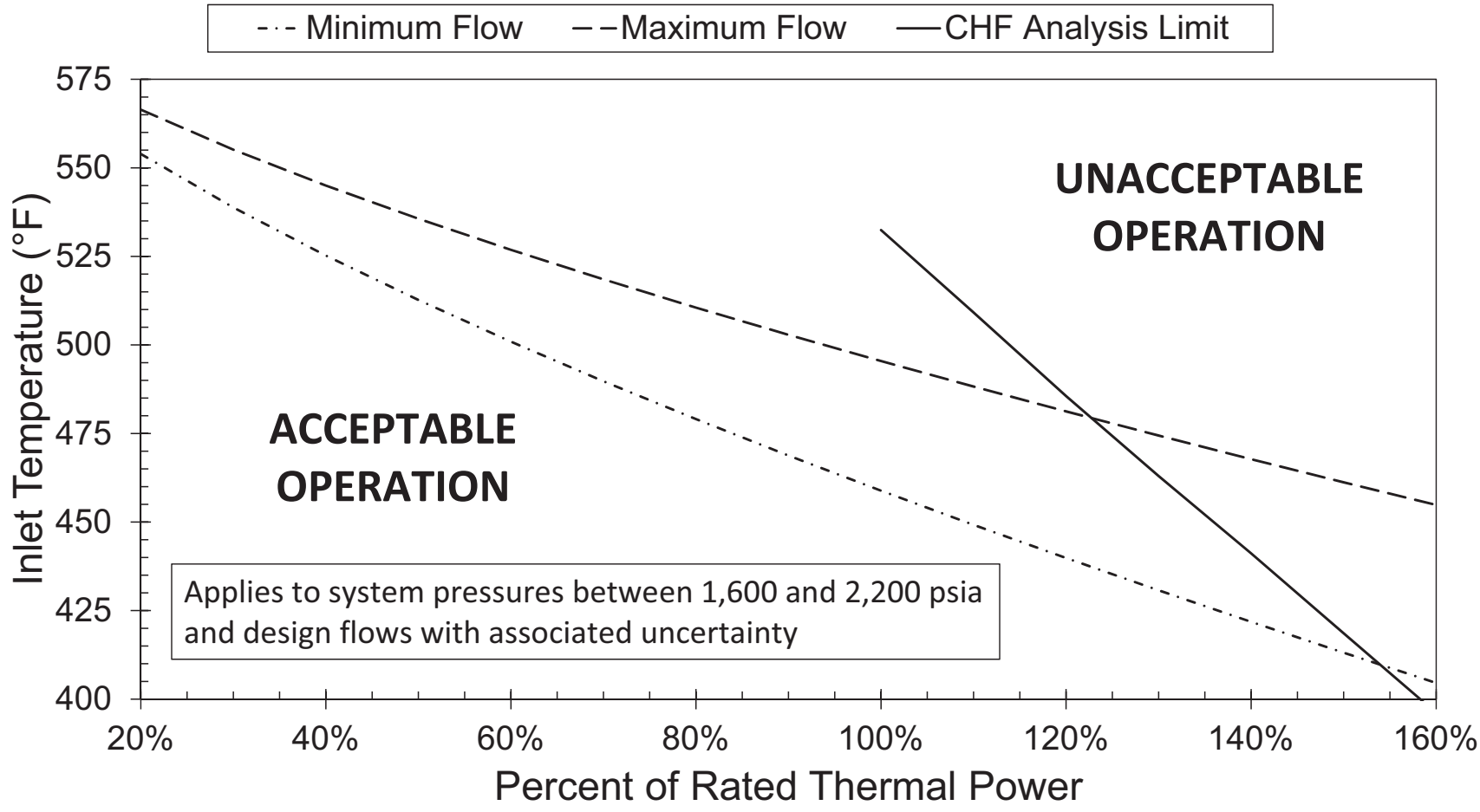

4.5 Reactor Materials

4.5.1 Control Rod Drive System Structural Materials

The control rod drive system (CRDS) consists of the control rod drive mechanisms (CRDMs) and the related mechanical components that provide the means for control rod assembly insertion into the core as described in Section 4.6. Portions of the CRDS are a part of the reactor coolant pressure boundary (RCPB) as described in Section 5.2.

The CRDS materials discussed in this section include the CRDMs and extend to the coupling interface with the control rod assemblies in the reactor vessel. Materials for the pressure-retaining components of the CRDMs are listed in Section 5.2.

Section 3.9.4 provides the details of the mechanical testing, seismic analysis of the CRDS, components life cycle testing, and mechanism functional tests.

4.5.1.1 Materials Specifications

The CRDMs are mounted above the pressurizer steam space on the reactor pressure vessel and inside the containment vessel. The CRDM internal components can be exposed to primary coolant or saturated steam and non-condensable gases. Before module movement for refueling, the containment vessel is partially flooded with borated water; therefore, the material design of the external surfaces of the CRDM include consideration of inadvertent submergence into borated water during module movement or refueling. The inside surfaces of the CRDM cooling water piping, tubes, and cooling jacket and the outside surfaces of the drive coil housings are exposed to component cooling water. The CRDM materials are selected to be compatible with the applicable fluid environments.

Portions of the CRDM that establish the RCPB are classified as Quality Group A and are designed, fabricated, constructed, tested, and inspected as Class 1 in accordance with Section III of the American Society of Mechanical Engineers (ASME) Boiler and Pressure Vessel Code (BPVC), 2017 Edition, and the applicable conditions promulgated in 10 CFR 50.55a.(b). These CRDM materials, including weld materials, conform to fabrication, construction, and testing requirements of BPVC, 2017 Edition, Section III, Subsection NB. Pressure retaining materials, including bolting materials and weld filler metal, selected for fabrication conform to the applicable material specifications provided in ASME BPVC, 2017 Edition, Section II and meet the requirements of ASME BPVC, Section III, 2017 Edition, Article NB-2000.

The CRDM cooling water pressure boundary and water connections external to the RCPB are designed in compliance with ASME BPVC, 2018 Edition, B31.1.

The seismic support plates of the rod position indication assembly are classified as ASME BPVC, 2017 Edition, Section III, Subsection NF Class 1 Supports and are constructed per the rules of ASME BPVC, 2017 Edition, Section III, Subsection NF.

Non-RCPB portions of the CRDM contained within the pressure housing are not categorized as ASME Code components. They are constructed to not adversely affect the integrity of the core support structures, and use materials that conform to either an ASME, Aerospace Material, or American Society for Testing and Materials (ASTM) material specification.

Non-RCPB CRDM component materials include Types 304, 316, 410, 410T, 440C, 630 H1100, AMS 5662, AMS 5698, AMS 5699, AMS 5662, AMS 5759, AMS 5894 or a low-cobalt alternative, UNS N07750, UNS N07718, and UNS N06625. Materials exposed to borated pool water, primary reactor coolant, saturated steam and non-condensable gases, or component cooling water are corrosion-resistant stainless steels, nickel-based alloys, and, to a limited extent, cobalt-based alloys. These materials are selected from those proven in light-water reactor operation and for their compatibility with the reactor coolant as specified in ASME BPVC, 2017 Edition, Section III, Paragraph NB-2160 and Subsubarticle NB-3120.

The CRDS pressure-retaining components are not fabricated or manufactured from cast austenitic stainless steel. Use of cold-worked austenitic stainless steel is avoided to the extent practicable during fabrication of CRDS structural components. Austenitic stainless steel with yield strength greater than 90,000 psi, as determined by the 0.2 percent offset method, is not used in fabricating CRDS structural components.

4.5.1.2 Austenitic Stainless Steel Components

Processing and welding unstablized American Iron and Steel Institute (AISI) Type 3XX series austenitic stainless steels for pressure-retaining parts comply with Regulatory Guide (RG) 1.44, Revision 1, to prevent sensitization and stress corrosion cracking. Austenitic stainless steel is procured in the solution-annealed condition. When rapidly cooled by means other than water quenching, non-sensitization of base materials is verified by test in accordance with Practice A or Practice E of ASTM A262 (Reference 4.5-1).

Unstabilized AISI Type 3XX series austenitic stainless steel base metals and weld filler metals have a maximum carbon content of 0.03 weight percent. This specification excludes base metals that are not welded or exposed to sensitizing temperatures in the range of 800 degrees F to 1500 degrees F subsequent to solution annealing.

The CRDM weld filler metals are in accordance, as applicable, with SFA-5.4 and SFA-5.9 of ASME BPVC, 2017 Edition, Section II, Part C. These include E308, E308L, E309, E309L, E316, E316L, E410, E430, ER308, ER308L, ER309, ER309L, ER316, ER316L, ER410, and ER430. They are analyzed for delta ferrite content and limited to a ferrite number (FN) of 5FN to 20FN in accordance with RG 1.31, Revision 4, and ASME BPVC, 2017 Edition, Section III, Paragraph NB-2433, except for Types 316 and 316L, which are limited to the range of 5FN to 16FN.

Section 5.2.3 describes the controls used to minimize the introduction of potentially harmful contaminants including chlorides, fluorides, and low-melting point alloys on the surface of austenitic stainless steel components that are part of the RCPB, including the CRDM reactor coolant pressure boundary components. Cleaning solutions, processing equipment, degreasing agents, and other foreign materials are removed during processing before elevated temperature treatments. Acid pickling is avoided on stainless steel and not used on sensitized austenitic stainless steel.

4.5.1.3 Other Materials

The use of martensitic stainless steel is limited to Types 410 and 440C. Type 410 is tempered at not less than 1050 degrees F to prevent temper embrittlement and stress-corrosion cracking.

Nickel-chromium-based alloy X-750 is used for the CRDM springs and cobalt-based-alloys Haynes 25 and Stellite 6 or 6B are used for wear-resistant parts. These materials have been used in existing pressurized water reactor CRDMs for the same function with satisfactory performance. The material of the pins associated with gripper components is Haynes 25. Stellite 6 or 6B material is limited to the CRDM gripper latch arms. To minimize the possibility of stress-corrosion cracking failures, the CRDM springs and wear-resistant parts are procured in the same heat treatment condition as previously used in the industry. Alloy X-750 spring material and heat treatment conform to the requirements of AMS 5698 or AMS 5699. There have been no operating experience reports of stress-corrosion cracking of Alloy X-750 CRDM springs fabricated from AMS 5698 and AMS 5699. For Alloy X-750, the cobalt impurity does not exceed 1 percent. To minimize cobalt intrusion into the reactor coolant, low-cobalt or cobalt-free alloys may be used for wear-resistant CRDM parts if their wear and corrosion resistance are qualified by testing. Alloy 625, Alloy 718, and Type 440C are used for improved strength in select CRDM components. Grades 8, B6, B8, and B8M are used for some screws and bolts. Type 630 H1100 is used for some fasteners and threaded rods. These materials have satisfactory performance in existing light-water reactors.

4.5.1.4 Material Cleaning and Cleanliness Control

Cleaning and cleanliness controls of CRDMs comply with the quality assurance requirements in Subpart 2.1 of ASME NQA-1 (Reference 4.5-2).

4.5.2 Reactor Internals and Core Support Structure Materials

Figure 3.9-1 through Figure 3.9-4 show the reactor vessel internals (RVI) subassemblies with components that comprise the RVI. The RVI do not contain any cast austenitic stainless steel components.

4.5.2.1 Materials Specifications

Materials used for the RVI consist of Type 304, F304, TP304, TP304 SMLS, TP321, XM-19, and UNS S21800, and strain-hardened Type 316 [Code Case

N-60-6 (Reference 4.5-3)] austenitic stainless steels in the following forms: SA-182, SA-193, SA-213, SA-240, SA-249, SA-312, SA-479, SA-508, SA-965, A-249, and A-580. Allowable weld materials are described in Section 4.5.2.4. The portions of the RVI performing a core support function are designed and fabricated as Class CS in accordance with ASME BPVC, 2017 Edition, Section III, Subsection NG. The materials for core support structures and threaded structural fasteners conform to the requirements of ASME BPVC, 2017 Edition, Section III, Subsubarticle NG-2120 and the applicable requirements of ASME BPVC, 2017 Edition, Section II, Part D, Tables 2A and 2B and Code Case N-60-6. The remaining portions of the RVI are designated as internal structures and are designed to conform to ASME BPVC, 2017 Edition, Section III, Paragraph NG-1122.

4.5.2.2 Control on Welding

The welding of RVI materials conforms to the applicable requirements of ASME BPVC, 2017 Edition, Section III, Articles NG-2000, NG-4000, and NG-5000. Welding is conducted using procedures qualified according to the rules of ASME BPVC, 2017 Edition, Section III, Subarticle NG-4300 and Section IX of the latest edition. Welders and welding operators are qualified in accordance with ASME BPVC Section IX of the latest edition and RG 1.71, Revision 1.

Electroslag welding is not permitted on RVI and core structural supports. Alloy 600 (UNS N06600) and associated weld filler materials are not used in the RVI.

4.5.2.3 Nondestructive Examination

Nondestructive examinations of core support structure materials, including tubular products, conform to the requirements of ASME BPVC, 2017 Edition, Section III, Subarticle NG-2500 using the methods of ASME BPVC, 2017 Edition, Section V and acceptance standards of Subarticle NG-5300.

4.5.2.4 Fabrication and Processing of Austenitic Stainless Steel Components

Austenitic stainless steel parts are fabricated from materials procured in the solution-annealed condition. Use of cold-worked austenitic stainless steel is avoided to the extent practicable during fabrication of the RVI and core support structures. Cold-worked austenitic stainless steel used in the RVI and core support components does not exceed a yield strength of 90,000 psi as determined by the 0.2 percent offset method.

Processing and welding unstablized AISI Type 3XX series austenitic stainless steels comply with RG 1.44, Revision 1 to prevent sensitization and stress-corrosion cracking. When rapidly cooled by means other than water quenching, non-sensitization of base materials is verified by test in accordance with Practice A or Practice E of ASTM A262 (Reference 4.5-1).

For unstabilized AISI Type 3XX series austenitic stainless steel subjected to sensitizing temperatures subsequent to solution heat treatment, the carbon content is limited to no more than 0.03 weight percent.

The RVI weld filler metals and associated specifications are in accordance with ASME BPVC, 2017 Edition, Section II, Part C. They are analyzed for delta ferrite content and limited to a ferrite number of 5FN to 20FN, except for Types 316 and 316L, which are limited to the range of 5FN to 16FN, in accordance with RG 1.31, Revision 4 and ASME BPVC, 2017 Edition Section III, Paragraph NG-2433. Carbon content of austenitic stainless steel weld filler metals is limited to no more than 0.03 weight percent.

Tools for abrasive work such as grinding, polishing, or wire brushing are not permitted to be contaminated by previous usage on ferritic carbon steel or other materials that could contribute to intergranular cracking or stress-corrosion cracking.

Section 5.2.3 describes the controls used to minimize the introduction of potentially harmful contaminants including chlorides, fluorides, and low melting point alloys on the surface of austenitic stainless steel components. Cleaning solutions, processing equipment, degreasing agents, and other foreign materials are removed during processing before elevated temperature treatments and acid pickling of sensitized stainless steel is avoided.

4.5.2.5 Other Materials

Only austenitic stainless steel is used for RVI materials.

4.5.3 References

4.5-1 American Society for Testing and Materials, “Standard Practices for Detecting Susceptibility to Intergranular Attack in Austenitic Stainless Steels,” ASTM A262-15 (2021), West Conshohocken, PA.

4.5-2 American Society of Mechanical Engineers, Quality Assurance Requirements for Nuclear Facility Applications, ASME NQA-1-2015 Addenda, New York, NY.

4.5-3 American Society of Mechanical Engineers Boiler and Pressure Vessel Code, Nuclear Code Case, N-60-6, “Material for Core Support Structures Section III, Division 1."

4.6 Functional Design of Control Rod Drive System

The control rod drive system (CRDS) performs the following safety-related functions:

- releases the control rod assemblies (CRAs) during a reactor trip
- maintains the pressure boundary of the reactor pressure vessel (RPV)

The CRDS performs the following non safety-related functions:

- latching, holding, and maneuvering the CRAs during reactor startup, power operation, and shutdown
- provides rod position indication

4.6.1 Description of the Control Rod Drive System

The CRDS includes the control rod drive mechanisms (CRDMs) and associated equipment used to operate the CRDMs. The CRDM includes the control rod drive shaft, which extends to the coupling interface with the CRAs in the RPV. The CRDS supports the CRAs by latching, holding, and maneuvering the CRAs during reactor startup, power operation, and shutdown in response to signals from the control rod drive power converter and controller assembly, and in releasing the CRAs during a reactor trip. The CRDS also includes the rod position indicator cabinets and cables, CRDM power cables, and cooling water supply and return piping inside containment. The mechanical design of the CRDM is described in Section 3.9.4 and the design of the CRA is described in Section 4.2.2. The instrumentation and controls for the CRDS are described in Chapter 7.

Figure 4.6-1 through Figure 4.6-6 illustrate the principal features of the CRDS. Figure 4.6-1 is a simplified drawing showing an overview of the location of components of the CRDS relative to the RPV and the containment vessel (CNV). The CRDMs are mounted on top of the RPV and laterally constrained in order to limit relative lateral seismic motion, yet allow for unrestricted axial expansion. The control rod drive shafts are located inside the RPV and aligned laterally by CRDS support structures that are part of the reactor vessel internals. Further details are provided in Section 3.9.4. The electromagnetic load transfer across the primary pressure boundary is facilitated by electromagnetic coils on the outside (Figure 4.6-3) that engage a set of magnetic poles connected to latches on the inside (Figure 4.6-5), in order to move the control rod drive shaft in a predetermined stepping sequence (Section 3.9.4). Figure 4.6-2 provides an illustration of the CRDM electromagnetic coils and housings, including the pressure housings. The power and cooling water connectors are located on top of the pressure housing and rod position indication coil stack assembly for ease of access through the removable cover on top of the CNV (Figure 4.6-1). Figure 4.6-3 illustrates the CRDM drive coil and cooling jacket assembly. Figure 4.6-4 shows the layout of the rod position indicator sensor coil assemblies, which are located external to the pressure housing in the region where the control rod drive shaft tip travels during insertion and withdrawal. Rod position indication is facilitated by means of electromagnetic induction in the sensor coils as the top of the control rod drive shaft travels upwards or downwards within the pressure boundary. Figure 4.6-5 is a representative overview of the latch mechanism

assembly that performs the rod withdrawal/insertion/reactor trip functions. Figure 4.6-6 illustrates the CRDM drive shaft interface with the CRA.

The CRDM assembly is an electro-mechanical device that moves the CRA in and out of the reactor core and holds the CRA at any elevation within the range of CRA travel. If electrical power is interrupted to the CRDM, the control rod drive shaft is released and the attached CRA drops into the reactor core.

The CRDMs are mounted on the RPV head, and the CRDM pressure housings are safety-related American Society of Mechanical Engineers (ASME) Class 1 pressure boundaries. The CRDS components internal to the reactor coolant pressure boundary are designed to function in borated primary coolant at primary coolant pressures and temperatures ranging from ambient conditions up to the RPV design pressure and temperatures above normal operating conditions. The lower portion of the drive rod is submerged in the primary coolant at hot leg temperature flowing upward through the upper riser and CRA guide tubes. The electric coil operating conditions require active cooling by water through a CRDS cooling water distribution header to cooling jackets surrounding the drive coils of each CRDM as shown in Figure 4.6-3. The cooling requirements for the CRDMs are provided by the reactor component cooling water system, which maintains the CRDM winding temperature below the maximum design temperature (Section 9.2.2).

The CRDS cooling line is branched into supply lines inside the CNV to each individual CRDM. After passing through the CRDM cooling jackets, the return lines rejoin into a single return header leaving containment. A thermal relief valve is provided on the return header to provide overpressure protection for the CRDS cooling piping during a containment isolation event.

The structural materials of construction for the CRDS are discussed in detail in Section 4.5.1.

4.6.2 Design Bases

This section describes how the design of the CRDS conforms to General Design Criteria (GDC) 4, 23, 25, 26, 27, 28, and 29 of 10 CFR 50, Appendix A.

GDC 4 is applicable to the CRDS design as it requires the SSC important to safety to be designed to accommodate the effects of and to be compatible with the environmental conditions during normal plant operation as well as during postulated accidents as a result of equipment failures and external events. The CRDS complies with GDC 4. The CRDS components located inside the containment are protected against dynamic effects as described in Section 3.6. The CRDS structures, systems, and components are located inside the Reactor Building, which provides protection from events and conditions outside the plant. The ability of the CRDS to perform the required safety-related functions is not compromised by adverse environmental conditions. The control rod drive shafts are immersed in 540 degrees F water during normal full power operation. The upper portion of the control rod drive shafts penetrate the pressurizer steam space and are exposed to a steam environment at approximately 636 degrees F. The control rod drive shafts and latch mechanisms are designed to 650 degrees F.

The CRDS complies with GDC 23. The CRDS provides positive core reactivity control through the use of movable CRAs. The movable CRAs provide reactivity control for modes of operation when the NuScale Power Module is installed in its operating location. The CRDS, in conjunction with the module protection system, actuates the control rods to perform safety-related functions when necessary to provide core protection during normal operation, AOOs, and accidents. The CRDS is designed to fail in a safe condition under adverse conditions, preventing damage to the fuel cladding and excessive reactivity changes during failure. Loss of electrical power to the reactor trip breaker initiates a reactor trip, causing the control rods to drop into the core and shut down the reactor.

The CRDS complies with GDC 25. Chapter 15 safety analyses demonstrate the CRDS is capable of performing a reactor trip when plant parameters exceed the reactor trip setpoint, given a credible failure of a single active component.

The CRDS complies with GDC 26 and GDC 27 as described in Section 4.3.

The CRDS complies with GDC 28. A postulated failure of the CRDS causing a rod ejection has the potential to result in a relatively high rate of positive reactivity insertion, which could challenge specified acceptable fuel design limits. The rod ejection accident is not analyzed as a loss-of-coolant accident event. To prevent a mechanical failure of the CRDM housings, the CRDM is made as a single-piece housing, with a top plug. The rod ejection analysis presented in Section 15.4 demonstrates GDC 28 is met.

GDC 29 is applicable to the CRDS design. The CRDS accomplishes safe shutdown (i.e., reactor trip) via gravity-dropping of the CRAs on a reactor trip signal or loss of electrical power. The CRDM pressure housing is an ASME Class 1 pressure boundary and maintains the reactor coolant pressure boundary during all ASME service levels.

The safety-related reactor trip function of the CRDS is initiated by the module protection system through the reactor trip system, which isolates the CRDS power converter and controller assembly from its motive power supply. Failures of the CRDS are evaluated in failure modes and effects analyses. Effectiveness of the CRDS, despite possible single failures, is demonstrated in Chapter 15, which shows the CRDS performs a reactor trip when plant parameters exceed the reactor trip setpoint. Therefore, the reactor is placed in a subcritical condition with the assumed credible failure of a single active component.

Section 3.6 demonstrates CRDS essential equipment is protected from common-mode failure caused by leakage or rupture of moderate- and high-energy lines, the dynamic and environmental effects of postulated breaks, and potential jet impingement to ensure compliance with GDC 4.

The CRDM components inside the CNV are located near high- and moderate-energy fluid system piping, such as reactor coolant system piping, feedwater piping, and steam piping. Loads from moderate- and high-energy line breaks are included in the stress analysis of the CRDM pressure housing, which is designed in accordance with the rules of the ASME Boiler and Pressure Vessel Code.

The jet impingement loads generated from high-energy line breaks inside the CNV are evaluated as described in Section 3.6, which states that circumferential and longitudinal breaks that could impinge on the CRDMs are not postulated. The other high-energy lines inside containment are small (NPS 2 or less). The line size limits the energy of jet impingement loads. Based on the low jet pressure load and heavy-walled construction of the CRDMs, jet impingement does not adversely affect CRDM scram functionality.

Jet impingement loads are expected from opening the reactor safety valves and the reactor vent valves, which vent to the containment. A fluid jet diffuser is provided at the outlet of the reactor vent valves to dissipate the energy of the fluid jet in order to protect the essential SSC in the region of containment near the RPV head. The CRDM design features described above ensure jet impingement loads resulting from opening the reactor safety valves do not adversely affect CRDM scram functionality.

The essential control elements of the CRDS (those required to provide reactor trip) are provided by the module protection system and are isolated from nonessential portions of the rod control system provided by the module control system, as described in Section 7.0.

4.6.3 Testing and Verification of the Control Rod Drive System

The CRDS prototype testing is described in Section 3.9.4 and Section 4.2.4. The testing of the prototype includes conceptual (mock-up) testing, prototype performance testing, stability testing, and endurance testing.

The pre-operational and initial startup tests that are performed to verify the proper function of the CRDS are described in Section 14.2. They include insertion, withdrawal and drop time testing, and hydrostatic tests. Inservice tests are conducted to verify the operability of the CRDS on a periodic basis and are described in the Technical Specifications.

4.6.4 Information for Combined Performance of Reactivity Systems

Single or common cause failures of the CRDS do not prevent proper operation of the reactor trip function. There are no reactor trip function failures that prevent proper functioning of the engineered safety features actuation system. Section 7.2 provides details that support this conclusion.

Section 4.3 provides information on the performance of reactivity control systems in accordance with GDC 26 and 27. Release of the CRAs credited in the design-basis safety analyses for reactivity control.

4.6.5 Evaluations of Combined Performance

Chapter 15 demonstrates for design-basis events, the reactor is maintained within acceptable limits.

Figure 4.6-1: Representative Overview of Control Rod Drive Mechanism Locations in Relation to the Reactor Pressure Vessel and Containment Vessel

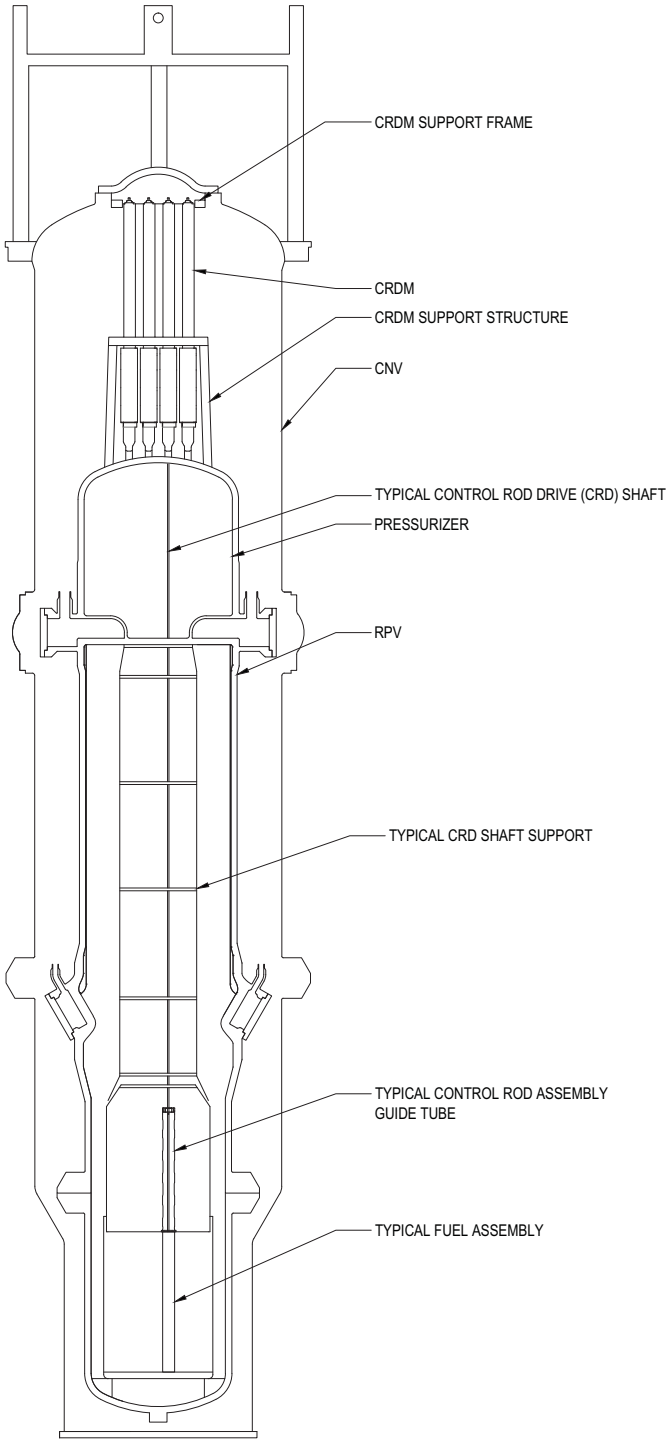

Figure 4.6-2: Representative Control Rod Drive Mechanism Coils and Housings

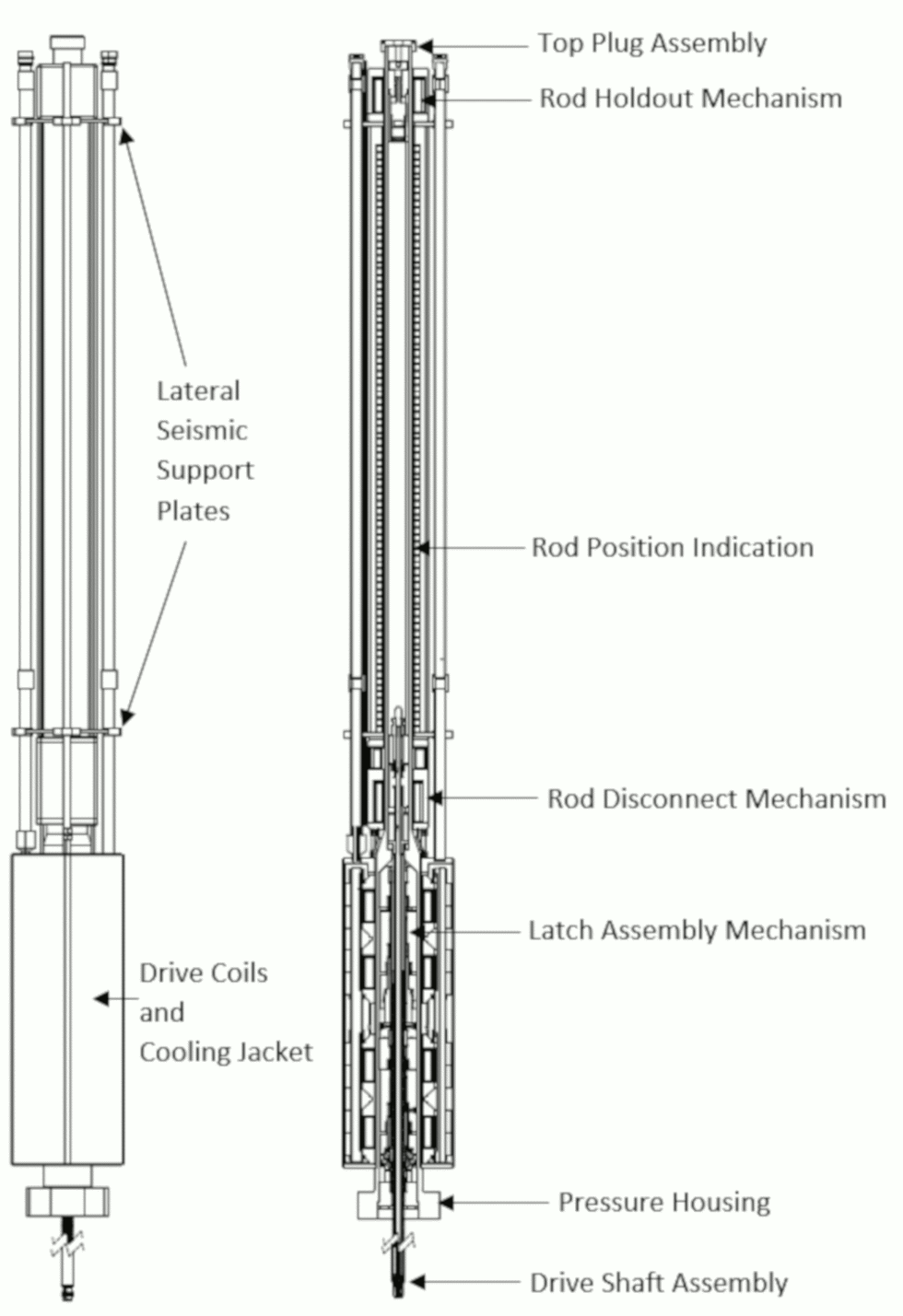

Figure 4.6-3: Representative Control Rod Drive Mechanism Drive Coil and Cooling Jacket Assembly

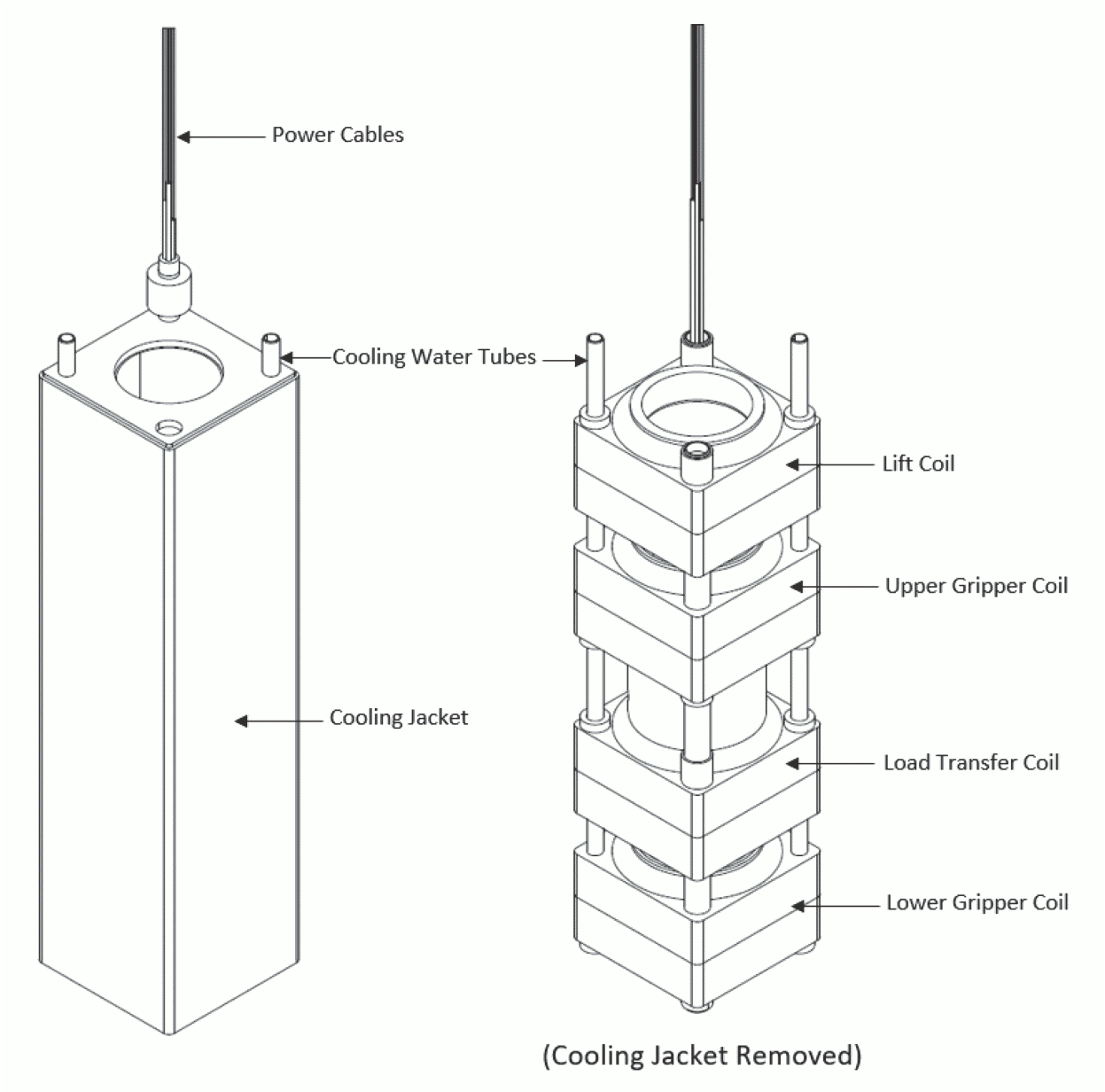

Figure 4.6-4: Representative Rod Position Indication Assembly

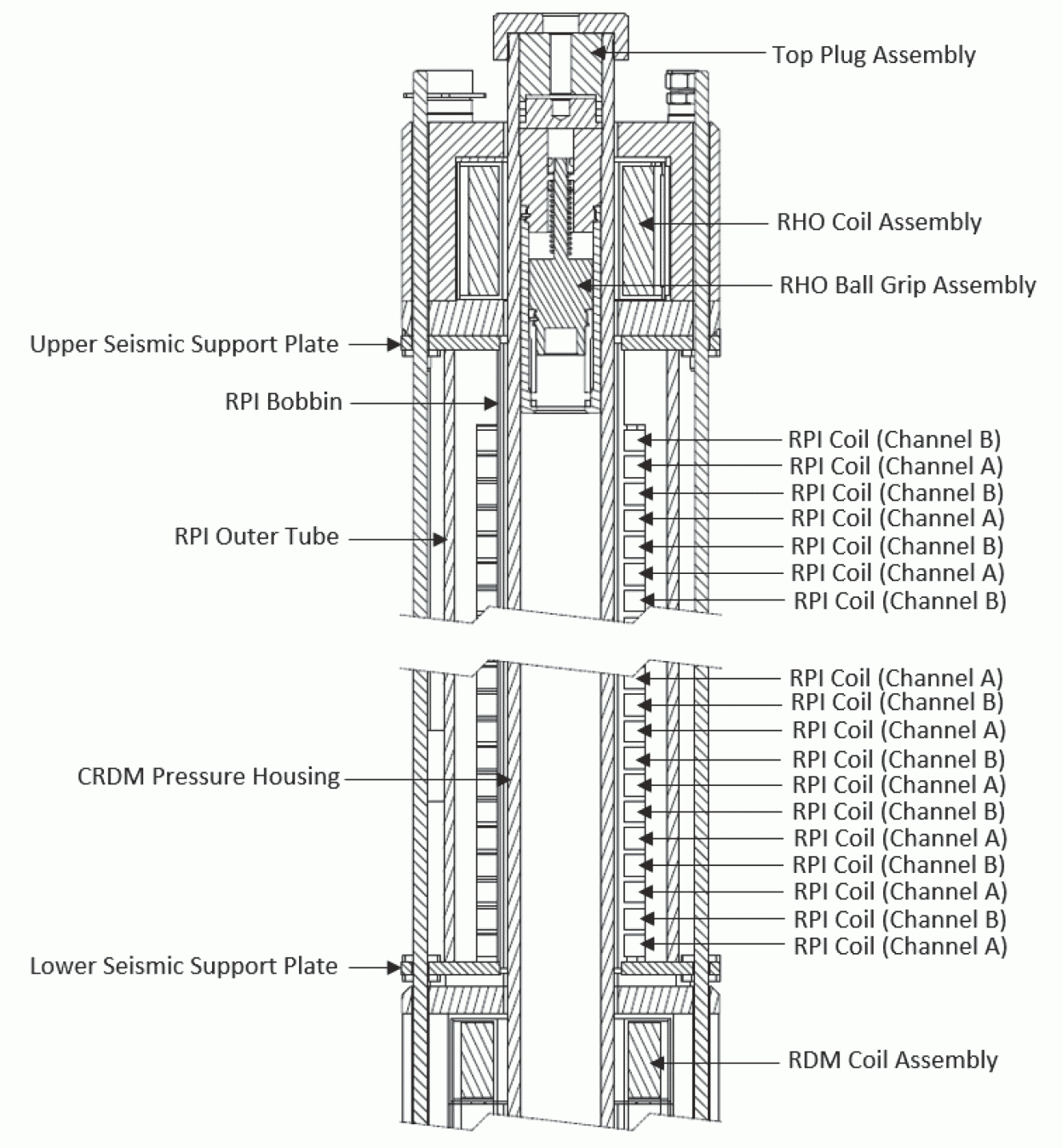

Figure 4.6-5: Representative Overview of Latch Mechanism Assembly

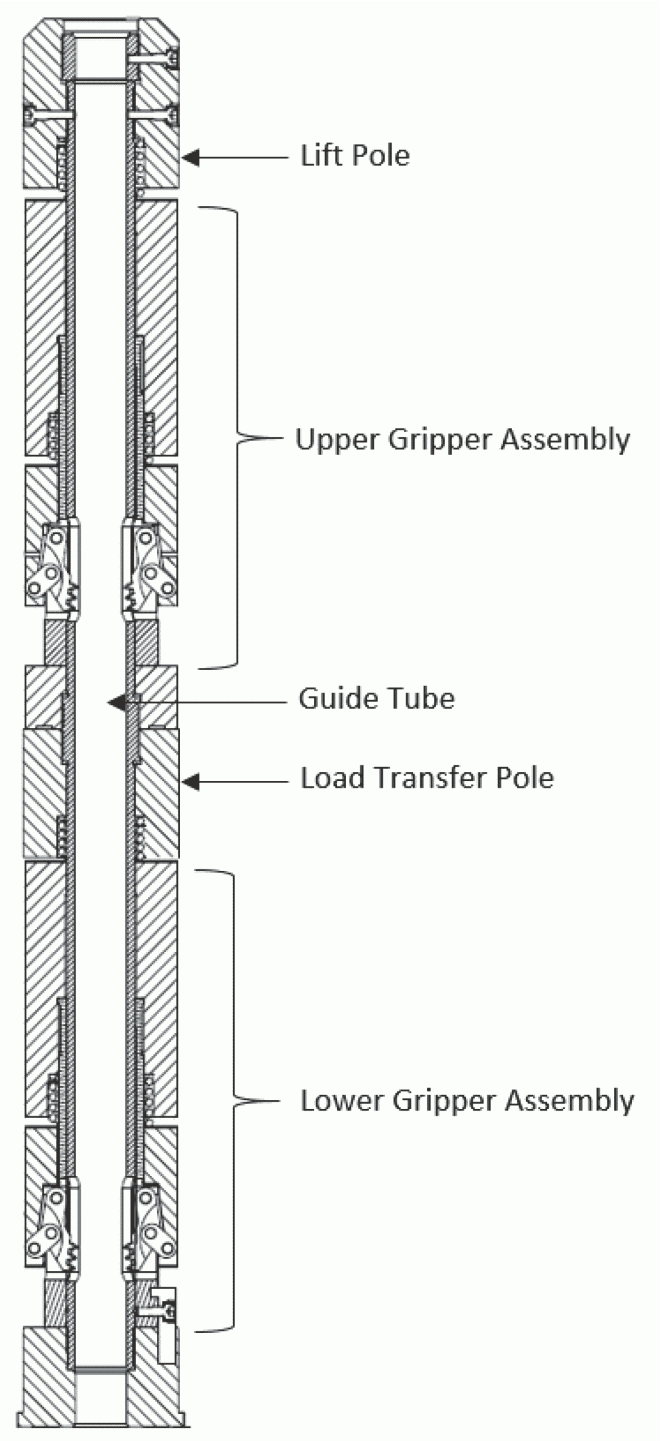

Figure 4.6-6: Representative Control Rod Drive Mechanism Drive Shaft Interface with Control Rod Assembly

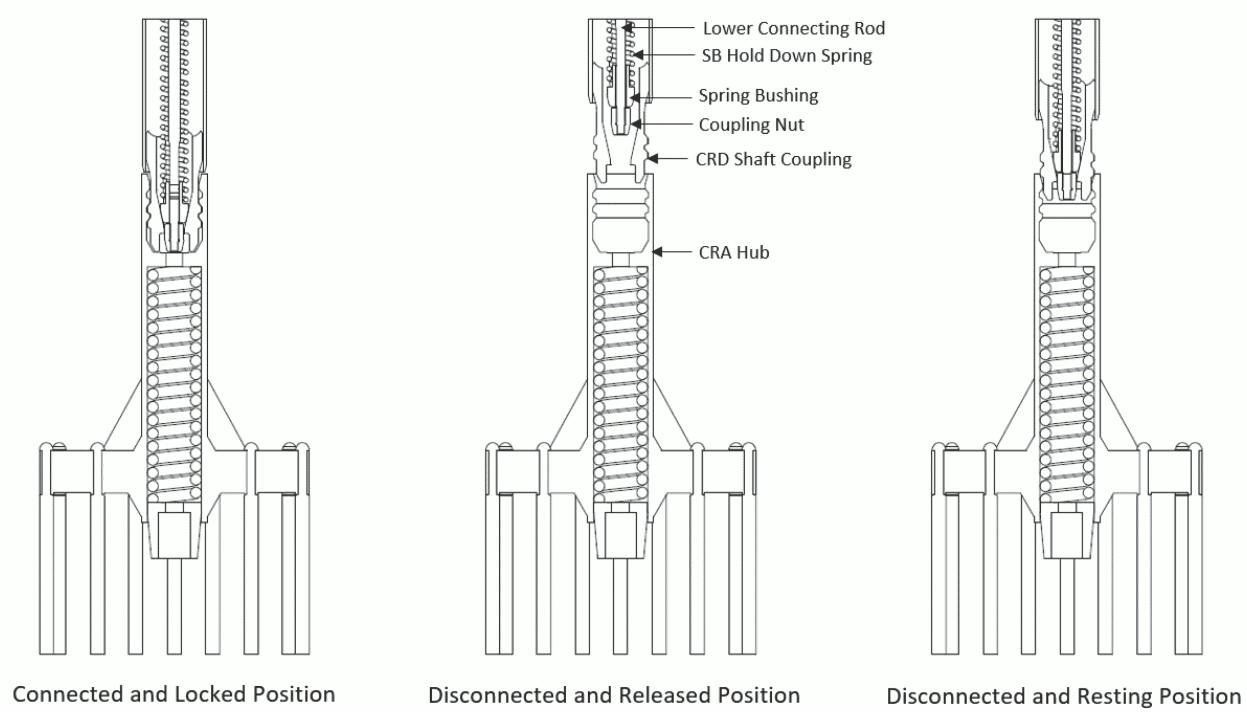

Section B

NuScale Power, LLC
1100 NE Circle Blvd., Suite 200 Corvallis, Oregon 97330 Office 541.360.0500 Fax 541.207.3928
www.nuscalepower.com

The table below provides NuScale's responses to each of the Nuclear Regulatory Commission readiness assessment observations on draft Chapter 4, "Reactor," of the Standard Design Approval Application.

Section	Observation	Response
4.4	All critical heat flux (CHF) correlations used in the application should be described in 4.4. The applicability ranges and limits should be included for the CHF correlations.	Additional discussion of the NuScale-developed NSPN-1 correlation for use with events characterized by a rapid system depressurization is in Section 4.4 of the Final Safety Analysis Report. Reference to the supporting topical reports is included throughout Section 4.4. The CHF correlations, associated ranges of applicability, and corresponding design limits are described in the topical reports.
4.4	Subsection 4.4.4.5.2 states that "conservatisms in the modeling of the subchannel analysis methodology have been determined to bound the effects of crud. "However, there is no reference for where this determination was made and is not included in the subchannel analysis TR.	Additional discussion is included in Section 4.4.4.5.2 of the Final Safety Analysis Report to provide the basis for the determination that the subchannel analysis methodology bounds the effects of crud.
4.3	The following information needed to evaluate the core design is missing from Section 4.3: - Fuel loading pattern - Peaking factor (FdH and FQ) curves - Differential boron worth curves - Radial relative power within fresh, once-, and twice-burned fuel assemblies - Power coefficient of reactivity - Assumed xenon concentration in refueling boron concentration calculation Additionally, some entries in Table 4.3-2 are blank.	Section 4.3 of the Final Safety Analysis Report includes the identified content.
4.3	Provide control rod worth (total for each bank, total from power-dependent insertion limit to full insertion, and differential) at the different operating modes and stages of the reactor and the associated uncertainty information to allow reviewers to make a determination regarding the adequacy of the shutdown margin at different stages of the reactor operations, e.g. beginning of cycle, emergency operations center and middle of the cycle. Because the control rod worth is dependent of the reactor core design, a new set of control rod worth for each bank should be provided for the new core design.	Section 4.3 of the Final Safety Analysis Report includes the identified content.
4.3	The DCA figure displaying power defect (i.e., Figure 4.3-15) was removed from the SDA. This information is related to the integrated power	Section 4.3 of the Final Safety Analysis Report includes the identified content.

Section	Observation	Response
	coefficient over the range of the power change. Reviewers will need this information to evaluate the shutdown margin.	
4.3	The role of the supplemental boron addition system in assuring long-term shutdown should be discussed.	Section 4.3 of the Final Safety Analysis Report includes the identified content.

Section C

NuScale Power, LLC
1100 NE Circle Blvd., Suite 200 Corvallis, Oregon 97330 Office 541.360.0500 Fax 541.207.3928
www.nuscalepower.com

TR Number	TR Title
TR-117605-NP Revision 0	NuFuel-HTP2™ Fuel and Control Rod Assembly Designs

NuScale Power, LLC
1100 NE Circle Blvd., Suite 200 Corvallis, Oregon 97330 Office 541.360.0500 Fax 541.207.3928
www.nuscalepower.com

Licensing Technical Report

NuFuel-HTP2™ Fuel and Control Rod Assembly Designs

December 2022

Revision 0

Docket: 52-050

NuScale Power, LLC
1100 NE Circle Blvd., Suite 200
Corvallis, Oregon 97330
www.nuscalepower.com

© Copyright 2022 by NuScale Power, LLC

Licensing Technical Report

COPYRIGHT NOTICE

This report has been prepared by NuScale Power, LLC and bears a NuScale Power, LLC, copyright notice. No right to disclose, use, or copy any of the information in this report, other than by the U.S. Nuclear Regulatory Commission (NRC), is authorized without the express, written permission of NuScale Power, LLC.

The NRC is permitted to make the number of copies of the information contained in this report that is necessary for its internal use in connection with generic and plant-specific reviews and approvals, as well as the issuance, denial, amendment, transfer, renewal, modification, suspension, revocation, or violation of a license, permit, order, or regulation subject to the requirements of 10 CFR 2.390 regarding restrictions on public disclosure to the extent such information has been identified as proprietary by NuScale Power, LLC, copyright protection notwithstanding. Regarding nonproprietary versions of these reports, the NRC is permitted to make the number of copies necessary for public viewing in appropriate docket files in public document rooms in Washington, DC, and elsewhere as may be required by NRC regulations. Copies made by the NRC must include this copyright notice and contain the proprietary marking if the original was identified as proprietary.

Licensing Technical Report

Department of Energy Acknowledgement and Disclaimer

This material is based upon work supported by the Department of Energy under Award Number DE-NE0008928.

Table of Contents

Table of Contents

Table of Contents

List of Tables

List of Figures

Abstract

This report describes the NuFuel-HTP2™ fuel and control rod assembly design, summarizes the key analysis results, and evaluates the fuel and control rod assembly design performance against regulatory requirements. The evaluations are focused on the mechanical aspects of the designs, consistent with Section 4.2 of NUREG-0800.

Executive Summary

This report describes the NuFuel-HTP2™ fuel and control rod assembly (CRA) design, summarizes the key analysis results, and evaluates the fuel and CRA design performance against regulatory requirements.

The fuel is designed and analyzed in accordance with regulatory requirements in NUREG-0800 Section 4.2 and the regulatory requirements from General Design Criterion (GDC) 2, GDC 10, GDC 27, Principal Design Criterion (PDC) 35, and 10 CFR 50.46.

Fuel Assembly

The fuel design is a reduced height 17x17 pressurized water reactor design. The assembly contains five spacer grids, 24 MONOBLOC™ guide tubes and a top and bottom nozzle. The bottom nozzle contains a mesh debris filter. The top nozzle is removable to allow for reconstitution of fuel rods if needed. The top four grids provide structural support for the fuel assembly and enhance mixing of the coolant. The bottom grid is primarily for structural support. The fuel rod cladding is M5®, an advanced zirconium alloy. The fuel is UO_2 enriched up to 4.95 weight percent ^{235}U, with gadolinia homogeneously mixed in some fuel pellets.

The fuel assembly is analyzed using established design criteria and methods to demonstrate that the fuel assembly is not damaged during normal operation, anticipated operational occurrences, and postulated accidents. Potential failure mechanisms include mechanical loading, fatigue, fretting, oxidation, growth, and distortion.

The fuel rod is analyzed using established design criteria and methods to demonstrate that the fuel rod is not damaged during normal operation, anticipated operational occurrences, and postulated accidents. Potential failure mechanisms include internal pressure, internal hydriding, creep collapse, centerline melting, pellet-cladding interaction, and mechanical loading. Certain design criteria (e.g., those associated with loss-of-coolant accidents) are addressed in other portions of the NuScale US460 Final Safety Analysis Report.

The design criteria and methods have been applied to fuel assembly and rod designs currently in power operation and have been demonstrated to be applicable to the NuFuel-HTP2™ design. The evaluations presented in this report demonstrate that the fuel rod design meets all applicable design criteria.

Mechanical testing is performed to characterize the mechanical performance of the fuel assembly. Test results support the design evaluations presented in this report. Thermal-hydraulic evaluations and tests are performed to characterize the hydraulic performance of the fuel assembly and demonstrate that the fuel design meets all applicable design criteria.

Evaluations and tests performed are comprehensive and demonstrate the acceptability of the fuel assembly design for use in the NuScale Power Module.

Control Rod Assembly

The CRA contains 24 individual control rods fastened to a stainless steel spider hub. The control rod tubes are stainless steel and contain silver indium cadmium (AIC) and boron carbide (B_4C) neutron absorbers.

The CRA design is analyzed using established design criteria and methods to demonstrate acceptable performance over the design lifetime. Potential failure mechanisms include stresses, strain, creep collapse, fatigue, wear, internal pressure, and component melting. Evaluations summarized in this report demonstrate that the CRA design meets all applicable criteria and is acceptable for use in the NuScale Power Module.

Testing is performed to confirm CRA drop times and CRA drop velocity, and to assess the impact of the maximum expected fuel assembly distortion and the misalignment of the lead screw and guides.

1.0 Introduction

NuScale Power, LLC (NuScale) has developed a 17x17 fuel assembly, NuFuel-HTP2™, and control rod assembly (CRA) design for use in the NuScale Power Module (NPM) based on existing Framatome methods and technology.

1.1 Purpose

This report describes the NuFuel-HTP2™ fuel assembly and CRA designs, summarizes the key analysis results, and demonstrates the designs meet regulatory requirements.

1.2 Scope

This report uses Framatome methodologies to evaluate the NuFuel-HTP2™ fuel design against the requirements of NUREG-0800 Section 4.2 (Reference 9.1.1). The evaluations are focused on the mechanical aspects of the design. Neutronic and thermal-hydraulic performance of the fuel assembly are addressed in the NuScale US460 Final Safety Analysis Report.

This report also summarizes the CRA design and analyses.

Chapter 2 provides the regulatory framework that identifies the requirements against which the fuel design is evaluated.

Chapter 3 describes the mechanical design and function of the fuel assembly and provides a brief description of applicable operating experience.

Chapter 4 summarizes the results of the fuel assembly design evaluations using NRC-approved methods.

- The NuFuel-HTP2™ fuel mechanical design is evaluated using generic mechanical design criteria for pressurized water reactor (PWR) fuel designs (Reference 9.1.2 and Reference 9.1.3).
- The COPERNIC Fuel Rod Design Computer Code (Reference 9.1.4) is used in the fuel performance analysis of the NuFuel-HTP2™ fuel design.
- The CROV code (Reference 9.1.5) is used to evaluate the cladding creep performance.
- The computational procedure for evaluating fuel rod bowing (Reference 9.1.6) is used to evaluate the impacts of fuel rod bow for the NuFuel-HTP2™ design.
- The PWR fuel assembly structural response to externally applied dynamic excitations (Reference 9.1.7) is used to perform seismic structural analysis on the fuel design.

The applicability of the fuel analysis methods is demonstrated in *Applicability of AREVA Fuel Methodology for the NuScale Design*, TR-0116-20825-P-A Revision 1 (Reference 9.1.8), *NuScale Applicability of AREVA Method for the Evaluation of Fuel Assembly Structural Response to Externally Applied Forces*, TR-0716-50351-P-A Revision 1 (Reference 9.1.9), and as supplemented for the US460 design *Framatome*

Fuel and Structural Response Methodologies Applicability to NuScale, Supplement 1 to TR-0116-20825-P-A, Revision 1, Supplement 1 to TR-0716-50351-P-A, Revision 1, TR-108553-P-A (Reference 9.1.10).

Chapter 5 describes the comprehensive testing performed to support the fuel assembly design and analysis.

Chapter 6 describes the CRA design and the analyses and testing that support the design.

Chapter 7 provides guidance for managing design changes to the fuel and CRA design. Criteria are provided to distinguish changes that require NRC approval.

Chapter 8 provides a summary and concludes that the NuFuel-HTP2™ fuel and CRA designs satisfy the applicable design requirements.

Table 1-1 Abbreviations

Term	Definition
AOO	anticipated operational occurrence
ASME	American Society of Mechanical Engineers
BOL	beginning of life
CFM	centerline fuel melt
CFR	Code of Federal Regulations
CRA	control rod assembly
CUF	cumulative usage factor
EFPY	effective full-power year
EOL	end of life
FCM	fuel centerline melt
FSAR	Final Safety Analysis Report
FIV	flow-induced vibration
GDC	General Design Criteria
LHR	linear heat rate
LOCA	loss-of-coolant accident
NPM	NuScale Power Module
NRC	Nuclear Regulatory Commission
OD	outside diameter
PDC	Principal Design Criterion
PHTF	portable hydraulic test facility (Richland)
PWR	pressurized water reactor
QD	quick disconnect
RCCA	rod control cluster assembly
RCS	reactor coolant system
RFT	reactor flange tool
RMS	root mean square
SRSS	square root of the sum of the squares
SSE	safe shutdown earthquake
TCS	transient cladding strain

2.0 Background

This report supports FSAR Section 4.2 . This section identifies the regulatory requirements that form the basis of the fuel design evaluation.

2.1 Regulatory Requirements

The mechanical design of the NuFuel-HTP2™ fuel assembly is evaluated against criteria established to be consistent with NUREG-0800 Section 4.2 (Reference 9.1.1). These criteria are specified in Section 4.0 of this report. Some of the NUREG-0800 acceptance criteria are addressed in plant transient analyses and are not addressed by this report, as noted in Section 4.0.

The following regulatory requirements apply to the fuel mechanical evaluations summarized in this report:

- General Design Criterion (GDC) 2, as it relates to designing fuel assemblies to withstand the effects of earthquakes
- GDC 10, as it relates to assuring that specified acceptable fuel design limits are not exceeded during any condition of normal operation, including the effects of anticipated operational occurrences (AOOs)
- GDC 27, as it relates to ensuring that fuel system damage is never so severe as to prevent control rod insertion when it is required
- 10 CFR 50.46, as it relates to ensuring that fuel assembly and fuel rod damage will not interfere with effective emergency core cooling

Additionally, as specified in FSAR Section 3.1, principle design criterion (PDC) 35 applies to the fuel mechanical evaluations as it relates to ensuring fuel damage does not interfere with effective emergency core cooling.

Section 4.0 identifies the approved methodologies used for evaluation of each criterion. These methodologies are demonstrated to be applicable to the design in Reference 9.1.8 and Reference 9.1.9 as supplemented for applicability to the US460 design in Reference 9.1.10.

3.0 NuFuel-HTP2™ Fuel Assembly Description

The NuFuel-HTP2™ fuel assembly (Figure 3-1) is a 17x17 PWR design that is approximately one-half the length of typical PWR nuclear plant fuel. Other than the shortened length, the assembly contains design features similar to those of proven HTP™ fuel designs. All components of the fuel assembly have relevant operating experience that demonstrates their suitability for use in reactor cores. The assembly is supported by five spacer grids, 24 guide tubes, and a top and bottom nozzle that together provide the structural skeleton for the 264 fuel rods. The fuel rod consists of M5® alloy cladding and uranium dioxide (UO_2) pellets with gadolinium oxide (Gd_2O_3) as a burnable absorber homogeneously mixed within the fuel pellets in select rod locations. Table 3-1 and Table 3-2 list key fuel design parameters.

Table 3-3 provides representative operating conditions for the NPM. The core contains 37 fuel assemblies. Sixteen of the fuel assembly locations contain CRAs. Figure 3-2 provides a representative core loading pattern showing the arrangement of the fuel assemblies in the reactor core.

The total, nominal height of the fuel assembly is 94 inches (excluding the hold-down spring height). Due to the assembly height and the use of span lengths between spacer grids that are typical for operating PWR plants, the assembly has a total of five spacer grids that provide lateral support for the fuel rods. Four HTP™ grids at the intermediate and top spacer locations are welded to the guide tubes, while the HMP™ lower grid at the bottom location of the fuel assembly is captured by rings welded to the guide tubes.

The fuel assembly materials (Table 3-4) are chosen for their low cobalt content to reduce plant dose, for corrosion resistance, and for desirable structural properties.

A summary of the NuFuel-HTP2™ components is provided below.

3.1 Top Nozzle

The top nozzle (Figure 3-3) consists of a stainless steel frame that interfaces with the reactor upper internals and the core components while providing for reactor coolant flow. The top nozzle flow hole pattern provides low pressure drop while satisfying strength requirements. A through-hole feature allows for insertion of the in-core instrumentation from above the fuel assembly.

The top nozzle is attached to the fuel assembly with quick disconnect (QD) features at each of the 24 guide tube locations. The QD features allow for removal of the top nozzle for fuel assembly reconstitution.

Two diagonally opposed corners of the top nozzle contain holes for accommodating the upper core plate alignment pins. Mounted on the other two corners are four two-leaf hold-down springs. The spring leaves maintain positive hold-down margin and are fastened to the top nozzle with clamp screws. The upper leaf has an extended tang that engages a cutout in the top plate of the nozzle to retain the spring leaves in the unlikely event of a leaf or clamp screw failure.

On one of the corners with leaf springs is a through-hole that allows for identification of rotational orientation of the assembly from above. Additionally, on the top left side of each face of the nozzle are marks that allow for identification of the orientation of the assembly from the side.

The hold-down spring system provides margin to fuel assembly lift off and helps to dampen axial motion of the fuel assembly caused by loss-of-coolant accident (LOCA) and seismic-induced core plate motions.

3.2 Bottom Nozzle with Mesh Filter Plate

The stainless steel bottom nozzle (Figure 3-4) consists of a cast frame of ribs. Twenty-four holes allow for connecting the guide tubes to the nozzle using cap screws and a center hole is provided for the instrument tube. A high-strength A-286 alloy mesh filter plate is pinned to the top of the frame to provide debris resistance and is captured by the guide tubes and cap screws. The four corners have concave feet with a radius designed to interface with the alignment pins of the lower core plate. As with the top nozzle, the top left side of each face of the bottom nozzle contains marks to allow identification of assembly orientation from the side.

The bottom nozzle height is designed as an anti-straddle feature to prevent the fuel assembly from being successfully set down over a shared fuel pin. This feature permits only one correct nozzle seating on the lower core plate.

3.3 Zircaloy-4 MONOBLOC™ Guide Tubes

The MONOBLOC™ guide tubes (Figure 3-5) have a constant outer diameter. The upper portion of the guide tube has a large internal diameter that allows for rapid insertion of the CRA during a reactor trip. The lower portion of the guide tube has a reduced inner diameter that acts as a dashpot that decelerates the CRA to limit the impact forces on the fuel assembly during a reactor trip. The guide tube has four holes located just above the top of the dashpot to allow for cooling flow for inserted CRAs and outflow during a reactor trip. The outside diameter of the guide tube is constant. The added thickness in the dashpot of the MONOBLOC™ guide tube increases the lateral stiffness of the fuel assembly and inhibits fuel assembly distortion and bow.

The guide tube lower end plug (Figure 3-6) is threaded to accept a stainless steel cap screw to secure the guide tube to the bottom nozzle. The cap screw has a through-hole that allows for cooling flow to the guide tube as well as outflow during a reactor trip. The design of the dashpot and cap screw hole are consistent with existing PWR designs.

The guide tube is connected to the top nozzle with a QD assembly (Figure 3-7). The QD consists of a double-spline sleeve made of Zircaloy-4 attached to the guide tube with multiple spot welds. Machined keyway-type features within the guide tube attachment holes in the top nozzle provide either clearance for removal or restraint for securing the nozzle, based on the radial orientation of the QD features.

3.4 Zircaloy-4 Instrument Tube

The Zircaloy-4 instrument tube has constant inner and outer diameters and is located at the center of the 17x17 array. It provides guidance for the in-core instrumentation, which is inserted from the top of the fuel assembly. The instrument tube is not attached to either of the fuel assembly nozzles, but has its axial position fixed by sleeves welded above and below the bottom HMP™ grid.

3.5 Zircaloy-4 HTP™ Upper and Intermediate Spacer Grids

The four HTP™ spacer grids (Figure 3-8 and Figure 3-9) that occupy the top four grid positions are formed from interlocking Zircaloy-4 strips that are welded at intersections to form a 17x17 matrix of square cells. Each grid strip includes a pair of strips welded back-to-back to create a doublet. The doublet is formed with flow channels that are angled at the outlets to create a swirling flow pattern. The flow channels are arranged so that there is no net hydraulic torque on the fuel assembly. The shape of the flow channel creates line contacts with the fuel rod that provide increased resistance to grid-to-rod fretting relative to traditional point-contact spacer grid designs. Sideplates are welded to the grid of doublets to complete the spacer grid design. The sideplates include lead-in tabs to eliminate hang-up during fuel movement.

The HTP™ spacer grids are spot welded to the guide tubes to limit axial movement and maintain alignment with adjacent fuel assemblies.

The HTP™ grids on the NuFuel-HTP2™ fuel design are identical to those used on Framatome's 17x17 PWR product that has extensive operating experience in the United States.

3.6 Alloy 718 HMP™ Lower Spacer Grid

The HMP™ spacer grid (Figure 3-10) resembles the HTP™ spacer grid with respect to spring design, rod-to-grid surface contact and manufacturing. The HMP™ spacer grid is made from low cobalt, precipitation-hardened Alloy 718 strip material, which provides enhanced strength and relaxation characteristics. The higher strength alloy allows thinner grid strips, resulting in reduced hydraulic resistance. The doublet flow channels are straight (non-mixing) flow channels that provide added reduction in hydraulic resistance. The grids are captured above and below by Zircaloy-4 sleeves spot welded to the guide tubes to maintain axial alignment.

The HMP™ grid on the NuFuel-HTP2™ design is identical to Framatome's 17x17 PWR product that has extensive operating experience in the United States.

3.7 Fuel Rod with Alloy M5® Fuel Rod Cladding

The fuel rod design (Figure 3-11) consists of ceramic UO_2 pellets contained in seamless M5® zirconium alloy tubing with end caps welded at each end. The M5® cladding material significantly improves the resistance to corrosion compared to other cladding materials.

M5® cladding material was first inserted in a U.S. reactor core in 1995. Twenty-two U.S. reactors have used M5® alloy in more than 7500 fuel assemblies. Globally, more than 5.8 million M5® fuel rods have operated in more than 23,000 fuel assemblies in 84 reactors. The operational experience of M5® cladding covers PWR fuel arrays from 14x14 up to 18x18.

The fuel stack height is 78.74 inches and rests on top of the lower end cap. The fuel rod has an internal spring in the upper plenum that axially restricts the position of the fuel stack within the rod, preventing the formation of gaps during shipping and handling while allowing for the expansion of the fuel stack during operation. The void volume of the fuel rod is designed to accommodate fission gas generation during operation to maintain rod internal pressure less than reactor coolant system (RCS) pressure.

The lower end cap has a bullet-nose shape to provide a smooth flow transition in addition to facilitating insertion of the rods into the spacer grids during assembly. The upper end cap has a grippable shape that allows for the removal of the fuel rods from the fuel assembly if necessary.

The fuel pellet has chamfered edges and is dished on the top and bottom. The chamfers allow for ease of loading and reduce pellet chipping. The dishing and chamfers accommodate pellet swelling during operation and reduce the tendency to produce an hour-glass shape, reducing pellet-to-cladding stress concentrations and the potential for pellet stack gaps.

The UO_2 pellets have a theoretical density of 96.5 percent with a maximum enrichment up to 4.95 weight percent ^{235}U consistent with current operating plant licensing requirements. The fuel rod design can utilize axial blanket and Gd_2O_3 fuel configurations.

Table 3-1 Fuel Assembly Parameters

Parameter	Value
Fuel rod array	17x17
Fuel rods per assembly	264
Guide tubes per assembly	24
Instrument tubes per assembly	1
Spacer grids per assembly	5
Fuel assembly height without holddown spring (inch)	94.0
Fuel rod pitch (inch)	0.496
Guide tube outside diameter (inch)	0.482
Guide tube inside diameter - upper region (inch)	0.450
Guide tube inside diameter - dashpot region (inch)	0.397
Instrument tube outside diameter (inch)	0.482
Instrument tube inside diameter (inch)	0.450
HTP™ outer/inner strip height (inch)	1.950 / 1.750
HTP™ outer/inner strip thickness (inch)	**[** **]**ECI
HMP™ outer/inner strip height (inch)	1.950 / 1.750
HMP™ outer/inner strip thickness (inch)	**[** **]**ECI

* Single strip thickness of a welded doublet

Table 3-2 Fuel Rod Parameters

Parameter	Value
Cladding material	M5®
Fuel rod length (inch)	85.90
Length of total active fuel stack (inch)	78.74
Cladding outer diameter (inch)	0.374
Cladding inner diameter (inch)	0.326
Cladding inner surface roughness (µin)	45
Fuel rod internal pressure (psig)	215
Fuel rod fill gas	Helium
Fuel rod plenum height (inch)	6.21
Fuel pellet outer diameter (inch)	0.3195
Fuel pellet length (inch)	0.400
Fuel pellet surface roughness (µin)	[ ]ECI
Fuel pellet density (% TD)	96.5
Resinter densification limits (24-hour test)	[ ]ECI
Fuel pellet grain size (µm)	[ ]ECI
Fuel pellet open porosity fraction	[ ]ECI
Sorbed gas	[ ]ECI
Fuel pellet dish volume, nominal/percent (mm^3)	[ ]ECI
Fuel pellet void volume, nominal/percent (cm^3)	[ ]ECI
Plenum spring free length (inch)	[ ]ECI
Plenum spring outer diameter (inch)	[ ]ECI
Plenum spring wire diameter (inch)	[ ]ECI
Plenum spring active coils	[ ]ECI
Plenum spring volume (in^3)	[ ]ECI
Lower end cap height (inch)	0.575

TD = theoretical density
UTL = upper tolerance limit
LCL = Lower confidence limit
UCL = Upper confidence limit

Table 3-3 Comparison of Operating Conditions

Parameter	NPM Design Value	Framatome 17x17 PWR Value
Rated thermal power (MWt)	250	3455
Average coolant velocity (ft/s)	3.6	16
System pressure (psia)	2000	2280
Core average temperature (°F)	540	584
Core average linear heat rate (LHR), approx. (kW/m)	12.8	18.0
RCS inlet temperature (°F)	480	547
RCS Reynolds number	86,000	468,000
Fuel assemblies in core	37	193
Fuel assembly loading (kgU)	251	455
Core loading (kgU)	9,269	87,815

Table 3-4 Fuel Assembly Materials

Component	Material
Top nozzle	Stainless steel
Bottom nozzle frame	Stainless steel
Mesh filter plate	Alloy 286
Guide tube and QD sleeves	Zr-4
Holddown leaf springs	Alloy 718
Holddown spring clamp screw	Alloy 718
Top connection (quick disconnect)	Zr-4 and Alloy 718
Bottom cap screw	AISI 316L stainless steel
HMP™ grid	Alloy 718
HTP™ grid	Zr-4
Fuel rod cladding	M5® - cold worked and recrystallized zirconium alloy
Fuel rod plenum springs	Alloy X-750
Fuel pellets	UO_2 and UO_2 plus Gd_2O_3

Note: Stainless steels are low cobalt.

Figure 3-1 Fuel Assembly General Arrangement

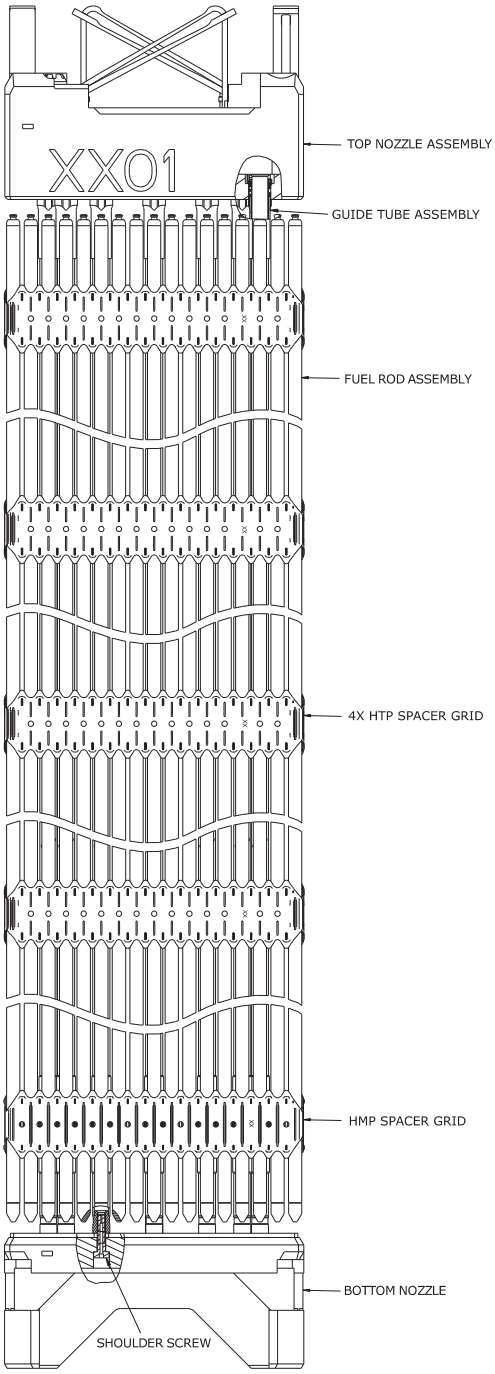

Figure 3-2 Representative Core Loading Pattern

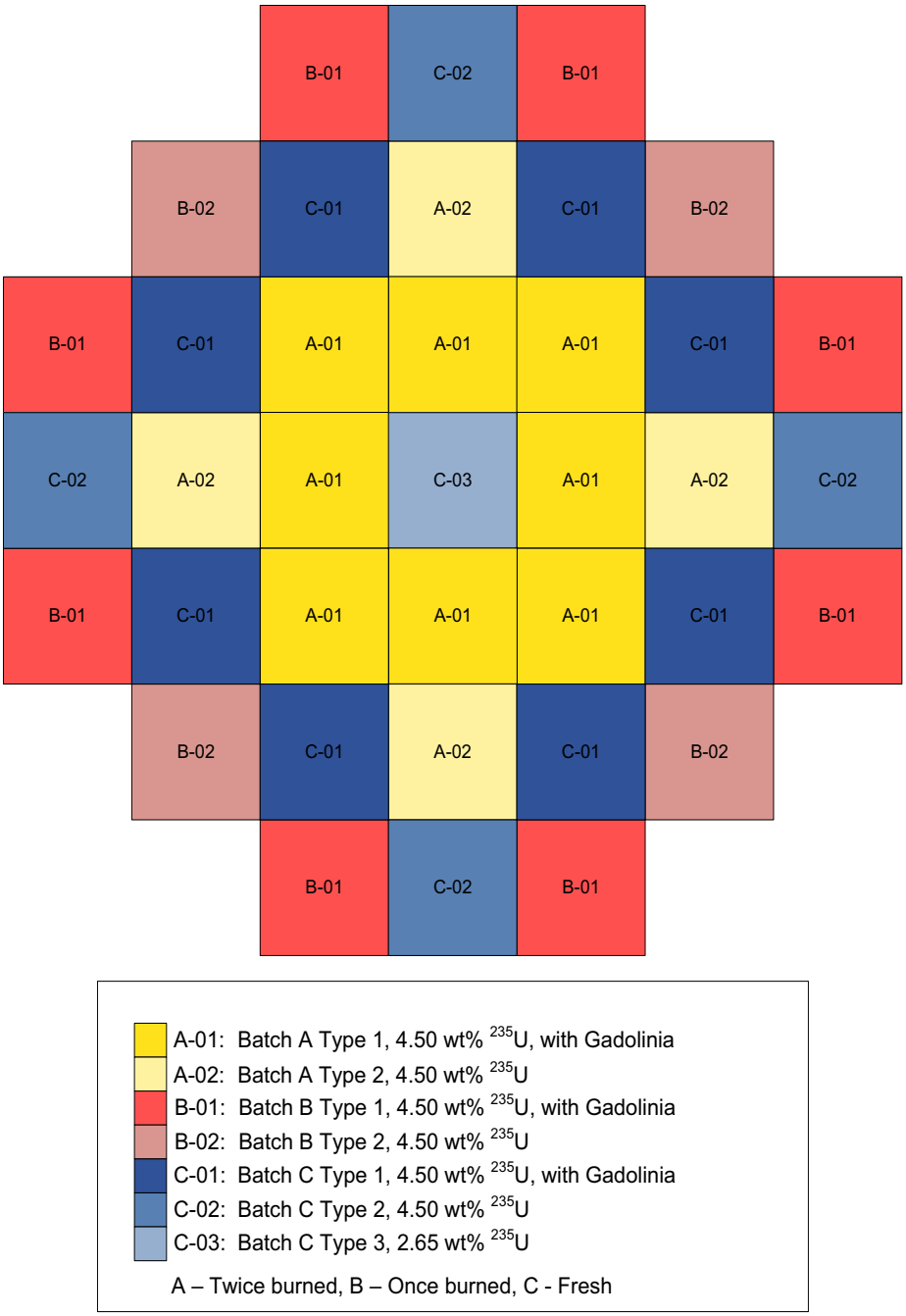

Figure 3-3 Top Nozzle

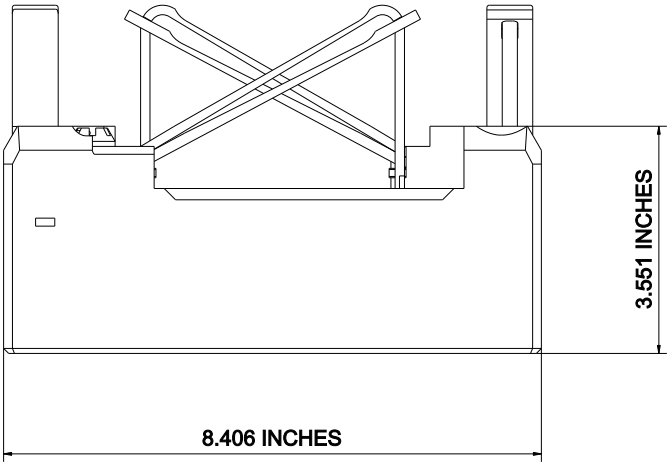

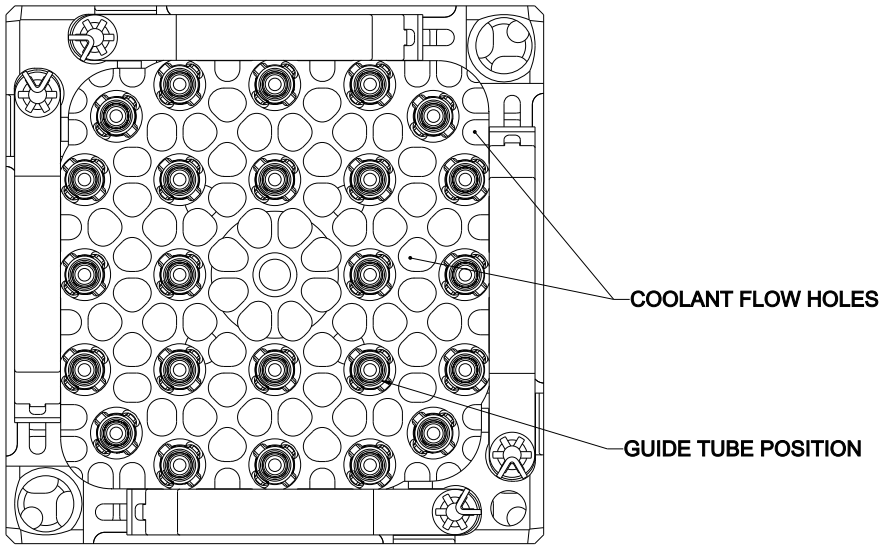

Figure 3-4 Bottom Nozzle

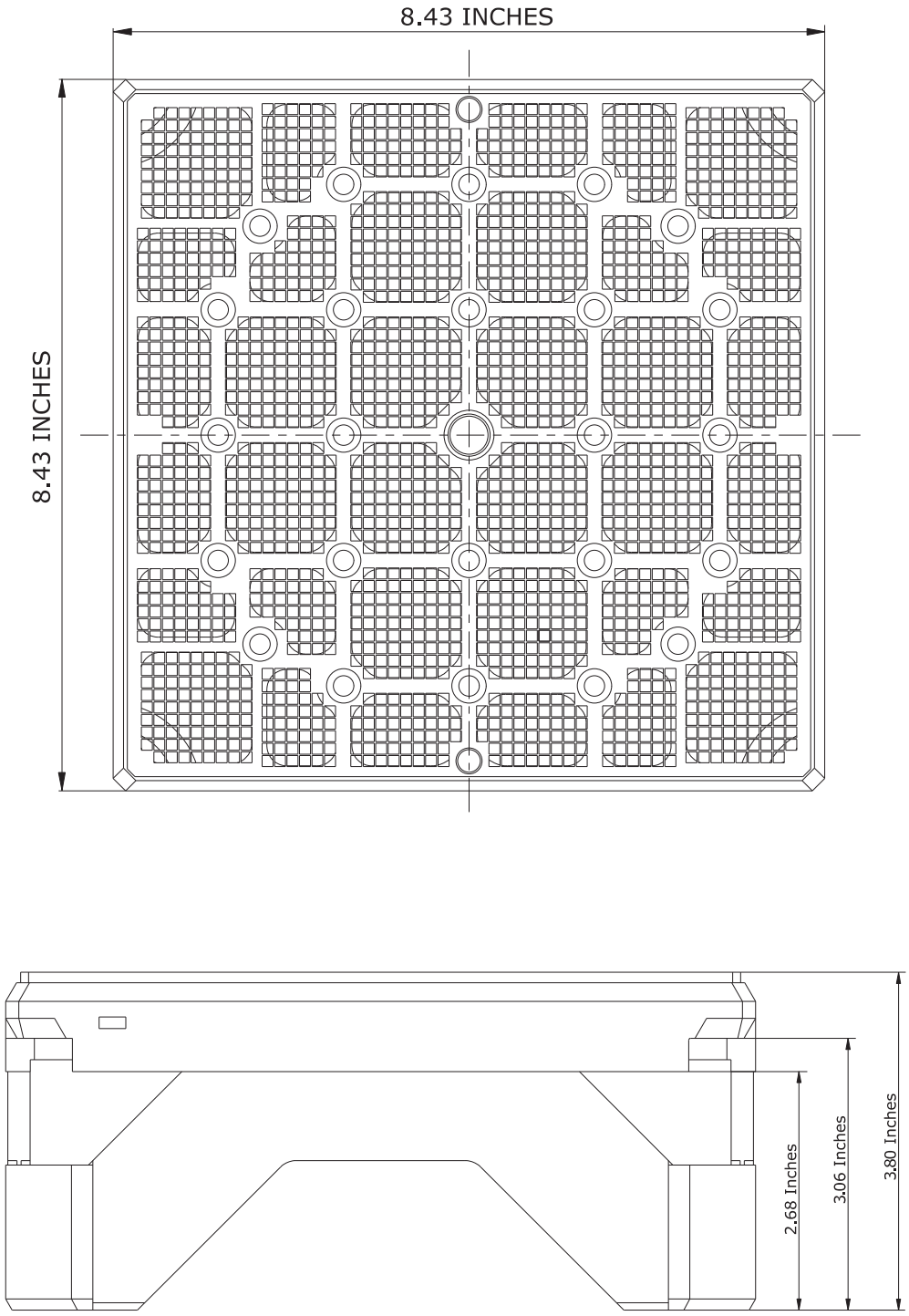

Figure 3-5 Guide Tube Assembly

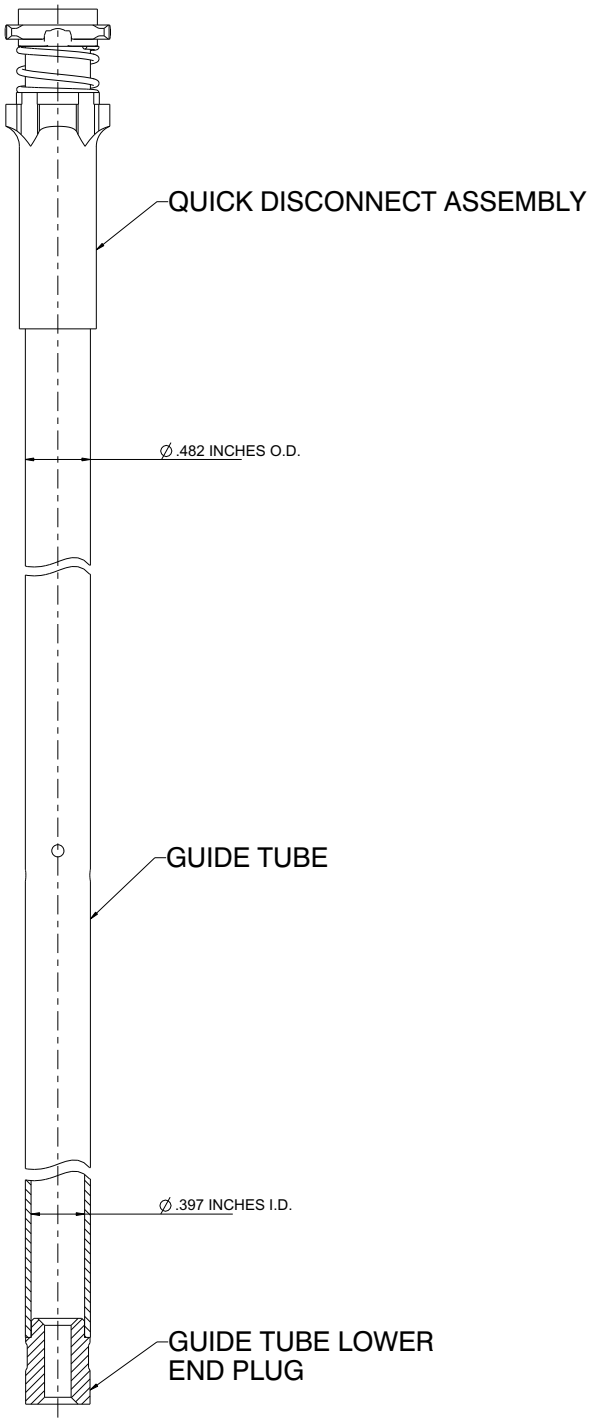

Figure 3-6 Cap Screw Bottom Nozzle Connection

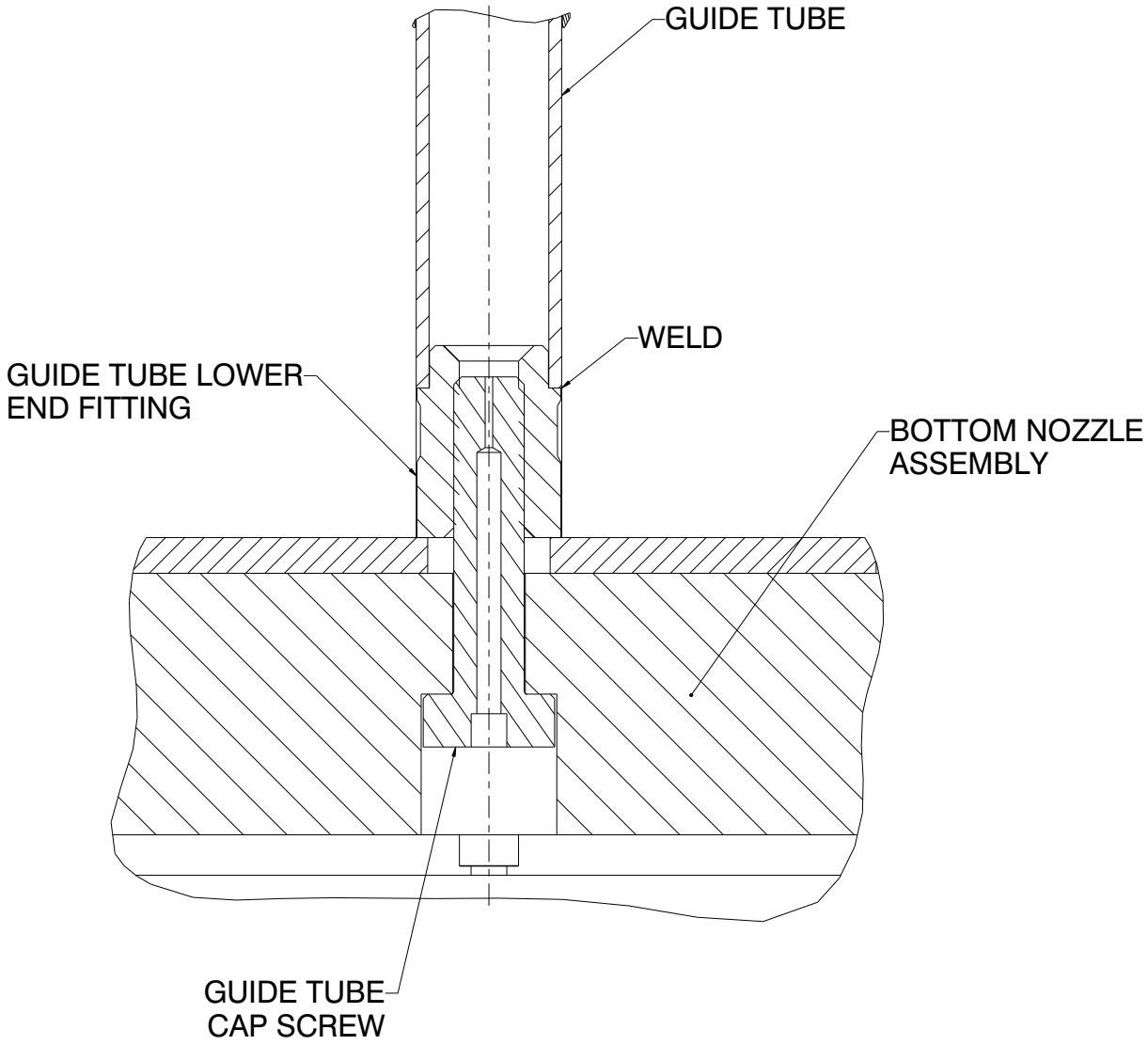

Figure 3-7 Guide Tube Quick Disconnect Top Nozzle Connection

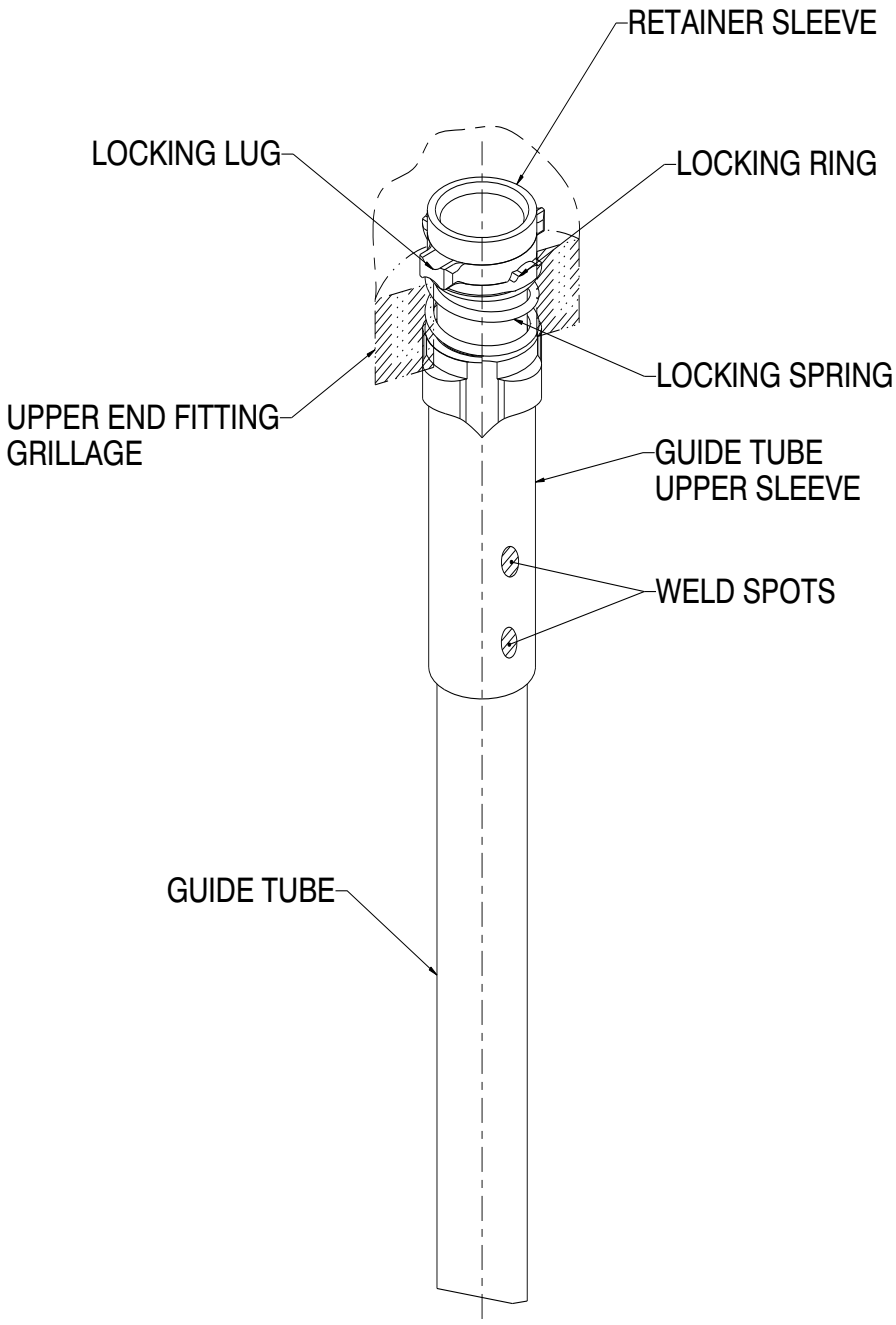

Figure 3-8 HTP™ Grid

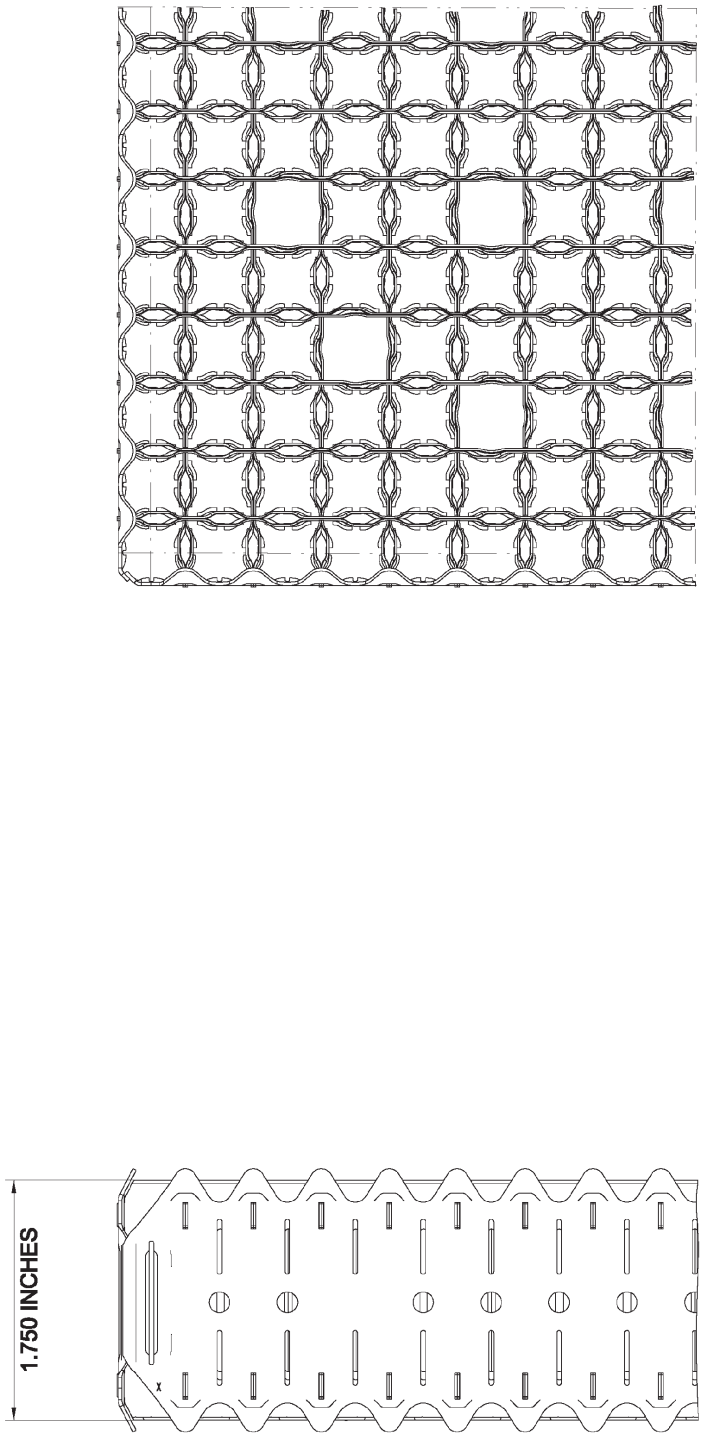

Figure 3-9 HTP™ Spacer Grid Characteristics

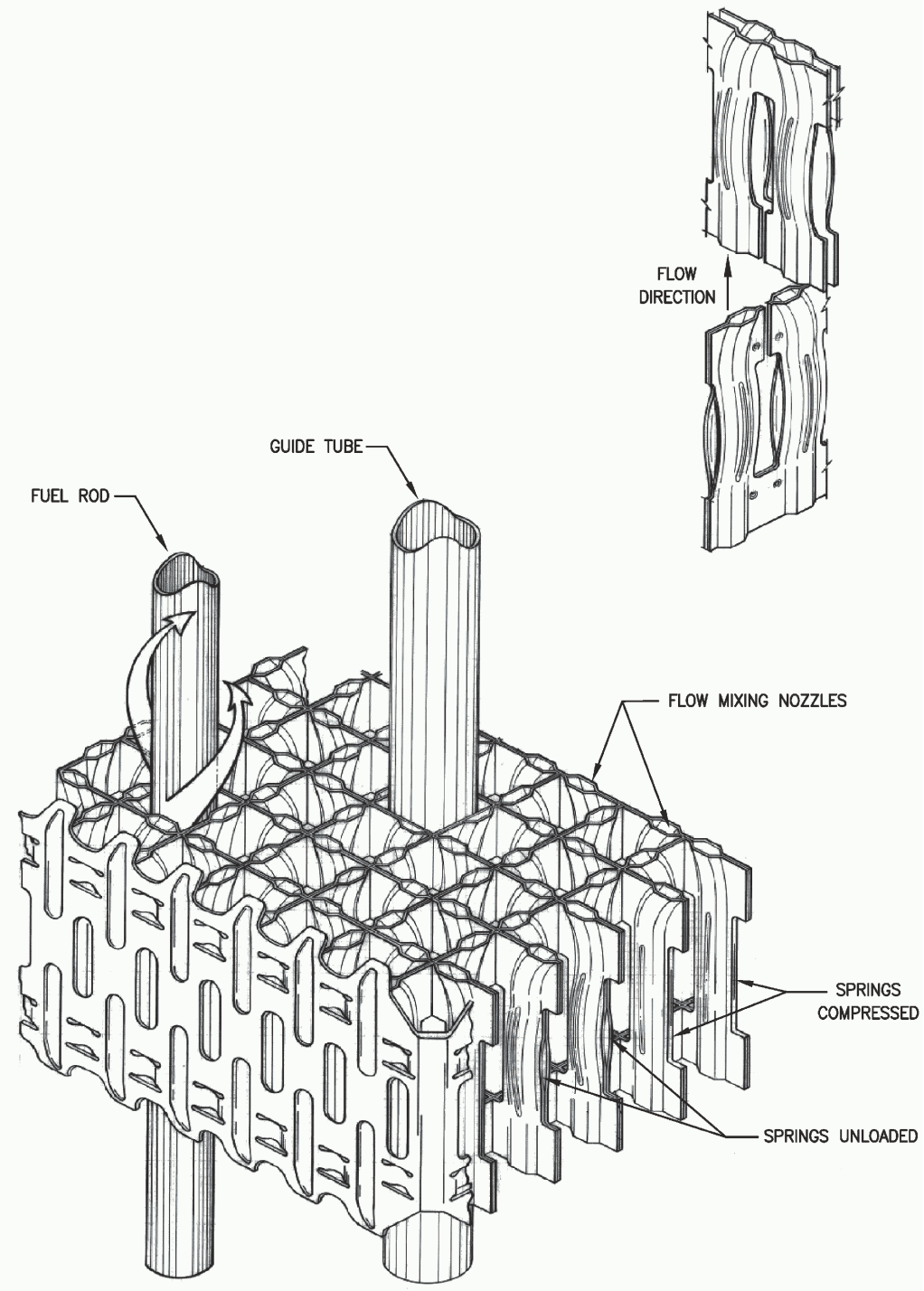

Figure 3-10 HMP™ Spacer Grid

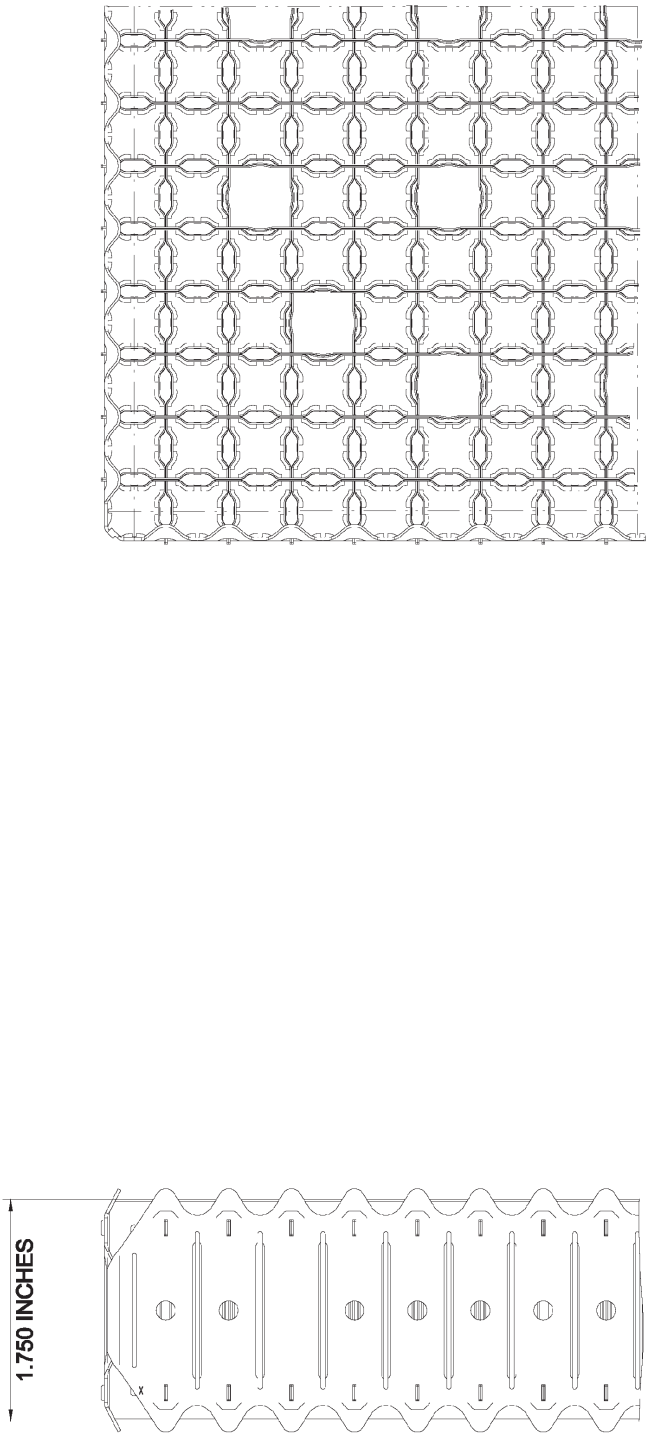

Figure 3-11 Fuel Rod Assembly

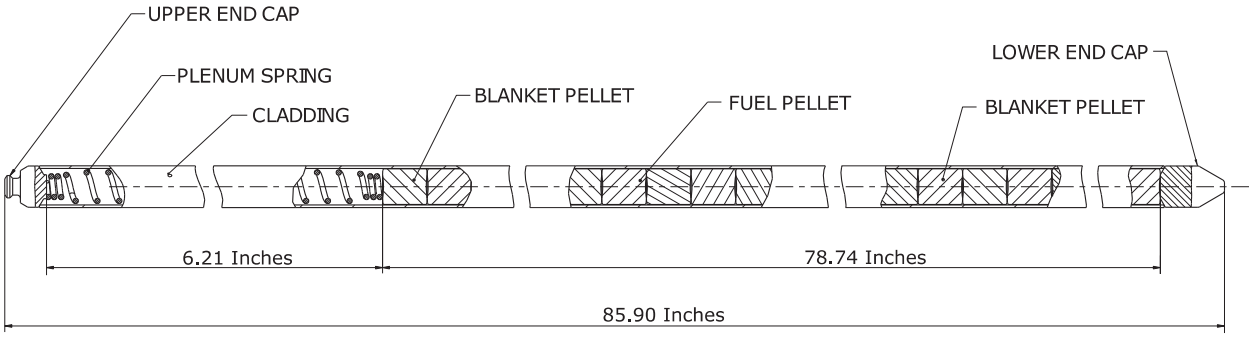

4.0 Design Evaluation

This section evaluates the NuFuel-HTP2™ design against criteria established consistent with Section 4.2 of NUREG-0800 (Reference 9.1.1), to provide assurance that

1. the fuel system is not damaged as a result of normal operation and AOOs.
2. the fuel system damage is never so severe as to prevent control rod insertion when it is required.
3. the number of fuel rod failures is not underestimated for postulated accidents.
4. core coolability is always maintained.

The design criteria are based on Framatome fuel design experience and are consistent with criteria established for previously approved fuel assembly designs.

Reference 9.1.8 identifies the NRC-approved codes and methods used to evaluate the fuel performance. Table 2-3 of Reference 9.1.8 associates the method with the corresponding Reference 9.1.1 acceptance criteria. Reference 9.1.9 identifies the method of analysis for the structural response of the fuel assembly to dynamic faulted loads. Reference 9.1.10 confirms the applicability of these methods for use with the SDAA. Use of well-established design criteria and evaluation methods provides assurance of acceptable fuel performance.

The results of the fuel performance analyses are applicable for operation in the NPM.

4.1 Fuel System Damage Criteria

4.1.1 Stress and Loading Limits

Design Criteria

Stress intensities for fuel assembly components shall be less than the stress limits based on ASME Code, Section III criteria (Reference 9.1.2).

Buckling of the guide tubes shall not occur during normal operation and AOOs.

The cumulative number of strain fatigue cycles on the structural components shall be less than the design fatigue lifetime.

NuFuel-HTP2™ Design Evaluation

In the normal operating analysis, a series of mechanical analyses demonstrate the fuel assembly can withstand stresses and buckling loads from start-up, steady-state operation, shutdown, and AOOs. Each structural component in the fuel assembly is evaluated against the ASME Code Section III, Level A service limits (Reference 9.1.11). The fuel assembly weight, hold-down spring forces, RCS hydraulic loads, thermal loads during plant heat-up, steady-state operation and cooldown, and CRA drop loads (sum of the CRA spring preload and the load from the

maximum travel of the CRA spring retainer) create the stress states that are evaluated in the analysis. The operating basis earthquake is less than one-third of the safe shutdown earthquake (SSE) ground motion and is enveloped by the SSE analysis. The fatigue analysis evaluates cyclic loading due to normal operation and AOOs combined with the OBE, for a total of 137 transients over the life of the fuel. The NUREG-0800 criterion for a safety factor of 2 on stress amplitude or 20 on the number of cycles is satisfied by the use of the O'Donnell-Langer curve (Reference 9.1.12) in the analysis.

Guide tube normal operating loads are evaluated for each fuel assembly span. Guide tube spans are separated by spacer grids that begin above the bottom nozzle and extend to the guide tube span below the top nozzle. The loads and material properties of the guide tubes and the other fuel assembly components are based on the bounding outlet temperature in order to conservatively evaluate the loads, design limit, and minimum design margins for fuel assembly components at normal operating conditions.

The guide tube buckling analysis evaluates a maximum guide tube eccentricity to create bounding load predictions when the fuel assembly weight, hold-down spring force, and CRA drop loads are simultaneously applied.

Guide tube stress calculations consider axial loading conditions that cause tensile stresses. Hydraulic loading is conservatively ignored because it reduces the CRA drop and weight loads. Secondary loads are also considered in the form of spacer grid slip loads. These loads are generated as fuel rod slip is resisted by the grids because of differential thermal expansion and irradiation growth between the fuel rods and guide tubes during normal operation. These frictional loads are evaluated for a condition where rods are unseated, or lifted, at beginning of life (BOL) and are conservative for the seated condition at end of life (EOL).

Guide tube primary membrane (P_m), primary membrane + bending ($P_m + P_b$), and primary + secondary ($P_m + P_b + Q$) stresses are evaluated against allowable stresses using the ASME Code Level A service limits based on the material yield and ultimate strengths.

The guide tube upper sleeve strength is bounded by the strength of the weld connections with the guide tubes. The guide tube upper sleeve seating appendages are also evaluated for bearing stress and shear stress, considering the loads applied through the top nozzle during a CRA drop.

For welded or threaded joints and various structural connections in the fuel assembly, the maximum load during normal operation is evaluated against ASME Code Level A service limits. The evaluated connections include the guide tube to spacer grid welds, the guide tube to upper sleeve welds, the guide tube upper sleeve to QD retainer weld, the guide tube to guide tube lower end fitting (GTLEF) weld, and the threaded connection between the GTLEF and the shoulder screw. The threaded connection is evaluated using ASME Code methods.

The bottom nozzle and top nozzle strengths are evaluated considering the maximum operating loads from the fuel assembly weight, hold-down spring force, and CRA drop events and the allowable ASME Code load limit based on prototype component tests. For both the bottom nozzle and top nozzle, testing determined the collapse load for each structural framework. In accordance with the ASME Code, each tested collapse load is multiplied by two-thirds in establishing the allowable load limit.

In consideration of corrosion effects, guide tube wall thinning due to corrosion is considered within EOL condition evaluations. This corrosion allowance is applied as a reduction to the inner and outer surface of the guide tube material. Similar wall thinning is not applied to stainless steel components given the minimal levels of corrosion observed for those components in reactor operating conditions.

The hold-down spring analysis shows that the spring meets ASME Code limits for stress and strain. Spring stresses do not remain within elastic limits. Rather, the springs shake down to elastic action. Following shakedown, they behave elastically up to a newly established yield point.

Table 4-1 provides a summary of the results for normal operation of the NuFuel-HTP2™ fuel assembly design. The results presented in Table 4-1 demonstrate that the assembly components meet the acceptance criteria.

Table 4-1 Summary of Results - Fuel Assembly Design Margins

[

]

Consistent with Reference 9.1.2, the fuel handling qualification includes a 2.5g axial load. The shipping qualification includes 4g axial and 6g lateral loads and grid clamp loads. Loads for shipping and pre-receipt handling are evaluated for fresh fuel conditions. The maximum stresses and loads on the fuel assembly components and structural connections during shipping and handling remain below the specified minimum strength, critical buckling loads, and below the ASME Code Level A service limits. For a 4g axial acceleration, the fuel rod plenum spring maintains a force against

the fuel stack sufficient to prevent column movement during handling. The evaluation also demonstrates that the fuel rods do not slip through the spacer grids under 4g axial loads.

4.1.1.1 Fuel Rod Cladding Stress and Buckling

Design Criterion

Fuel rod cladding stress shall not exceed the following stress limits defined in Reference 9.1.3:

- **[ ]**
- **[ ]**
- **[ ]**
- **[ ]**

The fuel rod shall not buckle based on **[ ]** criterion during the limiting overpressure transient at BOL.

NuFuel-HTP2™ Design Evaluation

The fuel rod stress and buckling analysis determines the in-core steady-state stress and buckling performance of the fuel rod design.

[

] Pressure and temperature inputs are chosen so that operating conditions for normal operation and AOOs are enveloped.

The stress analysis takes into account several sources of cladding stress: pressure differentials, ovality, thermal differentials, flow-induced vibration (FIV), fuel rod growth, and fuel rod to spacer grid (FR-SG) interaction. The following four stress categories are analyzed:

- Primary Membrane (P_m) - Pressure stresses
- P_m + Primary Bending (P_b) - Pressure, ovality and FIV stresses
- P_m + P_b + Local - Pressure, ovality, FIV, and FR-SG stresses
- P_m + P_b + Local + Secondary - Pressure , ovality, FIV, FR-SG , growth, and thermal stresses

At both the inner and outer diameter of the fuel rod, the maximum value of each individual stress is determined. The individual stresses within each stress component (tangential, axial, and radial) are added to find a maximum and

minimum stress value. The stress intensity for each category is determined by combining the maximum and minimum stresses. The stress intensity is compared with the allowable stress to determine the margin for the particular stress.

The cladding stress results, listed in Table 4-2, show positive margins for all stress categories. The minimum margin occurs on the cladding outer diameter in compression when combining primary membrane + bending + local stresses.

Table 4-2 Stress Results in Compression and Tension

[

]

The buckling pressure is calculated to be **[ ]** psi. The buckling pressure is higher than the maximum BOL pressure the fuel rod would experience during an overpressure event (2015 psi). Therefore, the design meets the buckling criterion.

The calculated critical bucking load is **[ ]** lbf. The critical bucking load is greater than the total compressive load of **[ ]** lbf. Therefore, the Euler buckling criterion is also met.

4.1.2 Cladding Fatigue

Design Criterion

The fuel rod cumulative usage factor shall not exceed 0.9 (Reference 9.1.3).

NuFuel-HTP2™ Design Evaluation

A bounding analysis of the core design is performed using the COPERNIC fuel rod analysis code (Reference 9.1.4) for both UO_2 and UO_2-Gd_2O_3 rods.

Plant operations result in fluctuating thermal, pressure, ovality, and pellet-clad contact stresses in the fuel rod cladding. The COPERNIC code predicts changes in cladding diameter, cladding temperature, and fuel rod internal pressure at each time step. These parameters are used to calculate the various stresses used in the fatigue calculation.

The transients considered in the fatigue analysis are provided in Table 4-3. The fuel rod life is conservatively assumed to be 10 years. With this assumption, the fuel rod experiences one-sixth of the number of transients identified in Table 4-3 for a sixty year plant design life.

The fuel rod behavior during each transient is analyzed using the COPERNIC fuel rod code, which predicts changes in cladding diameter and temperature and the fuel rod internal pressure for each time step. These parameters are used to calculate the various stresses used in the fatigue evaluation.

The maximum cumulative usage factor (CUF) for UO_2 fuel rods is **[ ]** and the maximum CUF for UO_2-Gd_2O_3 rods is **[ ]**. Both of these CUFs are well below the limit of 0.9.

Table 4-3 Summary of Transients Considered in the Fuel Rod Fatigue Analysis

Transient Identifier	Design Transient Name	Events for 60 Year Design Life
Condition I Events (Service Level A)		
A01-HTS	Reactor Heatup to Hot Shutdown	200
A02-RCD	Reactor Cooldown from Hot Shutdown	200
A03-PAC	Power Ascent from Hot Shutdown	700
A04-PWD	Power Descent to Hot Shutdown	300
A05-LFW	Load Following	19,750
A06-REG	Load Regulation	767,100
A07-SSF	Steady State Fluctuations	5,000,000
A08-RLI	Load Ramp Increase	2000
A09-RLD	Load Ramp Decrease	2000
A10-SLI	Step Load Increase	3000
A11-SLD	Step Load Decrease	3000
A12-LLD	Large Step Load Decrease	200
A13-REF	Refueling	60
A14-MKP	Reactor Coolant System Makeup	175,200
A15-SGI	Steam Generator Inventory Control from Hot Shutdown	600
A16-HPD	High Point Degasification	440
A17-CEV	Containment Evacuation	66,000
A18-CFD	Containment Flooding and Drain	400
A19-SLT	Secondary Leakage Tests	200
A20-HFT	Initial Test Program	20
Condition II Events (Service Level B)		
B01-FWD	Decrease in Feedwater Temperature	180
B02-FWI	Increase in Secondary Flow	30
B03-TTX	Turbine Trip without Bypass	90
B04-TTB	Turbine Trip with Bypass	180
B05-LOP	Loss of Normal Alternating Current Power	60
B06-SVC	Inadvertent Main Steam Isolation Valve Closure	30
B07-IOD	Inadvertent Operation of the Decay Heat Removal System	15
B08-TRP	Reactor Trip from Full Power	125
B09-DRP	Control Rod Misoperation	60
B10-PZM	Inadvertent Pressurizer Spray	15
B11-COP	Cold Overpressure Protection	30
B12-CMT	Chemical and Volume Control System Malfunctions	30
Condition III Events (Service Level C) (only one of the following is considered)		
C01-VNT	Spurious Emergency Core Cooling System (ECCS) Valve Actuation	5
C02-BDN	Inadvertent Opening of a Reactor Safety Valve	5
C03-SML	Chemical and Volume Control System Pipe Break	5
C04-SGT	Steam Generator Tube Failure	5
D01-SLB	Steam Piping Failures	1
D02-FLB	Feedwater Piping Failures	1
D03-CRE	CRA Ejection	1
T01-PHT	Primary Hydrostatic Test	10

Table 4-3 Summary of Transients Considered in the Fuel Rod Fatigue Analysis (Continued)

Transient Identifier	Design Transient Name	Events for 60 Year Design Life
T02-SHT	Secondary Hydrostatic Test	10
T03-CHT	Containment Hydrostatic Test	10

4.1.3 Fretting

Design Criterion

Fuel rod failures due to fretting shall not occur, as verified by fretting tests (Reference 9.1.2).

NuFuel-HTP2™ Design Evaluation

Fretting and vibration performance is validated by the 1000-hour life and wear test performed at the Richland portable hydraulic test facility (PHTF), in addition to other relevant HTP™ vibration and fretting tests.

- The 1000-hour life and wear test performed at the Richland PHTF was run for 1032 hours at a temperature of 300 degrees F at or above the target Reynolds number of 52,000. At the conclusion of the test, **[ ]** fuel rods were examined for grid-to-rod fretting performance. The test results show no wear abnormalities with results **[ ]** well within the performance base for historical test results of proven in-reactor designs. The fretting results are based on a conservative flow configuration with a test-to-reactor momentum flux ratio of approximately **[ ]**. The test assembly replicated the EOL condition **[ ]** The HMP™ grid for the EOL test assembly was relaxed to **[ ]** of the unirradiated grid-to-rod support.
- The predicted vibration response amplitude for the NuFuel-HTP2™ design is **[ ]**, which is less than the maximum measured rod amplitude of **[ ]** in the Hermes-T vibration and wear test performed for the 17x17 HTP™ fuel transition, which considered the effects of bundle-to-bundle cross flow.
- Fretting results for autoclave testing (8005 hours) of the 17x17 HTP™ grid design, which is identical to the HTP™ grid used on the NuFuel-HTP2™ design, show low wear **[ ]** for conservative imposed vibration amplitudes **[ ]**.
- Fretting results for autoclave testing (1000 hours) of the Advanced W17 HTP™ design with intermediate flow mixers, where the HTP™ and HMP™ grids are similar to the NuFuel-HTP2™ design, show low wear **[ ]** for conservative imposed vibration amplitudes and **[ ]**.

The predicted small vibration amplitudes for the NuFuel-HTP2™ design are a result of the lower NPM axial and cross flow velocities relative to those of a typical PWR. The NPM has a nominal flow rate of 395 gpm per fuel assembly compared to a best-estimate flow of approximately 2050 gpm per fuel assembly for a forced circulation PWR using a 17x17 fuel assembly design. The maximum calculated local cross flow velocity for NuFuel-HTP2™ fuel assemblies is {{ }}$^{2(a),(c),ECI}$ ft/sec for a uniform core compared to approximately **[ ]** ft/sec for a conventional PWR using a 17x17 fuel assembly design.

The robust fretting characteristics of the NuFuel-HTP2™ design provide confidence in the FIV performance of the fuel. The grid design provides line contact between the fuel rods and the spacer grid with large contact surfaces to mitigate wear. The grid-to-rod support also provides for higher damping to help suppress FIV and fretting wear. The grid-to-rod support conditions in the NuFuel-HTP2™ design are similar to the grid-to-rod support of other HTP™ fuel assemblies, of which more than 18,000 have been introduced into operating reactors globally. Thus, the HTP™ test results and operating experience pertaining to rod vibration and fretting is applicable for evaluating the NuFuel-HTP2™ design.

Based on the minimal fretting wear measured during the life and wear test in the Richland PHTF, the small predicted rod vibration amplitudes, and the extensive favorable operating and test experience with the HTP™ fuel design, the NuFuel-HTP2™ design is not expected to experience FIV or wear issues in the NPM, and fuel rod failures due to fretting do not occur. There are no limitations with respect to time or burnup for the conditions evaluated.

4.1.4 Oxidation, Hydriding, and Crud Buildup

Design Criterion

The fuel rod cladding peak oxide thickness shall not exceed a best-estimate predicted value of 100 microns. Hydrogen pickup is controlled by the corrosion limit. Crud buildup is limited by inclusion in the oxidation measurement (Reference 9.1.4).

NuFuel-HTP2™ Design Evaluation

A bounding analysis is performed using the COPERNIC fuel rod analysis code (Reference 9.1.4) for UO_2 rods with and without Gd_2O_3. The corrosion of the fuel rods is modeled in order to calculate the oxide thickness that develops on the outer surface of the rods during operation.

A bounding input power history, expressed in terms of effective full-power hours is used that bounds the individual rod power histories of the UO_2 and Gd_2O_3 rods in the equilibrium cores. The corrosion analysis primarily depends on the amount of energy transfer through the cladding and the irradiation time. It shows little sensitivity to the fuel rod design characteristics inside the rods. The use of a bounding power history envelope makes the analysis equally applicable to all fuel rod types.

The maximum predicted oxide thickness reaches {{ **[** **]** }}$^{2(a),(c),ECI}$ micrometers (Figure 4-1), which is well below the design limit of 100 micrometers.

Framatome and industry operating experience show that crevice corrosion is not a current cause of PWR fuel failures. Framatome PWR fuel designs and materials have shown no susceptibility to fuel reliability concerns driven by crevice corrosion. Specific to the M5® cladding, there are no significant crevices on the fuel cladding surface that could shield an area from the RCS flow, so there is no significant risk of crevice corrosion for the M5® fuel rod cladding.

Figure 4-1 Predicted Corrosion Results

{{ **[**

] }}$^{2(a),(c),ECI}$

4.1.5 Fuel Rod Bow

Design Criterion

There is no specific design criterion for fuel rod bow. Fuel rod bowing is evaluated with respect to the mechanical and thermal-hydraulic performance of the fuel assembly (Reference 9.1.6).

NuFuel-HTP2™ Design Evaluation

Fuel rod bow is the deviation from straightness of the fuel rods in the fuel assembly. The presence of fuel rod bow is identified by the deviation in water channel gap from nominal conditions. The primary effects of rod bow are a decrease in the critical heat flux ratio and an increase in local power peaking. Secondary effects of fuel rod bow

can include fuel clad fretting at 100 percent gap closure, although the probability of rod-to-rod contact is minimal.

The NuFuel-HTP2™ design does not introduce changes from current Framatome PWR fuel assembly designs that might adversely impact rod bow. Operating plant rod bow data for current Framatome PWR designs continue to be adequately covered by the existing rod bow correlation methodology.

The NuFuel-HTP2™ design is within the current experience base with regards to fuel rod bending stiffness and operating temperature and is less limiting regarding end grid slip loads and span length. The mechanical rod bow analysis concludes that fuel assembly performance is within current models and experience.

Rod bow penalties are derived for both linear heat generation rate (LHGR) and critical heat flux based on the NRC-approved methodology for quantifying fuel rod bowing.

4.1.6 Axial Growth

Design Criteria

For the fuel assembly, the axial clearance between core plates and the top and bottom nozzles shall allow sufficient margin for fuel assembly growth during the assembly lifetime.

For the fuel rod, adequate clearance shall be maintained between the fuel rod and the top and bottom nozzles to accommodate the differences in the growth of fuel rods and the growth of the fuel assembly (Reference 9.1.2).

NuFuel-HTP2™ Design Evaluation

The fuel assembly and its components grow during operation. There are two components of the growth: thermal expansion and irradiation growth. The minimum clearance between the fuel rods and the top and bottom nozzles and the clearance between the fuel assembly and core plates at the EOL condition are determined using worst case fuel rod and fuel assembly growth models and worst case initial dimensions.

[

]

The analysis shows that the allowable average assembly fast fluence is {{ }}$^{2(a),(c),ECI}$ n/cm^2 and the allowable maximum average fuel rod fast fluence is {{ }}$^{2(a),(c),ECI}$ n/cm^2. The minimum core plate to fuel assembly gap is **[ ]** inches at the allowable assembly fast fluence. The minimum fuel rod shoulder gap is **[ ]** inches (at a fuel assembly fluence of {{ }}$^{2(a),(c),ECI}$ n/cm^2 during hot operation).

A separate growth-based analysis was performed to demonstrate that adjacent fuel assemblies would maintain adequate spacer grid alignment given differing burnup profiles. The analysis applied a burnup differential of **[ ]** GWd/mtU between adjacent fuel assemblies.

The recommended allowable offset based on typical fuel assembly design requirements is that flat vertical surfaces of spacers on adjacent assemblies maintain a positive overlap at the worst-case conditions. The analysis demonstrates a maximum offset of **[ ]** inch, which maintains a positive overlap for the spacer grids that have a height of 1.750 inches.

4.1.7 Fuel Assembly Distortion Evaluation

The NuFuel-HTP2™ fuel has features, including spacer grids, structural connections, and guide tube diameters, similar to current Framatome 17x17 fuel but with a shorter overall length. The shorter length increases the lateral stiffness of the fuel assembly. As validation, fuel assembly lateral stiffness tests were performed for the NuFuel-HTP2™ fuel design in-air at BOL and EOL conditions.

Similar lateral stiffness tests have been conducted for current Framatome 17x17 fuel designs at EOL and BOL conditions. The test results show that the fuel assembly lateral stiffness is more than **[ ]** times greater than that of the current Framatome 17x17 fuel design. With this level of lateral stiffness and significantly lower hydraulic loads on the fuel assembly due to natural circulation flow, the fuel assembly has a high level of resistance to fuel assembly distortion.

Differential fuel rod and guide tube growth rates, coupled with spacer grid slip loads, can contribute to fuel assembly distortion during operation. The fuel design has the

same structural components and fuel rod cladding diameters and material (producing similar slip loads and growth rates) as the current Framatome 17x17 PWR designs; thus, the guide tube stresses from fuel rod and guide tube differential growth are bounded by Framatome design experience. The differential growth stresses imparted to the guide tubes are reduced compared to Framatome experience because of the reduced number of spacer grids over which tensile loads may accumulate on the guide tubes and the reduced length of the fuel rods and guide tubes, which results in lower differences in growth. These design characteristics ensure that the fuel rod and guide tube growth differential effects are within Framatome's recent PWR 17x17 fuel design experience.

Operating experience of the current Framatome 17x17 fuel assembly design demonstrates little in-reactor fuel distortion as evidenced by the absence of incomplete rod insertions and slow-to-settle observations where full insertion of the control rod is delayed. Therefore, control rod drop concerns related to assembly distortion are not expected for the NuFuel-HTP2™ fuel assembly design.

4.1.8 Fuel Rod Internal Pressure

Design Criterion

The internal gas pressure of the peak fuel rod in the reactor shall remain below a value that would cause the fuel-cladding gap to increase because of outward cladding creep during steady-state operation and extensive departure from nucleate boiling (critical heat flux) propagation to occur (Reference 9.1.4).

NuFuel-HTP2™ Design Evaluation

A bounding analysis is performed using the COPERNIC fuel rod analysis code (Reference 9.1.4) for UO_2 rods with and without Gd_2O_3. The maximum fuel rod internal pressure is conservatively compared to a design limit equal to nominal system pressure (2000 psia). Meeting this criterion demonstrates that the fuel-clad gap does not increase due to cladding outward creep during steady-state operation because a greater pressure external to the rod prevents outward creep and fuel-clad liftoff. This criterion also ensures that extensive departure from nucleate boiling propagation does not occur.

The COPERNIC pressure calculation is based on a best-estimate prediction plus an uncertainty allowance to take into account code uncertainties and manufacturing variations. The analysis considers steady-state and Condition I (normal operation) and Condition II (AOO) transients over the full burnup range. The transients are modeled in the COPERNIC input with appropriate axial flux shapes.

The maximum calculated internal pressure over the burnup history (for both UO_2 and Gd_2O_3 rods) is {{ }}$^{2(a),(c),ECI}$ psia compared to a limit of 2000 psia.

4.1.9 Assembly Liftoff

Design Criterion

The fuel assembly shall not lift off from the lower core plate under normal operating conditions and AOOs (Reference 9.1.2).

NuFuel-HTP2™ Design Evaluation

The fuel assembly lift-off analysis evaluates an {{ }}[2(a)(c)] AOO. To bound conditions for this event, the maximum flow rates at each corresponding power level are {{ }}[2(a)(c)]. The maximum hydraulic lift is **[ ]** lbf, resulting in a lift margin of **[ ]** lbf. There are large margins against lift-off at all normal operating, startup, and transient (AOO) conditions. Because the NPM relies on natural circulation of the coolant without mechanical pumps, the assumed flow rates envelope all operating conditions and AOOs.

4.2 Fuel Rod Failure Criteria

4.2.1 Internal Hydriding

Design Criterion

The fabrication limit for total hydrogen inside a fuel rod assembly is maintained at a minimal level to limit internal hydriding (Reference 9.1.2).

NuFuel-HTP2™ Design Evaluation

Fuel rod internal hydriding is controlled by fabrication limits for fuel pellet moisture. These controls, typical for Framatome fuel manufacturing, limit the total hydrogen content, including moisture, to ≤ **[ ]** ppm by weight, before rod final closure welding.

4.2.2 Cladding Collapse

Design Criterion

The predicted creep collapse life of the fuel rod shall exceed the maximum expected incore life (Reference 9.1.5 and Reference 9.1.3).

NuFuel-HTP2™ Design Evaluation

The cladding creep collapse analysis is performed using the methodology of Reference 9.1.5, extended to M5® applications in Reference 9.1.3.

A bounding analysis of the core design is performed using the COPERNIC fuel rod analysis code and the CROV creep ovalization code for both UO_2 and Gd_2O_3 rods. Reference 9.1.5 establishes the three collapse criteria to be analyzed:

- bifurcation buckling pressure
- yield stress
- deformation rate

COPERNIC simulates the performance of the fuel rod throughout the lifetime of the rod to generate the parameters required to perform the creep collapse analysis:

- rod internal pressure
- interior and exterior cladding temperatures
- coolant temperature and fast flux

The CROV code applies the initialization parameters from COPERNIC along with the fuel rod geometry (i.e., outside diameter, wall thickness, and ovality) to simulate the cladding creep-down deformations versus time. Consistent with Reference 9.1.5, when the ovality creep rate of the cladding exceeds 0.1 mils/hr, or the generalized stress within the cladding exceeds the yield stress, the cladding is considered to have failed. In addition, the bifurcation buckling pressure must not be exceeded. The three collapse criteria determine the predicted creep collapse life of the fuel, which must exceed the maximum expected incore life.

The CROV analysis demonstrates that the bifurcation buckling pressure limit is not exceeded. A bifurcation buckling pressure limit of approximately {{ }}$^{2(a),(c),ECI}$ psi is calculated that approximates the limit from the CROV analysis. The CROV analysis does not explicitly calculate the margin to the limit; however, the maximum pressure differential applied to the fuel rod in the CROV runs occurs at BOL and is approximately {{ }}$^{2(a),(c),ECI}$ psi, which indicates that the bifurcation buckling pressure collapse criterion is satisfied with significant margin.

Figure 4-2 and Figure 4-3 demonstrate that the fuel rod does not collapse as a result of stress beyond the yield point over the expected three cycle incore life.

Figure 4-2 Generalized Cladding Stress Versus Time

{{

}}2(a),(c),ECI

Figure 4-3 Cladding Deformation Rate Versus Time

{{

}}2(a),(c),ECI

All three collapse criteria are met. Therefore, the predicted creep collapse life of the fuel rod exceeds the maximum expected incore life of the fuel rod and cladding creep collapse does not occur.

4.2.3 Overheating of Cladding

Overheating of cladding is evaluated in the FSAR Chapter 15 transient analyses and is not addressed in this report.

4.2.4 Overheating of Fuel Pellets

Design Criterion

Fuel melting during normal operation and AOOs shall be precluded (Reference 9.1.4).

NuFuel-HTP2™ Design Evaluation

The fuel centerline melt (FCM) analysis is performed using the methodology of Reference 9.1.4.

A bounding analysis of the core design is performed using the COPERNIC fuel rod analysis code for both UO_2 and UO_2-Gd_2O_3 rods. The COPERNIC code predicts the transient LHRs where the onset of FCM occurs. **[**

]

[

]

Using the calculated LHR limits for each of the fuel rods, a bounding envelope is created, as shown in Table 4-4. Figure 4-4 and Figure 4-5 show the bounding FCM LHR limits for each fuel rod type. {{ **[**

] }}$^{2(a),(c),ECI}$

Table 4-4 Bounding Centerline Fuel Melt Limits

{{ [

] }}2(a),(c),ECI

Figure 4-4 Centerline Fuel Melt Bounding Envelopes for UO_2 Fuel

{{ [

] }}2(a),(c),ECI

Figure 4-5 Centerline Fuel Melt and Transient Cladding Strain Bounding Envelopes for 8 wt% Gd_2O_3 Fuel

{{ **[**

] }}2(a),(c),ECI

4.2.5 Excessive Fuel Enthalpy

Excessive fuel enthalpy from a reactivity initiated accident is addressed in FSAR Chapter 15 analyses.

4.2.6 Pellet-Cladding Interaction

Design Criteria

As stated in NUREG-0800 Section 4.2, there is no generic criterion for fuel failure resulting from pellet-cladding interaction or pellet-cladding mechanical interaction. Cladding strain and fuel melt criteria are applied as a surrogate.

The maximum uniform hoop strain (elastic plus plastic) shall not exceed 1 percent. Steady-state creep-down and irradiation growth are excluded (Reference 9.1.4).

The fuel melt criterion is stated in Section 4.2.4.

NuFuel-HTP2™ Design Evaluation

The transient cladding strain analysis is performed using the methodology of Reference 9.1.4.

A bounding analysis of the core design is performed using the COPERNIC fuel rod analysis code for both UO_2 and UO_2-Gd_2O_3 rods. The COPERNIC code predicts the transient LHRs where the cladding uniform hoop strain equals 1 percent.

[

]

Using the calculated LHR limits for each of the fuel rods, a bounding envelope is created, as shown in Table 4-5. Figure 4-6 and Figure 4-7 show the transient cladding strain LHR limits for each fuel rod type.

Table 4-5 Bounding Transient Cladding Strain Limits

{{ **[**

] }}$^{2(a),(c),ECI}$

Figure 4-6 Transient Cladding Strain Linear Heat Generation Rate Limits for UO_2 Fuel

{{ [

] }}2(a),(c),ECI

Figure 4-7 Transient Cladding Strain Linear Heat Generation Rate Limits for 8 wt% Gd_2O_3 Fuel

{{ [

] }}2(a),(c),ECI

4.2.7 Bursting

Swelling and rupture of the cladding relates to the ECCS performance evaluation in FSAR Chapter 15 analyses and is not addressed in this report.

4.2.8 Mechanical Fracturing

The seismic and LOCA load analysis summarized in Section 4.3.5 addresses externally applied forces on the fuel rod.

4.3 Fuel Coolability

4.3.1 Cladding Embrittlement

Cladding embrittlement relates to the ECCS performance evaluation and is not addressed in this report.

4.3.2 Violent Expulsion of Fuel

Because reactivity initiated accidents are addressed in FSAR Chapter 15 analyses, they are not addressed in this report.

4.3.3 Generalized Cladding Melting

As stated in NUREG-0800 Section 4.2, criteria for cladding embrittlement in Section 4.3.1 are more stringent than generalized cladding melting criteria. Therefore, additional specific criteria are not used.

4.3.4 Fuel Rod Ballooning

Burst strain and flow blockage caused by ballooning of the cladding relates to the ECCS performance evaluation and is not addressed in this report.

4.3.5 Fuel Assembly Structural Damage from External Forces

Design Criterion

The fuel assembly shall withstand the loads from an SSE and a LOCA. Specific acceptance criteria for fuel assembly components are identified in Reference 9.1.7.

NuFuel-HTP2™ Design Evaluation

The external load analysis is performed using the methodology of Reference 9.1.7 as modified by Reference 9.1.10. The analysis demonstrates positive margins to all applicable criteria.

Cladding Faulted

The faulted limits applied to the fuel rod cladding are shown in the far right column of Table 4-6. The table also shows the limits used in the previous faulted analysis that were based on Table 3-3 of the Framatome M5® Topical report (Reference 9.1.3). The middle column of values is derived from Table XIII-3110-1 and Article XIII-3420 of Reference 9.1.13. They are simplified for application to the cladding allowable stresses.

Table 4-6 Cladding Stress Intensity Limits

[

]

[

]

“Strengths of fuel assembly components other than spacer grids may be deduced from fundamental material properties or experimentation. Supporting evidence for strength values should be supplied. Since structural failure of these components (e.g., fracturing of guide tubes or fragmentation of fuel rods) could be more serious than grid deformation, allowable values should bound a large percentage (about 95 percent) of the distribution of component strengths. Therefore, ASME Code values and procedures may be used when appropriate for determining yield and ultimate strengths. Specification of allowable values may follow the ASME Code requirements and should consider buckling and fatigue effects.”

4.3.5.1 Analysis Inputs

4.3.5.1.1 Lateral Model

The lateral fuel assembly model is developed using the model parameters from Section 6.1 of Reference 9.1.7. Damping coefficients specific to the NuFuel-HTP2™ design are summarized in Table 4-7 and defined in Reference 9.1.9. The analysis uses values that are more conservative than those listed in Table 4-7.

Table 4-7 Summary of Fuel Assembly Damping Ratios

[

]

The following model parameters are established through design-specific characterization testing:

- **[** **]**
  - **[** **]**
  - **[** **]**
- **[** **]**
  - **[** **]**
  - **[** **]**

[

]

The application of the free and forced vibration test data from prototypical BOL and EOL NuFuel-HTP2™ fuel assemblies to define the fuel assembly dynamic characteristics is described in Appendix A of Reference 9.1.9.

Dynamic crush testing was performed on prototypical NuFuel-HTP2™ spacer grids in both a non-irradiated (BOL) and simulated-irradiated (EOL) condition to define the external spacer grid stiffness and damping characteristics. Grid corrosion is not directly modeled because the effect of oxidation on spacer grids is a small increase in strength and not accounting for it is conservative.

The **[ ]** is demonstrated in Appendix A of Reference 9.1.9. The dynamic crush test is also used to establish a grid load limit. **[**

] The grid loads are reported in Table 4-8.

Fuel assembly lateral impact testing was performed on prototypical NuFuel-HTP2™ fuel assemblies in both a BOL and EOL condition to establish the internal stiffness and damping parameters for the spacer grid.

4.3.5.1.2 Vertical Model

The vertical fuel assembly model is developed using the model parameters from Section 6.2 of Reference 9.1.7. The following model parameters are established through design-specific characterization testing:

- **[ ]**
  - **[ ]**
  - **[ ]**
- **[ ]**
  - **[ ]**
  - **[ ]**
  - **[ ]**

Spacer grid slip load tests define the grid-to-fuel rod slider slip load at BOL conditions. In this test, a prototypical NuFuel-HTP2™ spacer grid is loaded with cladding segments and a uniform load is applied across all of the cladding segments. The load at which the fuel rods are observed to begin slipping through the grid is identified as the global slip load. To simulate the EOL condition, **[ ]**
The Alloy 718 lower end grid is **[ ]**

An axial stiffness test was performed on full-scale prototypical NuFuel-HTP2™ fuel assemblies in both the BOL and EOL condition. The axial stiffness of the fuel assembly is measured at key axial locations (e.g., spacer grids and top nozzle). The measurements of location-specific axial stiffness are used to benchmark the stiffness of the grid-to-fuel rod slider elements in the vertical model.

In the event of a fuel assembly drop, two impact mechanisms require characterization. The nozzle-to-core plate gap stiffness and damping are established by a dynamic drop test of the fuel assembly. In this test, full-scale

prototypical NuFuel-HTP2™ fuel assemblies in both the BOL and EOL condition were dropped onto a rigid surface from varying heights. Impact loads, assembly velocity, and assembly position were recorded. **[**

]

The fuel rod-to-nozzle gap element is defined using dynamic drop test results performed on the EOL fuel assembly. In this test, **[**

]

[

]

4.3.5.1.3 Excitation Inputs

The excitation inputs for the external load analysis are NPM core plate displacement time histories for the SSE and LOCA events. The core plate displacement time histories include both horizontal and vertical motions.

The SSE input motions are the result of an evaluation of a single soil-structure profile, two module locations, two concrete conditions, and three stiffness profiles.

To account for the effect of uncertainty in the reactor module dynamic analysis, each time history variation is analyzed with three different scaled time intervals: the reference interval and plus or minus 15 percent. The frequency shift due to the 15 percent variation of the time scale is considered to be effectively equivalent to the broadening of spectral peaks that is done when generating in-structure response spectra. Considering the defined variations, a total of 12 time histories are considered in the analysis.

The LOCA time histories are derived from bounding high energy line breaks in the primary coolant system and inadvertent or spurious operation of reactor coolant pressure boundary valves. Core plate motions are the combined dynamic response due to asymmetric cavity pressurization of the

containment, depressurization of the reactor pressure vessel, and thrust force at the break or valve location. The LOCA events for the NPM also result in vertical hydraulic forces acting on the reactor internals. These forces are considered in addition to the core plate motions as a source of excitation for the fuel, as described in Reference 9.1.7.

4.3.5.2 Analysis Results

4.3.5.2.1 Lateral Analysis

The horizontal excitation of the full reactor core is considered in the analysis through a series of two dimensional row models with lengths of three, five, and seven fuel assemblies (Figure 3-2). Excitations in both horizontal directions are considered.

The peak impact loads for the base case seismic inputs and the margin to the grid impact load limit from all cases are summarized in Table 4-8. The peak impact loads for SSE and LOCA in a given direction are combined and margin is calculated against the impact load limit. The positive margin for these impact loads confirms that the spacer grid does not experience plastic deformation that exceeds the limit established in the Framatome methodology (Reference 9.1.7). Thus, the requirements for core coolability and control rod insertion are met.

Table 4-8 Peak Grid Impact Loads and Margins

[

]

4.3.5.2.2 Vertical Analysis

The single assembly vertical model is subjected to vertical core plate displacement time histories corresponding to the SSE and LOCA events. The maximum seismic impact load for the base case inputs, **[ ]** The maximum LOCA impact load is **[ ]** Component loads for the guide tubes, fuel rods, hold-down spring, nozzles, and guide tube connections are extracted from the vertical analysis for further load analysis.

4.3.5.2.3 Stress Analysis

The lateral and vertical analysis results are used as inputs to load and stress evaluations of the non-grid fuel assembly components. Lateral and vertical

loads are combined, along with steady-state normal operating loads, for each component for comparison to its respective acceptance criteria.

As defined in Section 8.1.2 of Reference 9.1.7, **[**

]

The results of the component evaluations are presented in Table 4-9.

Fuel rods

The accident loads on the fuel rod consist of the lateral bending stress, the axial stress from vertical loads, and an additional loading corresponding to impacts to the fuel assembly. The impact induced stress is a localized bending stress resulting from the portion of the grid impacts that are passed through the fuel rods (i.e., internal impact loads). The overall combined stress is the SRSS of the individual components combined with steady-state stresses to determine the maximum stress intensity.

The fuel rods are also evaluated for buckling under compressive loads.

Guide tubes

The accident loads on the guide tube consist of **[**
] The overall combined stress is calculated as the SRSS of the individual components combined with steady-state stresses to determine a maximum stress state. The allowable stress limits are based on ASME Code Level C service limits, consistent with Reference 9.1.7.

The guide tubes are also evaluated for buckling under compressive loads.

Guide tube-to-spacer connections

The vertical load acting on the guide tube-to-spacer grid connection is **[**

] The combined load is calculated as the SRSS of the individual components. The allowable strength of the guide tube-to-grid connections is based on the ASME Code Level D service limit and is established through testing.

Guide tube-to-nozzle connections

The loads considered in the evaluation of the guide tube-to-nozzle connections are **[**

] The allowable load for the top nozzle connection is based on the ASME Code Level C service limit and is established through strength testing. The allowable load for the bottom nozzle connection is based on ASME Code Level D service limits because the bottom nozzle cannot affect control rod insertion.

Top and bottom nozzles

The loads considered in the evaluation of the nozzles are the axial loads from the vertical analysis. The allowable strength of the top and bottom nozzle is established by testing. Because of the robustness of the nozzles, the testing is not carried to the extent of failure, and thus the allowable load and resulting margin are artificially low.

Table 4-9 Component Evaluation Margins

[

]

4.4 Thermal Hydraulic Evaluation

4.4.1 Core Pressure Drop Evaluation

An evaluation is performed of the fuel assembly pressure drop characteristics. The total pressure drop, including the recoverable and unrecoverable constituents, is determined for the limiting fuel assembly in the reactor core for rated core power and system flow conditions. Pressure loss coefficients based on testing are reported in Table 5-1 and are used in the evaluation.

The results of the pressure drop analysis indicate that the total pressure drop is dominated by the recoverable loss because of elevation change. For the full power case, the channel with the largest pressure drop has an elevation loss that is approximately {{ }}$^{2(a),(c),ECI}$ percent of the total pressure drop. The overall core total pressure drop for rated power conditions is {{ }}$^{2(a),(c),ECI}$

Figure 4-8 shows the total pressure drop axial profile for the limiting assembly in the core. As observed in the figure, the elevation pressure drop is gradual and linear between each grid or nozzle while the component pressure loss increases the pressure drop slope at the component axial location. The results are based on

operation at 100 percent rated power conditions with a bounding radial and axial core power distribution.

Figure 4-8 Best Estimate Axial Pressure Drop for Limiting Assembly

{{

}}2(a),(c),ECI

4.4.2 Guide Tube Boiling

The guide tube boiling analysis determines the water temperature profile inside the guide tubes of all assemblies, with the limiting conditions found in those fuel assemblies that contain CRAs. The analysis considers the limiting CRA positions and power levels (i.e., the normal parked all rods out position and the power dependent insertion limit position). The design criterion is that long term bulk boiling in the guide tube is precluded. This criterion is satisfied by demonstrating that the coolant flow inside the guide tube remains below the saturation temperature under conservative thermal-hydraulic conditions and assembly relative power.

The guide tube coolant temperatures are dependent on the coolant flow rates inside the guide tubes, the amount of radiation heating of the control rod, the direct heating of the water inside the guide tube, and the direct heating of the guide tube itself. Heat transfer with the surrounding assembly subchannels is modeled with conduction through the guide tube wall and convection with axial fluid flow.

Conservative analyses are performed by evaluating normal operation as a function of power and RCS flow rate. Core geometry parameter uncertainties are considered in the areas of {{

}}2(a),(c),ECI

The guide tube heating analysis determines the coolant flow distribution in the core, including rodded and unrodded guide tubes as a function of elevation. Flow enters the guide tube through holes in the side of the guide tube and from below the bottom nozzle by way of the through-hole in the cap screw.

Analysis results for the 100-percent full-power case and 75-percent power case indicate that bulk boiling does not occur at any location within the guide tube under steady-state conditions for the equilibrium core and control rod power dependent insertion limit depths. Results are shown for 100-percent and 75-percent power in Figure 4-9 and Figure 4-10, respectively. The 100-percent power case is limiting {{

}}2(a),(c),ECI

Figure 4-9 Internal Guide Tube Temperature for 100 Percent Power

{{

}}2(a),(c),ECI

Figure 4-10 Internal Guide Tube Temperature for 75 Percent Power

{{

}}2(a),(c),ECI

4.4.3 Control Rod Drop Analysis

The control rod drop analysis predicts the insertion rate and impact velocity of the CRA during a reactor trip. The calculated impact velocity is compared to the maximum acceptable impact velocity for the CRA spring in Section 6.2.9.

When the CRA is dropped into a fuel assembly, water in the guide tube is displaced through several flow paths. The rate of displacement depends on the number, size, and location of the holes along the guide tube. The fuel assembly design has 24 guide tubes, each containing two pairs of side flow holes at the entrance to the dashpot. In addition, water is forced out through the top annulus of the guide tube and through the hole in the cap screw at the bottom of the guide tube assembly.

A best-estimate, mechanistic model is used to evaluate the maximum impact velocity based on the guide tube and control rod geometry, nonlinear coefficients for drag loss (hydraulic and mechanical), and the equation of motion. Drag coefficients were developed with control rod drop measurements from a 17x17 PWR plant with a similar fuel geometry and from CRA drop testing. Coolant flow velocity through the guide tube is conservatively assumed to be zero to maximize the impact velocity.

The CRA impact velocity limit is defined in Section 6.2.9 based on the CRA spring design. The control rod drop analysis predicts an impact velocity of 2.09 ft/sec, which is below the impact velocity limit, and a drop time of 1.14 sec, where drop time is defined as the time between the start of rod movement and the time of full insertion. Figure 4-11 shows axial position versus time for the CRA drop based on a 75.982 inch travel distance for the control rod from its initial position to full insertion. Figure 4-12 shows CRA velocity versus time.

Figure 4-11 Control Rod Position Versus Time

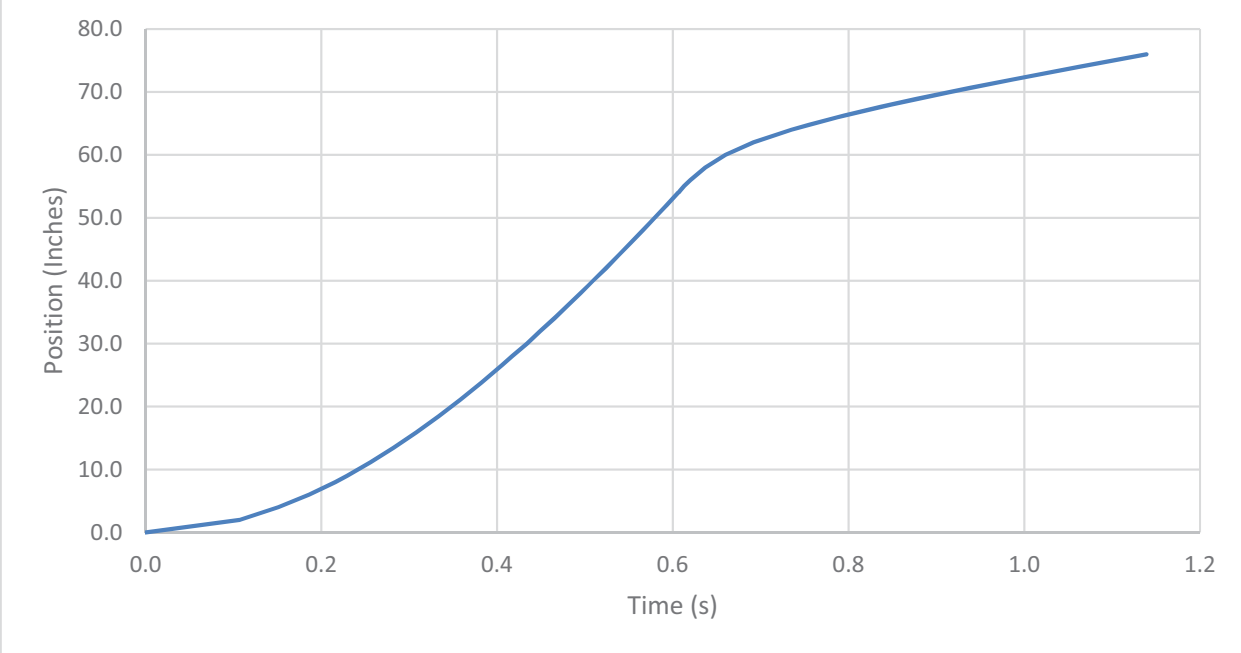

Figure 4-12 Control Rod Velocity Versus Time

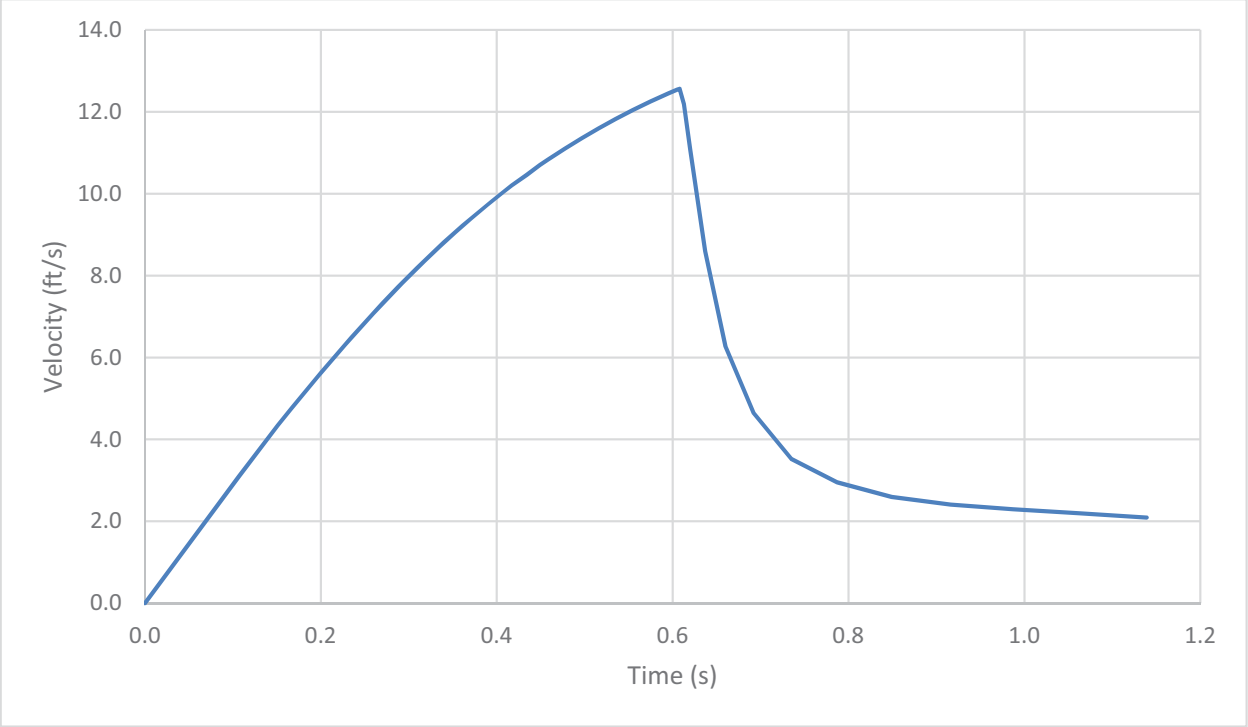

5.0 Fuel Assembly Testing

5.1 Mechanical Testing Summary

A comprehensive test program was conducted at Framatome's Richland Test Facility to characterize the mechanical performance of the NuFuel-HTP2™ fuel design. The test results are used in the fuel assembly normal operation and seismic analyses to determine the acceptability of the design for in-reactor operation.

Prototypical fuel assemblies for BOL and EOL conditions were fabricated and mechanically tested. The BOL assembly spacer grids are in the as-fabricated BOL condition. The EOL assembly simulates the EOL conditions with grid cells relaxed and fuel rods seated on the bottom nozzle.

The fuel assembly characterization tests and their use in modeling and analysis are further described in Reference 9.1.7.

5.1.1 Fuel Assembly Lateral Load Deflection (Stiffness) Test

The lateral load deflection (stiffness) test is performed to characterize the static, lateral structural response of the fuel assembly at BOL and EOL. The assembly is secured in prototypical upper and lower core plate interfaces. The test is performed by laterally deflecting the center of the test assembly at the second HTP™ spacer grid from the bottom to a displacement along one axis. The force required to deflect the assembly and the corresponding displacement are recorded continuously for the complete loading and unloading cycle.

5.1.2 Fuel Assembly Free Vibration (Lateral Pluck) Test

The free vibration (lateral pluck) test is performed to characterize the dynamic, lateral response of the fuel assembly over a large range of amplitudes at BOL and EOL. The assembly is secured in prototypical upper and lower core plate interfaces. The test is performed by laterally deflecting at the second HTP™ spacer grid from the bottom of the test fuel assembly to a given displacement, and obtaining the response of the assembly when the applied force is suddenly released. Deflection versus time is measured and is used to establish the fuel assembly first mode and damping.

5.1.3 Fuel Assembly Lateral Impact Test

The lateral impact test is performed to characterize the dynamic, lateral impact behavior of the fuel assembly at BOL and EOL. The test is performed in two phases. In the first phase, the test consists of deflecting the fuel assembly to a given displacement at the second HTP™ spacer grid from the bottom and then suddenly releasing the load allowing it to impact on a baffle plate at the third spacer grid from the bottom location. In the second phase, the test consists of deflecting the fuel assembly to a given displacement at the third spacer grid location from the bottom and then suddenly releasing the load allowing it to impact on a baffle plate at the second spacer grid from the bottom location. The assembly response is obtained in

the form of deflection versus time measured at two spacer elevations corresponding to the pull and impact locations. Instrumentation is also used to monitor out of plane movement and twist during the test. A load cell attached between the baffle plate and the support measures the test assembly impact force.

5.1.4 Fuel Assembly Lateral Forced Vibration Test

The lateral forced vibration test is used to characterize the dynamic, lateral response of the fuel assembly at BOL and EOL. This test complements the free vibration test by providing information on higher modes of the fuel assembly natural frequency, but is typically limited to smaller amplitudes than the free vibration test. This test is performed by applying a dynamic horizontal motion to the test assembly. The fuel assembly is installed on the seismic test stand, and secured in a prototypical support fixture, in order to achieve fixed-fixed end boundary conditions. The input is applied at the first and second intermediate spacer grids. These locations are selected in order to be able to excite all modes of interest. For each mode, the fuel assembly response is measured by accelerometers and displacement sensors attached at the HTP™ grid locations. **[ ]**, the evolution of frequency versus vibration amplitude is analyzed.

5.1.5 Fuel Assembly Axial Stiffness Test

The axial stiffness test is performed to characterize the static, axial structural response of the fuel assembly at BOL and EOL. The test is performed in the same fixture used for the free and forced vibration testing. The fuel assembly is secured at the top and bottom plates with a simulated core plate fixture. A jack screw is mounted between the simulated core plate and the upper support structure. A load cell is mounted between the lower support plate and the floor plate. The jack is used to apply the load, and the load cell measures the applied load. The axial deflection of the fuel assembly, under load, is measured at key locations with respect to a fixed reference. Instrumentation is also used to monitor lateral movement of the fuel assembly.

5.1.6 Fuel Assembly Drop Test

The drop test is performed to characterize the dynamic, axial structural response of the fuel assembly at BOL and EOL. The test fuel assembly is suspended a specified distance above a plate attached to a load cell. The assembly is released and allowed to fall onto the plate and load cell. The displacement of the fuel assembly bottom nozzle is measured throughout the test.

Because the use of this data is to calibrate the impact behavior of the vertical seismic model, it is necessary to collect data on force and displacement as a function of time.

5.1.7 Spacer Grid Tests

The mechanical performance of the spacer grids was confirmed through a series of structural tests on prototype grids.

Dynamic crush tests are performed on HTP™ spacer grids at unirradiated and simulated-irradiated conditions. The tests determine the through-grid stiffness and damping values for the lateral seismic models and the crushing load limits for the grids.

The static crush characteristics (static stiffness and elastic load limit) are used to establish allowable grid clamping loads applied during shipping.

Grid slip load testing defines the grid-to-fuel rod slip load at non-irradiated (BOL) conditions for both the HTP™ and HMP™ grids. Grid slip load testing is not performed at irradiated (EOL) conditions because the fuel rods are not actively restrained in the grid. The slip load values are used in the fuel assembly evaluation.

5.1.8 Top and Bottom Nozzle Tests

Strength testing of the bottom nozzle is performed to establish the axial load limit for evaluation. A prototypical bottom nozzle is tested at room temperature in static axial compression by applying a load to 24 springs on the guide tube positions. The spring stiffness is set to be equal to the guide tubes stiffness in order to simulate the load distribution of the guide tubes.

A maximum room temperature test load is applied without collapse of the structure. This tested maximum load is used to demonstrate the structural adequacy in the design evaluation by comparison with the normal operating and faulted loads.

Strength testing of the top nozzle is also performed to establish the axial load limit for evaluation. A prototypical top nozzle is tested at room temperature in static axial compression by applying a load to the top of the top nozzle, which is set on 24 springs at the guide tube positions. The spring stiffness is set to be equal to the guide tubes stiffness in order to simulate the real load distribution of the guide tubes.

A room temperature test load is applied that exceeds the design load and resulted in no plastic deformation of the structure. This tested maximum load is used to demonstrate the structural adequacy in the design evaluation by comparison with the shipping and handling, normal operating, and faulted loads.

5.2 Thermal-Hydraulic Testing Summary

5.2.1 Pressure Drop and Liftoff Testing and Pressure Loss Coefficient Development

Pressure drop and liftoff testing was performed on a full-scale NuFuel-HTP2™ prototype fuel assembly in the PHTF at the Framatome Richland Test Facility. The testing configuration simulated the upper and lower core supports in the NPM. The test data obtained from the pressure drop and liftoff testing are used to develop pressure loss coefficients for subsequent thermal-hydraulic and mechanical analyses.

The pressure loss coefficients for the spacer grids and the overall loss for the NuFuel-HTP2™ fuel assembly are dependent on the Reynolds number. The coolant

flow in the NPM is driven by natural circulation. At nominal flow conditions, the Reynolds number is approximately 86,000. Pressure drop data are reduced to Reynolds number dependent values and are used in the development of the pressure drop coefficient correlation. The pressure loss coefficients for assembly components and the overall fuel assembly are given in Table 5-1.

In addition to the pressure drop test, a hydraulic liftoff test was performed in the PHTF to acquire data to develop a correlation to be used in fuel assembly hydraulic lift analyses. The liftoff test is performed on a prototypical fuel assembly at six different temperatures for characterization over a range of Reynolds numbers. At each temperature, the flow is adjusted to obtain a conservative lift point, which is defined as the flow and temperature state at which the assembly is barely seated. Pressure drop measurements are taken at the conservative lift point and at a state point where the assembly lifts measurably. An overall pressure loss coefficient for use in hydraulic lift analyses is determined and is given in Table 5-1.

5.2.2 Flow-Induced Vibration Testing

A 1000-hour life and wear test was performed at the Richland PHTF to validate the fretting performance of the fuel assembly structure. The life and wear test is run for 1032 hours at a temperature of 300 degrees F at or above the target Reynolds number of 52,000. At the conclusion of the test, **[ ]** fuel rods are examined for grid to rod fretting. The test results are summarized in Section 4.1.3.

Table 5-1 Pressure Loss Coefficients Derived from Testing

[

]

6.0 Control Rod Assembly

6.1 Control Rod Assembly Description

The CRA includes 24 individual control rods fastened to a one-piece cast stainless steel spider and coupling hub (Figure 6-1). Table 6-1 provides major CRA design parameters. The top end of each individual control rod attaches to the spider by a nut, pin, and weld combination. Compared to Framatome's standard rod control cluster assembly (RCCA) design, the individual control rods are shortened to match the reactor core height, but retain the same basic design features and materials. Framatome's standard RCCA design has been implemented in twelve 17x17 PWRs in the United States, comprising over 600 individual assemblies.

The combination of the pin, nut, upper end plug, and spider boss form a flex joint, which provides flexibility to accommodate potential misalignment between the CRA and fuel assembly guide tubes. The upper end plug has a reduced diameter shank and lower shoulder to provide lateral clearance with the interior diameter of the spider finger. The clearance allows for elastic deflection of the upper end plug for any misaligned control rod, fuel assembly, upper internals, or fuel handling equipment.

A preloaded helical spring is assembled into a skirt internal to the bottom of the spider hub and provides for energy absorption during a CRA trip. The spring is preloaded and maintained within the hub by a retaining ring and tension bolt. During a refueling outage or after a reactor trip, the spring retaining ring rests on the fuel assembly top nozzle. The CRA interfaces with the control rod drive mechanism coupling through a cavity at the top of the CRA spider (Figure 6-2) that matches the male coupling dimensions on the drive shaft, similar to current designs in operation.

A 302 stainless steel plenum spring is used within the individual rods to restrain motion of the absorber materials within the cladding during shipping and handling. The absorber material is a combination of B_4C pellets and silver-indium-cadmium (AIC) bar. The lower AIC absorber is located in the higher flux region because it has lower swelling under irradiation than B_4C.

A stack support resides within the annulus of the lowermost AIC absorber to reduce compressive loads on the bottom segment of AIC, thus reducing thermal creep of the AIC during operation. The control rod cladding is 304L stainless steel tubing with stainless steel end plugs welded to each end, encapsulating the rod internals to complete the rod assemblies (Figure 6-3).

The design differences between the Framatome standard RCCA and the NuScale CRA are the length of the rod components, the cladding material, and spider spring and retainer modifications. Framatome operating experience has identified two life-limiting phenomena for control rod assemblies: cladding strain and cladding wear. Strain behavior of the CRA is similar given the diametral equivalence of the rods. The minor difference in cladding material should not be a significant factor in the allowable cladding strain. Cladding wear is expected to be acceptable on the CRA given the low axial flow rates of the NPM.

The changes to the spider spring and retainer design relative to the standard Framatome RCCA design are made to increase the spring preload and decrease the spring solid height. These changes allow the CRA spider to absorb the energy from a higher impact force than is experienced in typical PWR applications.

Control rod assembly materials exposed to reactor coolant are either low carbon stainless steels or Alloy 718, all of which are resistant to corrosion from reactor coolant exposure. These materials have been used extensively and successfully in operating PWRs. The B_4C and AIC absorber materials are encapsulated in a 304L stainless steel tube that is welded at both ends, which protects the absorbers from coolant interaction. Control rod integrity is confirmed by inspection during initial refueling outages. Table 6-2 identifies CRA component materials.

Table 6-1 Control Rod Design Parameters

Parameter	Value
CRA total weight (lb)	43
CRA total height (inch)	94.37
Control rod length - short/medium/long (inch)	87.065 / 87.425 / 87.875
Control rod outer diameter (inch)	0.381
Control rod inner diameter (inch)	0.344
Control rod bottom end plug length (inch)	1.913
B_4C outer diameter (inch)	0.333
B_4C stack length (inch)	62.0
AIC outer diameter (inch)	0.336
AIC stack length (inch)	12.0
Height of CRA spider assembly (inch)	10.387
CRA shaft outer diameter (inch)	1.804

Table 6-2 Control Rod Assembly Materials

Component	Material
Spider	304L stainless steel
Rod end plugs	308L stainless steel
Cladding	304L stainless steel
Solid spacer, lock pin, nuts, tension bolt	304L stainless steel
Spring retainer	17-4 PH stainless steel
Spider spring	Alloy 718
Control rod plenum spring	302 stainless steel
Absorber materials	80% Ag - 15% In - 5% Cd and B_4C
Stack support	Alloy X750

Figure 6-1 Control Rod Assembly General Arrangement

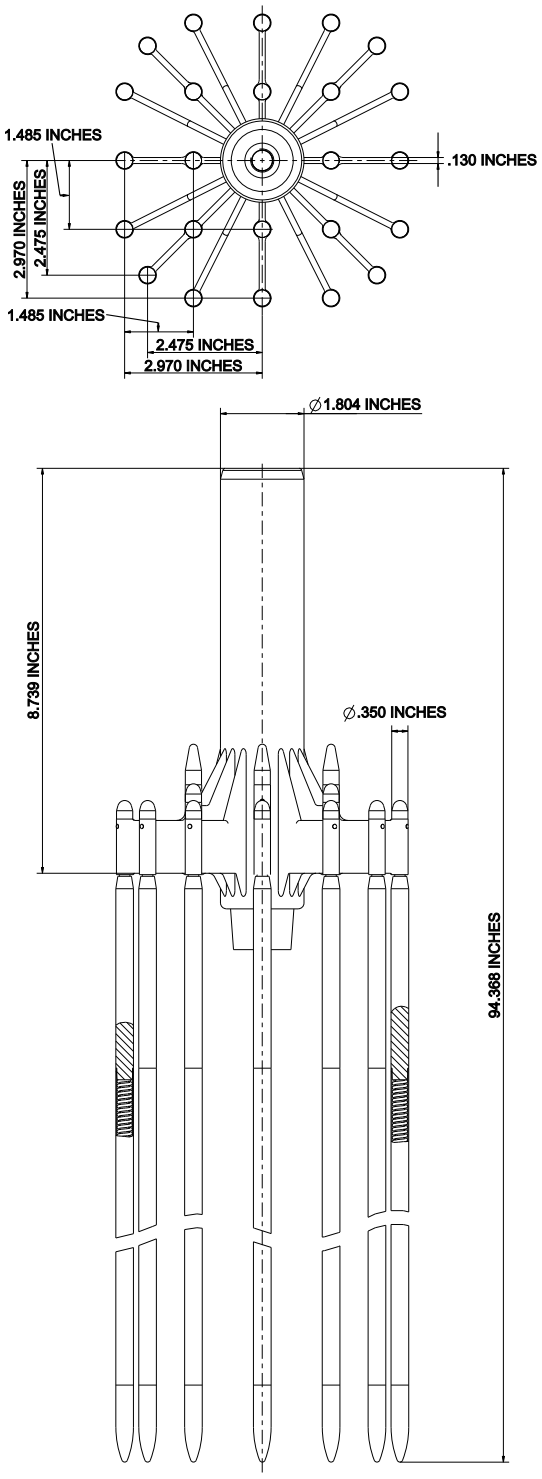

Figure 6-2 Control Rod Assembly Cut-Away

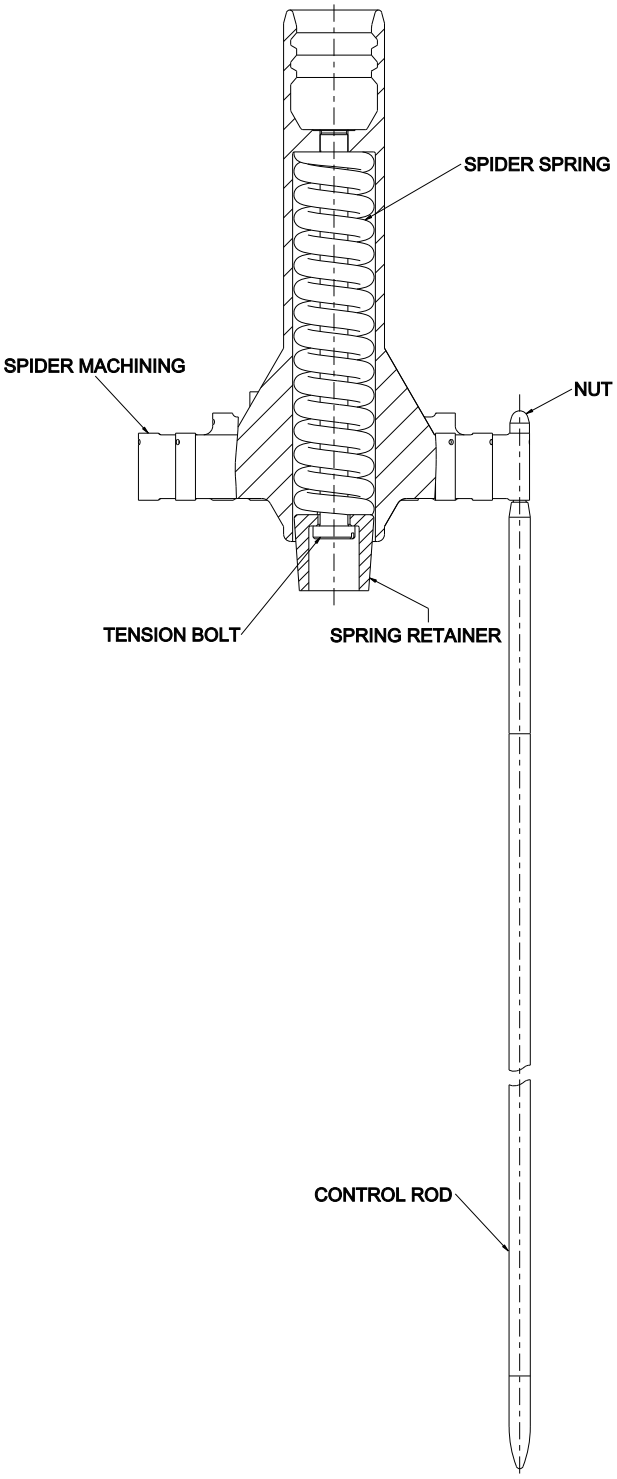

Figure 6-3 Control Rod Design

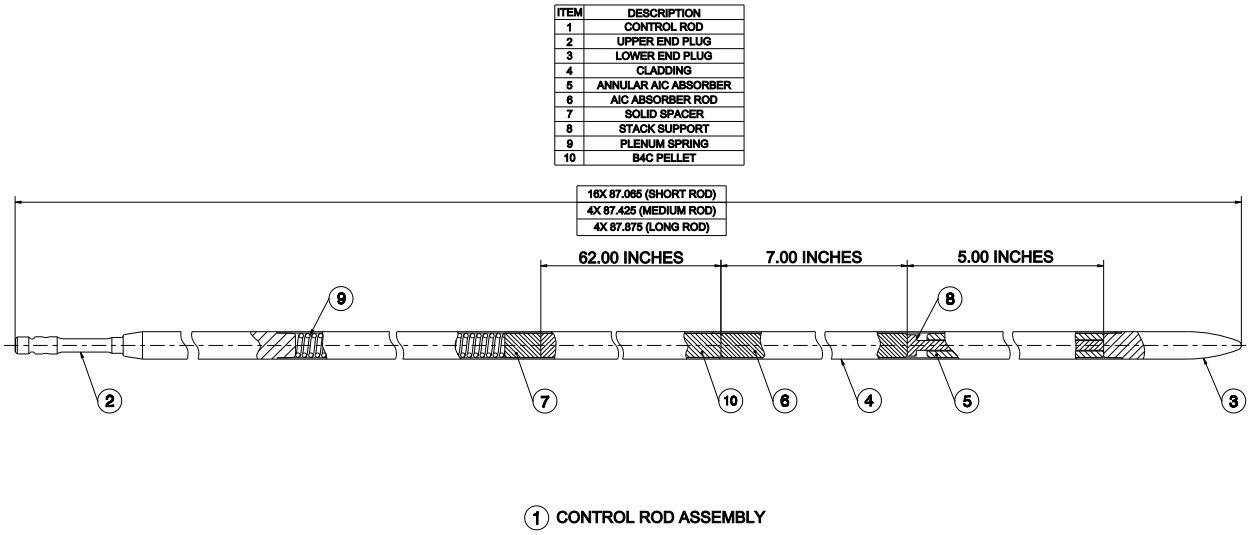

6.2 Control Rod Assembly Evaluation

This section evaluates the CRA design against typical criteria to demonstrate acceptable performance under all conditions of operation over a 20 effective full power year (EFPY) design lifetime.

6.2.1 Cladding Strain

The potential for control rod cladding strain is primarily a result of swelling of the control rod absorber material caused by neutron fluence. The analysis considers elevation-specific fluence values and thermal expansion of the absorber and cladding. The calculated cladding and absorber temperatures are based on the flux predicted for various axial positions along the control rods. Volumetric swelling rates of the B_4C pellets and the AIC absorber are based on models benchmarked to measurements from in-reactor control components.

The strain calculation is performed at the following axial elevations:

- bottom of the annular AIC bar, where the fluence is highest
- bottom of the solid AIC bar
- bottom of the B_4C pellet stack

Cladding strain is limited to **[ ]** percent to maintain ductility for irradiated 304L stainless steel cladding. The strain calculation determines that the cladding strain limit is met for greater than 20 EFPY of operation.

6.2.2 Cladding Creep Collapse

Cladding creep collapse evaluations include short-term and long-term collapse analyses.

In the short-term collapse analysis, the differential pressure across the control rod cladding must not exceed the critical buckling pressure. Two critical buckling pressures are calculated:

- bifurcation buckling pressure of a perfectly circular shell (P_{cr}), to confirm the elastic stability of the cladding
- yield-point buckling pressure (P_{yp}) accounting for initial tubing ovality

The calculated buckling pressures at hot and cold conditions exceed the system pressure of 2000 psia and a conservative maximum reactor system pressure of 2310 psia, providing margin to the buckling criteria.

In the long-term collapse analysis, changes in cladding ovalization and cladding stress over time are predicted using the CROV creep ovalization code. The analysis assumes no cladding support by the control rod internals. Creep collapse is evaluated at the lowest tip of the control rod because this region experiences the largest fast flux.

The CROV analysis demonstrates that after 20 EFPY, the cladding ovality remains within acceptance limits, the cladding stress remains below the material yield strength, and the maximum cladding diameter as a result of ovalization is less than the inner diameter of the guide tube dashpot.

6.2.3 Cladding Stress

Control rod cladding stresses are categorized, calculated, and compared to service limits in accordance with the ASME Code. Cladding stresses are calculated based on

- differential pressure.
- differential temperature.
- cladding ovality.
- loads from control rod drive mechanism stepping and reactor trip.
- bending due to misalignment.
- seismic conditions.
- FIV.
- shipping and handling conditions (evaluated in isolation from other conditions).
- stuck rod condition (evaluated in isolation from other conditions).

The design stress intensity, S_m, is two-thirds of the cladding yield strength **[ ]**. Table 6-3 defines the allowable stresses for each of the four ASME Code stress categories. The calculated stresses result in a minimum design margin of **[ ]**, which occurs for primary membrane stresses at hot conditions, where margin is defined as the allowable stress divided by the calculated stress.

Table 6-3 Control Rod Cladding Allowable Stresses

Stress Category	Temperature, °F	ASME Allowable Stress, psi
A: Primary membrane $P_m \le S_m$	70 650	**[**
B: Primary membrane + bending $P_m + P_b \le 1.5S_m$	70 650	
C: Primary and secondary membrane + bending $P_m + P_b + Q \le 3.0S_m$	70 650	
D: Faulted $P_m \le S_m$ $P_m + P_b \le 2.25S_m$	70 650 70 650	**]**

6.2.4 Cladding Fatigue

The control rod cladding is analyzed for fatigue from stepping loads and FIV bending loads, assuming no wear. The analysis conservatively assumes infinite cycles from FIV and control rod stepping. The analysis concludes that the fatigue stress is below the endurance stress limit of the cladding material based on the ASME Code fatigue curve (12 ksi), and therefore fatigue failure does not occur.

6.2.5 Cladding Wear

Control rod cladding wear limits are determined by reducing the cladding wall thickness in mechanical analyses until the margin to acceptance limits is reduced to zero. This method is consistent with the industry approach for PWRs. Because of the potential for leaching of the B_4C pellets and subsequent impact on shutdown capability if the cladding barrier is breached, a **[ ]** reduction in the minimum cladding wall thickness is conservatively applied to calculate the wear limits. The calculated wear limits address circumferential wear and azimuthally localized wear.

The following limits are calculated:

- maximum wear depth of **[ ]** inch, independent of geometry

- minimum cross-sectional area of **[ ]** inch^2 remaining after wear (uniform circumferential wear)
- minimum cross-sectional area of **[ ]** inch^2 remaining after wear (azimuthally localized wear, considering **[ ]**)

Wear limits are used in conjunction with wear rates specific to the NPM design to determine an allowable wear-based design life. After initial irradiation and operation of the CRA design, inspections are performed so that actual rod wear rates can be compared with the predetermined wear limits to demonstrate acceptable performance.

The operating environment for the CRAs is expected to be less severe with respect to rod wear than the environment typical of operating PWRs. Axial flow rates in the reactor core and in the guide tubes are significantly lower and cross flows at and above the fuel assembly top nozzles are very low (approximately {{ }}$^{2(a),(c),ECI}$ feet/second). The absence of outlet flow nozzles in the upper internals reduces the cross flows compared to a typical PWR. These flow conditions create a more benign flow environment, reducing mechanical interactions with the guide cards and fuel assemblies. Based on this assessment, the CRA design lifetime is not expected to be limited by control rod wear.

6.2.6 Control Rod Internal Pressure

The control rod internal pressure analysis predicts the maximum internal rod pressure using a conservative model that calculates the depletion in the B_4C pellets and release of helium to the rod plenum volume. The calculation includes helium backfill, residual, and sorbed gases in the determination of the final maximum internal pressure. The AIC material is not a source of gases.

During normal operation, the CRAs are positioned such that the B_4C pellets are located above the active fuel. Over the lifetime of the CRA, there is very low depletion, which results in insignificant helium production. In addition, the large porosity of the B_4C absorber material provides sufficient volume to accommodate any helium produced. However, the analysis conservatively assumes **[ ]** percent release and retention of the helium due to depletion of the B_4C pellets.

For a 20 EFPY control rod assembly design life, a ^{10}B depletion of **[ ]** percent creates a maximum rod internal pressure of **[ ]** psia, which meets the criterion of being less than RCS pressure (2000 psia).

6.2.7 Component Melt Analysis

The control rod is analyzed to ensure that each component remains below the melt temperature. The analysis uses conservative values for heating rates and gap conductance. The worst case calculated temperatures for all rod components are well below the material melt limits.

6.2.8 Spider Assembly Structural Analysis

The spider assembly structural analysis evaluates the static and fatigue stresses in the CRA spider assembly and the control rod to spider connections. The following loads are analyzed:

- reactor trip and CRA stepping
- stuck rod
- shipping and handling
- hydraulic load during reactor trip

The following elements of the spider assembly are analyzed:

- spider arm
- CRA spring
- spring retainer
- spring tension bolt
- spring flange
- spring housing
- spider coupling splines
- upper end plug, nut, and spider connection

Calculated stresses are compared to ASME Code minimum material strength values. The results demonstrate positive margins for all components, validating the structural integrity of the spider assembly and connections during normal operation and faulted conditions.

6.2.9 Control Rod Assembly Impact Velocity Limit

The kinetic energy absorption capacity of the CRA spring is analyzed to determine the CRA maximum allowable impact velocity during a reactor trip. The design has a longer and heavier CRA driveline than is typical for PWRs and has lower axial flow rates, resulting in a higher CRA impact velocity. The spider spring is designed to absorb the kinetic energy of the CRA during a reactor trip using the available spring retainer travel to prevent the CRA spider hub from impacting the fuel assembly top nozzle.

The maximum allowable impact velocity is **[ ]** ft/sec. Section 4.4.3 describes a calculation performed that determined an impact velocity of 2.09 ft/sec.

6.3 Control Rod Assembly Testing

The CRA is similar to existing 17x17 control rod assemblies except for the shorter length. The CRA drive shaft is longer than typically used in the industry. Prototype testing was

performed to confirm CRA drop times, to assess the propensity for wear, and to assess the impact of the maximum expected misalignment of the fuel assembly guide tubes, guide cards, and riser supports predicted to occur during a concurrent LOCA and seismic event. The combination of misalignments resulting in the slowest drop produced a drop time of approximately 1.2 seconds. Section 4.4.3 describes the calculation performed to determine the impact velocity.

7.0 Design Change Process

The following defines the mechanical design change process for the NuFuel-HTP2™ fuel design. The design change process is modeled after the NRC-approved change process defined in Reference 9.1.2 and is in conformance to the NuScale design control requirements and 10 CFR 50 Appendix B Quality Assurance Program.

The fuel design criteria for the NuFuel-HTP2™ design are distributed across several sources. Reference 9.1.8, Table 7-1 identifies the mechanical design criteria and source of applicability to the NuFuel-HTP2™ design. The design criteria sources are

- Framatome methodologies that are applicable to the NuFuel-HTP2™ design provided in Reference 9.1.4, Reference 9.1.5, Reference 9.1.6, Reference 9.1.7, Reference 9.1.2, and Reference 9.1.3.
- NuScale methodologies provided in Reference 9.1.8, Reference 9.1.9, and Reference 9.1.10.
- the remaining criteria that are evaluated by the methodologies as approved in the FSAR.

Applicable design criteria are summarized in Section 4.0. Compliance to these criteria is demonstrated by

- documenting the fuel system and fuel assembly design drawings.
- performing analyses with the NRC-approved models and methods described in Section 4.0.
- using lead test assemblies, prototypic testing and engineering analyses, where appropriate, to demonstrate that analytical methods and acceptance criteria remain applicable and to demonstrate in-reactor performance.
- continuing irradiation surveillance programs, including post irradiation examinations, to confirm fuel assembly performance.
- using the quality assurance procedures, quality control inspection program, and design control requirements set forth in the NRC-approved NuScale Quality Assurance Program.

Design changes can be made without NRC review and approval if the following conditions are met:

- demonstrating compliance with the approved criteria as defined above
- changes in plant technical specifications are not required
- the applicability of NRC-approved methodologies as described in Section 4.0 is demonstrated to be valid
- burnup limits are within those approved by the NRC

Examples of changes that would potentially meet these conditions:

- a change in the attachment of the spacer grid to the guide tubes
- a change in the strip thickness of the spacer grid
- a change in cladding thickness

Examples of changes that would not meet these conditions:

- new cladding material
- a spacer grid with a new mixing behavior or new rod support mechanism
- a change that would alter the fuel behavior relative to the NRC-approved models, for example rod growth, assembly growth, or clad corrosion

8.0 Summary and Conclusions

This report describes the NuFuel-HTP2™ fuel assembly design and corresponding CRA design. The designs incorporate features with extensive operating experience and are evaluated using NRC-approved evaluation methods. The testing and design evaluations demonstrate that the designs meet regulatory criteria and perform acceptably in the NPM.

9.0 References

9.1 Source Documents

9.1.1 NUREG-0800, U.S. NRC Standard Review Plan Section 4.2, Revision 3, “Fuel System Design,” March 2007.

9.1.2 EMF-92-116(P)(A), Rev. 0, “Generic Mechanical Design Criteria for PWR Fuel Designs,” February 2015.

9.1.3 BAW-10227P-A, Rev. 1, “Evaluation of Advanced Cladding and Structural Material (M5®) in PWR Reactor Fuel,” June 2003.

9.1.4 ANP-10231PA-01, “COPERNIC Fuel Rod Design Computer Code,” January 2004.

9.1.5 ANP-10084PA-03, “Program to Determine In-Reactor Performance of B&W Fuels - Cladding Creep Collapse” (CROV computer code), October 1980.

9.1.6 XN-75-32 (P) (A), Supplements 1-4, Computational Procedure for Evaluating Fuel Rod Bowing, February 1983.

9.1.7 ANP-10337P-A, Rev. 0, “PWR Fuel Assembly Structural Response to Externally Applied Dynamic Excitations,” April 2018.

9.1.8 TR-0116-20825-P-A, Applicability of AREVA Fuel Methodology for the NuScale Design, June 2016, Revision 1.

9.1.9 TR-0716-50351-P, NuScale Applicability of AREVA Method for the Evaluation of Fuel Assembly Structural Response to Externally Applied Forces, December 2019, Revision 1.

9.1.10 TR-108553-P-A, Framatome Fuel and Structural Response Methodologies Applicability to NuScale, Supplement 1 to TR-0116-20825-P-A, Revision 1, Supplement 1 to TR-0716-50351-P-A, Revision 1, October 2022, Revision 0.

9.1.11 ASME Boiler and Pressure Vessel Code, Section III, Division 1 - Subsection NG, Core Support Structures, 2010 Edition with 2011a Addenda, July 1, 2011.

9.1.12 O’Donnell, W.J. and B.F. Langer, “Fatigue Design Basis for Zircaloy Components,” Nuclear Science and Engineering, Volume 20, pp. 1-12, September 1964.

9.1.13 ASME Boiler and Pressure Vessel Code, Section III, Division 1, 2019 Edition.

Enclosure 3:

Affidavit of Carrie Fosaaen, AF-131682

NuScale Power, LLC
1100 NE Circle Blvd., Suite 200 Corvallis, Oregon 97330 Office 541.360.0500 Fax 541.207.3928
www.nuscalepower.com

NuScale Power, LLC

AFFIDAVIT of Carrie Fosaaen

I, Carrie Fosaaen, state as follows:

(1) I am the Senior Director of Regulatory Affairs of NuScale Power, LLC (NuScale), and as such, I have been specifically delegated the function of reviewing the information described in this Affidavit that NuScale seeks to have withheld from public disclosure, and am authorized to apply for its withholding on behalf of NuScale

(2) I am knowledgeable of the criteria and procedures used by NuScale in designating information as a trade secret, privileged, or as confidential commercial or financial information. This request to withhold information from public disclosure is driven by one or more of the following:

(a) The information requested to be withheld reveals distinguishing aspects of a process (or component, structure, tool, method, etc.) whose use by NuScale competitors, without a license from NuScale, would constitute a competitive economic disadvantage to NuScale.

(b) The information requested to be withheld consists of supporting data, including test data, relative to a process (or component, structure, tool, method, etc.), and the application of the data secures a competitive economic advantage, as described more fully in paragraph 3 of this Affidavit.

(c) Use by a competitor of the information requested to be withheld would reduce the competitor's expenditure of resources, or improve its competitive position, in the design, manufacture, shipment, installation, assurance of quality, or licensing of a similar product.

(d) The information requested to be withheld reveals cost or price information, production capabilities, budget levels, or commercial strategies of NuScale.

(e) The information requested to be withheld consists of patentable ideas.

(3) Public disclosure of the information sought to be withheld is likely to cause substantial harm to NuScale's competitive position and foreclose or reduce the availability of profit-making opportunities. The accompanying report reveals distinguishing aspects about the component by which NuScale develops its Reactor.

NuScale has performed significant research and evaluation to develop a basis for this component and has invested significant resources, including the expenditure of a considerable sum of money.

The precise financial value of the information is difficult to quantify, but it is a key element of the design basis for a NuScale plant and, therefore, has substantial value to NuScale.

If the information were disclosed to the public, NuScale's competitors would have access to the information without purchasing the right to use it or having been required to undertake a similar expenditure of resources. Such disclosure would constitute a misappropriation of NuScale's intellectual property, and would deprive NuScale of the opportunity to exercise its competitive advantage to seek an adequate return on its investment.

(4) The information sought to be withheld is in the enclosed report entitled Reactor. The enclosure contains the designation "Proprietary" at the top of each page containing proprietary information. The information considered by NuScale to be proprietary is identified within double braces, "{{ }}" in the document.

(5) The basis for proposing that the information be withheld is that NuScale treats the information as a trade secret, privileged, or as confidential commercial or financial information. NuScale relies upon the exemption from disclosure set forth in the Freedom of Information Act ("FOIA"), 5 USC §

552(b)(4), as well as exemptions applicable to the NRC under 10 CFR §§ 2.390(a)(4) and 9.17(a)(4).

(6) Pursuant to the provisions set forth in 10 CFR § 2.390(b)(4), the following is provided for consideration by the Commission in determining whether the information sought to be withheld from public disclosure should be withheld:

(a) The information sought to be withheld is owned and has been held in confidence by NuScale.

(b) The information is of a sort customarily held in confidence by NuScale and, to the best of my knowledge and belief, consistently has been held in confidence by NuScale. The procedure for approval of external release of such information typically requires review by the staff manager, project manager, chief technology officer or other equivalent authority, or the manager of the cognizant marketing function (or his delegate), for technical content, competitive effect, and determination of the accuracy of the proprietary designation. Disclosures outside NuScale are limited to regulatory bodies, customers and potential customers and their agents, suppliers, licensees, and others with a legitimate need for the information, and then only in accordance with appropriate regulatory provisions or contractual agreements to maintain confidentiality.

(c) The information is being transmitted to and received by the NRC in confidence.

(d) No public disclosure of the information has been made, and it is not available in public sources. All disclosures to third parties, including any required transmittals to NRC, have been made, or must be made, pursuant to regulatory provisions or contractual agreements that provide for maintenance of the information in confidence.

(e) Public disclosure of the information is likely to cause substantial harm to the competitive position of NuScale, taking into account the value of the information to NuScale, the amount of effort and money expended by NuScale in developing the information, and the difficulty others would have in acquiring or duplicating the information. The information sought to be withheld is part of NuScale's technology that provides NuScale with a competitive advantage over other firms in the industry. NuScale has invested significant human and financial capital in developing this technology and NuScale believes it would be difficult for others to duplicate the technology without access to the information sought to be withheld.

I declare under penalty of perjury that the foregoing is true and correct. Executed on 12/28/2022.

Carrie Fosaaen

Enclosure 4:

Affidavit of Morris Byram, Framatome Inc.

A F F I D A V I T

1. My name is Morris Byram. I am Product Manager, Licensing & Regulatory Affairs for Framatome Inc. (Framatome) and as such I am authorized to execute this Affidavit.

2. I am familiar with the criteria applied by Framatome to determine whether certain Framatome information is proprietary. I am familiar with the policies established by Framatome to ensure the proper application of these criteria.

3. I am familiar with the Framatome information contained in the Document TR-117605-P, Revision 0, "NuFuel-HTP2™ Fuel and Control Rod Assembly Designs," within Enclosure 1 to the NuScale Power, LLC letter Number LO-131679 with subject "NuScale Power, LLC Submittal of the NuScale Standard Design Approval Application Part 2 – Final Safety Analysis Report, Chapter 4, 'Reactor,' Revision 0," and referred to herein as "Document." Information contained in this Document has been classified by Framatome as proprietary in accordance with the policies established by Framatome for the control and protection of proprietary and confidential information.

4. This Document contains information of a proprietary and confidential nature and is of the type customarily held in confidence by Framatome and not made available to the public. Based on my experience, I am aware that other companies regard information of the kind contained in this Document as proprietary and confidential.

5. This Document has been made available to the U.S. Nuclear Regulatory Commission in confidence with the request that the information contained in this Document be withheld from public disclosure. The request for withholding of proprietary information is made in accordance with 10 CFR 2.390. The information for which withholding from disclosure is

requested qualifies under 10 CFR 2.390(a)(4) “Trade secrets and commercial or financial information.”

6. The following criteria are customarily applied by Framatome to determine whether information should be classified as proprietary:

(a) The information reveals details of Framatome’s research and development plans and programs or their results.

(b) Use of the information by a competitor would permit the competitor to significantly reduce its expenditures, in time or resources, to design, produce, or market a similar product or service.

(c) The information includes test data or analytical techniques concerning a process, methodology, or component, the application of which results in a competitive advantage for Framatome.

(d) The information reveals certain distinguishing aspects of a process, methodology, or component, the exclusive use of which provides a competitive advantage for Framatome in product optimization or marketability.

(e) The information is vital to a competitive advantage held by Framatome, would be helpful to competitors to Framatome, and would likely cause substantial harm to the competitive position of Framatome.

The information in this Document is considered proprietary for the reasons set forth in paragraph 6(b), 6(c), and 6(d) above.

7. In accordance with Framatome’s policies governing the protection and control of information, proprietary information contained in this Document has been made available, on a limited basis, to others outside Framatome only as required and under suitable agreement providing for nondisclosure and limited use of the information.

8. Framatome policy requires that proprietary information be kept in a secured file or area and distributed on a need-to-know basis.

9. The foregoing statements are true and correct to the best of my knowledge, information, and belief.

I declare under penalty of perjury that the foregoing is true and correct.

Executed on: (12/23/2022)

BYRAM Morris Digitally signed by BYRAM Morris
Date: 2022.12.23 19:04:30 -08'00'

(NAME)

Email: morris.byram@framatome.com
Phone: 434-221-1082